

Chemical tools to probe carbohydrate recognition and glycoconjugate biosynthesis

Irina Ivanova

This thesis is submitted in fulfilment of the requirements of the degree of
Doctor of Philosophy at the University of East Anglia

Department of Biological Chemistry

John Innes Centre

Norwich

June 2015

© This copy of the thesis has been supplied on condition that anyone who consults it is understood to recognise that its copyright rests with the author and that no quotation from the thesis, or information derived therefrom, may be published with the author's prior, written consent.

Date

30/06/2015

I declare that the work contained in this thesis, submitted by me for the degree of Doctor of Philosophy, is to the best of my knowledge my own original work, except where due reference is made.

Signed

Irina Ivanova

Abstract

In eukaryotes the assembly of complex glycoconjugate structures takes place in the endoplasmic reticulum (ER) and Golgi apparatus, where a number of specific membrane-bound glycosyltransferases transfer sugar moiety from soluble or lipid linked activated sugar nucleotides to variety of acceptors with correct stereo and regioselectivity. Many glycoconjugates structures have been elucidated; however, most glycosyltransferases involved in their biosynthesis have not been identified and characterised. Currently, cell-free radiolabelled assays are widely used to detect their activities. These types of assays are sensitive and broadly applicable, but can be complicated by well-known factors related to the application of radioactive substances.

The purpose of this study was the development of simple and sensitive fluorescence-based methodology to detect membrane-bound glycosyltransferases activities, which could replace traditional radiolabelled methods used in the field. Fluorescent acceptors, such as 4-(1-(7-hydroxy-coumarin-3-yl)-1H-1,2,3-triazol-4-yl)-propyl α -D-mannopyranoside (α -Man-HTC) (**2.12**) and 4-(1-(7-hydroxy-coumarin-3-yl)-1H-1,2,3-triazol-4-yl)-propyl α -D-mannopyranosyl-(1 \rightarrow 6)- α -D-mannopyranoside (α -Man-1,6- α -Man-HTC) (**2.13**) were designed to have linkages that mimic the authentic acceptors. The fluorescence-based assays were benchmarked against established radiolabelled assays to detect mannosyltransferase activities involved in the biosynthesis of lipoarabinomannan in *Mycobacterium smegmatis* and galactosyltransferase activities involved in the decoration of GPI anchor in *Trypanosoma brucei*. Further application of this methodology allowed detection and characterisation of mannosyltransferase activities responsible for biosynthesis of *N*-glycans in *Euglena gracilis*, along with detection of *N*-acetylglucosamine-1-phosphate transferase activity.

In a separate study, a series of linear and cyclic 1,4/1,5-triazole-linked-*pseudo*-galctooligomers were synthesised from 2-(2-(2-azidoethoxy)ethoxy)ethyl 6-*O*-(prop-2-ynyl)- β -D-galactopyranoside (**4.07**) utilising Cu(I)-catalysed click reactions. These compounds were used to mimic authentic substrates for *Trypanosoma cruzi trans*-sialidases in order to block *Trypanosoma cruzi* macrophage invasion.

“Wherever you go, go with all your heart.”

Confucius

Acknowledgements

To begin with, I would like to thank my supervisor Prof Rob Field for giving me this opportunity to be a part of your group and to work alongside with so many remarkable people. Thank you for your patience and positive approach to life, for continuous support, constant encouragement and lots of helpful advices during the whole period of my PhD. You allowed me to grow and developed from a hesitant undergraduate to a more confident scientist. And who can forget, I will always be grateful to you for allowing me to experience Chinese science and culture, and making it a worry-free experience. You are an amazing supervisor, Thank you.

I also would like to thank my second supervisor Prof Sarah O'Connor for your inquisitive questions and helpful advices relating to my project during our progress meetings. And a warm thank you to Prof Biao Yu for hosting me in your group at Shanghai Institute of Organic Chemistry and allowing me to learn new aspects of carbohydrate synthesis. I would especially like to thank Dr. Sergey Nepogodiev and Dr. Martin Rejzek for your invaluable guidance related to the carbohydrate chemistry, for teaching me to be very thorough in my experimental approaches and for all those stimulating conversations we had over these years. I also thank Gerhard Saalbach and Lionel Hill for their help and advice with analytical aspect of this project.

I would like to thank all the past and present members of Rob Field's group Matt Donaldson, Ellis O'Neill, Stephan Goetz, Mike Rugen, Ben Wagstaff, Edward Hems, and Sue Sakonwan for making it an enjoyable place to work and helping me with any queries I had. I would like to thank my newly made and old friends Matilde Aguilar-Moncayo, Giulia Pergolizzi, Ivone Carvalho, Ausra Jablonskyte and Amanda Hill for being there for me when I needed you the most.

I would like to thank my father for setting up an example that it is never too late to study and my mother for your unconditional love and support.

And finally, I would like to thank Douglas Powell for putting up with my late evenings and weekends, for letting me gallivanting to all places without ever complaining, for feeling so proud of my achievements, and therefore, I dedicate this thesis to you.

Table of Contents

1	INTRODUCTION.....	1
1.1	Essentials of glycoconjugates	2
1.2	The structures and biosynthesis of glycoconjugates of interest.....	2
1.2.1	Glycosylphosphatidylinositol anchors	3
1.2.2	Mycobacterial lipoarabinomannan	6
1.2.3	Eukaryotic <i>N</i> -linked glycoproteins.....	8
1.2.4	Eukaryotic <i>O</i> -linked glycoproteins	15
1.3	Glycosyltransferases involved in the biosynthesis of glycoconjugates	17
1.4	Methods to probe activities of glycosyltransferases.....	19
1.4.1	Radiolabelled methodologies to probe glycosyltransferase activities.....	20
1.4.2	Fluorescence-based methodologies to probe glycosyltransferase activities	21
1.5	Requirement for the new fluorescence-based methodology.....	26
1.6	Project aims and objectives.....	28
2	DEVELOPMENT AND VALIDATION OF FLUORESCENCE-BASED METHODOLOGIES TO PROBE BIOSYNTHESIS OF GLYCOCONJUGATES	29
2.1	Underlying aspects of fluorescence-based methodologies	30
2.2	Design of non-fluorescent and fluorescent mannoside substrates for fluorescence-based methodologies.....	34
2.3	Chemical synthesis of non-fluorescent and fluorescent α-D- mannopyranoside derivatives for methodology I.....	37
2.3.1	Chemical synthesis of non-fluorescent azidocoumarinyl α -D-mannopyranoside derivatives	37

2.3.2	Chemical synthesis of fluorescent coumarinyl α -D-mannopyranoside derivative under strain-promoted click conditions	38
2.4	Chemical synthesis of non-fluorescent and fluorescent α-D-mannopyranoside derivatives for methodology II	39
2.4.1	Chemical synthesis of non-fluorescent 5-hexynyl α -D-mannopyranoside derivatives	39
2.4.2	Chemical synthesis of fluorescent coumarinyl α -D-mannopyranoside derivatives under Cu(I)-catalysed click conditions.....	40
2.5	Spectroscopic studies of fluorescent coumarinyl α-D-mannopyranoside derivatives.....	42
2.6	Examination of detection limits of fluorescently labelled coumarinyl α-D-mannopyranoside derivatives	46
2.6.1	TLC analyses.....	46
2.6.2	Solution analyses.....	47
2.7	Validation of fluorescence-based methodologies against established radiolabelled assay	49
2.7.1	Insight into studying biosynthesis of glycoconjugates in mycobacteria.....	49
2.7.2	Literature radiolabelled assay to probe α -1,6-mannosyltransferase activities responsible for the biosynthesis of LAM in mycobacterial species	50
2.7.3	Fluorescence-based methodologies to probe α -1,6-mannosyltransferase activities in <i>Mycobacterium smegmatis</i>	52
2.7.4	TLC results from the fluorescence-based methodology I	53
2.7.5	TLC results from the fluorescence-based methodology II.....	54
2.7.6	Identification of fluorescent products by LC-MS	56
2.7.7	Linkage analysis through <i>exo</i> -mannosidase digestions.....	58
2.7.8	Summary of fluorescence-based methodologies in <i>Mycobacterium smegmatis</i>	59
2.8	Validation of fluorescence-based methodology II against established radiolabelled assay	60
2.8.1	Insight into studying biosynthesis of glycoconjugates in <i>Trypanosoma brucei</i>	60

2.8.2	Literature radiolabelled assay to probe galactosyltransferase activities responsible for decoration of GPI anchors in <i>Trypanosoma brucei</i>	61
2.8.3	Fluorescence-based methodology II to probe galactosyltransferase activities responsible for α -galactosylation of GPI anchors in <i>Trypanosoma brucei</i>	64
2.8.4	Identification of fluorescent product by LC-MS	68
2.8.5	Linkage analysis through <i>exo</i> -galactosidase digestions	68
2.8.6	Investigation of number of isomeric structures by IM-MS	70
2.8.7	Summary of fluorescence-based methodology II in <i>Trypanosoma brucei</i>	71
2.9	Conclusion and future work	72
3	THE QUEST FOR GLYCOSYLTRANSFERASE ACTIVITIES IN <i>EUGLENA GRACILIS</i>	76
3.1	Insight into <i>Euglena</i>	77
3.2	Fluorescence-based methodology II to probe mannosyltransferase activities in <i>Euglena gracilis</i>	79
3.2.1	Microsomal membranes as a source of glycosyltransferases	80
3.2.2	Fluorescence assays to probe mannosyltransferase activities	81
3.2.3	Purification of fluorescent products by HPLC	82
3.2.4	Identification of fluorescent products by LC-MS	84
3.2.5	Linkage analysis through <i>exo</i> -mannosidase digestions	85
3.2.6	Confirmation of newly formed linkages in fluorescent mannoside products by LC-MS	88
3.2.7	Investigation of number and nature of isomeric structures in fluorescent products by IM-MS	90
3.2.8	Summary of fluorescence-based methodology II used to investigate mannosyltransferase activities in <i>Euglena gracilis</i>	91
3.3	Exploration of other glycosyltransferases in <i>Euglena gracilis</i>	94
3.3.1	Fluorescence assays to probe glycosyltransferase activities	95
3.3.2	Purification of fluorescent products by HPLC	99

3.3.3	IM-MS analyses on number of isomeric structures present in trisaccharide fluorescent product obtained from UDP-Glc incubation	100
3.3.4	Identification of fluorescent products obtained from incubation of UDP-Glc by LC-MS	101
3.3.5	Identification of fluorescent products obtained from incubation with UDP-GlcNAc by LC-MS	104
3.3.6	Investigation of newly formed linkages in fluorescent products through enzymatic and chemical degradations	106
3.3.7	Characterisation and confirmation of fluorescent product by NMR spectroscopy.....	108
3.3.8	Summary of fluorescence-based methodology II used to investigate glycosyltransferase activities in <i>Euglena gracilis</i>	111
3.4	Conclusion and future work	114
4	SYNTHESIS OF TRIAZOLE-LINKED LINEAR AND CYCLIC OLIGOMERS TO OBSTRUCT <i>TRYPANOSOMA CRUZI</i> MACROPHAGE INFECTION.....	120
4.1	Introduction.....	121
4.2	Synthesis of azido-alkyne galactose-containing monomer	126
4.3	Cyclisation and oligomerisation through CuAAC reactions based on azido-alkyne-containing galactose monomer	127
4.4	Fluorescent labelling of 1,4-triazole linked linear oligomers	133
4.5	Uncatalysed 1,3-dipolar cycloaddition of azido-alkyne-containing galactose monomer	135
4.6	Cyclic triazole-linked oligomers as acceptor substrates for <i>Trypanosoma cruzi</i> trans-sialidase (TcTS)	137
4.7	Preliminary biological evaluation of triazole-linked oligomers.....	139
4.8	Conclusion and future work	141
5	MATERIALS AND METHODS.....	143

5.1	Chemical methods	144
5.1.1	General experimental section	144
5.2	Chemical synthesis of non-fluorescent and fluorescent α-D-mannopyranoside derivatives to utilise in fluorescence-based methodology I.....	148
5.2.1	Chemical synthesis of non-fluorescent azidocoumarinyl α -D-mannopyranoside derivatives	148
5.2.2	Chemical synthesis of fluorescent coumarinyl α -D-mannopyranoside derivative under strain-promoted click condition	152
5.3	Chemical synthesis of non-fluorescent and fluorescent α-D-mannopyranoside derivatives to utilise in fluorescence-based methodology II....	154
5.3.1	Chemical synthesis of non-fluorescent 5-hexynyl α -D-mannopyranoside derivatives	154
5.3.2	Chemical synthesis of fluorescent coumarinyl α -D-mannopyranoside derivatives under Cu(I)-catalysed click conditions.....	158
5.4	Chemical synthesis of azido-alkyne galactose-containing monomer.....	161
5.5	Cu(I)-catalysed oligomerisation of azido-alkyne galactose-containing monomer	164
5.5.1	General procedure for catalysed cyclisation and oligomerisation	164
5.6	Uncatalysed oligomerisation of azido-alkyne galactose-containing monomer	167
5.6.1	General procedure for uncatalysed cyclisation and oligomerisation	167
5.7	Biological methods	168
5.7.1	General experimental section	168
5.8	<i>Mycobacterium smegmatis</i>	172
5.8.1	Fluorescence-based assays to probe mannosyltransferase activities in <i>Mycobacterium smegmatis</i>	172
5.9	<i>Trypanosoma brucei</i>	173

5.9.1	Fluorescence-based assays to probe galactosyltransferase activities in <i>Trypanosoma brucei</i>	173
5.10	<i>Euglena gracilis</i>	174
5.10.1	Preparation of <i>Euglena gracilis</i> cells	174
5.10.2	Isolation of microsomal membranes from <i>Euglena gracilis</i> ¹⁶¹	175
5.10.3	Fluorescence-based assays to probe glycosyltransferase activities in <i>Euglena gracilis</i>	175
5.10.4	Generation of product carrying <i>N</i> -acetylglucosamine-6-Phosphate motif for structural characterisation	176
5.11	<i>Trypanosoma cruzi</i>.....	177
5.11.1	<i>Trans</i> -sialidase-mediated sialylation of triazole-linked <i>pseudo</i> -galactooligomers	177
5.11.2	Macrophage invasion assays	177
6	APPENDICES.....	179
7	REFERENCES	187

List of Figures

Figure 1.1 Structural variations of GPI anchors in protozoan, yeast and mammalian systems.	3
Figure 1.2 Diagrammatic schemes of GPI anchor biosynthesis in <i>Trypanosoma brucei</i>	5
Figure 1.3 Representative examples of the main components of the mycobacterial cell surface; structural similarities and differences between LAM in <i>Mycobacterium tuberculosis</i> and <i>Mycobacterium smegmatis</i>	6
Figure 1.4 Diagrammatic scheme of LAM biosynthesis in non-pathogenic <i>Mycobacterium smegmatis</i>	7
Figure 1.5 Representative biosynthetic pathway of <i>N</i> -linked glycosylation at the ER membrane in eukaryotic cells.	9
Figure 1.6 Structural variations of lipid-linked <i>N</i> -glycan precursors in eukaryotic system.	10
Figure 1.7 Processing and maturation of oligosaccharide moiety of the <i>N</i> -linked glycoprotein at the ER and Golgi apparatus membranes.	11
Figure 1.8 Structural variants of <i>N</i> -linked glycoproteins.	12
Figure 1.9 Diagrammatic representation of <i>N</i> -linked glycoprotein phosphorylation. ...	13
Figure 1.10 Diagrammatic representation of phosphorylation of a newly synthesised <i>N</i> -linked lysosomal glycoprotein and its subsequent transfer to the lysosome.	14
Figure 1.11 Structural variation of the mucin type <i>O</i> -glycans.	16
Figure 1.12 Diagrammatic representation of scintillation proximity assay utilising radiolabelled donor and impregnated bead to detect α -1,3-fucosyltransferase activity.	21
Figure 1.13 Chemical structures of widely used fluorophores.	22
Figure 1.14 Schematic representation of fluorescence-based ligand-displacement assay for inhibitory screening.	23
Figure 1.15 Chemical structures of selected fluorescently-labelled sugar nucleotides and acceptor substrates used in the literature GT assays.	24

Figure 1.16 Representative example of enzymatic reactions of fluorescent GM1 and lactose acceptor substrates and their products derived from the glycolipid metabolism detected by CE-LIF.....	26
Figure 2.1 General outline of fluorescence-based methodology to detect enzymatic activities of membrane-bound glycosyltransferases.	30
Figure 2.2 Schematic representation of structures of glycoconjugates from <i>Trypanosoma brucei</i> and <i>Mycobacterium smegmatis</i> and synthetic fluorescent and non-fluorescent glycoside acceptors to be used in detection of glycosyltransferase activities.	34
Figure 2.3 Authentic and synthetic acceptor substrate analogues of D-GlcN α -1,6-D- <i>myo</i> -inositol-1-PO ₄ - <i>sn</i> -1,2-diacylglycerol utilised in the literature research.	35
Figure 2.4 Structures of non-fluorescent and fluorescent acceptor substrates designed to be used in methodology I and II to probe activities of membrane-bound glycosyltransferases.	36
Figure 2.5 Coumarin-derived fluorophores with the highest quantum yield described in the literature.	43
Figure 2.6 Structural differences of fluorescently labelled coumarinyl α -D-mannopyranoside derivatives can affect their photophysical properties.	43
Figure 2.7 Fluorescent properties of coumarinyl α -D-mannopyranoside derivatives. .	44
Figure 2.8 The effect in change of pH level on the fluorescent properties of coumarinyl α -D-mannopyranoside derivatives.	45
Figure 2.9 Comparison of TLC detection range of fluorescently labelled coumarinyl α -D-mannopyranoside derivatives.	47
Figure 2.10 The detection range of fluorescently labelled coumarinyl α -D-mannopyranoside derivatives in solution.	47
Figure 2.11 Diagrammatic representation of lipoarabinomannan biosynthesis in <i>Mycobacterium smegmatis</i>	50
Figure 2.12 Structure of acceptor substrates used in the literature cell-free radiolabelled assays.	51
Figure 2.13 Structures of non-fluorescent and fluorescent compounds used to benchmark fluorescence-based methodology I and II against literature radiolabelled assay.	52

Figure 2.14 TLC analyses of enzymatic assays of non-fluorescent and fluorescent mannoside acceptors to detect mannosyltransferase activities in <i>Mycobacterium smegmatis</i> membranes using fluorescence-based methodology I.	54
Figure 2.15 TLC analyses of enzymatic assays of non-fluorescent and fluorescent mannoside acceptors to detect mannosyltransferase activities in <i>Mycobacterium smegmatis</i> microsomal membranes using fluorescence-based methodology II.	55
Figure 2.16 LC-MS analyses of reaction mixtures obtained from incubation of non-fluorescent and fluorescent acceptors with GDP-Man in the presence of <i>Mycobacterium smegmatis</i> microsomal membranes.	57
Figure 2.17 TLC analyses of <i>exo</i> -mannosidase digestions of fluorescent mannoside products with <i>exo</i> -mannosidase.	59
Figure 2.18 Schematic representation of α -1,6-mannosyltransferase reaction with non-fluorescent and fluorescent acceptor substrates using fluorescence-based methodology II.	60
Figure 2.19 Diagrammatic representation of GPI anchor biosynthesis in <i>Trypanosoma brucei</i>	62
Figure 2.20 Structures of acceptor substrates used in the literature cell-free radiolabelled assays.	63
Figure 2.21 Structures of non-fluorescent and fluorescent compounds used to benchmark fluorescence-based methodology II against radiolabelled literature assay.	65
Figure 2.22 TLC analyses of enzymatic assays of non-fluorescent and fluorescent acceptors used in detection of galactosyltransferase activities in <i>Trypanosoma brucei</i> membranes utilising fluorescent methodology II.	66
Figure 2.23 TLC analyses of enzymatic assays of fluorescent mannoside acceptor to improve galactosyltransferase activities in <i>Trypanosoma brucei</i> microsomal membranes utilising fluorescent methodology II.	67
Figure 2.24 UPLC analyses of reaction mixture obtained from incubation of fluorescent acceptor with UDP-Gal in the presence of <i>Trypanosoma brucei</i> microsomal membranes.	68
Figure 2.25 Analyses of <i>exo</i> -glycosidase digestion of fluorescent products with α -galactosidase from green coffee beans and β -galactosidase from <i>Escherichia coli</i> . (A) The TLC plate after <i>exo</i> -galactosidase digestion.	69

Figure 2.26 Ion mobility spectrum to represent isomeric structures present in trisaccharide fluorescent products obtained from incubation of UDP-Gal with <i>Trypanosoma brucei</i> membranes.	70
Figure 2.27 Diagrammatic representation of fluorescent acceptor mimicked sites on the GPI anchor and resulted fluorescent products.	71
Figure 2.28 Structural comparison between acceptors used in the literature radiolabelled assays and in the fluorescence-based methodology.....	74
Figure 3.1 The <i>Euglena gracilis</i> cell.	77
Figure 3.2 Diagrammatic representation of conserved <i>N</i> -glycan and GPI anchor biosynthesis to illustrate limited information available on glycosyltransferases present in <i>Euglena gracilis</i>	79
Figure 3.3 Schematic and chemical structures of fluorescent acceptors used in fluorescence-based methodology II to probe mannosyltransferases activities in <i>Euglena gracilis</i> microsomal membranes.	80
Figure 3.4 TLC analyses of fluorescence-based assays to assess mannosyltransferase activities in <i>Euglena gracilis</i> microsomal membranes.	81
Figure 3.5 HPLC analyses of reaction mixtures obtained from incubation of fluorescent acceptors with GDP-Man in the presence of <i>Euglena gracilis</i> microsomal membranes.	83
Figure 3.6 Structural identification of fluorescent products obtained from enzymatic reactions with GDP-Man and <i>Euglena gracilis</i> microsomal membranes by LC-MS.	84
Figure 3.7 TLC analyses to assess stereoselectivity and regioselectivity of disaccharide fluorescent products by <i>exo</i> -glycosidase digestions.	86
Figure 3.8 TLC analyses to assess stereoselectivity and regioselectivity of trisaccharide fluorescent products by <i>exo</i> -glycosidase digestions.	87
Figure 3.9 Formation of two fluorescent disaccharide isomeric compounds confirmed by LC-MS analysis.	88
Figure 3.10 Presence of one fluorescent trisaccharide compound confirmed by LC-MS analysis.	89
Figure 3.11 Drift time IM-MS spectra to represent number and nature of isomeric structures present in fluorescent mannoside products obtained from incubation with GDP-Man and <i>Euglena gracilis</i> microsomal membranes.	91

- Figure 3.12** Schematic enzymatic reaction of monosaccharide acceptor and structural relationship between its disaccharide products and authentic *N*-glycan and GPI anchor intermediates. 92
- Figure 3.13** Schematic enzymatic reaction of disaccharide acceptor and structural relationship between its disaccharide products and authentic *N*-glycan and GPI anchor intermediates. 93
- Figure 3.14** Structural variations of *N*-linked glycoproteins in plants, mammalian and yeast systems..... 94
- Figure 3.15** Structures of fluorescent acceptors used in fluorescence-based methodology II to probe mannosyltransferases activities present in *Euglena gracilis* microsomal membranes. 96
- Figure 3.16** TLC analyses of enzymatic assays involving incubation of monosaccharide fluorescent acceptor substrate with number of sugar nucleotides in the presence of *Euglena gracilis* microsomal membranes. 97
- Figure 3.17** TLC analyses of enzymatic assays involving incubation of disaccharide fluorescent acceptor substrate with number of sugar nucleotides in the presence of *Euglena gracilis* microsomal membranes. 98
- Figure 3.18** HPLC analyses of reaction mixtures obtained from incubation of fluorescent acceptors with UDP-Glc and UDP-GlcNAc in the presence of *Euglena gracilis* microsomal membranes. 99
- Figure 3.19** . UPLC and ion mobility analyses of isomeric structures present in glucosylated product obtained from incubation of UDP-Glc with *Euglena gracilis* microsomal membranes. 101
- Figure 3.20** LC-MS analyses to investigate the nature of glucosylated products obtained from enzymatic biotransformation with UDP-Glc in the presence of *Euglena gracilis* microsomal membranes. 102
- Figure 3.21** LC-MS analyses to investigate the structure of fluorescent products obtained from enzymatic biotransformation with UDP-Glc in the presence of *Euglena gracilis* microsomal membranes. 103
- Figure 3.22** LC-MS analyses to investigate the nature of fluorescent products obtained from enzymatic biotransformation with UDP-GlcNAc in the presence of *Euglena gracilis* microsomal membranes. 105
- Figure 3.23** TLC analyses to investigate presence of terminal phosphate in fluorescent products through application of enzymatic hydrolysis with alkaline phosphatase. 106

- Figure 3.24** Diagrammatic representation of sequential chemical and enzymatic degradation of fluorescent trisaccharide and tetrasaccharide products containing phosphodiester bond. 107
- Figure 3.25** TLC analyses to investigate the presence of phosphodiester bond in fluorescent products through application of chemical degradation and enzymatic hydrolysis. 108
- Figure 3.26** Characterisation of fluorescent phosphodiester-linked product by the NMR spectroscopy. 109
- Figure 3.27** Characterisation of fluorescent phosphodiester-linked product by the NMR spectroscopy. 110
- Figure 3.28** Proposed structure and assignment of fluorescent phosphodiester-linked compound for NMR analysis. 111
- Figure 3.29** Schematic representation of enzymatic activities detected in *Euglena gracilis* microsomal membranes. 112
- Figure 3.30** Diagrammatic representation of mimicked *N*-glycan sites by synthetic fluorescent acceptors and their resulting products in *Euglena gracilis*. 114
- Figure 3.31** Chemical structures of authentic fluorescent acceptors to aid with detection of mannosyltransferase activities in *Euglena gracilis* microsomal membranes. 116
- Figure 4.1** Diagrammatic representation of *Trypanosoma cruzi* invasion and differentiation inside the vector and mammalian host cells. 122
- Figure 4.2** Representative transfer of sialic acid from the host glycoconjugate to the parasite cell surface mucin glycoprotein catalysed by *Trypanosoma cruzi* trans-sialidase. 123
- Figure 4.3** Representative examples of potent and moderate TcTs inhibitors. 124
- Figure 4.4** Schematic representation of cyclooligomerisation approach to the synthesis of cyclic *pseudo*-oligosaccharides. 125
- Figure 4.5** Schematic representation of cell surface-presented *Trypanosoma cruzi* trans-sialidase and potential for its blocking by 1,2,3-triazole-linked linear and cyclic *pseudo*-galactooligomers resulting in potential prevention of host cells invasion. 126
- Figure 4.6** Reverse phase HPLC and normal phase TLC analyses of cyclic and linear products obtained from azido-alkyne 1,3-dipolar cycloaddition reactions of galactose monomer. 128

- Figure 4.7** Linear oligomerisation products from the reaction of azido-alkyne-containing galactose under CuAAC conditions. 130
- Figure 4.8** Characterisation of cyclic and linear 1,4-triazole-linked galactose dimers by NMR spectroscopy. 132
- Figure 4.9** Normal phase TLC image and reverse phase HPLC chromatogram of fluorescently labelled 1,4-triazol-linked linear compounds obtained from azido-alkyne 1,3-dipolar cycloaddition reactions of mixed 1,4-triazole-linked linear compounds in the presence of 3-azido-7-hydroxy-coumarin. 133
- Figure 4.10** Fluorescent linear oligomerisation products from the reaction of azido-alkyne-containing galactose under CuAAC conditions. 134
- Figure 4.11** Reverse phase HPLC and normal phase TLC analyses of cyclic and linear products obtained from azido-alkyne 1,3-dipolar cycloaddition reactions of galactose monomer. 136
- Figure 4.12** TLC analyses of enzymatic transformations of 1,4-triazole-linked cyclic monomer **4.08**, 1,5-triazole-linked cyclic monomer **4.26**, 1,4-triazole-linked cyclic dimer **4.09** and 1,4 triazole-linked cyclic trimer **4.10** into mono-, di- and tri-sialylated cyclic compounds in the presence of TcTS and a fetuin donor. 138
- Figure 4.13** Inhibition of *T. cruzi* invasion of bovine macrophages in the presence of 1,4/1,5-triazole-linked cyclic dimers (**C2**), trimer (**C3**), tetramer (**C4**), pentamer (**C5**), hexamer (**C6**), heptamer (**C7**) and a series of mixed 1,4/1,5-triazole-linked linear oligomers. 140
- Figure 4.14** Representative images illustrating amastigote-form parasite numbers present inside macrophages infected with *T. cruzi*. 141
- Figure 6.1** LC-MS data of peak 1 of fluorescent disaccharide (**3.03**) product obtained from incubation of monosaccharide acceptor substrate with UDP-Glc in the presence of *Euglena gracilis* microsomal membranes..... 179
- Figure 6.2** LC-MS data of peak two of fluorescent disaccharide (**3.03**) product obtained from incubation of monosaccharide acceptor substrate with UDP-Glc in the presence of *Euglena gracilis* microsomal membranes..... 180
- Figure 6.4** The ^1H NMR spectra of fluorescent phosphodiester-linked product. 182
- Figure 6.5** The ^{31}P NMR spectra of fluorescent phosphodiester-linked product..... 182
- Figure 6.6** The HRMS spectrum of the series of 1,4-triazole-linked linear products obtained from CuAAC oligomerisation of galactose monomer. 186

List of Tables

Table 2.1 Outline schemes of fluorescence-based methodologies for pre- and post-enzymatic transformation labelling in detecting enzymatic activities of membrane-bound glycosyltransferases.	33
Table 2.2 Photophysical properties of fluorescently labelled coumarinyl α -D-mannopyranoside derivatives.	44
Table 3.1 Percentage conversion of fluorescent products obtained from enzymatic reactions with <i>Euglena gracilis</i> microsomal membranes.	83
Table 3.2 Percentage conversion of fluorescent products obtained from enzymatic reactions with UDP-Glc and UDP-GlcNAc in the presence of <i>Euglena gracilis</i> microsomal membranes.	100
Table 3.3 <i>Euglena gracilis</i> percent identity of mannosyltransferase to known protein sequences from other organisms.	115
Table 4.1 Yields of 1,4-triazole-linked cyclic and linear products from CuAAC reactions of galactose monomer.	129
Table 4.2 HRMS data of 1,4-triazole-linked cyclic products and linear oligomers.....	130
Table 4.3 HRMS data of fluorescent 1,4-triazole-linked linear products.	134
Table 4.4 MALDI-TOF data of 1,4- and 1,5-triazole-linked cyclic oligomers.	136
Table 4.5 HRMS data for products of enzymatic sialylation of triazole-linked cyclic oligomers.	138
Table 5.1 Solvents mixtures used for TLC elution.	168
Table 6.1 MS and MS2 data from LC-MS analysis of glucosylated fluorescent products obtained from 2.12 and 2.13	181
Table 6.2 MS and MS2 data from LS-MS analysis of products obtained from 2.12 with UDP-Glc.	181
Table 6.3 MS and MS2 data from LS-MS analysis of products obtained from 2.13 with UDP-GlcNAc.	181
Table 6.4 <i>Euglena gracilis</i> percent identity, similarity and gaps of <i>EgAlg3</i> to known protein sequences.	183

Table 6.5 *Euglena gracilis* percent identity, similarity and gaps of *EgAlg9* to known protein sequences. 184

Table 6.6 *Euglena gracilis* percent identity, similarity and gaps of GlcNAc-P-Tase to known protein sequences. 186

List of Schemes

Scheme 1.1 Mechanisms for inverting and retaining glycosyltransferases.	19
Scheme 2.1 Azido coumarin-based fluorophore becomes fluorescent upon reaction with strain or terminal alkyne to form a triazole ring under click conditions.	31
Scheme 2.2 Synthetic route to 2-(3-azido-coumarin-7-yloxy)ethyl α -D-mannopyranoside.	38
Scheme 2.3 Synthetic route to fluorescent coumarinyl α -D-mannopyranoside derivative through strain-promoted click conditions.	39
Scheme 2.4 Synthetic route to hexyn-5-yl α -D-mannopyranoside and hexyn-5-yl α -D-mannopyranosyl-1,6- <i>O</i> - α -D-mannopyranoside.	40
Scheme 2.5 Synthetic routes to fluorescent coumarinyl α -D-mannopyranoside derivatives through Cu(I)-catalysed click conditions.	41
Scheme 2.6 Reaction schemes of azido-alkyne compounds leading to formation of 5,5-bistriazole by-products under Cu(I)-catalysed click conditions as described in the literature.	42
Scheme 2.7 Enzymatic transformations of synthetic acceptor substrate by galactosyltransferases responsible for branching of GPI anchors as detected by literature radiolabelled assay.	64
Scheme 4.1 Synthetic route to azido-alkyne-containing galactose monomer.	127
Scheme 4.2 Cyclisation and oligomerisation of azido-alkyne-containing galactose through CuAAC.	129
Scheme 4.3 Spontaneous cyclisation and oligomerisation of azido-alkyne-containing galactose leading to a mixture of compounds incorporating both 1,4-linked and 1,5-linked 1,2,3-triazole residues.	135
Scheme 4.4 Structures of proposed sialylated products obtained from enzymatic transformation of compound 4.10	139

Abbreviations

[α] _D	optical rotation
°C	degree Celsius
Å	Ångstrom
Ac	acyl
AcOH	acetic acid
AG	arabinogalactan
AgOTf	silver triflate
AGP	arabinogalactan protein
Alg	asparagine-linked glycosyltransferases
AP	alkaline phosphatase
APTS	8-aminopyrene-1,3,6-trisulfonic acid
aq	aqueous
Ar	aromatic
Asn	asparagine
<i>At</i>	<i>Arabidopsis thaliana</i>
ATP	adenosine triphosphate
b.p.	boiling point
BMMO	macrophages derived from bone marrow
BODIPY	4,4-difluoro-4-bora-3a,4a-diaza-s-indacene
BP	by-product
BSA	bovine serum albumin
BzCl	benzoyl chloride
<i>c</i>	concentration
CAD	corona charged aerosol detector
CDGS	carbohydrate deficiency glycoprotein syndrome
CE-LIF	capillary electrophoresis-laser induced fluorescence
CH ₂ Cl ₂	dichloromethane
CH ₃ CN	acetonitrile
CHCl ₃	chloroform
COSY	correlation spectroscopy
CuAAC	Cu(I)-catalysed azido-alkyne cycloaddition
d	doublet
DBU	1,8-diazabicyclo[5.4.0]undec-7-ene
dd	doublet of doublets
DMAP	4-dimethylaminopyridine
DMF	<i>N,N</i> -dimethylformamide
Dol-PP	dolichylpyrophosphate
DP	degradation product
DTT	dithiothreitol
Em _{max}	emission maximum
ER	endoplasmic reticulum
ESI	electro spray ionisation
Et ₃ N	triethylamine

EtNPO ₄	phosphoethanolamine
EtOAc	ethyl acetate
EtOH	ethanol
Ex _{max}	excitation maximum
FRET	Förster (fluorescence) resonance energy transfer
FTIR	Fourier transform infrared
Fuc	L-fucose
FucT	fucosyltransferase
Gal	D-galactose
Gal ^f	D-galactofuranose
GalNAc	<i>N</i> -acetyl-D-galactosamine
GalNAcT	<i>N</i> -acetylgalactosaminyltransferase
Gal _p	D-galactopyranose
GalT	galactosyltransferase
GalT	galactosyltransferase
GlcNAc	<i>N</i> -acetyl-D-glucosamine
GC-MS	gas chromatography–mass spectrometry
GDP	guanosine diphosphate
Glc	D-glucose
GlcA	D-glucuronic acid
GlcN	D-glucosamine
GlcNAc-PI	<i>N</i> -acetylglucosamine-phosphatidyl-myo-inositol
GlcNAc-P-Tase	<i>N</i> -acetylglucosamine-1-phosphate transferase
GlcNAcT	<i>N</i> -acetylglucosaminyltransferase
GlcT	glucosyltransferase
GPC	gel permeation chromatography
GPI anchor	glycosylphosphatidylinositol anchor
GPI-T	glycosylphosphatidylinositol transamidase
GT	glycosyltransferase
H BP	hydrolysed by-product
HEPES	4-(2-hydroxyethyl)-1-piperazineethanesulfonic acid
HMBC	heteronuclear multiple bond correlation
HPLC	high performance liquid chromatography
HPTLC	high performance thin layer chromatography
HRMS	high resolution mass spectrometry
HSQC	heteronuclear single quantum coherence
HTS	high throughput screening
Hyp	hydroxyproline
Hz	Hertz
IM-MS	ion-mobility–mass spectrometry
iPrOH	isopropanol
IR	infrared
<i>J</i>	coupling constant
K	Kelvin
kDa	kiloDalton
KO ^t Bu	Potassium t-butoxide

kV	kiloVolts
LAM	lipoarabinomannan
LC	liquid chromatography
LC-MS	liquid chromatography–mass spectrometry
LDA	lithium diisopropylamide
LM	lipomannan
m	multiplet
<i>m/z</i>	mass to charge ratio
M6P	mannose-6-phosphate
MALDI-TOF	matrix-assisted laser desorption ionization time of flight
Man	D-mannose
ManH	mannosidase
ManT	mannosyltransferase
MeOH	methanol
MHz	megaHertz
MOPS	3-(<i>N</i> -morpholino)propanesulfonic acid
MPR	mannose-6-phosphate receptor
ms	milliseconds
mU	milliunit
N	normal
NaAsc	sodium ascorbate
NaOMe	sodium methoxide
OT	oligosaccharyl transferase
PI	phosphatidyl- <i>myo</i> -inositol
PIM	phosphatidyl- <i>myo</i> -inositol mannoside
<i>pK_a</i>	acid dissociation constant
ppGlcNAcT	UDP-GlcNAc:polypeptide N-acetylglucosaminyltransferase
ppm	parts per million
Py	pyridine
r.p.m	rotation per minute
Rf	retention factor
Rha	L-rhamnose
RP	reverse phase
Sia	<i>N</i> -acetyl-neuraminic acid
TB	tuberculosis
TcTS	<i>Trypanosoma cruzi</i> <i>trans</i> -sialidase
<i>t_D</i>	drift time
TFA	trifluoroacetic acid
THF	tetrahydrofuran
TLC	thin layer chromatography
TMS	tetramethylsilane
TMSOTf	trimethylsilyl trifluoromethanesulfonate
TrCl	trityl chloride
Tris	tris(hydroxymethyl)aminomethane
U	unit
UDP	uridine diphosphate

UPLC	ultra performance liquid chromatography
UV	ultraviolet
VSG	variant surface glycoprotein
Xyl	D-xylose
δ	chemical shift
ε	extinction coefficient
λ_{em}	emission wavelength
λ_{ex}	excitation wavelength
ϕ_f	quantum yield

1 Introduction

1.1 Essentials of glycoconjugates

Glycoconjugates are vital components of prokaryotic and eukaryotic cell surface. They consist of a variety of complex carbohydrate structures that are covalently linked to non-sugar moieties, such as proteins, peptides, and lipids. The carbohydrate moiety of the glycoconjugate can incorporate a variety of monosaccharides, which can be arranged through different linkages, chain length and branching points, and can have different sequences and covalent attachment of terminal modifying groups.^{1,2} Due to these complexities and variability of the terminal carbohydrate sequences, glycoconjugates can participate in a variety of biological functions. In bacteria and parasites, glycoconjugates are constituents of the cell wall where they play an important role in protection against the immune system of the host, and aid with infectivity inside the vector and host organisms.^{3,4} In animals and plants, glycoconjugates that occupy the intercellular spaces determine the cell adhesion and involved in signal transduction,⁵ cell-cell or bacterial-host interactions^{6,7} as well as cell development and fertility.^{8,9} However, the central function of glycosylation is the involvement of carbohydrate moiety in correct folding of polypeptides¹⁰ and consequent maintenance of protein solubility as well as protection against the proteases inside the cell.^{11,12}

The assembly of these complex structures takes place in the endoplasmic reticulum (ER) and Golgi apparatus where a series of specific membrane-bound glycosyltransferases transfer sugar moieties from soluble sugar nucleotides or lipid linked activated sugars to variety of oligosaccharide, lipid or peptide acceptors with the correct stereo- and regio-selectivity. The structures and biosynthesis of glycoconjugates have been extensively studied using radiolabelled methodologies; however, we are still far from the characterising and understanding construction of most glycoconjugates.

1.2 The structures and biosynthesis of glycoconjugates of interest

In this study, we looked at the detection of membrane-bound glycosyltransferase activities involved in the biosynthesis of GPI anchor in *Trypanosoma brucei*, lipoarabinomannan in *Mycobacterium smegmatis* and N-linked glycoproteins in *Euglena gracilis*. We also looked at the mimetic of O-linked glycoproteins in

Trypanosoma cruzi. Therefore, a description on what is known about these glycoconjugate structures and their biosynthesis is described below.

1.2.1 Glycosylphosphatidylinositol anchors

Glycosylphosphatidylinositol (GPI) anchors are present in all eukaryotic cells and are widely distributed in protozoa, plants, yeast, fungi, insects and mammals (Fig. 1.10).¹³ Their main function is the attachment and transport of proteins, glycoproteins and glycolipids to the plasma membrane.¹⁴ GPI anchored components can then play a vital role in a variety of biological functions, for example in immune responses, signal transduction and cancer cell invasion, as well as pathophysiology of the parasites.^{3, 15} The importance of GPI anchored proteins during mouse embryonic developmental stages was apparent from lethality in GPI deficient mice.¹⁶

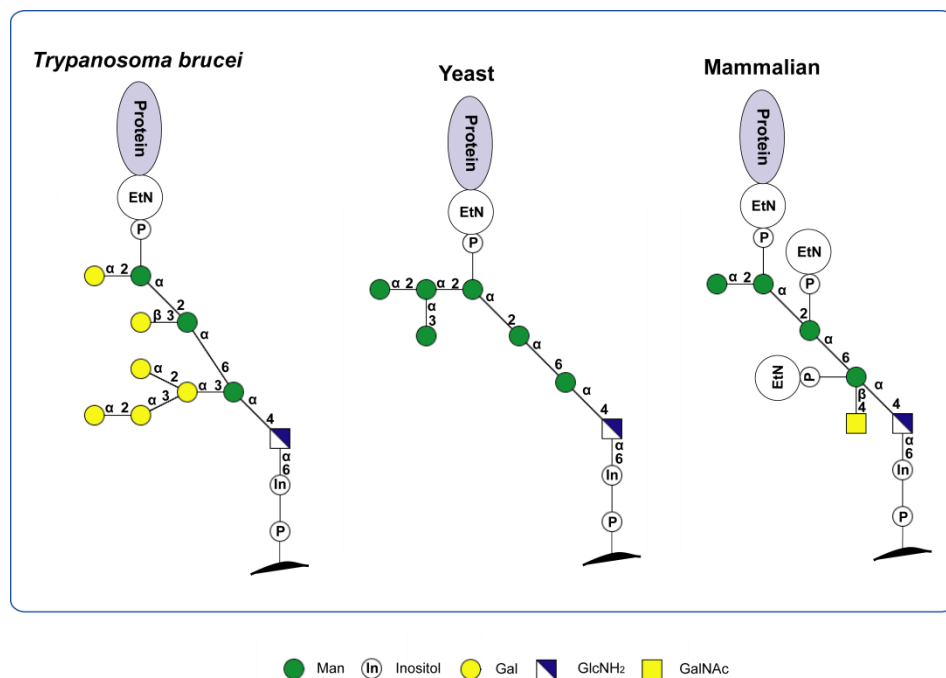


Figure 1.1 Structural variations of GPI anchors in protozoan, yeast and mammalian systems.

The core structure of GPI anchors, EtNPO₄-6-Man-α-1,2-Man-α-1,6-Man-α-1,4-GlcN-α-1,6-*myo*-inositol-P-lipid, is conserved throughout all eukaryotic cells and the structural complexity originates from variations on either side-chains or/and the lipid moieties (Fig 1.1). The side chain modifications include decoration of conserved core structure with galactose residues in *Trypanosoma brucei*, addition of a fourth mannose branching in yeast and additional phosphoethanolamine residues added to the first and

second mannose in mammals.¹⁷ The functional significance of these side modifications is largely unknown; although, the addition of galactose residues in *Trypanosoma brucei* was assigned as a requirement to fill the space between proteins in order to preserve their distribution and functional integrity.¹⁸

The intact GPI precursors were first identified in *Trypanosoma brucei* and were used to develop a first cell-free system to assist in delineating the biosynthetic pathway for GPI biosynthesis.¹⁹ This method was then successfully adopted to define biosynthetic pathways in yeast²⁰ and mammalian cells.²¹ The biosynthesis of core GPI anchors begins on the cytoplasmic side of the ER with the transfer of GlcNAc residue from UDP-GlcNAc to a phosphatidyl-*myo*-inositol (PI) precursor to give GlcNAc-PI (Fig. 1.2). The resulting GlcNAc-PI precursor is then deacetylated to form glucosamine (GlcN)-PI, which is flipped through the lipid bilayer to the luminal side of the ER. The biosynthesis of GPI precursor proceeds on the luminal side of the ER by addition of three mannose residues from lipid-activated sugars (Dol-PP-Man) to GlcN-PI mediated by α -1,4-ManT (MT-I), α -1,6-ManT (MT-II) and α -1,2-ManT (MT-III) to generate Man₃-GlcN-PI. The significant difference between mammalian and *Trypanosoma brucei* biosynthesis at this point is the relative order of acylation of inositol and mannosylation. In mammalian systems the attachment of acyl group to the inositol of the GlcN-PI precursor is followed by mannosylation while in *Trypanosoma brucei* mannosylation of GlcN-PI precedes the acylation of inositol. Furthermore, in mammalian systems one ethanolamine phosphate (EtNP) is added to the first mannose residue of core GPI precursor, while it is absent in *Trypanosoma brucei*. These apparent differences in the substrate specificities (GlcN-PI vs GlcN-(acyl)-PI in MT-I and Man₂-GlcN-PI vs EtNP-Man₂-GlcN-(acyl)-PI in MT-III) made these enzymes attractive targets to design inhibitors of GPI anchor biosynthesis in *Trypanosoma brucei*.^{22, 23}

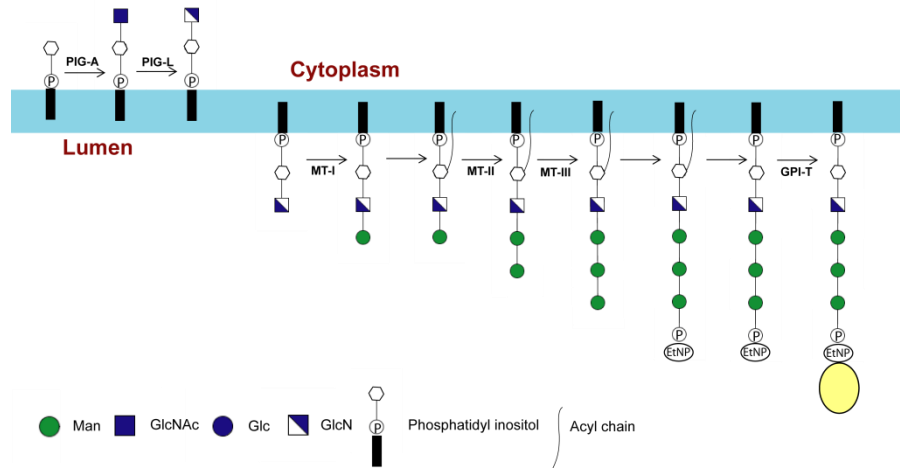


Figure 1.2 Diagrammatic schemes of GPI anchor biosynthesis in *Trypanosoma brucei*. The biosynthesis initiates with transfer of GlcNAc to PI followed by deacetylation of GlcNAc and transfer of GlcN-PI to the luminal side of the ER. In the luminal side of the ER the GPI precursor acylated, mannosylated with three mannose residues and transferred to the nascent protein.

Attachment of GPI precursor to the nascent protein takes place on the luminal side of the ER via a transamidation reaction catalysed by GPI transamidase (GPI-T). The polypeptide chain requires a specific C-terminal signal sequence for the attachment to GPI precursor by GPI-T. During its activation, GPI-T identifies and cleaves the C-terminal signal sequence leading to formation of a new amide bond between the carbonyl group of the polypeptide chain and the amine group of the GPI precursor.²⁴ After the GPI has been attached to the protein, the glycoconjugate is transported to the Golgi apparatus where side chain modification of the core structure and lipid remodelling takes place. The completed GPI anchored proteins are then transported from the Golgi to the plasma membrane where their specific cell surface location depends on the function of the protein concerned.

Despite the importance of GPI anchors in plants,²⁵ little work has been done to elaborate their structural composition or biosynthetic pathway. In fact, to date the only plant GPI structure so far determined is from *Pyrus communis*.²⁶ This GPI anchor has the conserved core structure, which is consistent with those found in protozoa, mammals and yeast; however, it is modified with β -1,4-galactosyl substitution of the 6-linked mannose residue. The GPI biosynthetic pathway in plants has not been studied experimentally; it has only been proposed on the basis of a structural study from *Pyrus communis* and bioinformatics analysis, which identified orthologous genes to mammalian and yeast GPI biosynthetic systems.²⁶

1.2.2 Mycobacterial lipoarabinomannan

The cell surface of pathogenic *Mycobacterium tuberculosis* and non-pathogenic *Mycobacterium smegmatis* possess a series of amphipathic glycolipids, such as lipoarabinomannan (LAM), lipomannan (LM) and phosphatidyl-*myo*-inositol mannoside (PIM), which are non-covalently attached to the cell membrane through a phosphatidyl-*myo*-inositol (PI) anchor (Fig. 1.3).

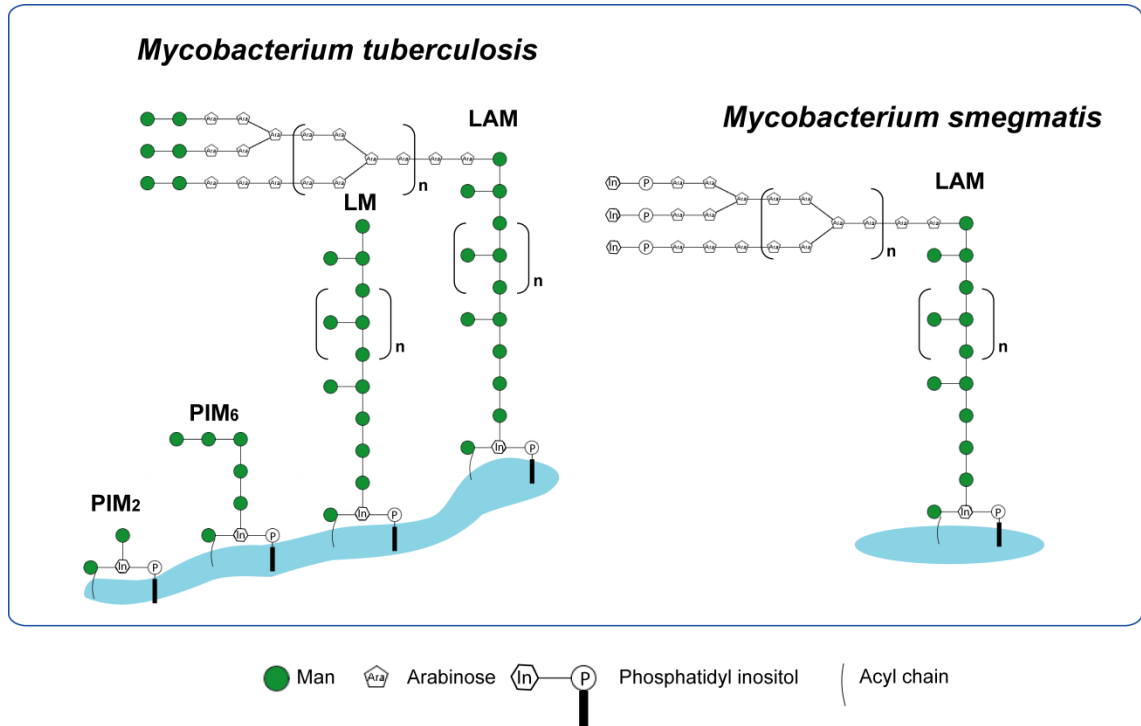


Figure 1.3 Representative examples of the main components of the mycobacterial cell surface; structural similarities and differences between LAM in *Mycobacterium tuberculosis* and *Mycobacterium smegmatis*.

The mannosylated PIM structures contain between two and six mannose residues in α -1,6 and α -1,2 linkages and can be acylated by transfer of fatty acid to one of the core mannose residues, resulting in final AcPIM₆ species. The LM structure is composed of a longer α -1,6-linked mannan backbone, which is elaborated with α -1,2-linked mannose residues forming short side chains. The backbone of the LAM is then extended with α -1,5-linked arabinofuranose residues modified with α -1,3-linked branching chains. The terminal α -1,2-linked arabinofuranose residues are then modified with a specific capping motif, which is species dependent. In slow-growing *Mycobacterium tuberculosis*, the capping motif was assigned to small manno oligosaccharides (ManLAM), while in fast-growing *Mycobacterium smegmatis* to phospho-inositol (PILAM) (Fig. 1.3).²⁷ The ManLAM of *Mycobacterium tuberculosis* plays an important role in regulating the host immune response by interaction with different

receptors which contributes to the survival of the slow-growing pathogenic bacterium in the host.²⁸ The current model of LAM biosynthesis follows a linear pathway from PI→PIM→LM→LAM with some diversion in the biosynthesis of AcPIM₆ (Fig. 1.4).⁴

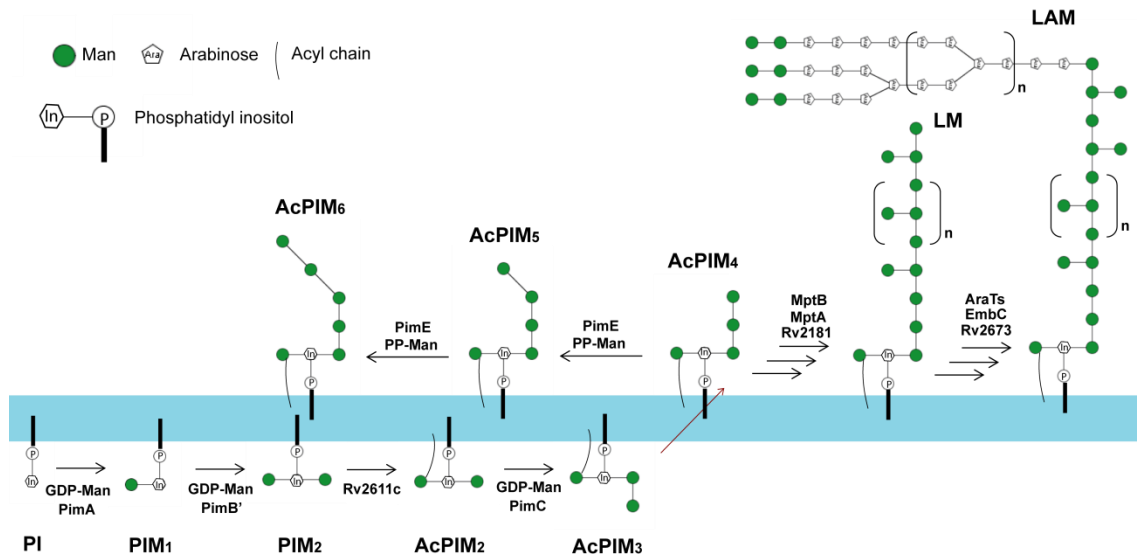


Figure 1.4 Diagrammatic scheme of LAM biosynthesis in non-pathogenic *Mycobacterium smegmatis*. The biosynthesis begins on the cytoplasmic face of the plasma membrane by mannosylation of inositol with two mannose residues to form PIM₂ which is then further acylated and mannosylated to yield AcPIM₃. The AcPIM₃ is transported to the outer face of the plasma membrane where it is mannosylated to AcPIM₄ which either leads to formation of AcPIM₆ or proceed further to the biosynthesis of LM and LAM.

LAM biosynthesis initiates with the transfer of a mannose residue to the 2-position of the *myo*-inositol ring of PI, which is catalysed by a ManT, termed PimA, yielding a PIM₁. This enzyme has been well characterised using biochemical experiments and its crystal structure was solved in the presence of acceptor and donor, which gave an understanding of the enzymes catalytic mechanism.^{29, 30} The *myo*-inositol is then mannosylated by a ManT, termed PimB' to give PIM₂, which is acylated by acyltransferase (Rv2611c) to form AcPIM₂.³¹ The latter is then mannosylated to AcPIM₃ and AcPIM₄, where AcPIM₄ is believed to be a branching point intermediate leading to either formation of AcPIM₆ or further elongation to LM and LAM. The transition of AcPIM₃ has been determined to occur from mannosyltransferases located on the cytoplasmic face of the plasma membrane, which utilise soluble GDP-Man sugar nucleotide to the glycosyltransferases that utilise lipid-linked-activated (polyprenol phosphate (PP)) sugars located on the luminal side of the ER. This was supported by inhibiting the biosynthesis of AcPIM₄ with amphomycin, which is a selective inhibitor of polyprenyl-phosphate-ManT.³² The enzyme involved in formation of AcPIM₅ and

AcPIM₆ is α -1,2-ManT, termed PimE; however, it is still not clear if it is solely responsible for the biosynthesis of both intermediates.

The biosynthesis of LM involves two recently identified α -1,6-ManT, termed MptB and MptA. The first α -1,6-ManT (MptB) enzyme is involved in the initial stage of AcPIM₄ elongation, while the second α -1,6-ManT (MptA) is involved in further elongation of LM precursor to produce mature LM.³³ Deletion of genes encoding for MptB and MptA enzymes in *Corynebacterium glutamicum*, a species that shares similar orthologues involved in cell wall assembly with *Mycobacterium tuberculosis* and *Mycobacterium smegmatis*, resulted in the absence of LM and LAM structures when compared to the wild type.^{34, 35} The core LM structure is branched by α -1,2-ManT enzyme (Rv2181) resulting in characteristic α -1,2-linked branches. The initial decoration of mannose core structures of mature LM with arabinose residues involves as yet uncharacterised arabinofuranosyltransferase (AraT) enzyme. Decorated LAM is then further extended by α -1,5-AraT (EmbC)³⁶ and at this point formation of branching is assigned to α -1,3-AraT (Rv2673).³⁷ The branched LAM is then extended by unidentified α -1,5-AraT and finally β -1,2-AraT introduces terminal tetra and hexa-arabinofuranoside structures.³⁸

1.2.3 Eukaryotic N-linked glycoproteins

The majority of the genetic and biochemical characterisation of N-glycosylation has been established in eukaryotic cells and the biosynthetic pathway can be divided into three major stages. The first stage involves assembly of the lipid-linked oligosaccharide and occurs at the ER; the second stage involves transfer of newly synthesised oligosaccharide from the lipid-linked precursor to the asparagine residue of proteins, finally, the third stage involves further modification of oligosaccharide on the protein and takes place in Golgi apparatus (Fig. 1.5).³⁹ The first two stages are remarkably conserved in all eukaryotic cells ranging from unicellular organisms, such as yeast to the multicellular, such as animal, plant and humans.⁴⁰ In contrast, the third stage is cell, tissue and organism specific.

During the first stage, the assembly of the lipid-linked oligosaccharide requires a series of membrane-bound glycosyltransferases that belong to the *Alg* family (asparagine-linked glycosyltransferases). The ordered addition of sugar residues to the growing

intermediate is maintained through remarkable substrate specificity of these enzymes. It all begins with the synthesis of dolichylpyrophosphate (Dol-P-P) carrier at the cytoplasmic face of the ER membrane. Once the assembly of this carrier is complete, the first step of *N*-glycosylation begins with transfer of *N*-acetylglucosamine residue from UDP-GlcNAc to the Dol-P-P carrier giving rise to GlcNAc-P-P-Dol. *N*-Acetylglucosaminyl phosphate transferase (*Alg7*) involved in this catalysis is very sensitive to inhibition by tunicamycin, which is naturally occur in several bacteria including *Streptomyces clavuligerus*, and it was originally developed as an antiviral substance.^{41, 42} The next step involves transfer of a second GlcNAc residue to GlcNAc-P-P-Dol followed by sequential addition of five mannose residues to give $\text{Man}_5\text{GlcNAc}_2\text{-P-P-Dol}$. After completion, the $\text{Man}_5\text{GlcNAc}_2\text{-P-P-Dol}$ intermediate is translocated to the luminal side of the ER by a process which is believed to involve proteins, termed flippases; however, the overall process is still unclear.⁴³

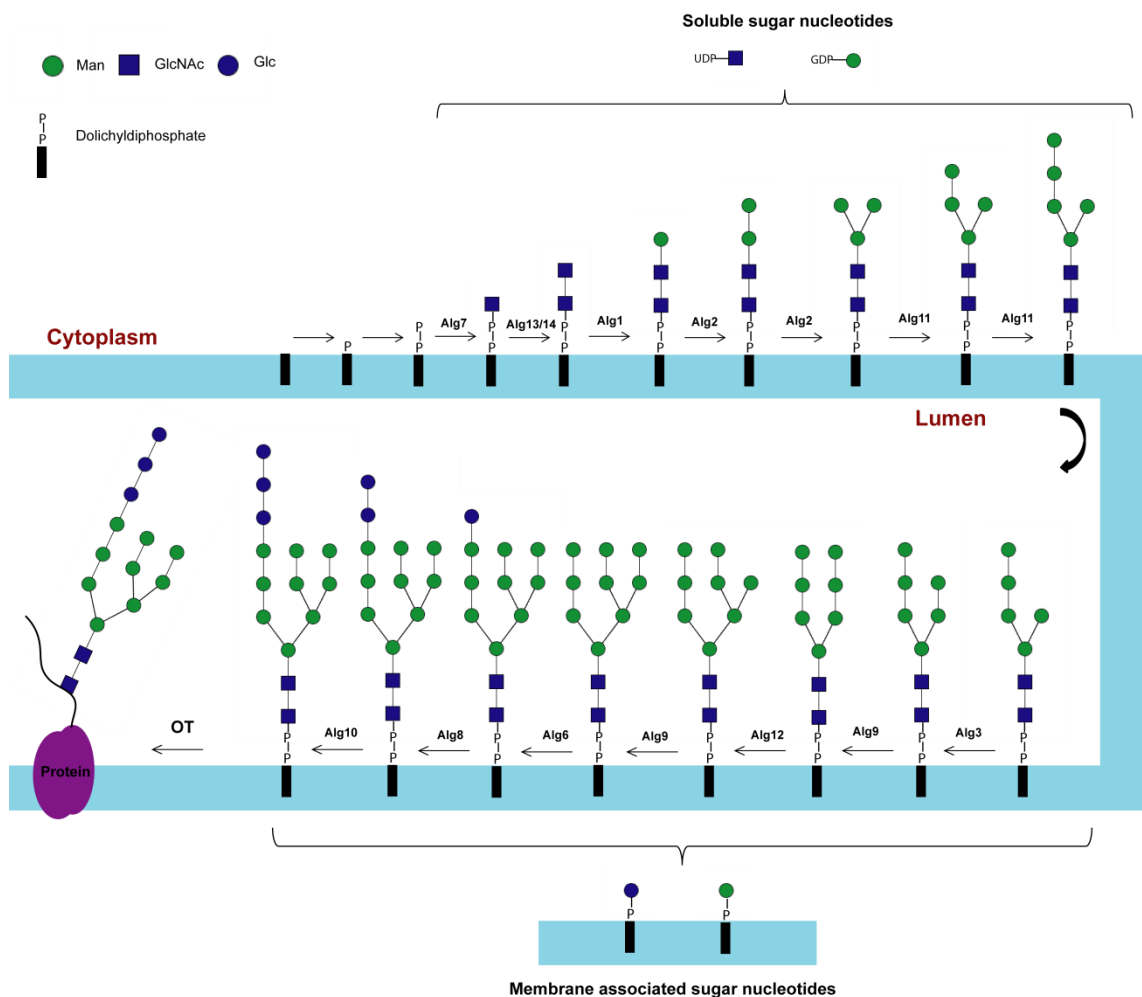


Figure 1.5 Representative biosynthetic pathway of *N*-linked glycosylation at the ER membrane in eukaryotic cells.³⁹

On the luminal side of the ER the $\text{Man}_5\text{GlcNAc}_2\text{-P-P-Dol}$ intermediate is elongated with four mannose residues to give $\text{Man}_9\text{GlcNAc}_2\text{-P-P-Dol}$. These mannosylations are catalysed by *Alg3*, *Alg12* and *Alg9*, where *Alg3* and *Alg12* transfers an α -1,3- and α -1,6-linked mannose residues respectively, and *Alg9* two α -1,2-linked mannose residues.^{44, 45} Addition of the remaining three glucose residues is catalysed by glucosyltransferases (GlcT) *Alg6*, *Alg8* and *Alg10*, which complete the biosynthesis of lipid-linked $\text{Glc}_3\text{Man}_9\text{GlcNAc}_2\text{-P-P-Dol}$ precursor (Fig 1.5). It is worth mentioning that all glycosyltransferases involved in the biosynthesis of lipid-linked precursor on the cytosolic side of the ER utilise soluble sugar nucleotides, such as UDP-GlcNAc and GDP-Man. In contrast, all glycosyltransferases on the luminal side of the ER utilise lipid-activated sugar nucleotides such as Dol-P-Man and Dol-P-Glc as donors that are synthesised on the cytosolic side of the ER and translocated to the luminal side.

As mentioned above, the structure of lipid-linked $\text{Glc}_3\text{Man}_9\text{GlcNAc}_2\text{-P-P-Dol}$ precursor is conserved; nevertheless, several species of parasitic protozoa such as *Trypanosoma brucei* ($\text{Man}_{9-8-7}\text{GlcNAc}_2\text{-P-P-Dol}$) and *Leishmania* ($\text{Man}_{7-6}\text{GlcNAc}_2\text{-P-P-Dol}$) are known to synthesise truncated forms of lipid-linked oligosaccharide.⁴⁶ This is due to the inability of trypanosomatids to synthesise Dol-P-Glc sugars as well as the lack of certain ManT and GlcT in these parasitic protozoa (Fig. 1.6).⁴⁷

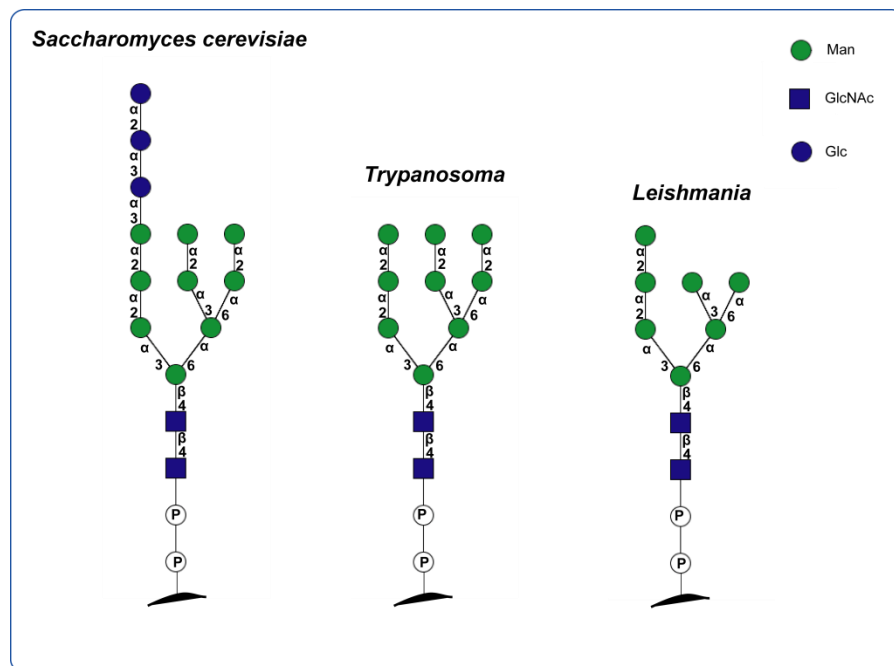


Figure 1.6 Structural variations of lipid-linked N-glycan precursors in eukaryotic system.

During the second stage of *N*-glycosylation, newly synthesised $\text{Glc}_3\text{Man}_9\text{GlcNAc}_2\text{-P-P-Dol}$ precursor is transferred *en bloc* from a dolichol-P-P carrier to the asparagine residue of the nascent polypeptide chain on the luminal side of the ER. This enzymatic reaction is catalysed by the integral membrane oligosaccharyl transferase (OT) (Fig. 1.7).⁴⁸ Glycosylation of asparagine occurs within an Asn-X-Thr/Ser sequence, where X can be any amino acid residue except proline; in particular OT has a slight preference for threonine. After glycosylation, the protein undergoes an elaborate quality control that monitors the protein folding in the ER (Fig. 1.7). The quality control is performed by two lectins, such as membrane-bound calnexin and its soluble homolog calreticulin.⁴⁹ The process of quality control begins with removal of two glucose residues by the action of glucosidases I and II to give $\text{GlcMan}_9\text{GlcNAc}_2\text{-Asn-Protein}$. This precursor is then recognised by the two lectins that prevent protein aggregation and misfolding. Once the protein is properly folded, the removal of remaining glucose residues by glucosidase II liberates the $\text{Man}_9\text{GlcNAc}_2\text{-Asn-Protein}$ from calnexin and calreticulin. However, if protein fails to fold, which can be due to several factors, such as spontaneous errors during transcription, genetic mutations, toxic compounds or a cellular stress, it undergoes the ER-associated degradation process that employs proteasomes.⁵⁰

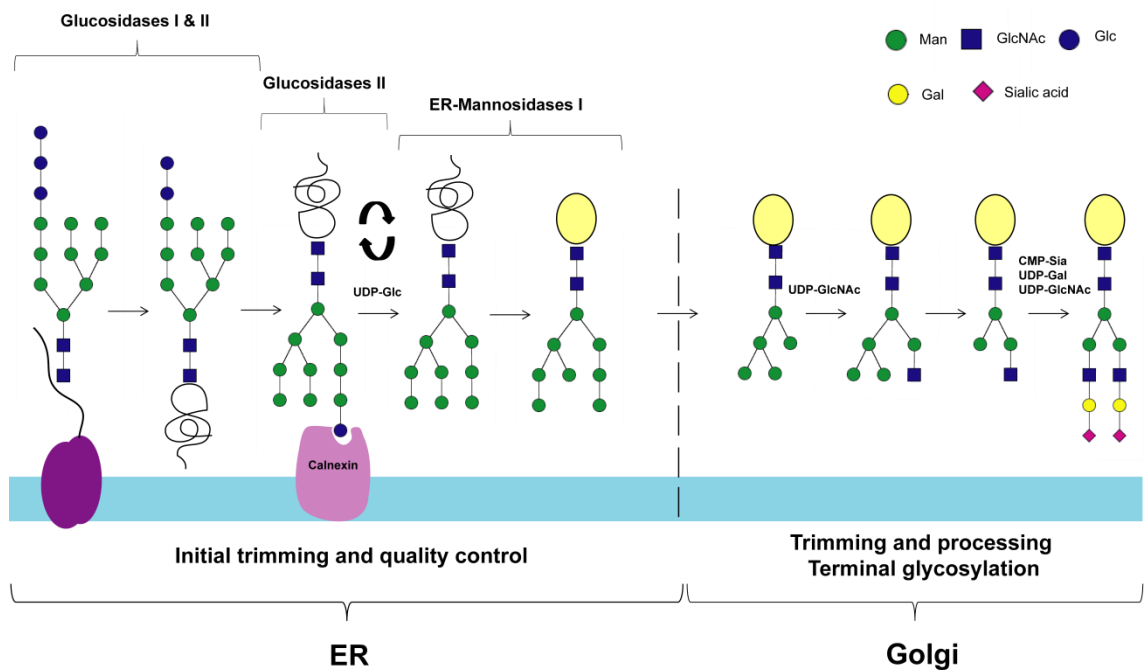


Figure 1.7 Processing and maturation of oligosaccharide moiety of the *N*-linked glycoprotein at the ER and Golgi apparatus membranes.⁴⁰

The third stage occurs mainly in higher eukaryotic cells, as in mammals and plants. In contrast, in yeast the number of mannose residues is not reduced but rather extended with more than 100 mannose residues onto a single glycosylation site forming an outer chain.⁵¹ In the case of higher eukaryotic cells, the correctly folded $\text{Man}_8\text{GlcNAc}_2\text{-Asn-Protein}$ is transported to the Golgi where it undergoes a series of hydrolytic reactions, known as processing and trimming (Fig. 1.7).⁵² This process starts by the addition of a GlcNAc residue to the $\text{Man-}\alpha\text{-1,3-Man}$ arm of the $\text{Man}_5\text{GlcNAc}_2\text{-Asn-Protein}$, catalysed by $\beta\text{-1,2-}N\text{-acetylglucosaminyl transferase I}$ (GlcNAc-T I). Subsequent removal of two mannose residues catalysed by mannosidases II produce a substrate for $\beta\text{-1,2-GlcNAc-T II}$, which transfers GlcNAc residue to the $\text{Man-}\alpha\text{-1,6-Man}$ arm of the $\text{Man}_3\text{GlcNAc}_3\text{-Asn-Protein}$. These two steps are an evolutionary requirement for the next steps that involve building antennae by adding various numbers of Gal, sialic acid and fucose (xylose in plants). It is worth mentioning again that these last enzymatic reactions, which produce the final *N*-glycan structures, involve glycosidases and glycosyltransferases with high substrate specificities that use soluble sugar nucleotides donor substrates.⁵³ Deduction of *N*-linked oligosaccharide final structures from a variety of animal and plant sources using NMR spectroscopy allowed characterisation of *N*-linked glycans and their classification into three main categories that were defined as high-mannose, hybrid and complex (Fig. 1.8).⁵⁴

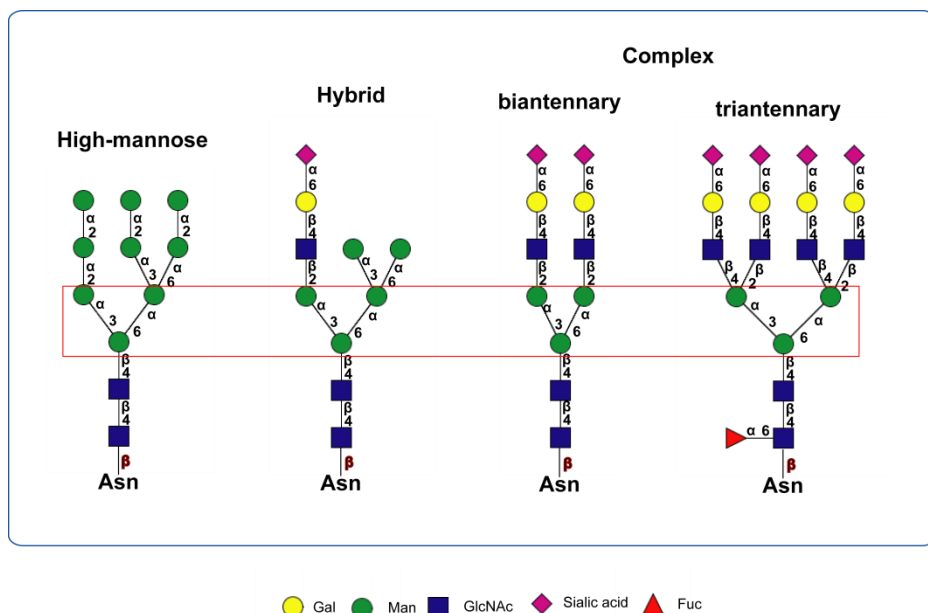


Figure 1.8 Structural variants of *N*-linked glycoproteins. The core structure shared between all types of *N*-linked glycoproteins is indicated by a red box.

All three types of *N*-linked glycoproteins share a common Man₃GlcNAc₂-Asn core structure and differ in the outer branching (Fig. 1.8).⁵⁵ The high-mannose *N*-glycans typically have two to six additional mannose residues attached to the common core structure, whereas complex-type contain several outer branches (bi-, tri-, and tetra-antennary) that typically ends with a sialyl lactosamine sequence. The complex-type *N*-glycans also could have *N*-acetylglucosamine residue attached to the core mannose residue and a fucose residue to the innermost *N*-acetylglucosamine residue. The hybrid-type *N*-glycans share both features of high-mannose and complex-type oligosaccharides (*N*-acetylglucosamine residue attached to the core mannose residue). Furthermore, some *N*-linked glycoproteins can undergo further post-translational modifications, including phosphorylation of mannose residue, sulfation of mannose and *N*-acetylhexosamine residues and *O*-acetylation of sialic acid residue.

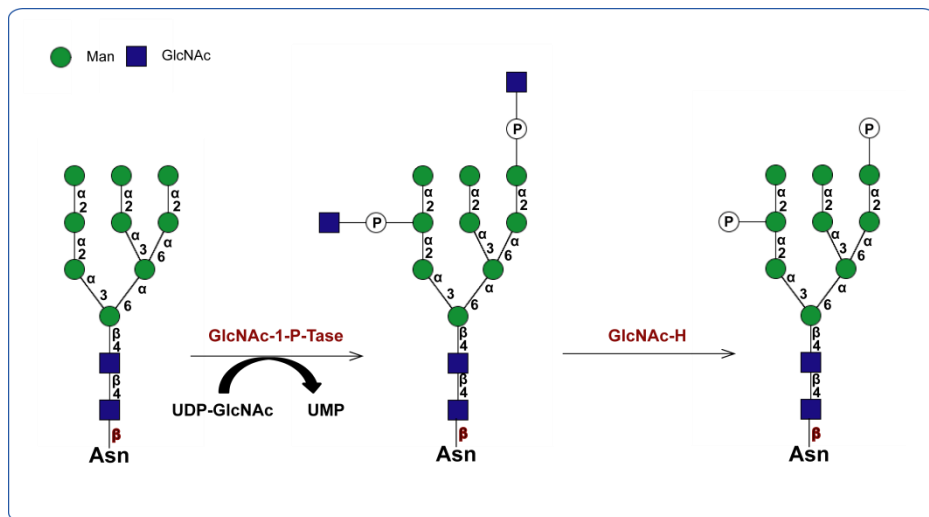


Figure 1.9 Diagrammatic representation of *N*-linked glycoprotein phosphorylation.

One example of post-translational modification is phosphorylation of mannose residues of the *N*-glycan attached to the lysosomal hydrolases, which are destined to be transported to the lysosomes where these enzymes are involved in the degradation of many different substrates accumulated inside the cell.⁵⁶ Like all *N*-glycosylated proteins, lysosomal hydrolases are synthesised and *N*-glycosylated in the ER. When they move along the secretory pathways in the Golgi, these proteins are selectively recognised by UDP-*N*-acetylglucosamine 1-phosphotransferase (GlcNAc-1-P-Tase) (Fig. 1.9).^{57, 58} This enzyme initiates the transfer of GlcNAc-1-P from the UDP-GlcNAc to C-6-hydroxyl group of selected high-mannose type residues of the lysosomal hydrolases.⁵⁹ The enzyme is capable of transferring GlcNAc-1-P to three

different mannose residues and can accept substrates that already carry one phosphorylated mannose residue in high-mannose oligosaccharides.⁶⁰ The next step involves the removal of terminal GlcNAc residue by *N*-acetylglucosamine-1-phosphodiester α -*N*-acetyl-glucosaminidase (uncovering enzyme) in order to expose mannose-6-phosphate (M6P) (Fig. 1.9).⁶¹ The M6P residue of the glycoprotein serves as a recognition site for cation-dependent and cation-independent mannose-phosphate receptors (MPR) in order to transport labelled hydrolases into the lysosomes (Fig. 1.10).⁶² The MPRs are transmembrane glycoproteins localised in the *trans*-Golgi compartment, where they bind to M6P residue of the proteins at pH 6.5-6.7 and release the lysosomal hydrolases at pH 6 inside late endosomes. Interestingly, some lysosomal hydrolases can escape binding to the MPR in the *trans*-Golgi compartment and end up secreted into the extracellular fluid. The MPRs then travel to the plasma membrane to retrieve the escaped lysosomal hydrolases and return them back to the lysosome.⁶³

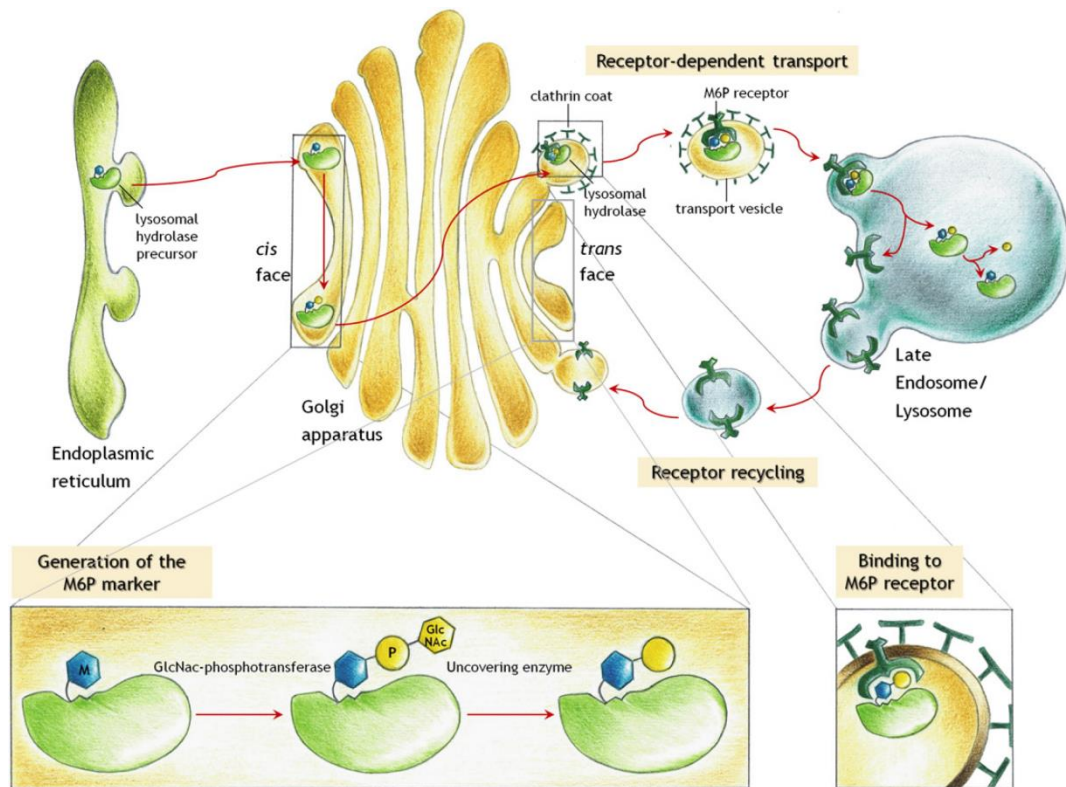


Figure 1.10 Diagrammatic representation of phosphorylation of a newly synthesised *N*-linked lysosomal glycoprotein and its subsequent transfer to the lysosome.⁶³

1.2.4 Eukaryotic *O*-linked glycoproteins

O-Glycosylation is the second major type of post-translational modification of proteins. During this modification a single sugar residue is covalently attached to an amino acid containing hydroxyl group, followed by stepwise elongation of carbohydrate moiety to form a rather compact structure. Furthermore, any amino acid that contains hydroxyl groups such as serine, threonine, tyrosine, hydroxyproline and hydroxylysine can be implicated in the process of glycosylation compared to *N*-glycosylation, where the only amino acid which can be glycosylated is asparagine. This type of modification occurs with either α - or β -anomeric configuration at the carbohydrate protein site compared to only β -anomeric configuration present in *N*-glycoproteins. The *O*-linked glycans are less easy to characterise due to their diversity. However, depending on the nature of the glycosidic bond between a single sugar residue and the protein there are several types of *O*-glycosylation. In mammals, the *O*-linked *N*-acetylgalactosamine (GalNAc) to serine or threonine residues is known as mucin-type glycosylation;⁶⁴ in protozoa, the *O*-linked *N*-acetylglucosamine to serine or threonine residues is also known as mucin type glycosylation⁶⁵ and in plants the *O*-linked galactose to hydroxyproline is known as arabinogalactan (AGP) proteins.²⁵ In addition, many other sugars such mannose, fucose, glucose, and xylose are known to be *O*-linked to proteins.⁶⁶

Mucin type *O*-glycosylation is initiated by the transfer of single GalNAc residue to the serine or threonine amino acid of protein catalysed by UDP-GalNAc:polypeptide *N*-acetylgalactosaminyltransferases (GalNAcT).⁶⁷ In the past, the search for the specific consensus sequence for this type of glycosylation has been unsuccessful, thus concluding that the enzyme responsible for this transfer had a broad specificity. Only recently, it has been realised that there are more than one enzyme involved in the first step of *O*-glycosylation in mucins. At the moment, there is evidences for about 20 isoforms of GalNAcT present in humans,⁶⁸ which makes mucin-type *O*-glycosylation unique compared to *N*-glycosylation, which is controlled by only one protein complex (OT) (Fig. 1.11 A). Within this family of isoforms, there is hierarchy of action, where certain members act as initiating transferases and add GalNAc residue to unmodified polypeptide, while others favour previously glycosylated proteins adding the GalNAc residue adjacent to previous site of glycosylation.⁶⁹ This hierarchy of enzymatic activities allows the build-up of rod-like structures of mucin. Indeed, after the initial addition of GalNAc residue, the chain is extended in a stepwise fashion to generate the

vast majority of glycan structures (Fig. 1.11 A). Core 1 is the most common modification which is known as Tn antigenic structure.⁷⁰ This structure is formed by the action of core 1 galactosyltransferase (Gal-T), that transfer galactose residue to the existing GalNAc- α -1-*O*-serine or threonine moiety to form a β -1,3-linkage. Conversely, core 3 is generated by β -1,3-GlcNAcT, this time by addition of GlcNAc residue to the existing GalNAc- α -1-*O*-serine or threonine moiety.⁷¹ Core 1 and 3 structures can be further modified to form core 2 and 4 by β -1,6-GlcNAc-T action. These core structures are further extended with other sugars such as Gal, GlcNAc, Fuc and sialic acid, creating linear or branched short chain structures. The *O*-glycan structure in mammals is usually terminated with the negatively charged sialic acid that constitutes a target for various lectins and antibodies.⁷²

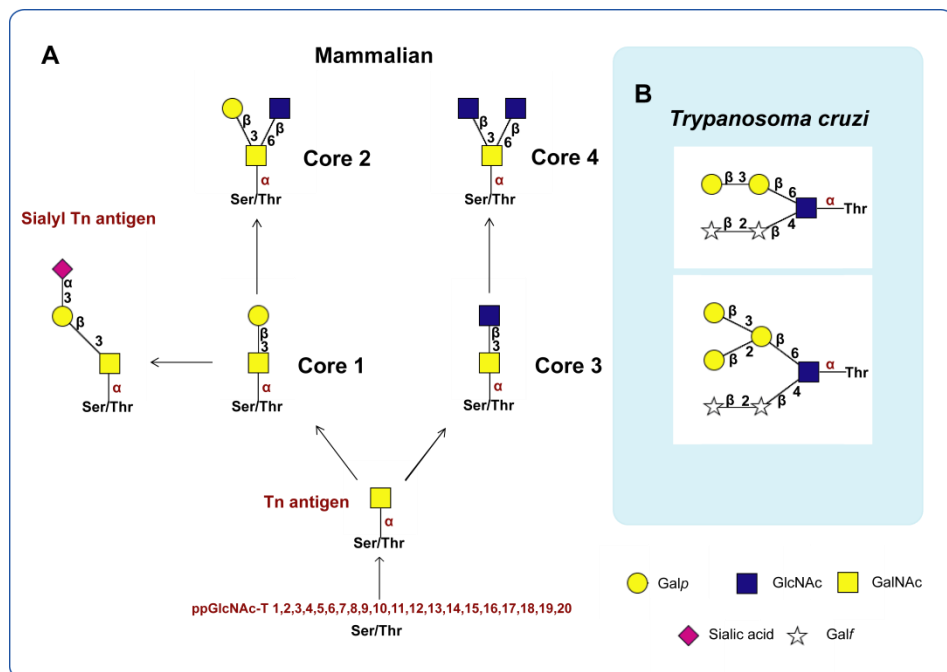


Figure 1.11 Structural variation of the mucin type *O*-glycans. (A) Biosynthesis of mucin type *O*-glycans in mammals. (B) Representative examples of mucin type *O*-glycans in *Trypanosoma cruzi*.^{64, 65}

Serine and threonine *O*-glycosylation through α -*N*-acetylglucosamine-linkages in protozoa is also known as a mucin type *O*-glycosylation (Fig. 1.11 B). This type of modification is mainly found on the mucin proteins located on the cell-surface of pathogens, such as *Trypanosoma cruzi*.⁶⁵ *Trypanosoma cruzi* is an intracellular parasite and it is the etiologic agent of Chagas' disease. Protein glycosylation in this parasite at different developmental stages is the important post-translational modification that causes host-parasite interactions and determines the outcome of infection. The protein domain of *Trypanosoma cruzi* mucin (Tc-mucin) is rich in threonine and serine with *O*-

glycosylation occurring more frequently on the threonine residue.⁷³ The first step of *O*-glycosylation is initiated in the Golgi apparatus by the UDP-GlcNAc:polypeptide *N*-acetylglucosaminyltransferase (ppGlcNAcT), which catalyse transfer of GlcNAc residue to the threonine side chain leading to formation of GlcNAc- α -1-*O*-threonine linkages.⁷⁴ These residues are further extended by addition of galactopyranose (Galp) and galactofuranose (Galf) monosaccharides through the action of β -1,6; β -1,4; β -1,3; β -1,2-Galp-transferases and β -1,4; β -1,2-Galf-transferases (Fig.1.11 B). Terminal β -linked galactose residues serve as substrates for the parasite-specific *trans*-sialidases that transfer sialic acid from exogenous host donor to the parasite acceptor (see Chapter 4).⁷⁵

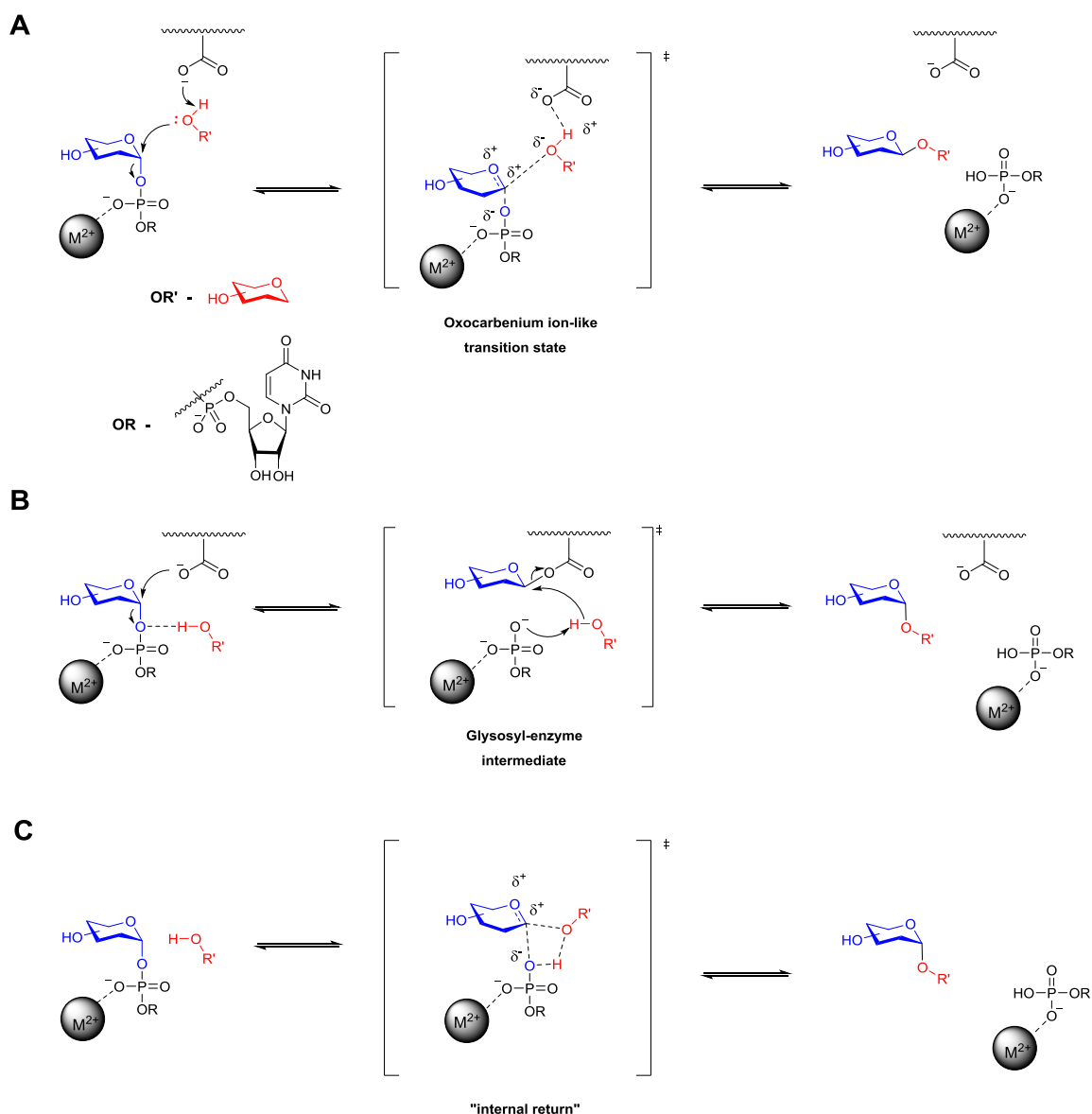
1.3 Glycosyltransferases involved in the biosynthesis of glycoconjugates

GTs are a large family of enzymes, which can be found in the CAZy database (EC 2.4.x.y, CAZy).⁷⁶ They consist of around 200,000 GTs designated by sequence homology into 97 families. GTs catalyse the transfer of a sugar moiety from either a soluble or a lipid-linked activated sugar to acceptor substrates, such as oligosaccharides, peptides, lipids or small molecules. This leads to formation of glycosidic bonds, thereby creating a diverse range of saccharides and glycoconjugates in nature. According to the stereochemistry of the substrate and product glycosyltransferases can be classified as either inverting or retaining enzymes.⁷⁷ Inverting GTs transfer sugar residues from the sugar nucleotide with inversion of stereochemistry of the anomeric centre *e.g.* UDP- α -Glc to β -glycoside. In contrast, retaining GTs retain the same stereochemistry around the anomeric centre *e.g.* UDP- α -Glc to α -glycoside.

The mechanism for the inverting GTs is well understood and follows a direct displacement via an S_N2-like mechanism (Scheme 1.1 A). During the enzymatic reaction, a side chain in the active site acts as a base catalyst and deprotonates the nucleophilic acceptor substrate, which in its turn attacks at C-1 position of the nucleotide donor substrate. The C-1 atom of the donor substrate forms an oxocarbenium-ion-like transition state leading to formation of the glycosidic bond between the donor and acceptor with the inversion of the stereochemistry at the anomeric carbon.

In contrast, the catalytic mechanism used by retaining GTs is still debatable. The current literature describes two hypothetical mechanisms first is a double-displacement mechanism and second is a S_{Ni} -like or “internal return” mechanism. During a double-displacement mechanism, a suitable base on the protein side chain attacks the donor substrate and forms a glycosyl-enzyme intermediate with inversion of the configuration at the anomeric carbon. In the second displacement, the nucleotide phosphate leaving group acts as a base and deprotonates the hydroxyl group of the incoming acceptor substrate. Subsequently, the acceptor substrate attacks the glycosyl-enzyme intermediate resulting in transfer of glycosyl moiety to the acceptor with inversion of configuration at the anomeric carbon (Scheme 1.1 B). This method was based on the knowledge about mechanism of retaining glycosidases;⁷⁸ however, despite numerous efforts no such glycosyl-enzyme intermediates have been trapped. The second proposed “internal return” mechanism (Scheme 1.1 C) suggests a direct attack of the acceptor from the same side as the leaving group departs leading to formation of new glycosidic linkage on the same side of the sugar ring. Currently, this mechanism was supported by mechanistic evidence utilising trehalose-6-phosphate synthases.⁷⁹

GTs involved in the biosynthesis of a majority variety of glycoconjugates described above are membrane-bound enzymes located in the ER and Golgi apparatus.⁸⁰ Subcellular localisation of GTs has been experimentally confirmed by overexpressing them fused with green or red fluorescent proteins in the system of interest and then examining their intracellular distribution using confocal fluorescent scanning microscopy.⁸¹ The ER and Golgi apparatus GTs are type II transmembrane enzymes, with a short single transmembrane domain flanked by a short amino-terminal domain (cytosolic tail), stem region and a large C-terminal domain that possess a catalytic domain that points to the lumen of the ER and Golgi apparatus. GTs are difficult to study when compared to soluble enzymes because of their microsomal membrane association, which presents a major challenge for the isolation of this type of enzymes from the membrane with retained enzymatic activities. Often, the isolation leads to denaturation with subsequent loss of activity. There are also additional difficulties to produce them in high yield in the recombinant form and to obtain crystal structures as they often exist as multi-domain proteins⁴⁸ and can undergo substantial conformational changes.



Scheme 1.1 Mechanisms for inverting and retaining glycosyltransferases. (A) Direct displacement SN₂ mechanism for inverting glycosyltransferases. (B) Double displacement mechanism for retaining glycosyltransferases. (C) Internal return mechanism.

1.4 Methods to probe activities of glycosyltransferases

In order to assess GT activities in both recombinant and cell-free systems a broad range of assay formats, such as radiolabelled, fluorescent, chromatographic, spectroscopic and immunological, were developed and employed to detect one or more product species from GT biotransformations. Most assays require insertion of either a radiolabel or a fluorophore into a donor or acceptor substrates in order to detect GT enzymatic activities because during formation of glycosidic bond there is no obvious fluorescence

or absorbance change. Presence of the label allows monitoring of enzymatic reactions through either depletion of donor or acceptor as well as separation and detection of products formed during these enzymatic reactions. Furthermore, some excellent label-free pH-sensitive and mass spectrometry-based assays have been developed and used to investigate GT substrate specificities. Two excellent reviews by Palcic⁸² and Wagner⁸³ summarise all experimental formats currently used to detect GT and in this thesis section only radiolabelled and fluorescent methods are discussed.

1.4.1 Radiolabelled methodologies to probe glycosyltransferase activities

Radiolabelled assays are the most popular and generic methods to probe glycosyltransferase activities. Indeed, they provide high sensitivity allowing detection of low level of enzymatic activities in natural sources. For this reason, they have been used in a variety of different studies.⁸² Radiolabelled assays mainly utilise radiolabelled ³H- or ¹⁴C-labelled sugar nucleotides. All mammalian radiolabelled donors are commercially available and some radiolabelled acceptors, such as lipids can also be found. Generally, during the assay a radiolabelled donor and acceptor substrate are incubated with a recombinant enzyme of interest or a crude extract of microsomal membranes, which contain membrane-bound glycosyltransferases. During the incubation, the radiolabelled monosaccharide is transferred from the activated donor to the acceptor leading to formation of radiolabelled products. The typical assay can be set up either in the discontinuous or continuous fashion. During the discontinuous assays the enzyme of interest is incubated with a specific acceptor and radiolabelled donor, and the whole reaction is quenched at the time where the formation of product is still linear. In contrast, in discontinuous assays aliquots are taken at set time intervals for the analysis and quantification of formed products.⁸⁴ Subsequently, quantification of radiolabelled products can be performed by standard liquid scintillation counting. Purification of radiolabelled products from unreacted radiolabelled starting material is achieved by a variety of methods, which depend on the type of acceptor used. In general, most carbohydrate acceptors are neutral and water soluble; therefore, a negatively charged unreacted radiolabelled donor can be removed by anion exchange column. In this way, unreacted donor binds to the column and the soluble product elutes with water. In contrast, enzymatic reactions that produce glycosides containing large hydrophobic aglycones can be easily purified by a single extraction with organic

phase⁸⁵ or by application of reverse phase column cartridges.⁸⁶ Obtained radiolabelled products are subjected to further analysis using thin layer chromatography (TLC), where products are identified by co-migration with known standards, as well as HPLC and mass spectrometry. The chemical structure can be assigned using enzymatic or chemical degradation followed again by TLC analysis.^{87, 88}

The above radiolabelled methods are laborious and time consuming requiring extensive product separation and purification. In order to address these issues scintillation proximity assays were developed and used to detect α -1,3-fucosyltransferase (FucT) activities responsible for the biosynthesis of sialyl Lewis X from human leukocytes.^{89, 90} This method is based on the principle of scintillation proximity and utilises microscopic beads coated with a suitable acceptor that contain a scintillant inside the beads. During these assays the microspheres impregnated with acceptors are incubated with the radiolabelled nucleotide donor and enzyme. The transfer of the radiolabelled donor to the acceptor brings the radio-emitter in close proximity to the microsphere resulting in the emission of light detected by photometer (Fig. 1.12).

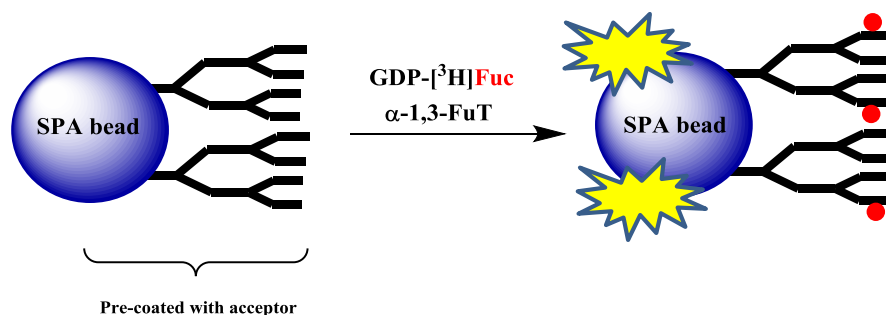


Figure 1.12 Diagrammatic representation of scintillation proximity assay utilising radiolabelled donor and impregnated bead to detect α -1,3-fucosyltransferase activity.⁸⁹ During the biotransformation fucosyltransferase transfer fucose residue to the acceptor coated on the SPA bead resulting in a scintillation proximity signal increase. SPA (scintillation proximity assay).

1.4.2 Fluorescence-based methodologies to probe glycosyltransferase activities

Fluorescence-based methodology provides high sensitivity, operational simplicity, and, most importantly, the fluorescence-based assays are free from radioactivity, so the outcome could be analysed with any modern analytical instrumentation. In order to assess glycosyltransferase activities a fluorophore can be chemically attached to either a donor or an acceptor substrate depending on the prerequisite of a particular

investigation. In almost all fluorescence-based assays the focus lies on a small family of fluorophores, such as BODIPY (4,4-difluoro-4-bora-3a,4a-diaza-s-indacene), fluoresceins, rhodamines and umbelliferones (coumarin-based) (Fig. 1.13).⁹¹

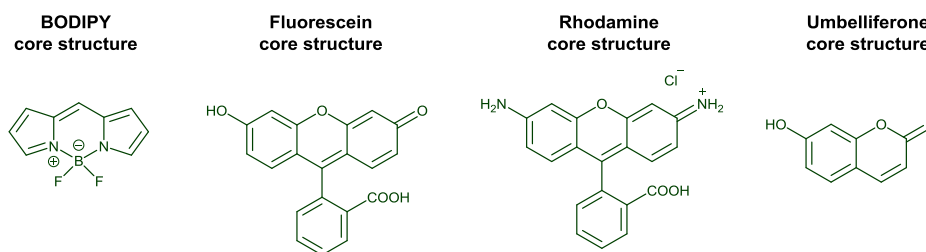


Figure 1.13 Chemical structures of widely used fluorophores.

These are fairly large aromatic compounds that can influence either substrate association with membranes or substrate solubility, and all provide different fluorescent properties.⁹¹ BODIPY-based fluorophores possess unique photophysical properties, such as a small Stokes shift, high fluorescent quantum yield, sharp excitation and emission peaks and high molar extinction coefficient.⁹² Moreover, this fluorophore is not affected by solvent polarity and pH, compared to fluorescein- and coumarin-based fluorophores. The common limitations of this fluorophore are its poor water solubility and lack of functional groups for conjugation; however, introduction of various substituents can be modulated to suit various applications.⁹³ Fluorescein-based fluorophores possess good water solubility, high fluorescent yield and it has two groups, such as carboxyl and hydroxyl group, which can be used to attach acceptor or donor. Nevertheless, these types of fluorophores have several significant drawbacks, including, pH sensitive fluorescence and especially high rate of photobleaching that requires storage and all manipulations to be performed in the dark. Rhodamine-based fluorophores have good photostability compared to the fluorescein-based fluorophores, a high extinction coefficient and high fluorescence quantum yield. Although, conjugation of rhodamine-based fluorophores to protein known to precipitate from solution. Coumarin-based fluorophores are the most interesting set of fluorophores because their photophysical properties (especially quantum yield) can be altered by adding different substituents on the coumarin scaffold.⁹⁴ They are fairly small and easy to synthesise but they could also show pH sensitivity, due to the presence of hydroxyl group at the 7-position of coumarin rings but can be modified to avoid this limitations. Moreover, placing the azido group at the 3-position quenches the fluorescence

completely and it can be restored on formation of the triazole ring (see Chapter 2 section 2.1).

Fluorescence-based methodologies utilising sugar nucleotides and acceptors

Naturally occurring sugar nucleotide donors are poor light emitters and therefore a variety of strategies have been developed to generate fluorescent donor analogues to target GTs activities (reviewed in Wagner's publication⁸³). In these strategies, a fluorophore is always attached to the donor site that does not interfere with the active site of investigated enzymes. One of these fluorescence-based methodologies utilises a ligand-displacement format because it provides a more practical and cheaper way to identify GT enzyme inhibitors where labelling of acceptors require substantial time and effort. This assay simply monitors changes in fluorescence polarisation occurring when the fluorescent donor substrate analogues bind to active sites of GT enzymes and following their displacement by inhibitors introduced into the reaction mixture (Fig. 1.14). The general principle underlying these assays is that the fluorescence polarisation of the fluorescent label is lower when it is attached to a small molecule and higher when it is attached to a larger one.⁹⁵

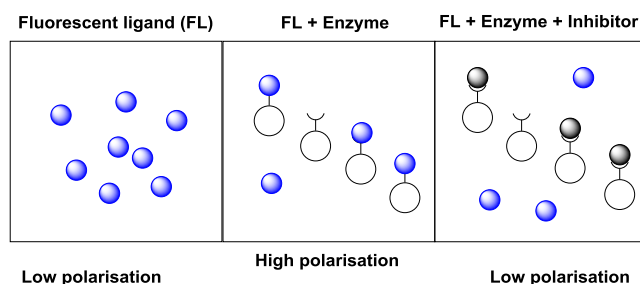


Figure 1.14 Schematic representation of fluorescence-based ligand-displacement assay for inhibitory screening.⁹⁶

More specifically, this method has been used to identify inhibitors of *O*-GlcNAc transferase, which, as discussed in section 1.2.4, transfer *N*-acetylglucosamine from UDP-GlcNAc to serine and threonine residues of newly synthesised proteins. For this assay fluorescent UDP-GlcNAc donor was generated by conjugation of fluorophore to the *N*-acetyl functional group of UDP-GlcNAc (Fig. 1.15 A(i)).⁹⁷ This donor substrate was then screened in HTS assays against library of 64,416 commercial compounds

using a microplate reader to measure changes in fluorescent polarisation. The output identified 102 compounds which acted as very strong inhibitors. Their identification prompted authors to look into effect of these compounds in cell cultures where reduction in *O*-GlcNAc transferase activity could assess the biological function of this enzyme *in vivo*; however, no further publication to illustrate this point has been produced.

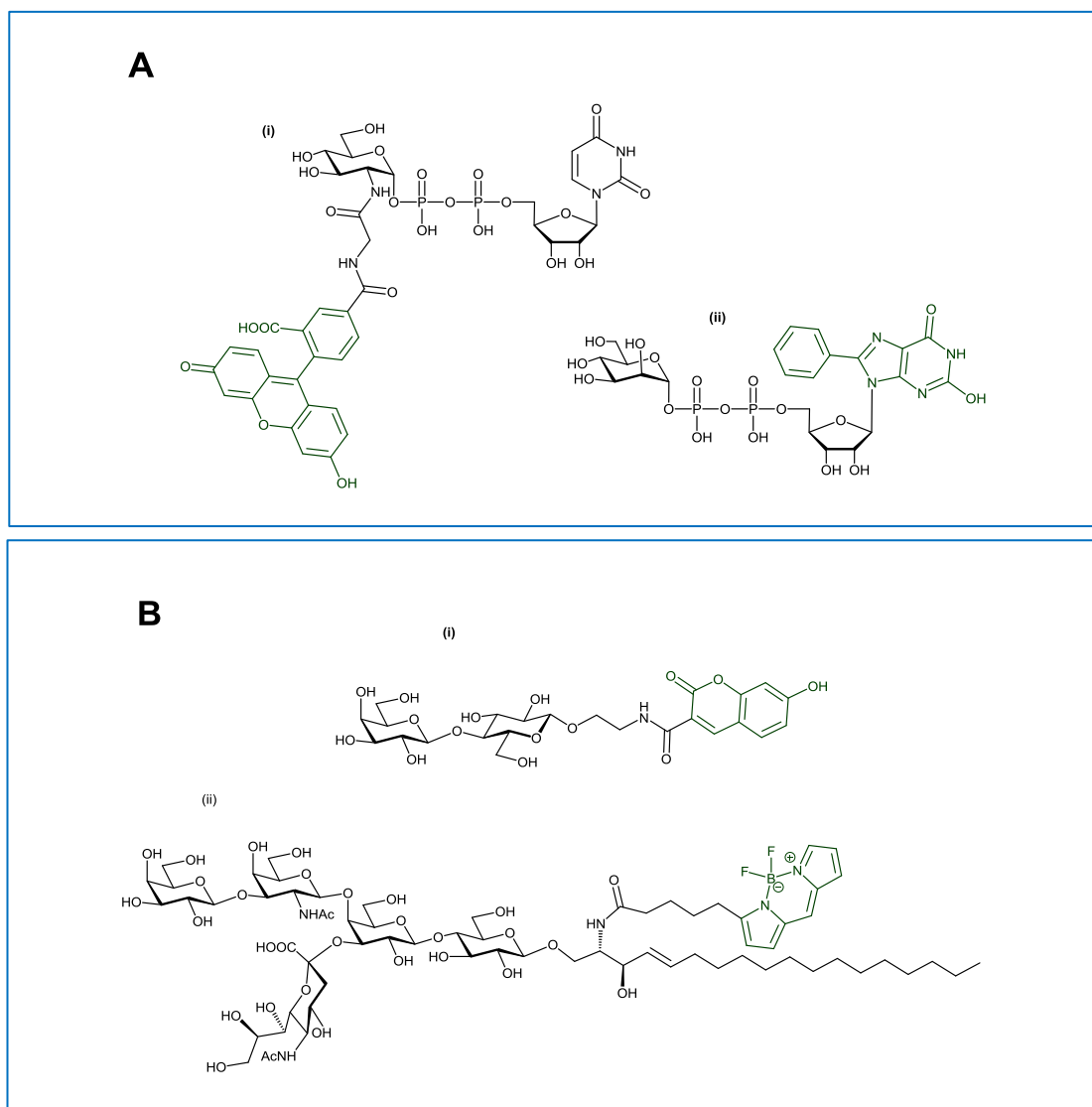


Figure 1.15 Chemical structures of selected fluorescently-labelled sugar nucleotides and acceptor substrates used in the literature GT assays. (A) Fluorescently labelled sugar nucleotides;⁸³ (B) Fluorescently labelled acceptor substrates.

An alternative approach to the one described above looked at the installation of a fluorophore into the nucleotide part of the GDP-Man donor following utilisation of this modified sugar nucleotide to screen inhibitor candidates of mycobacterial α -1,6-ManT, such as PimA and PimB' (section 1.2.2). The enzymes involved in the biosynthesis of

LM represent prospective targets for novel chemotherapeutic agents. In this study, a series of GDP-Man donor analogues, which incorporated aryl or heteroaryl substituents at position 8 on the guanine nucleobase were synthesised by Suzuki-Miyaura cross-coupling chemistry (Fig. 1.15 A(ii)).⁹⁸ The extension of the aromatic system with aryl or heteroaryl substituents resulted only in subtle differences in fluorescence characteristics of these compounds, having λ_{em} around 400 nm and similar Stokes shifts. In further research performed by Besra's group, only the brominated derivative of GDP-Man, used as a precursor for Suzuki-Miyaura cross-coupling reaction, has been co-crystallised with PimB' in order to assess structural and mutational analysis of the active site.⁹⁹

Fluorescent labelling of acceptors has been used in HTS screening to check for activities of engineered glycosyltransferases and identify mutants which possess the highest activities. One of these studies described in the literature¹⁰⁰ used fluorescently labelled acceptors to identify activities of engineered sialosides in intact *Escherichia coli* cells by fluorescence-activated cell sorting (FACS). This technique is based on using flow cytometry to separate intact cells according to their size and fluorescence.¹⁰¹ In this assay, a series of lactose and galactose acceptors fluorescently labelled with coumarin, fluoresceine and BODIPY fluorophores were synthesised (Fig. 1.15 B(i)) with prerequisite that these acceptors substrates can freely be transported in and out of cells. Engineered cells were then incubated with fluorescent acceptors and, as the reaction took place, sialylated galactoside products were trapped inside the cell due to their size and charge, while unreacted acceptor substrates were washed away. The washing step was important to get rid of any fluorescent background in order to facilitate detection of minimal enzymatic activities. In the last step intact cells were subjected to the fluorescence-activated cell sorting. Using this method, it was possible to screen libraries of $>10^6$ engineered mutants in less than two hours and to detect mutants with increased enzymatic activities compared to the wild type. In addition, it was demonstrated that using fluorescence-activated cell sorting techniques two different fluorescent acceptors with different fluorophores attached could be used in parallel and their transfer reactions monitored simultaneously.

Another fascinating study described in the literature was performed in Palcic's group.¹⁰² In this study, fluorescently labelled acceptor substrate analogues were utilised to analyse glycosphingolipids (glycolipid) metabolism on the single cell scale by capillary

electrophoresis (CE) with laser induced fluorescence (LIF) detection.¹⁰² To begin with, fatty acids of the ceramide lipid moiety of GM1 and lactose glycosphingolipid were replaced with a fluorophore, such as BODIPY and tetramethylrhodamine (Fig. 1.15 B(ii)). The fluorescent GM1 and lactose glycolipid were then modified *in vitro* employing recombinant sialyltransferases and commercially available glycosidases resulting in a variety of fluorescent glycolipid structures. These fluorescently labelled glycolipid intermediates were used as standards in CE-LIF analysis. Incubation of fluorescent lactose and GM1 glycolipids with cells culture and subsequent product separation using CE-LIF method revealed detection of glycosyltransferases as well as hydrolase activities involved in the metabolism of glycosphingolipids (Fig. 1.16 A and B).

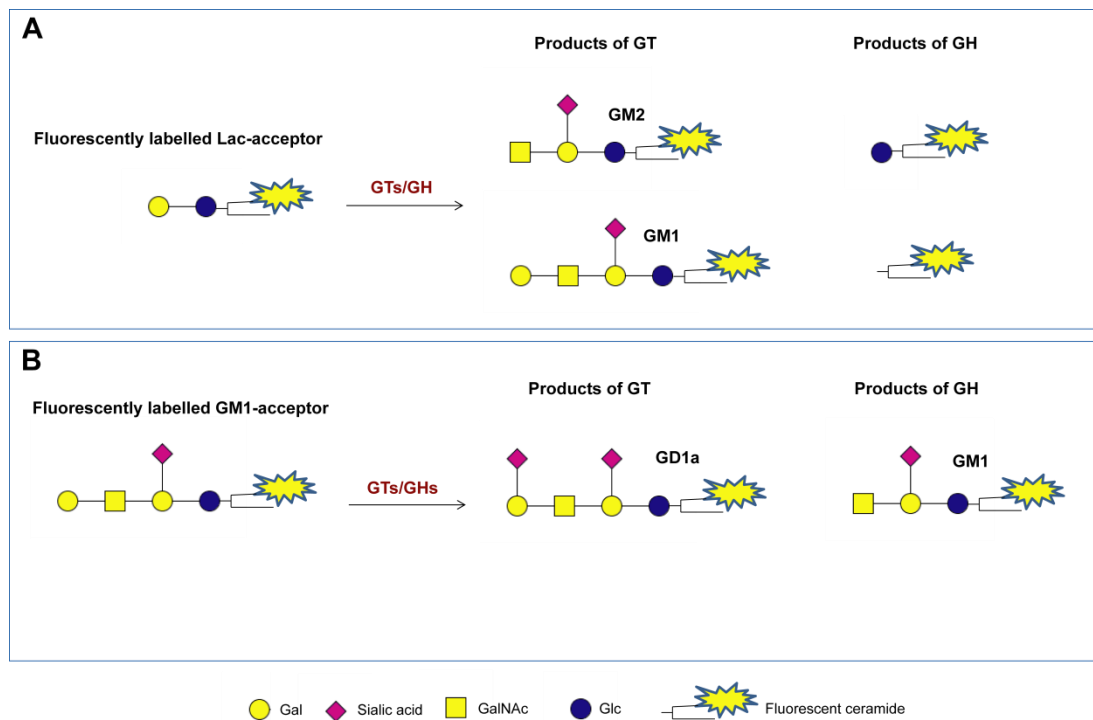


Figure 1.16 Representative example of enzymatic reactions of fluorescent GM1 and lactose acceptor substrates and their products derived from the glycolipid metabolism detected by CE-LIF.

1.5 Requirement for the new fluorescence-based methodology

Despite the sensitivity and applicability of radiolabelled assays, they can be complicated by a number of factors. There is a limited availability of radiolabelled sugar nucleotides, especially in the case of complex glycosides that come from bacterial or

plant systems. The separation of reaction mixtures using ion-exchange columns can also generate high background values due to donor decomposition leading to high scintillation count reading. The requirement for specially designed and equipped labs, personnel trained in handling radiolabelled materials and long preparations of health hazard assessments and standard operating procedures extends the preparation and experimental times. Radiolabelled sugar nucleotides that contain ^3H or ^{14}C have low or moderate specific activities, therefore requiring long processing times to obtain meaningful results; for example, it can take up to a week to develop a TLC plate using autoradiography. Other limitations include health hazards associated with handling and waste disposal of radioactive material.

Fluorescence-based methodologies described above allow screening of already identified and overexpressed glycosyltransferases involved in biosynthesis of glycoconjugates. These assays illustrate that modification of acceptors or donor with a fluorophore does not impair activities of the glycosyltransferases, and these enzymes are still able to transfer sugar residue from sugar nucleotide to the acceptor analogues. Therefore, there is scope to develop a fluorescence-based methodology to probe activities of membrane-bound glycosyltransferases involved in the biosynthesis of various glycoconjugates. The research has shown that donors modified on the nucleobase are good substrates and can be compatible with enzyme active site. It is less likely that this strategy would be applied because modification of donor with a fluorophore would require additional chemical synthesis of donor as well as acceptor, which is not always trivial and easily applicable. In contrast, it is more plausible to develop a new fluorescence-based methodology that incorporates a fluorophore on the acceptor and especially on the aglycone part of the molecule because it could aid with substrate presentation and recognition by membrane-bound enzymes and it would not interfere with the active site of detected enzymes. Furthermore, this would give the desired experimental flexibility as well as provide opportunity to investigate the effect of aglycone hydrophobicity and bulkiness on enzymatic activities of investigated membrane-bound glycosyltransferases.

1.6 Project aims and objectives

The initial aim of this project was to design several novel fluorescent based methodologies which can probe activities of membrane-bound glycosyltransferases responsible for the biosynthesis of multiple glycoconjugates from various biological systems with the purpose to replace traditional radiolabelled methods used in the laboratory environment. The prerequisite of these methodologies would be sensitive, quick and simple in operation and to employ standard analytical techniques for product analyses.

The second aim was to validate and benchmark designed fluorescence-based methodologies against the established radiolabelled assays used to detect glycosyltransferase activities involved in the biosynthesis of lipoarabinomannan in *Mycobacterium smegmatis* and GPI anchors in *Trypanosoma brucei*. Furthermore, fluorescence-based methodologies should be able to illustrate diversities in targeting several membrane-bound glycosyltransferases from two different organisms so in the future it could be used for detection of various enzyme activities with little modifications.

The third aim was to utilise the most promising fluorescence-based methodology to detect glycosyltransferases responsible for the biosynthesis of *N*-glycans and GPI anchors in *Euglena gracilis* in order to use it as a model organism.

An additional aim of this project was to synthesise a series of *Trypanosoma cruzi* mucin glycan mimetic based on the linear and cyclic 1,4/1,5-triazole-linked oligomers utilising Cu(I)-catalysed click reactions of an azido-alkyne-functionalised galactose building block. Subsequently, to test these linear and cyclic 1,4/1,5-triazole-linked oligomers for their ability to act as substrates for *T. cruzi* *trans*-sialidases with the scope to illustrate their potential ability to block *T. cruzi* macrophage invasion.

2 Development and validation of fluorescence-based methodologies to probe biosynthesis of glycoconjugates

2.1 Underlying aspects of fluorescence-based methodologies

The primary aim of this study was to design and develop a universal fluorescence-based methodology that is capable of probing membrane-bound glycosyltransferases (GTs) involved in the biosynthesis of glycoconjugates in a variety of biological systems. In general, we envisaged our fluorescence-based methodology would incorporate the chemical synthesis of a fluorescently labelled acceptor substrate capable of mimicking the authentic intermediates involved in the biosynthesis of a number of glycoconjugates. The labelled acceptor would then undergo enzymatic transformation in the presence of a sugar nucleotide and a crude microsomal membrane extract (ER/Golgi), with subsequent product visualisation by thin layer chromatography (TLC), product purification by high performance liquid chromatography (HPLC) and product analysis using a variety of analytical, spectroscopic, and enzymatic digestion methods (Fig. 2.1).

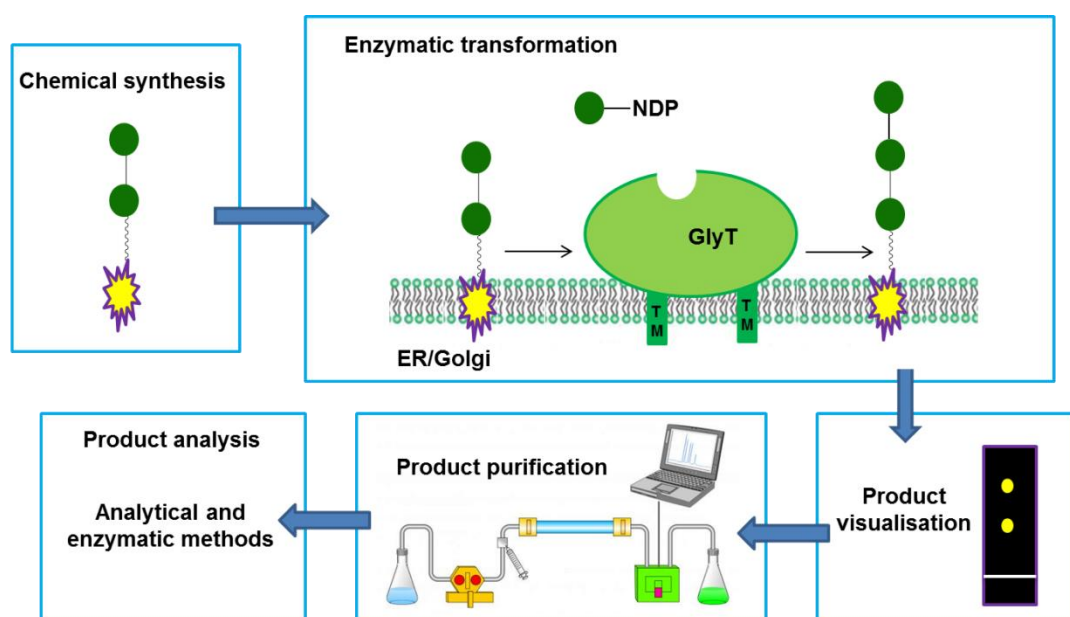
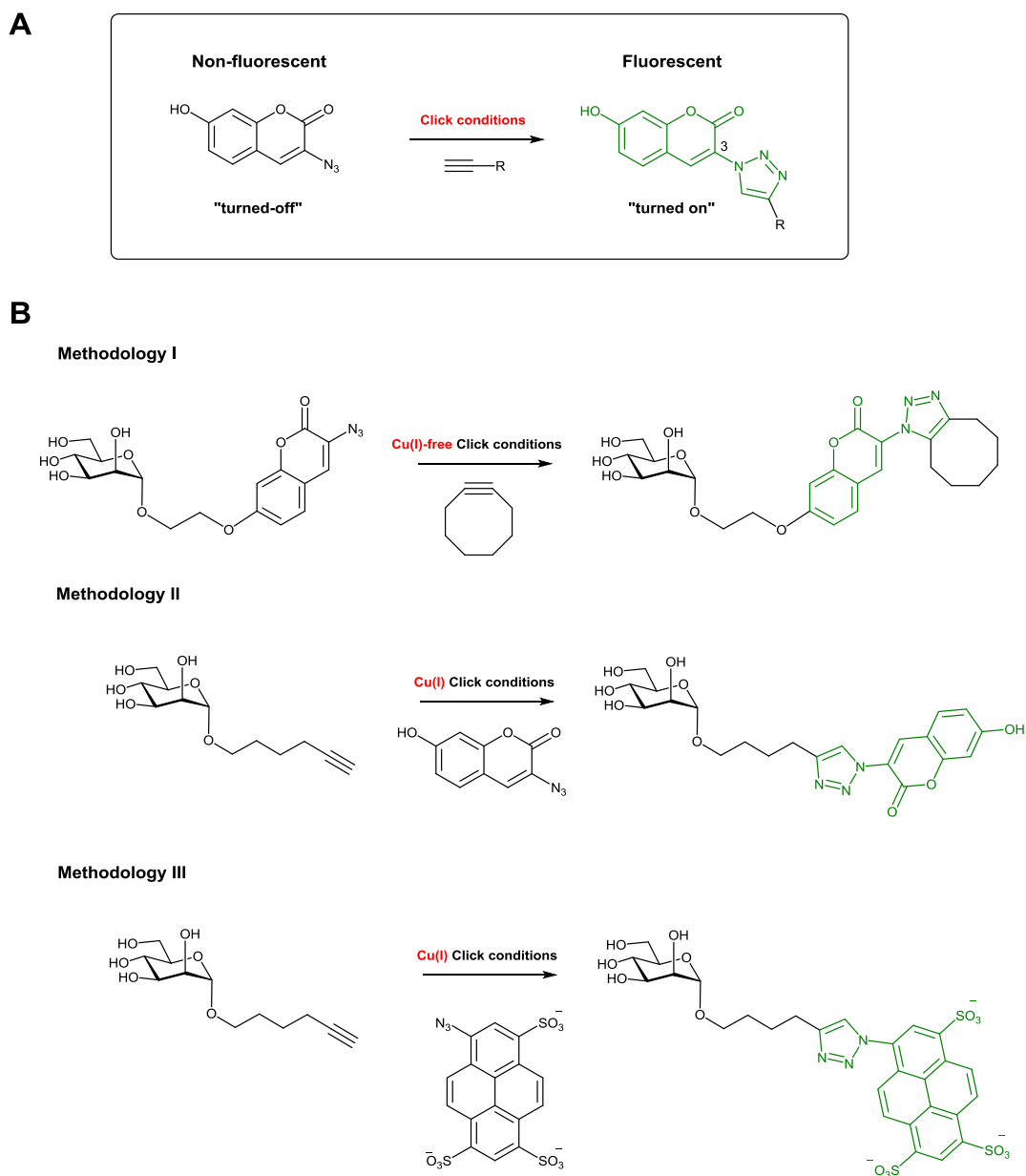


Figure 2.1 General outline of fluorescence-based methodology to detect enzymatic activities of membrane-bound glycosyltransferases.

Three fluorescence-based approaches were initially considered. Methodology I includes chemical syntheses of a non-fluorescent and fluorescent glycoside acceptor substrates with a hydrophobic linker that incorporates either a “turned off” or an activated coumarin-based fluorophore, such as 3-azido-7-hydroxycoumarin (Table 2.1 Methodology I). In the “turned off” state this label possesses no fluorescence due to a quenching effect from the electron rich α -nitrogen of azido group. However, once it undergoes the azido-alkyne 1,3-dipolar cycloaddition under click conditions the

fluorescence of azido coumarin-based fluorophore is “turned on” or activated due to extension of the conjugation exhibited through the 1,2,3-triazole ring formation on the coumarin ring (Scheme 2.1 A).^{103, 104}



Scheme 2.1 Azido coumarin-based fluorophore becomes fluorescent upon reaction with strain or terminal alkyne to form a triazole ring under click conditions. (A) A general scheme to represent “turned off and on” fluorescent properties of 3-azido-7-hydroxycoumarin. (B) Underlying chemical reactions of each methodology. Fluorophores are shown in green.

The activation of the “turned off” azidocoumarin-based fluorophore could be performed either before or after enzymatic transformations. In both cases, activation of an azidocoumarin-based fluorophore happens as result of azido-alkyne 1,3-dipolar cycloaddition reaction with a triple bond of the cyclooctyne under Cu(I)-free strain-promoted click conditions (Scheme 2.1 B, Methodology I).¹⁰⁵ Fluorophore activation

after the enzymatic transformations would be performed directly on the TLC plate in order to have means of visualising the progress of enzymatic reactions. Presence of fluorophore allows tracking of fluorescent material throughout manipulations, quick access to information on the reaction progress by TLC methods and product separation and analysis.

Methodology II and III include chemical syntheses of a non-fluorescent and fluorescent glucoside acceptor substrates with a hydrophobic linker that contains either a terminal alkyne group, required for the attachment of fluorescent label or an activated fluorophore. The choice of fluorophore attached to the terminal alkyne functional group would depend entirely on the analytical method to be used in further analyses (Table 2.1 Methodology II and III). In methodology II we proposed to use a “turned off” azidocoumarin-based fluorophore that undergoes an azido-alkyne 1,3-dipolar cycloaddition with a terminal alkyne group under Cu(I)-catalysed click conditions (Scheme 2.1 B, Methodology II).¹⁰⁶ The labelling of the terminal alkyne group with the azidocoumarin-based fluorophore before enzymatic transformations would give a set of fluorescent compounds that could be visualised on TLC plates without further modification and that could be taken forward for further purification and analysis. The labelling of the terminal alkyne group with the azido coumarin-based fluorophore after enzymatic transformations would be done on the reaction mixture in solution to aid with product visualisation on the TLC plate (Table 2.1 Methodology II).

In methodology III, we proposed to use a negatively charged 8-azidopyrene-1,3,6-trisulfonic acid (AzPTS) that undergoes an azido-alkyne 1,3-dipolar cycloaddition with terminal alkyne group of the acceptor under Cu(I)-catalysed click conditions (Scheme 2.1 B, Methodology III). The azido group on the AzPTS dramatically quenches the fluorescence resulting in 24-fold reduction in the quantum yield compared to 8-azidopyrene-1,3,6-trisulfonic acid (APTS), and on formation of the 1,2,3-triazole ring could be restored.¹⁰⁷ The labelling of glycoside acceptor with AzPTS after enzymatic transformation would allow product separation and identification by the capillary electrophoresis with laser induced fluorescence detection (CE-LIF) (Table 2.1 Methodology III).¹⁰⁸ In past research in Field’s group, a related mode of labelling has been successfully used by Dr. Goetz to evaluate the synthetic pathways of polysaccharides present in plant cell walls.¹⁰⁹ In these studies, labelling was achieved through reductive amination of reducing sugar terminus with 8-aminopyrene-1,3,6-

trisulfonic acid (APTS). The detection of APTS-labelled products proved to be highly sensitive, allowing detection on fluorescent products on femtomole scale. Indeed, CE-LIF techniques of separation and detection have been successfully used in other studies to probe fatty acid, phosphoinositide and sphingolipid metabolism.¹¹⁰⁻¹¹² However, it should be noticed that this technique not the most robust and adaptable method.

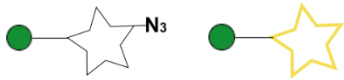
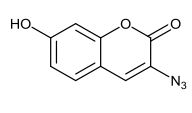
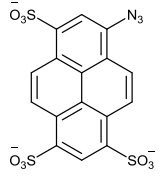
	Methodology I	Methodology II	Methodology III
	Chemical synthesis of acceptors		
			
Work flow	Enzymatic reaction		
	TLC visualisation using Strain-promoted click reaction	Cu(I)-catalysed click reaction	
			
		TLC visualisation	Capillary electrophoresis
	Product separation	Product separation	
	Product analyses	Product analyses	

Table 2.1 Outline schemes of fluorescence-based methodologies for pre- and post-enzymatic transformation labelling in detecting enzymatic activities of membrane-bound glycosyltransferases.

2.2 Design of non-fluorescent and fluorescent mannoside substrates for fluorescence-based methodologies

Non-fluorescent and fluorescent monosaccharide and disaccharide acceptor substrates were designed to have mannose residue as well as α -1,6-mannosidic linkage similar to that present in authentic glycoconjugate structures, such as GPI anchors, *N*-glycans and lipomannans (Fig. 2.2). Such monosaccharides and disaccharides could mimic the authentic intermediates involved in the biosynthesis of these glycoconjugates during biotransformation. In essence allowing generic mannoside acceptors to be used in the detection of α -1,6-ManT activities in *Mycobacterium smegmatis* and α -1,3-GalT activities in *Trypanosoma brucei* required for initial validation and benchmarking of fluorescence-based methodologies against established radiolabelled assays as well as further investigation into biosynthesis of *N*-glycans and GPI anchors in *Euglena gracilis*.

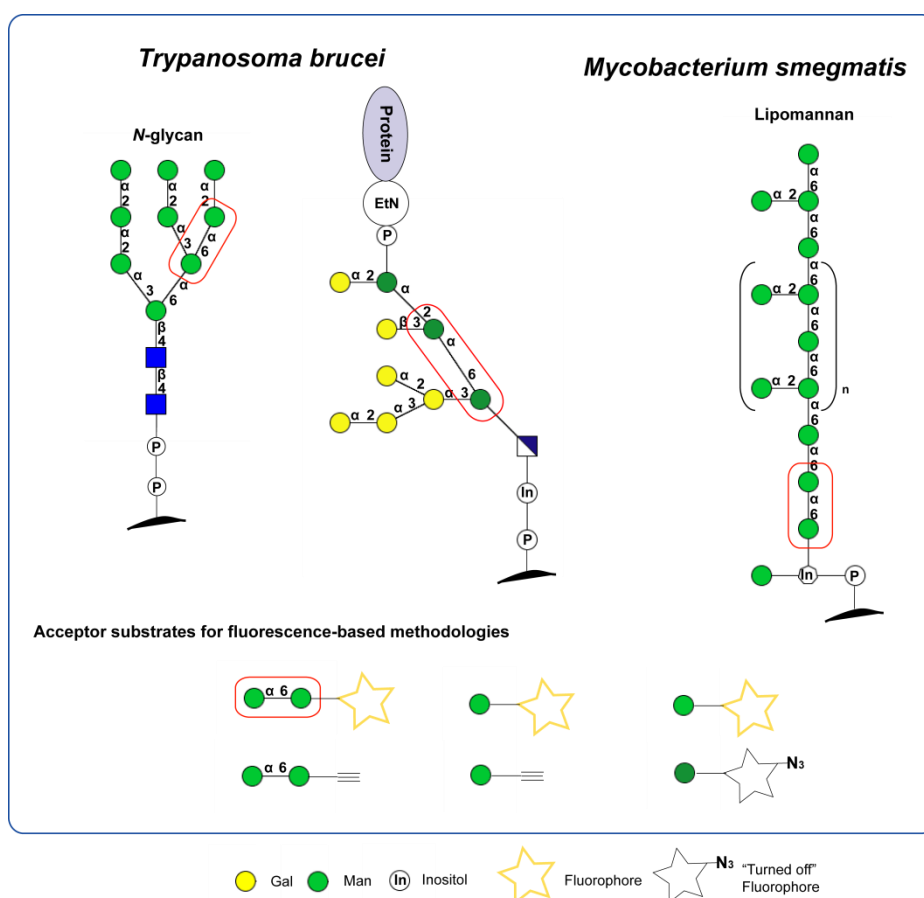


Figure 2.2 Schematic representation of structures of glycoconjugates from *Trypanosoma brucei* and *Mycobacterium smegmatis* and synthetic fluorescent and non-fluorescent glycoside acceptors to be used in detection of glycosyltransferase activities.

Previous research on the enzyme specificities of the Dol-P-Man:GlcNH₂-PI α -1,4-ManT, which is responsible for transfer of mannose residue to the GlcNH₂-PI intermediate during the GPI anchor biosynthesis in *Trypanosoma brucei*, showed that the acceptor substrate required the presence of full diacylglycerol structure.¹¹³ In these investigations, synthetic GlcN-inositol-glycerol substrate that lacks two fatty-acid components, showed much less enzymatic efficiency compared to the natural substrate D-GlcN- α -1,6-D-myoinositol (GlcN-PI) that contains 1,2-diacylglycerol fatty acid. The removal of glycerol or glycerol phosphate moieties from the synthetic acceptor further reduced enzymatic activities and the removal of inositol resulted in hardly any activities (Fig. 2.3). These data suggested that the presence of lipid moiety is important in substrate presentation and recognition by membrane bound enzymes.

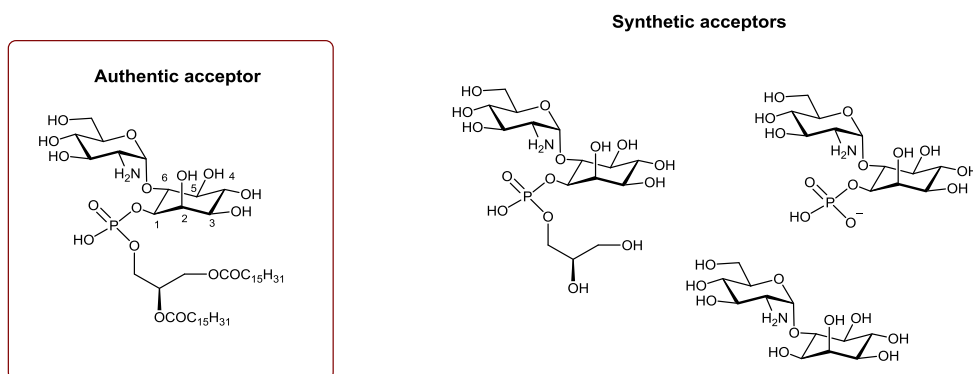


Figure 2.3 Authentic and synthetic acceptor substrate analogues of D-GlcN α -1,6-D-myoinositol-1-PO₄-sn-1,2-diacylglycerol utilised in the literature research.¹¹³

Other research on acceptor substrate specificities of the GlcNAc-phosphatidylinositol (GlcNAc-PI) de-*N*-acetylase enzyme present in *T. brucei* showed that a synthetic acceptor with a simple C18:0 alkyne chain in place of *sn*-1,2-dipalmitoylglycerol proved to be a better substrates.¹¹⁴ This suggests that the precise lipid structure and stereochemistry are not essential for substrate recognition in GlcNAc-PI de-*N*-acetylase. Furthermore, the alkyl chain can be replaced with steroidal moieties without decrease in the GlcNAc-PI de-*N*-acetylase activity.¹¹⁵ Evidently, if the lipid moiety provides enough hydrophobicity to associate with the lipid bilayer, the activity of this enzyme remained unperturbed.

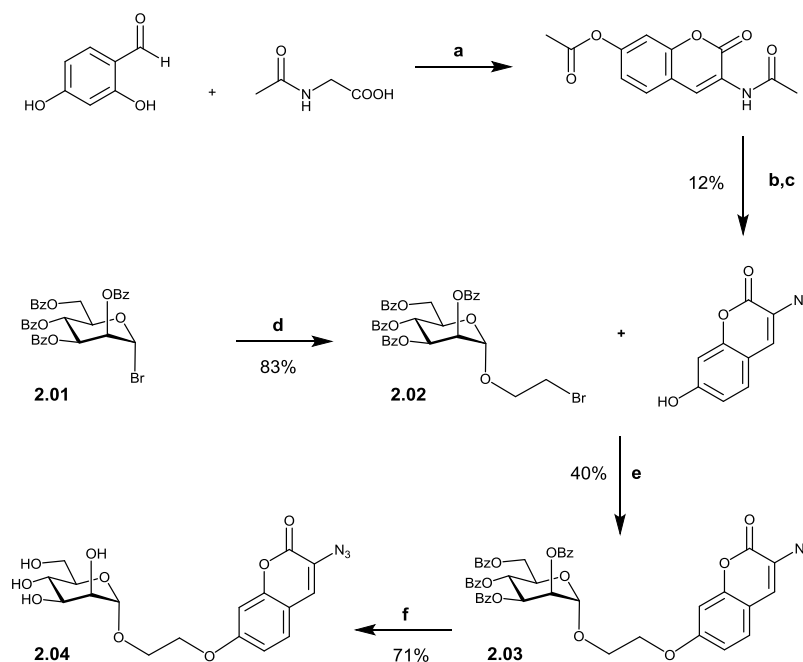
Based on these research data, all synthetic non-fluorescent and fluorescent acceptor substrates used in our fluorescence-based methodologies incorporated a hydrophobic aglycone (Fig. 2.4). This gives the desired experimental flexibility as well as provided opportunity to investigate the effect of aglycone hydrophobicity and bulkiness on

2.3 Chemical synthesis of non-fluorescent and fluorescent α -D-mannopyranoside derivatives for methodology I

In order to establish scope and limitations of fluorescence-based methodology I, the non-fluorescent α -Man-EtC (**2.04**) and fluorescent α -Man-EtTC (**2.05**) compounds were synthesised.

2.3.1 Chemical synthesis of non-fluorescent azidocoumarinyl α -D-mannopyranoside derivatives

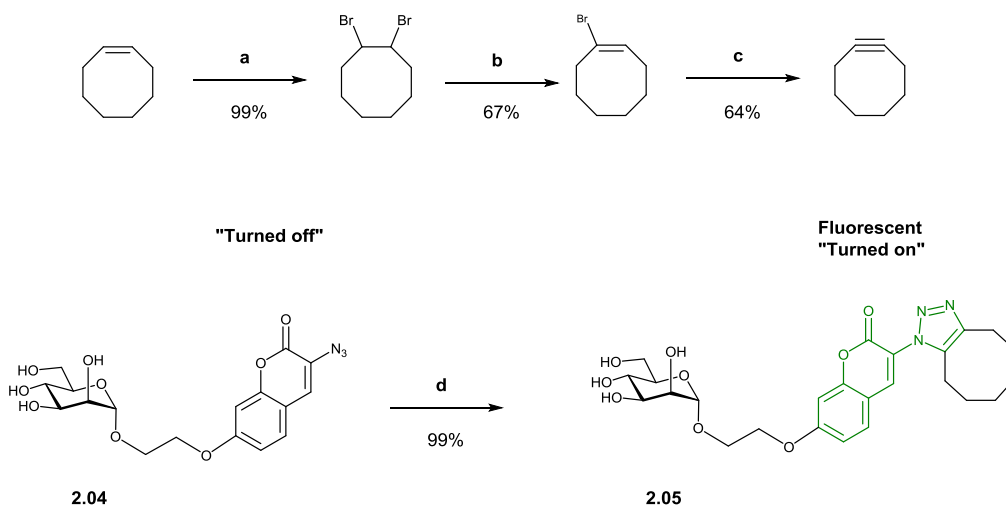
The 2-(3-azido-coumarin-7-yloxy)ethyl α -D-mannopyranoside (α -Man-EtC (**2.04**)) was synthesised from 2-bromoethyl mannoside (**2.02**) and 3-azido-7-hydroxycoumarin in three steps (Scheme 2.2). Known glycosyl bromide donor (**2.01**),¹¹⁶ was obtained by reaction of perbenzoylated mannose with HBr-AcOH in 97% yield. The glycosyl bromide donor (**2.01**) was activated with AgOTf and reacted with 2-bromoethanol to give α -glycoside **2.02** in 83% yield. The α -configuration of **2.02** was determined by ¹³C NMR spectroscopy of the anomeric carbon signal (δ_{C-1} 97.8 ppm, J_{C-H} =171.0 Hz).¹¹⁷ 3-Azido-7-hydroxycoumarin was synthesised through cyclisation, hydrolysis and diazotation of corresponding 2,4-dihydroxybenzaldehyde and *N*-acetylglycine following a literature procedure in 12% overall yield.¹¹⁸ Compound **2.02** was then treated with K₂CO₃ (modified Williamson ether synthesis)¹¹⁹ in the presence of 3-azido-7-hydroxycoumarin and 18-crown-6 to give **2.03** in a moderate 40% yield. De-*O*-benzoylation of **2.03** afforded target α -Man-EtC (**2.04**) in 71% yield.



Scheme 2.2 Synthetic route to 2-(3-azido-coumarin-7-yloxy)ethyl α -D-mannopyranoside. Reagents and conditions: a) NaOAc, Ac₂O, reflux; b) HCl/EtOH (v/v 1:1), reflux; c) NaNO₂, NaN₃, 0 °C; d) Bromoethanol, AgOTf, CH₂Cl₂; e) K₂CO₃, 18-crown-6, DMF; f) NaOMe, MeOH.

2.3.2 Chemical synthesis of fluorescent coumarinyl α -D-mannopyranoside derivative under strain-promoted click conditions

The hydrophobic aglycone of **2.04** incorporates a “turned off” 3-azido-7-hydroxycoumarin attached to the carbohydrate moiety through the 2xCH₂ linker. The exposed azido group is used to generate fluorescent **2.05** under the strain-promoted click conditions,¹⁰⁵ as depicted in Scheme 2.3. The synthesis of cyclooctyne was performed according to the literature procedure,¹²⁰ starting from commercially available cyclooctene, which was first dibrominated to form 1,2-dibromocyclooctane followed by two consecutive dehydrobrominations; first with KOt-Bu and then with lithium diisopropylamide (LDA) to afford the desired strained cyclic product. The fluorescent α -Man-EtTC (**2.05**) was then synthesised using strain-promoted reaction with cyclooctyne in almost quantitative yield. Product formation was evident from the appearance of new set of signals between 2.96 and 1.55 ppm in ¹H NMR spectrum that corresponded to six CH₂ groups of the triazole-fused cyclooctyne ring. It should be noted that compound **2.04** possessed limited stability at room temperature.



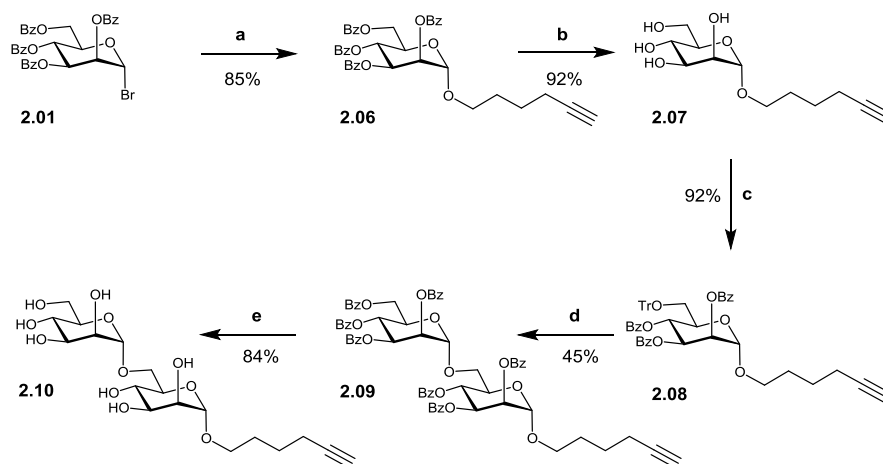
Scheme 2.3 Synthetic route to fluorescent coumarinyl α -D-mannopyranoside derivative through strain-promoted click conditions. Reagents and conditions: a) Br_2 , CH_2Cl_2 ; b) KOtBu , THF; c) LDA, THF, $-25\text{ }^\circ\text{C}$; d) cyclooctyne, MeOH, rt.

2.4 Chemical synthesis of non-fluorescent and fluorescent α -D-mannopyranoside derivatives for methodology II

To establish fluorescence-based methodology II, two non-fluorescent compounds, such as monosaccharide H- α -Man (**2.07**) and disaccharide H- α -Man α -1,6-Man (**2.10**) as well as two fluorescent compounds: α -Man-HTC (**2.12**) and α -Man-1,6- α -Man-HTC (**2.13**) were synthesised.

2.4.1 Chemical synthesis of non-fluorescent 5-hexynyl α -D-mannopyranoside derivatives

A non-fluorescent monosaccharide H- α -Man (**2.07**) was synthesised in two steps starting from known glycosyl bromide¹¹⁷ **2.01**, as outlined in Scheme 2.4. The glycosylation step was performed upon activation of **2.01** with halophilic promoter AgOTf ¹²¹ followed by reaction with 5-hexyn-1-ol, which gave α -glycoside **2.06** in 85% yield. The α -configuration of **2.06** followed from the characteristic anomeric carbon signal (δ 98.4 ppm, $J_{\text{C-H}}=171.9$ Hz) in the ^{13}C NMR spectrum.¹¹⁷ De-*O*-benzylation of **2.02** afforded target hexyn-5-yl α -D-mannopyranoside H- α -Man (**2.07**) in 92% yield.

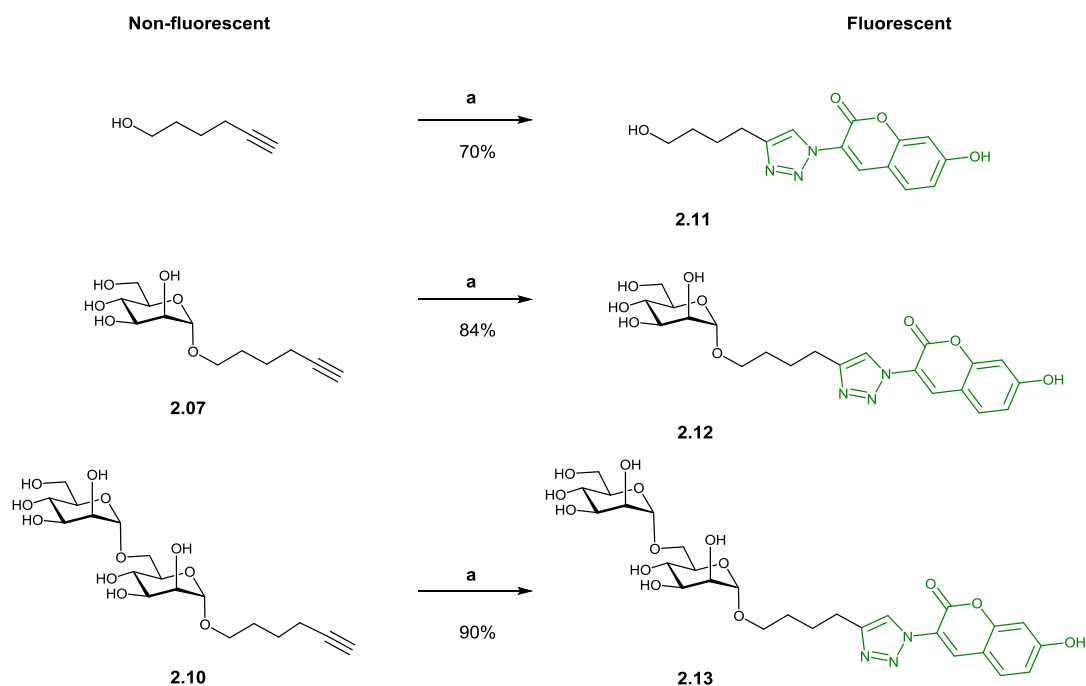


Scheme 2.4 Synthetic route to hexyn-5-yl α -D-mannopyranoside and hexyn-5-yl α -D-mannopyranosyl-1,6-O- α -D-mannopyranoside. Reagents and conditions: a) **2.01**, AgOTf, CH₂Cl₂, 5-hexyn-1-ol; b) NaOMe, MeOH; c) TrCl, DMAP, BzCl, Py; d) **2.01**, AgOTf, CH₂Cl₂, **2.08**; e) NaOMe, MeOH.

Non-fluorescent disaccharide H- α -Man α -1,6-Man (**2.10**) compound was synthesised in three steps using α -glycoside **2.07** as a starting material (Scheme 2.4). The 6-OH group of **2.07** was regioselectively protected with trityl group followed by per-*O*-benzoylation to afford **2.08**, which was isolated in 92% yield. AgOTf-promoted glycosylation of **2.08** with glycosyl bromide **2.01** gave α -glycoside **2.09** in 45% yield. De-*O*-benzoylation of **2.09** afforded target H- α -Man α -1,6-Man (**2.10**) in 84% yield. The α -configuration of **2.10** was confirmed by the anomeric carbon signal ($J_{C-H} = 171$ Hz) in the ¹³C NMR spectrum.

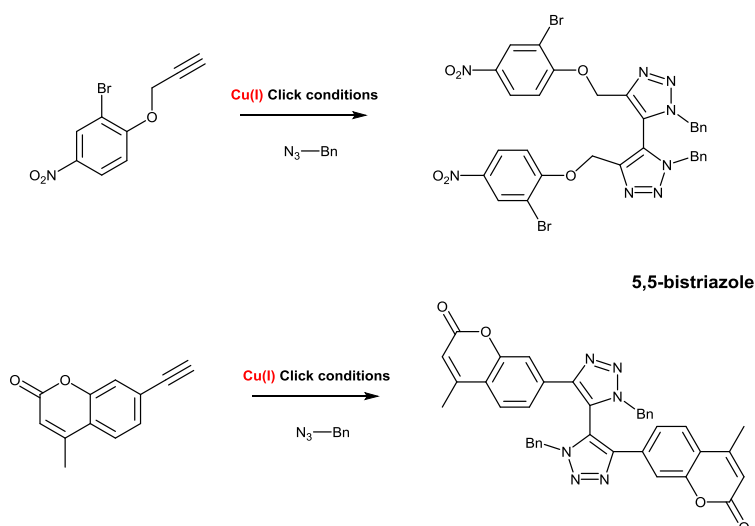
2.4.2 Chemical synthesis of fluorescent coumarinyl α -D-mannopyranoside derivatives under Cu(I)-catalysed click conditions

The alkyne functional group on the 5-hexyn-1-ol, H- α -Man (**2.07**) and H- α -Man α -1,6-Man (**2.10**) was employed to attach a non-fluorescent 3-azido-7-hydroxycoumarin to generate fluorescent HTC (**2.11**), α -Man-HTC (**2.12**) and α -Man-1,6- α -Man-HTC (**2.13**) as outlined in Scheme 2.5.



Scheme 2.5 Synthetic routes to fluorescent coumarinyl α -D-mannopyranoside derivatives through Cu(I)-catalysed click conditions. Reagents and conditions: a) 3-azido-7-hydroxycoumarin, CuSO₄/NaAsc, MeOH/H₂O (1:1), rt.

Fluorescent 1,4-triazole-linked HTC (**2.11**), α -Man-HTC (**2.12**) and α -Man-1,6- α -Man-HTC (**2.13**) were synthesised using Cu(I)-catalysed click reactions of alkyne precursors with 3-azido-7-hydroxycoumarin, the synthesis of which is described in section 2.3.1. These reactions were generally complete after 2 h at room temperature, resulting in good yields (70-90%) (Scheme 2.5). The 1,4-triazole ring formation was confirmed by the presence of singlets at δ 8.24 ppm for HTC (**2.11**), δ 8.17 ppm for α -Man-HTC (**2.12**) and δ 8.5 ppm for α -Man-1,6- α -Man-HTC (**2.13**) in ¹H NMR spectra; peaks at around 122.3 and 124.2 ppm in ¹³C NMR spectra further confirmed formation of triazole rings. The efficiency of all three reactions were affected by formation of by-products with R_f values in each case slightly lower compared to R_f values of the desired products but identities of these by-products were not pursued. The reported data in literature with related alkyne coumarin-based fluorophores¹²² and other azido-alkyne compounds¹²³ also indicated formation of a by-product under Cu-(I)-catalysed click conditions. This by-product was isolated and shown to have a 5,5-bistriazole structure, which can form as a major product under basic conditions (Scheme 2.6).^{123, 124} In our synthesis this is not be the case because the R_f value of bistriazole compound would differ by TLC significantly.



Scheme 2.6 Reaction schemes of azido-alkyne compounds leading to formation of 5,5-bistriazole by-products under Cu(I)-catalyzed click conditions as described in the literature.^{123, 124}

2.5 Spectroscopic studies of fluorescent coumarinyl α -D-mannopyranoside derivatives

The photophysical properties of α -Man-EtTC (**2.05**) and α -Man-1,6- α -Man-HTC (**2.13**) only were investigated in this study as these compounds have different substituents attached at the 3- and 7- positions of the coumarin scaffold and modifications at these sites have been shown to have a strong impact on photophysical properties.⁹⁴ Investigation of structure and optical properties of coumarin-based fluorophores showed that the extension of the π -system with an aromatic group at the 3-position and the electron donating group, such as an amino group, at 7-position resulted in compounds with the highest quantum yields (Fig. 2.5).⁹⁴

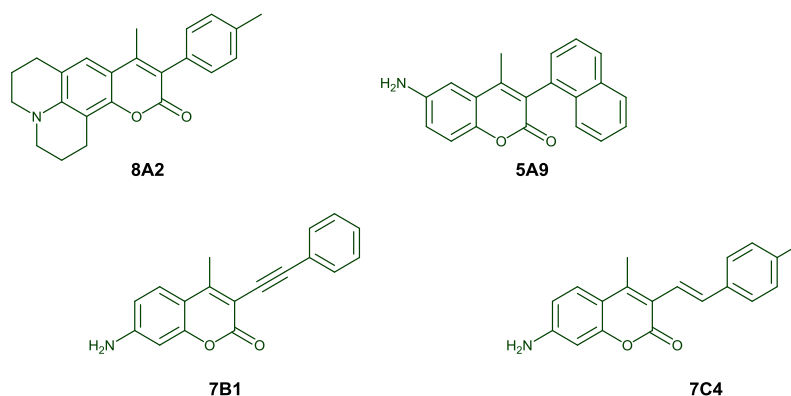


Figure 2.5 Coumarin-derived fluorophores with the highest quantum yield described in the literature.⁹⁴ Photophysical properties of depicted compounds in ethanol 8A2 ($\lambda_{\text{abs}} = 395$ nm, $\lambda_{\text{em}} = 478$ nm, $\phi_f = 0.90$), 7C4 ($\lambda_{\text{abs}} = 393$ nm, $\lambda_{\text{em}} = 480$ nm, $\phi_f = 0.62$), 5A9 ($\lambda_{\text{abs}} = 373$ nm, $\lambda_{\text{em}} = 535$ nm, $\phi_f = 0.18$) and 7B1 ($\lambda_{\text{abs}} = 397$ nm, $\lambda_{\text{em}} = 455$ nm, $\phi_f = 0.98$) External standard 9,10-diphenylanthracene ($\phi_f = 0.95$ in cyclooctene).

In our case, both α -Man-EtTC (**2.05**) and α -Man-1,6- α -Man-HTC (**2.13**) compounds have electron donating groups at the 7-position and at the 3-position the π -system of α -Man-EtTC (**2.05**) compound is extended through triazole ring connected to cyclooctene and of α -Man-1,6- α -Man-HTC (**2.13**) compound is extended through the triazole ring connected to the alkyne (Fig. 2.6). These structural differences could influence photophysical properties of these compounds. In contrast, carbohydrate moieties, which are well separated from the fluorophore in **2.05** and **2.13** should impose no influence on photophysical properties of the fluorophore.¹²⁵ Fluorescent derivatives HTC (**2.11**) and α -Man-HTC (**2.12**) were omitted from this investigation due to the structural similarity with α -Man-1,6- α -Man-HTC (**2.13**).

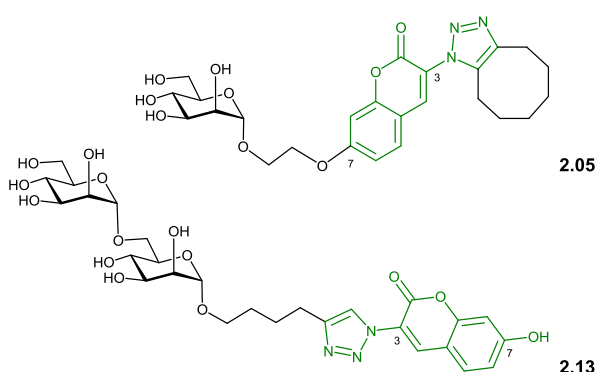


Figure 2.6 Structural differences of fluorescently labelled coumarinyl α -D-mannopyranoside derivatives can affect their photophysical properties.

Spectral characterisation of **2.05** and **2.13** were performed in methanol due to limited aqueous solubility and water, respectively at concentration (10×10^{-5} M) at room temperature. The structural differences associated with coumarin fluorophore as described above showed a direct influence on the photophysical properties of **2.05** and

2.13 that are reflected in the values obtained for the UV-vis absorbance, extinction coefficient, fluorescence excitation, emission and Stokes shift (Table 2.2). The emission of **2.05** at 405 nm gives rise to a blue colour, whereas the emission of **2.13** at 469 nm associates with the intense green colour in solutions (Fig. 2.7 A1 and A2). The separation between excitation and emission peaks in **2.05** is greater compared to **2.13** which results in a larger Stokes shift (Fig 2.7 B1 and B2). Obtained values of extinction coefficients for both compounds could assist with the estimation of product concentration of purified samples in later fluorescence-based methodologies as required.

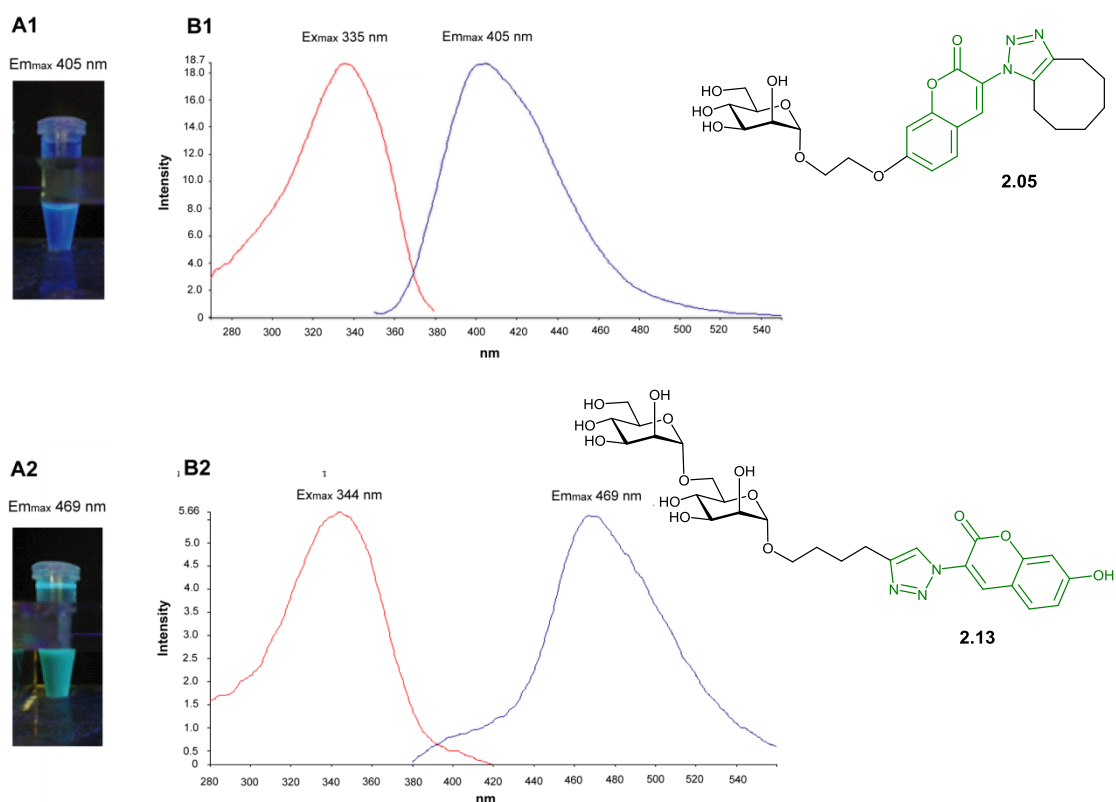


Figure 2.7 Fluorescent properties of coumarinyl α -D-mannopyranoside derivatives. (A) Visual fluorescence of coumarinyl α -D-mannopyranoside derivatives in solution (A1) **2.05** and (A2) **2.13**; (B) The excitation and emission spectra (B1) **2.05** (10×10^{-5} M) in water and (B2) **2.13** (10×10^{-5} M) in MeOH.

	Absorption λ (nm)	Extinction coefficient ϵ ($M^{-1}cm^{-1}$)	Excitation λ E_{xmax} (nm)	Emission λ E_{mmax} (nm)	Stokes shift $\Delta\lambda$ (nm)
2.05	336	19300	335	405	70
2.13	344	10302	347	469	122

Table 2.2 Photophysical properties of fluorescently labelled coumarinyl α -D-mannopyranoside derivatives.

The presence of a free hydroxyl group at the 7-position of the coumarin ring makes the fluorophore pH sensitive and affects the fluorescence intensity as the pH level changes from neutral to basic. The pH dependence of fluorescence in **2.05** and **2.13** were investigated by preparing solutions of known concentration using “universal” buffer (0.04 M H₃BO₃, H₃PO₄ and CH₃COOH) in the range of pH from 2 to 11. Subsequently, fluorescence intensities of each solution at different pH were measured and data analysed (Fig. 2.8 A).

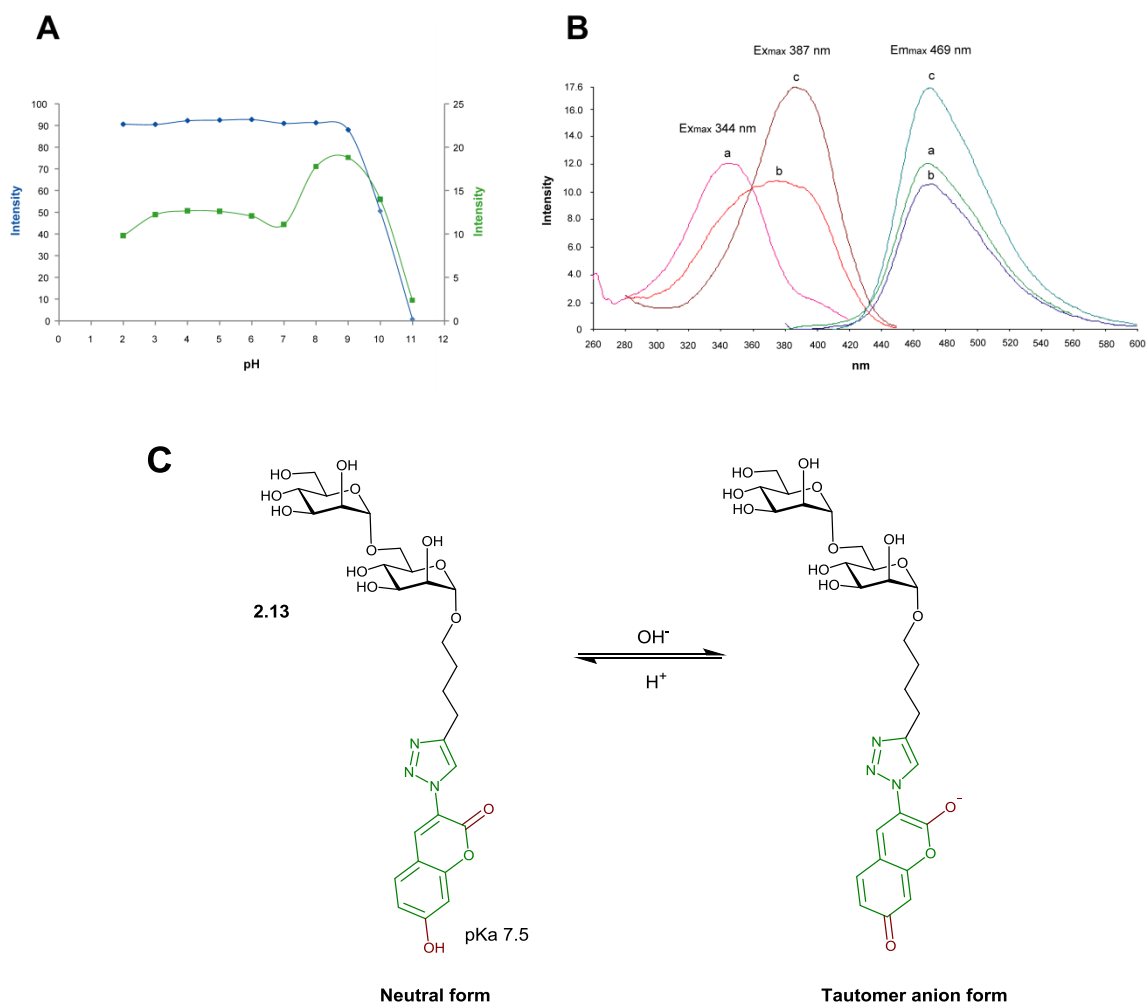


Figure 2.8 The effect in change of pH level on the fluorescent properties of coumarinyl α -D-mannopyranoside derivatives. (A) The pH dependence on fluorescence intensities in the presence and absence of hydroxyl group at the 7-position on the coumarin ring. (Blue trace) **2.05** (20×10^{-6} M) Em_{max} 405 nm and (Green trace) **2.13** (20×10^{-7} M) Em_{max} 469 nm. (B) Excitation and emission spectra of **2.13** to represent the bathochromic shift. Solutions of **2.13** (20×10^{-7} M) were prepared using universal buffer (a) pH 6; (b) pH 7; (c) pH 8. (C) Equilibrium between neutral and anion tautomer forms of **2.13** that occur with change in pH level from neutral to basic.

Fluorescence intensity of **2.13** slightly increases from pH 7 reaching its highest at pH 9 (Fig. 2.8 A green trace). This observation can be explained by the deprotonation of the hydroxyl group as the pH level changes from neutral to basic, leading to formation of new tautomer anion species that possesses a different excitation optimum resulting in

slight increase of fluorescent intensity at pH 9 (Fig. 2.8 C).¹²⁶ In contrast, no significant changes in the fluorescence intensity of **2.05** were detected as pH level increased because it lacks free hydroxyl group on the coumarin scaffold (Fig. 2.8 A blue trace). The decrease in the fluorescent intensity at pH above 10 for both **2.05** and **2.13** could be due to lactone ring hydrolysis. The fully deprotonated new tautomer anion species of **2.13** causes the bathochromic shift of excitation wavelength from 347 nm at pH 2-6 to 367 nm at pH 7 and to 387 nm at pH 8-10 (Fig. 2.8 B). The emission wavelength remains at 469 nm despite the change in the excitation wavelength.

In fluorescence-based methodology II the progress of enzymatic reaction would be visualised on the TLC plate; therefore the fluorescent intensity of **2.13** and its enzymatic products could be enhanced, as required, by spraying the TLC plate with basic solution prior visualisation.¹¹²

2.6 Examination of detection limits of fluorescently labelled coumarinyl α -D-mannopyranoside derivatives

2.6.1 TLC analyses

The lowest amounts of fluorescent α -Man-EtTC (**2.05**) and α -Man-1,6- α -Man-HTC (**2.13**) compounds that could be detected on TLC plates using UV-light were determined in the series of experiments.

The fluorescent method of detection was then compared to orcinol staining, which is a standard method of carbohydrate detection.¹²⁷ For this purpose solutions of **2.05** and **2.13** in a wide range of concentrations were prepared and 2 μ L aliquots were loaded onto glass-backed TLC plates containing no fluorescent indicator. Each TLC plate was eluted with an appropriate solvent system and then visualised with a mid-wave length UV light for fluorescence detection (Fig. 2.09 A1 and A2) and then stained with orcinol for standard carbohydrate detection (Fig. 2.09 B1 and B2). The results indicated that the fluorescent method of detection for **2.05** and **2.13** is ca. 100 fold more sensitive than orcinol staining, allowing detection of fluorescent mannoside acceptors at the 25 ng or 40 pmols level for **2.13** and 20 ng or 40 pmols for **2.05**. Values obtained with fluorescence method of detection are lower compare to the typical limits of detection using radiolabelling.

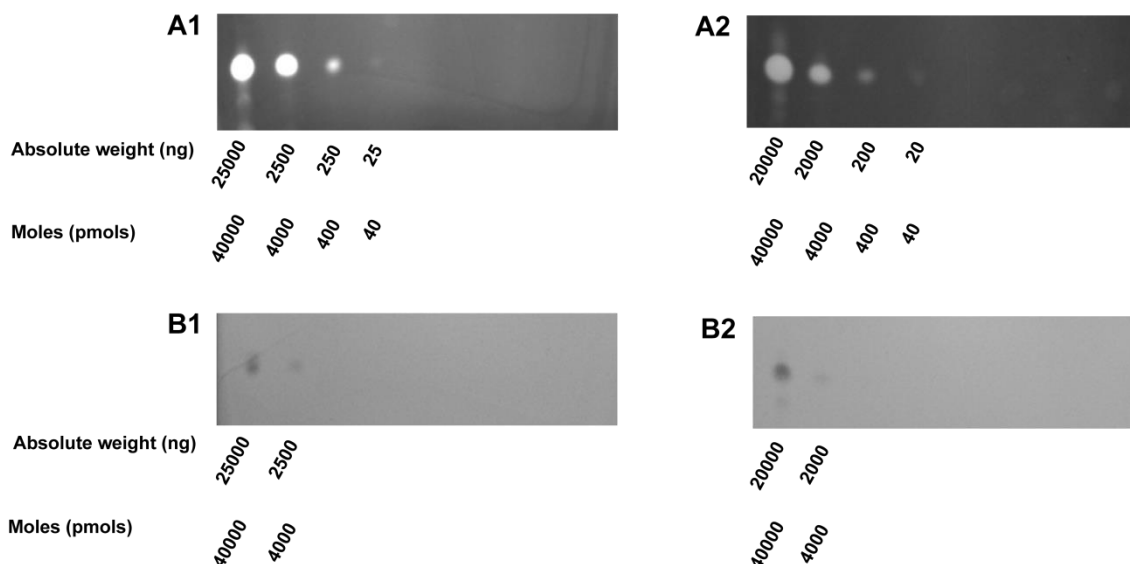


Figure 2.9 Comparison of TLC detection range of fluorescently labelled coumarinyl α -D-mannopyranoside derivatives. (A) The TLC plate visualised with mid-wave length UV light (**A1**) **2.13** and (**A2**) **2.05**. (B) The TLC plate developed with orcinol staining (**B1**) **2.13** and (**B2**) **2.05**. TLC conditions: 2 μ L of 2×10^{-2} M, 2×10^{-3} M, 2×10^{-4} M, 2×10^{-5} M aliquots in water for **2.13** and in MeOH for **2.05** were loaded onto the TLC and eluted with (CH_2Cl_2 :MeOH:H₂O (80:20:3)) for **2.13** and (CH_2Cl_2 :MeOH (9:1)) for **2.05**.

2.6.2 Solution analyses

In order to achieve quantification of fluorescently labelled glycoside products obtained from the enzymatic biotransformation the detection limits of α -Man-EtTC (**2.05**) and α -Man-1,6- α -Man-HTC (**2.13**) were examined in solution (Fig 2.10).

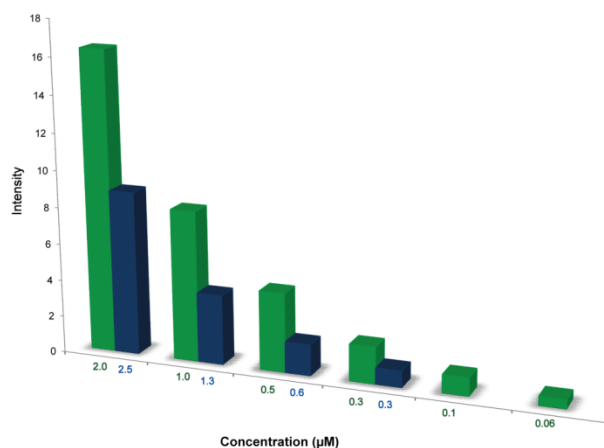


Figure 2.10 The detection range of fluorescently labelled coumarinyl α -D-mannopyranoside derivatives in solution. (■) Solution of **2.13** pH 9 (universal buffer), Ex_{max} 344 nm, Em_{max} 469 nm; (■) Solution of **2.05** pH 6 (universal buffer), Ex_{max} 335 nm, Em_{max} 405 nm;

As for results described in section 2.5 a range of concentrations of **2.05** and **2.13** were prepared at the pH level with the highest fluorescence intensity observed, for **2.13** at pH

9 and for **2.05** at pH 6. The fluorescence intensity was measured as the concentration of each compound decreased. The analysis of results showed that concentrations as low as 0.06 μM for **2.13** and 0.3 μM for **2.05** could be detected in solution.

2.7 Validation of fluorescence-based methodologies against established radiolabelled assay

In order to develop fluorescence-based methodologies the initial validation and benchmarking against published protocols of radiolabelled assays utilised to investigate the biosynthesis of cell surface glycoconjugates in *Mycobacterium smegmatis* was performed. In these studies we targeted α -1,6-ManT responsible for the biosynthesis of lipomannan in *Mycobacterium smegmatis*.

2.7.1 Insight into studying biosynthesis of glycoconjugates in mycobacteria

Pathogenic *Mycobacterium tuberculosis* is the causative agent of tuberculosis (TB). According to the World Health Organisation it infects about 9.0 million and kills 1.5 million people worldwide every year. Treatments for this disease with four front-line drugs, such as isoniazid, rifampicin, pyrazinamide and ethambutol, are often require administration of several drugs for a long period of time, which leads to the development of multiple drug-resistant and extremely drug-resistant mycobacterial strains, making the development of new drugs even more essential.¹²⁸ Difficulties in treatment of TB arise from the unique structure of the mycobacterial cell wall, which is composed of peptidoglycans, arabinogalactans, long fatty acids (mycolic acids), glycolipids and lipoglycans that are tightly packed side by side and layered on top of the plasma membrane. This hydrophobic complex layer around the cell wall provides mycobacterial species with a formidable permeability barrier to hydrophobic drugs and other harmful substances.¹²⁹ Intervention with the biosynthesis of any of these components through understanding the specificity of the glycosyltransferases involved could lead to new antimicrobial drugs. Lipoarabinomannan (LAM), lipomannan (LM) and phosphatidyl-*myo*-inositol mannoside (PIM) are major components of mycobacterial cell wall that have been extensively studied (see section 1.2.2). The terminal capping motif of the LAM has shown to contribute to the survival of *M. tuberculosis* in the host through regulating the host immune responses by interaction with different host receptors in the course of TB.²⁸ Compounds that prevent the formation and installation of these capping motives should have potential as anti TB agents.

2.7.2 Literature radiolabelled assay to probe α -1,6-mannosyltransferase activities responsible for the biosynthesis of LAM in mycobacterial species

The proposed biosynthesis of mycobacterial LAM follows a linear pathway starting from a decoration of phosphatidyl-*myo*-inositol (PI) with four mannose residues to give phosphatidyl-*myo*-inositol mannoside (PIM₄), which is then elaborated to linear α -1,6-linked LM and further decorated with α -1,2-linked single mannose residue to form mature LM and finally the addition of arabinose moieties completes the biosynthesis of LAM (see Chapter 1 section 1.2.2).¹³⁰ The biosynthesis of linear α -1,6-linked LM involves several α -1,6-mannosyltransferases. The first two α -1,6-ManT enzymes (PimA and PimB) catalyse the transfer of mannose residue from the soluble GDP-Man donor to PI to form PIM₂ intermediate. While another two recently identified α -1,6-ManT enzymes (MptB and MptA) involved in the elongation of linear α -1,6-linked LM and catalyses transfer of mannose residue from the lipid linked polyprenyl-phosphate-mannose (P-P-Man) donor to PIM₄ intermediate (Fig. 2.11). Another set of mannosyltransferases that catalyse transfer of mannose residue from GDP-Man donor to a variety of polyprenol monophosphate donors are also present and can be inhibited by amphomycin in the presence of calcium ion through chelation with polyprenol monophosphate.¹³¹

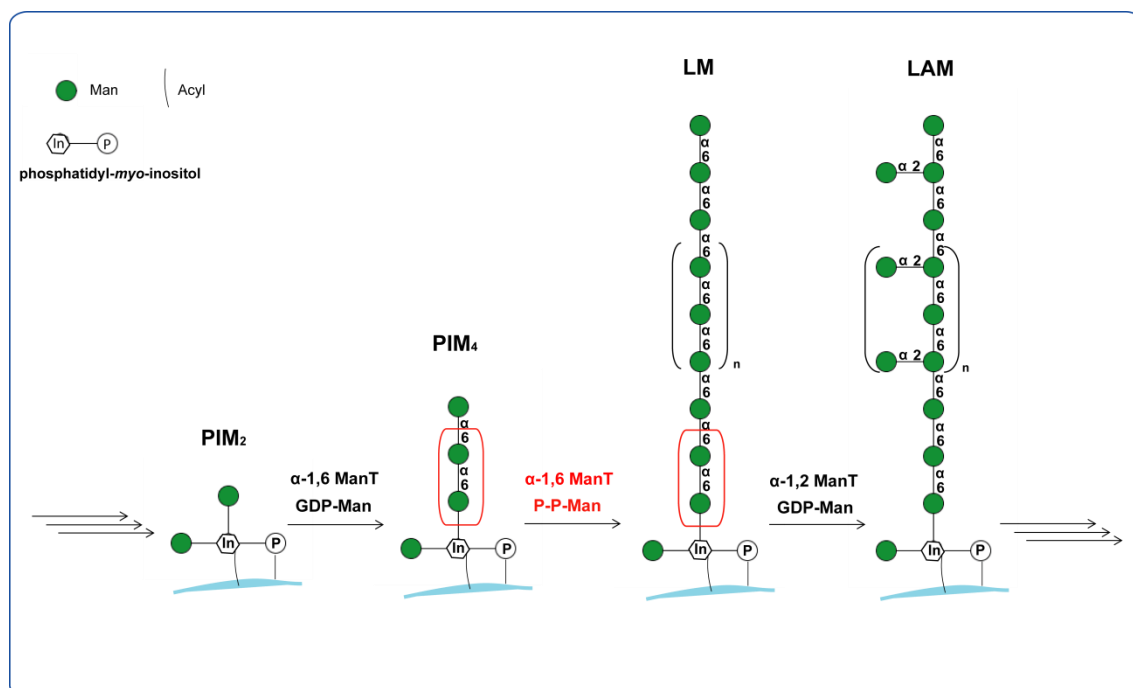


Figure 2.11 Diagrammatic representation of lipoarabinomannan biosynthesis in *Mycobacterium smegmatis*. The red box area indicates the site of authentic intermediate mimicked by the synthetic acceptors used in the literature radiolabelled assays.

In order to understand the biosynthesis of LAM, cell-free radiolabelled assays were developed by Dr. Brown and used in Professor Besra's group to study the biosynthetic pathways and substrate specificities of these glycosyltransferases in mycobacterial species.^{132, 133} One of these radiolabelled assay that looked at the substrate activities of chemically synthesised substrates for ManT responsible for elongation of LM structure was used to benchmark our fluorescence-based methodologies.⁸⁷ In their study, chemically synthesised compounds, such as octyl 6-*O*- α -D-mannopyranosyl- α -D-mannopyranoside (**2.14**) and octyl 6-*O*- α -D-mannopyranosyl-1-thio- α -D-mannopyranoside (**2.15**) (Fig. 2.12) were designed to mimic LM intermediates and to target α -1,6-ManT (MptB and MptA) involved in the elongation of α -1,6-linked LM. During these assays acceptor substrates were incubated with the radiolabelled GDP-[¹⁴C]Man in the presence of *M. smegmatis* membranes. [*M. smegmatis* is a fast growing non-pathogenic bacterium that has a similar cell wall composition to the *M. tuberculosis* and is used as a model organism.]

Acceptor substrates used in the literature radiolabelled assays

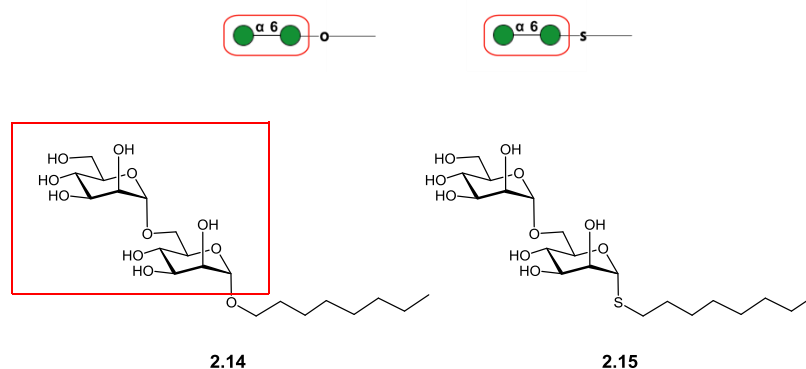


Figure 2.12 Structure of acceptor substrates used in the literature cell-free radiolabelled assays. (Top image) The diagrammatic representation of acceptor substrates. The red box area indicates the site of authentic intermediate mimicked by the synthetic acceptors.

The reported results demonstrated that both compounds acted as acceptor substrates for these enzymes, leading to formation of two radiolabelled mannoside products, as evaluated by HPTLC and autoradiography. The nature of α -1,6-glycosidic linkage in these assays has been confirmed through *exo*-glycosidase digestion and permethylation analysis by GC-MS, which indicated formation of a major α -1,6-linked trisaccharide and minor α -1,6-linked tetrasaccharide radiolabelled products. Therefore, in order to benchmark our fluorescence-based methodologies we were looking to obtain similar results.

2.7.3 Fluorescence-based methodologies to probe α -1,6-mannosyltransferase activities in *Mycobacterium smegmatis*

The immediate question that we wanted to ask through the initial benchmarking against the above radiolabelled assays was which of our non-fluorescent and fluorescent mannoside compounds could act as acceptor substrates for α -1,6-mannosyltransferases present in *M. smegmatis* membranes? Could we observe formation of the two products, as described in the cell-free radiolabelled assays and/or could our acceptors be more effective substrates and extended beyond a tetramer? In what way does the length and hydrophobicity of aglycone affect the efficiency of α -1,6-ManT activities and finally could we detect α -1,2-ManT with our acceptor substrates? In an attempt to answer these questions, two chemically synthesised non-fluorescent compounds α -Man-EtC (**2.04**) and H- α -Man- α -Man (**2.10**) and two fluorescent compounds α -Man-EtTC (**2.05**) and α -Man-1,6- α -Man-HTC (**2.13**) were chosen to be examined. Each methodology included one fluorescent and one non fluorescent compound (Fig. 2.13).

Acceptor substrates for fluorescence-based methodologies

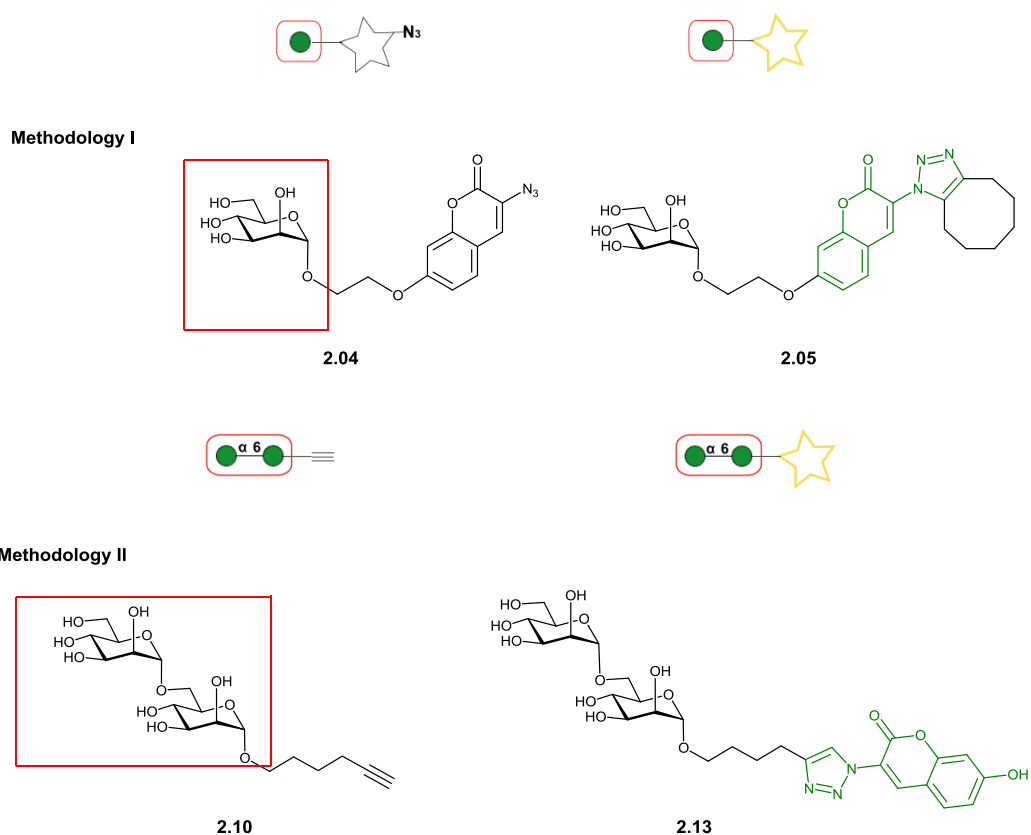


Figure 2.13 Structures of non-fluorescent and fluorescent compounds used to benchmark fluorescence-based methodology I and II against literature radiolabelled assay. The red box area indicates the site of authentic intermediate mimicked by the synthetic acceptors.

Mycobacterial membranes, kindly donated by Professor Besra's group, were obtained by growing *M. smegmatis* (strain mc²155) in media (Bacto Nutrient Broth) to mid-log phase (about 24 h). The harvested cells were then lysed, centrifuged to remove larger cell particles and ultracentrifuged to obtain the required mycobacterial membranes.⁸⁷ Compounds **2.04**, **2.05**, **2.10** and **2.13** were incubated with GDP-Man in the presence of washed mycobacterial membranes under the same conditions used in the radiolabelled assays. The progress of each enzymatic reaction for both methodology I and II, during 18 h and 29 h of incubation at 37 °C, was monitored by TLC.

2.7.4 TLC results from the fluorescence-based methodology I

During enzymatic assays 20 µL aliquots at 20 min, 40 min, 60 min, 2 h, 4 h and 18 h were taken and stopped by addition of methanol-chloroform (1:1). Reaction mixtures (2 µL) of each time point, from the non-fluorescent α -Man-EtC (**2.04**) acceptor, were applied onto the TLC plate and eluted. In order to visualise the progress of enzymatic reaction from the non-fluorescent acceptor substrate the TLC plate was sprayed with the solution of cyclooctyne in EtOAc (1:1) and visualised under UV light (Fig. 2.14 A). Reaction mixtures (2 µL) of each time point from the fluorescent α -Man-EtTC (**2.05**) acceptor were applied onto the TLC, eluted and visualised without further manipulations (Fig. 2.14 B).

TLC analysis of enzymatic reactions with non-fluorescent and fluorescent acceptors showed no enzymatic transformations. The TLC plate from the incubation of **2.05** contained one faint fluorescent band with lower R_f value compared to the starting acceptor. This fluorescent band was associated with formation of some degradation product (DP) which was formed after 18 h of incubation at 37 °C. In the event of formation of disaccharide product the expected R_f value would be lower compared to the observed value of the degradation product when utilising this eluent system. According to these results no further analysis of these reaction mixtures were performed.

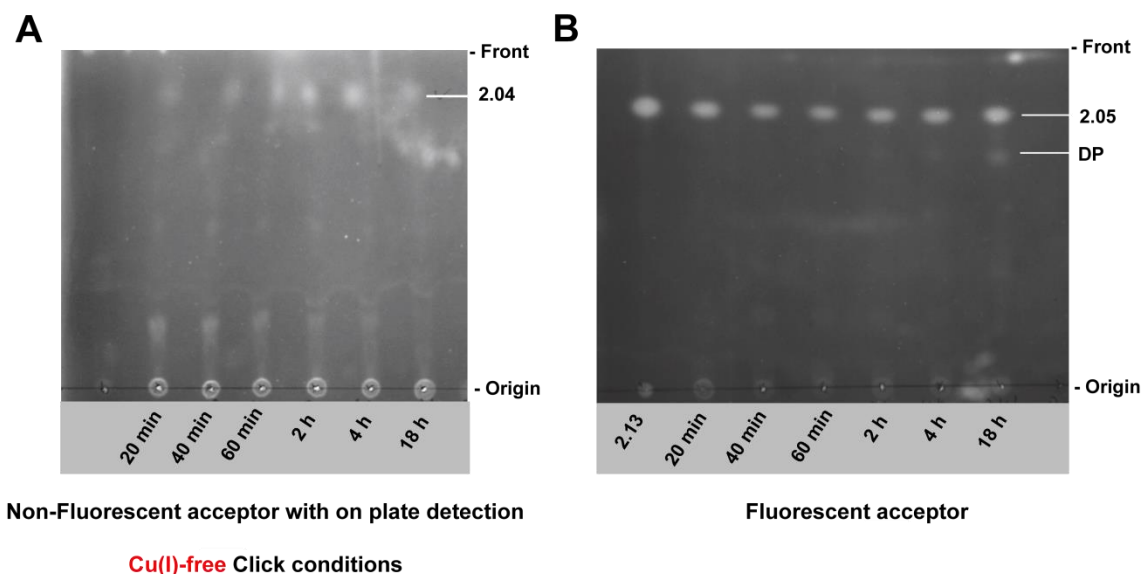


Figure 2.14 TLC analyses of enzymatic assays of non-fluorescent and fluorescent mannoside acceptors to detect mannosyltransferase activities in *Mycobacterium smegmatis* membranes using fluorescence-based methodology I. (A) The TLC plate features reaction mixtures of a non-fluorescent acceptor (**2.04**) after fluorescent labelling with cyclooctyne; (B) The TLC plate features reaction mixtures of a fluorescent acceptor (**2.05**). Assay conditions: acceptor substrate (0.5 mM); GDP-Man (1 mM); reaction buffer MOPS/KOH (50 mM, pH 7.9), MgCl₂ (10 mM), DTT (5 mM); *M. smegmatis* microsomal membranes (50 μ L, 500 μ g of total protein); Total reaction volume of 200 μ L. TLC plates were eluted with CH₂Cl₂:MeOH:H₂O (6:4:1) and visualised using mid-wave length range UV light. Reaction time points are shown below the corresponding TLC image and starting acceptors and DP (degradation product) are shown to the left of the TLC image.

2.7.5 TLC results from the fluorescence-based methodology II

During enzymatic assays 20 μ L aliquots at 2 h, 4 h, 6 h, and 29 h were taken and stopped by addition of methanol-chloroform (1:1). Subsequently, each reaction mixture incorporating non-fluorescent H- α -Man- α -1,6-Man (**2.10**) acceptor was made fluorescent in solution by addition of 3-azido-7-hydroxycoumarin, catalytic CuSO₄ and sodium ascorbate (NaAsc). The Click reactions continued overnight to ensure complete fluorescent labelling of starting compound and possible products. In order to visualise the progress of enzymatic reaction 2 μ L from each aliquot were spotted onto the TLC plate that were eluted and visualisation under the UV light (Fig. 2.15 A). Enzymatic reactions that involved fluorescent α -Man-1,6- α -Man-HTC (**2.13**) acceptor were visualised on the TLC plate without further modifications (Fig. 2.15 B). The fluorescent labelling of H- α -Man- α -1,6-Man (**2.10**) under Cu(I)-catalysed click conditions with coumarin-based fluorophore should generate fluorescent α -Man-1,6- α -Man-HTC (**2.13**) and fluorescent products that would be expected to have the same structures as fluorescent products obtained from **2.13** (Fig. 2.15 C).

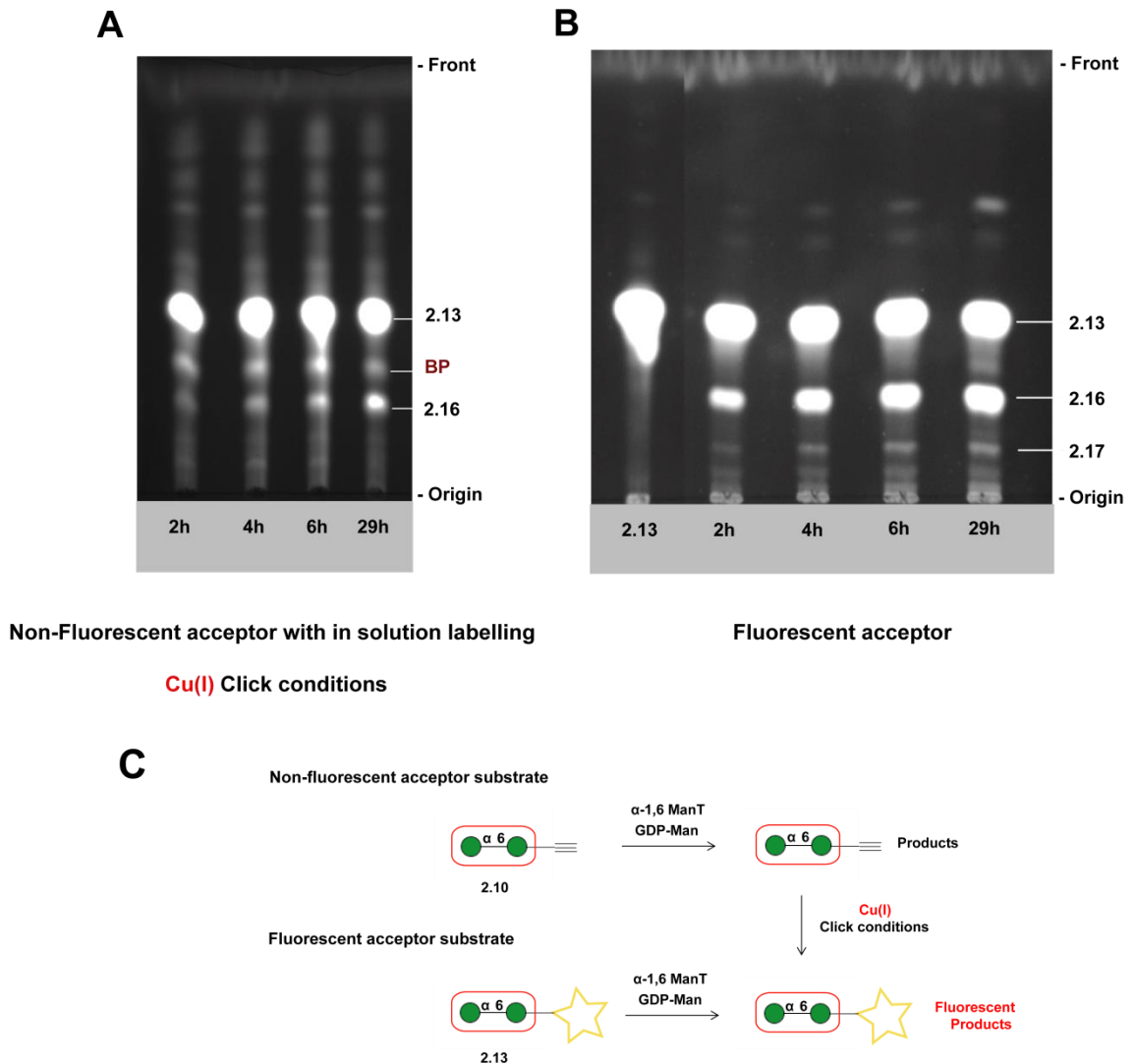


Figure 2.15 TLC analyses of enzymatic assays of non-fluorescent and fluorescent mannoside acceptors to detect mannosyltransferase activities in *Mycobacterium smegmatis* microsomal membranes using fluorescence-based methodology II. (A) The TLC plate features reaction mixtures of a non-fluorescent acceptor (**2.10**) after fluorescent labelling with 3-azido7-hydroxycoumarin; (B) The TLC plate features reaction mixtures of a fluorescent acceptor (**2.13**); Assay conditions: acceptor substrate (1 mM), GDP-Man (4 mM), reaction buffer MOPS/KOH (50 mM, pH 7.9), MgCl₂ (10 mM), DTT (5 mM); *M. smegmatis* microsomal membranes (250 μ L, 4000 μ g of total protein); Total reaction volume of 1 mL. (A) TLC plates were eluted with CHCl₃:MeOH:H₂O (10:6:1) visualised using mid-wave length range UV light. Reaction time points are shown below the corresponding TLC image and starting acceptors and products are shown to the left of the TLC image. (BP) by-product. (C) Schematic representation of reaction mixture obtained from **2.10** leading to the same products as from **2.13** after fluorescent labelling occurred.

TLC analysis of enzymatic reaction obtained from H- α -Man- α -1,6-Man (**2.10**) showed formation of two new fluorescent bands (Fig. 2.15 A). The fluorescent band with the lowest R_f value began to form after 2h incubation with a gradual increase in intensity through to 29 h of incubation. This fluorescent band was tentatively assigned as a trisaccharide (**2.16**) product with a possible transfer of one mannose residue to the non-fluorescent H- α -Man- α -1,6-Man (**2.10**) acceptor. The second fluorescent band between the acceptor and product had the same fluorescent intensity at each time point. This

fluorescent band was attributed to the formation of by-product (BP) which has been observed previously when synthesising the fluorescent compounds using Cu(I)-catalysed click conditions (see section 2.4.2).

TLC analysis of the enzymatic reaction from α -Man-1,6- α -Man-HTC (**2.13**) acceptor also showed formation of two new fluorescent bands (Fig. 2.15 B). The most intense band below the starting acceptor was tentatively assigned to formation of trisaccharide (**2.16**) product and the less intense band with the lower R_f value was assigned as tetrasaccharide (**2.17**) product. The fluorescent band of trisaccharide products had the same R_f value on TLC plates obtained from both incubation of H- α -Man- α -1,6-Man (**2.10**) and α -Man-1,6- α -Man-HTC (**2.13**), indicating that the presence and absence of fluorescent aglycone in the acceptor did not influence which glycosyltransferases were targeted. Fluorescent bands with higher R_f value compared to both acceptor substrates indicated a possible hydrolysis of H- α -Man- α -1,6-Man (**2.10**) and α -Man-1,6- α -Man-HTC (**2.13**) (Fig. 2.15 A and B). At this stage, structures of enzymatically mannosylated fluorescent products obtained from fluorescence-based methodology II needed to be established.

2.7.6 Identification of fluorescent products by LC-MS

In order to confirm formation of fluorescent mannoside products, reaction mixtures from H- α -Man- α -1,6-Man (**2.10**) after 18 h incubation and α -Man-1,6- α -Man-HTC (**2.13**) after 29 h incubation were submitted to the LC-MS analysis. LC-MS method provides separation of fluorescent carbohydrate products using either normal phase (amino-modified stationary phase) or reverse phase (C18 stationary phase) methods and when coupled to the mass spectrometry it allows mass analysis of each separated compound. The derivatisation of carbohydrate acceptor substrates with the fluorophore also allowed utilisation of UV-detection in LC methods, simplifying the identification of fluorescent products amongst other components of reaction mixture. Normal phase LC was chosen in the first instance because it provided superior resolution of mixtures of carbohydrates that differ in monosaccharide composition and inter-glycosidic linkage types when compared to reverse phase LC methods.^{134, 135}

Normal phase LC coupled with UV-detection allowed separation of fluorescent products and revealed one peak at retention time 7.7 min (**2.16**) for the reaction mixture

involving H- α -Man- α -1,6-Man (**2.10**) and two peaks at retention time 7.2 min (**2.16**) and 8.0 min (**2.17**) for the reaction mixture involving α -Man-1,6- α -Man-HTC (**2.13**) (Fig. 2.16 A1 and A2). Slight inconsistency in the retention time of **2.16** from **2.10** and **2.13** could be due to the instrumental issue.

The analysis of MS data of fluorescent (**2.16**) product confirmed addition of single mannose residue to H- α -Man- α -1,6-Man (**2.10**) and α -Man-1,6- α -Man-HTC (**2.13**), thus major signal observed in both MS spectrum had m/z of 788.18 and 788.25, respectively, corresponding to $[M+H]^+$ of a trisaccharide molecular ion (Fig. 2.16 B1 and B2a). The MS data for fluorescent (**2.17**) product confirmed addition of two mannose residue to α -Man-1,6- α -Man-HTC (**2.13**) with m/z of 950.13 corresponding to $[M+H]^+$ of a tetrasaccharide molecular ion (Fig. 2.16 B2b). LS-MS data were in agreement with the preliminary TLC observations.

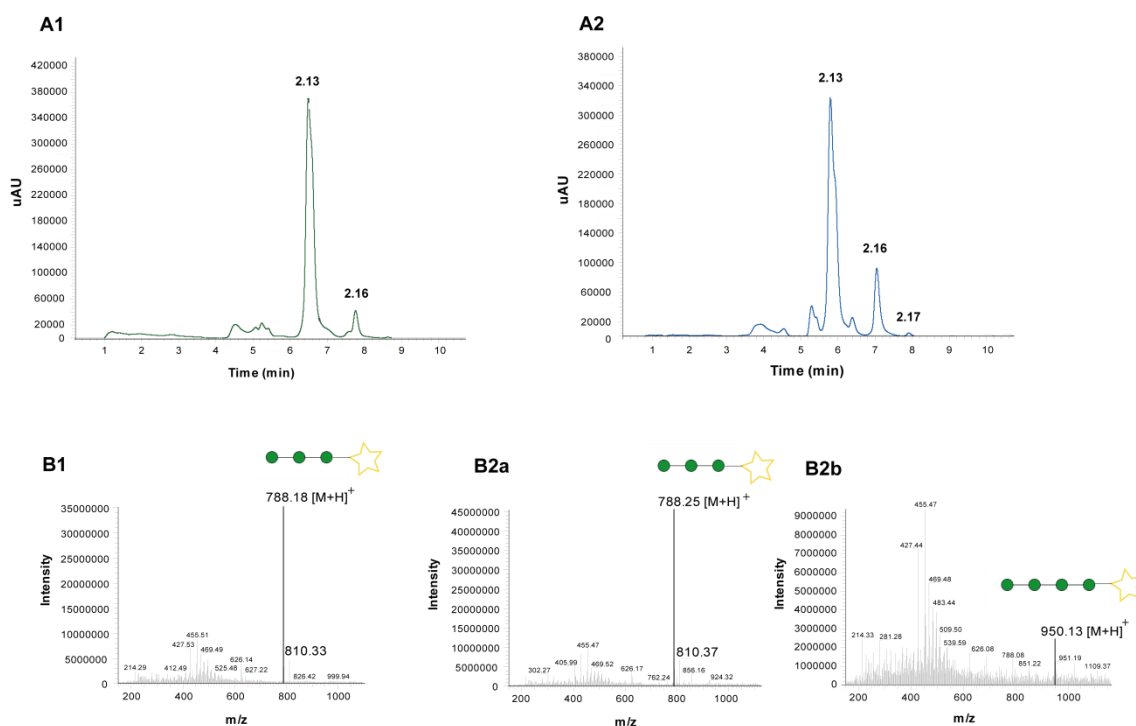


Figure 2.16 LC-MS analyses of reaction mixtures obtained from incubation of non-fluorescent and fluorescent acceptors with GDP-Man in the presence of *Mycobacterium smegmatis* microsomal membranes. (A) UV chromatogram (A1) reaction mixture from **2.10**, (A2) reaction mixture from **2.13**. LC conditions: Kinetex LUNA NH₂ (100 mm/2.0 mm/3 μ m), mobile phase: CH₃CN-water (0.1% TFA) (10 to 90 %, 32 min, flow rate: 1 mL/min) UV detector at 347 nm. (B) MS spectra (B1) **2.16** obtained from the non-fluorescent acceptor (**2.10**); (B2) **2.16** obtained from the fluorescent acceptor (**2.13**); (B3) **2.17** obtained from the fluorescent acceptor (**2.13**).

2.7.7 Linkage analysis through *exo*-mannosidase digestions

The newly formed linkages in fluorescent trisaccharide (**2.16**) and tetrasaccharide (**2.17**) products were assessed through the application of *exo*-mannosidase digestion with a hydrolase of well-defined α -1,6-specificity. For this purpose, both enzymatic reactions were scaled up to obtain sufficient amount of fluorescent products to be analysed. The purification of **2.16** from H- α -Man- α -1,6-Man (**2.10**) and **2.16/2.17** from α -Man-1,6- α -Man-HTC (**2.13**) was attempted by a normal phase HPLC method. Disappointingly, the obtained fractions contained mixed products as some interactions of coumarin-based fluorophore with the amino column were observed, which resulted in tailing of peaks for all fluorescent compounds. Semi-purified fraction containing mixed trisaccharide (**2.16**) and by-product (BP) from H- α -Man- α -1,6-Man (**2.10**) reaction (Fig. 2.17 A, lane 1) was subjected to *exo*-mannosidase digestion with *Xanthomonas manihotis* α -1,6-mannosidase and the progress of this reaction was monitored by TLC (Fig. 2.17 A, lane 2). TLC analysis indicated that α -1,6-mannosidase hydrolysed trisaccharide (**2.16**) and removed two mannose residues releasing fluorescent α -Man-HTC (**2.12**). Interestingly, the by-product of Cu(I)-catalysed click reaction was also hydrolysed by α -1,6-mannosidase; therefore, indicating that the structural deviations possibly lies in aglycone.

HPLC purification of the reaction mixture from α -Man-1,6- α -Man-HTC (**2.13**) gave two mixed fractions. First semi-purified fraction contained mixed trisaccharide (**2.16**) product, a faint amount of α -Man-1,6- α -Man-HTC (**2.13**) and product of hydrolysis α -Man-HTC (**2.12**) (Fig. 2.17 B, lane 1). Second semi-purified fraction contained tetrasaccharide (**2.17**) product, small amount of trisaccharide (**2.16**) as well as **2.13** and **2.12** (Fig. 2.17 B, lane 3). Both fractions were subjected to *exo*-mannosidase digestion with *Xanthomonas manihotis* α -1,6-mannosidase (Fig. 2.17 B, lane 2 and 4). TLC analysis indicated that hydrolysis of trisaccharide (**2.16**) and tetrasaccharide (**2.17**) products with α -1,6-mannosidase resulted in formation of α -Man-HTC (**2.12**) (Fig. 2.17 B, lane 2 and 4). The obtained data indicates that both non-fluorescent H- α -Man- α -1,6-Man (**2.10**) and fluorescent α -Man-1,6- α -Man-HTC (**2.13**) compounds can act as acceptor substrates for α -1,6 ManT present in *M. smegmatis* membranes.

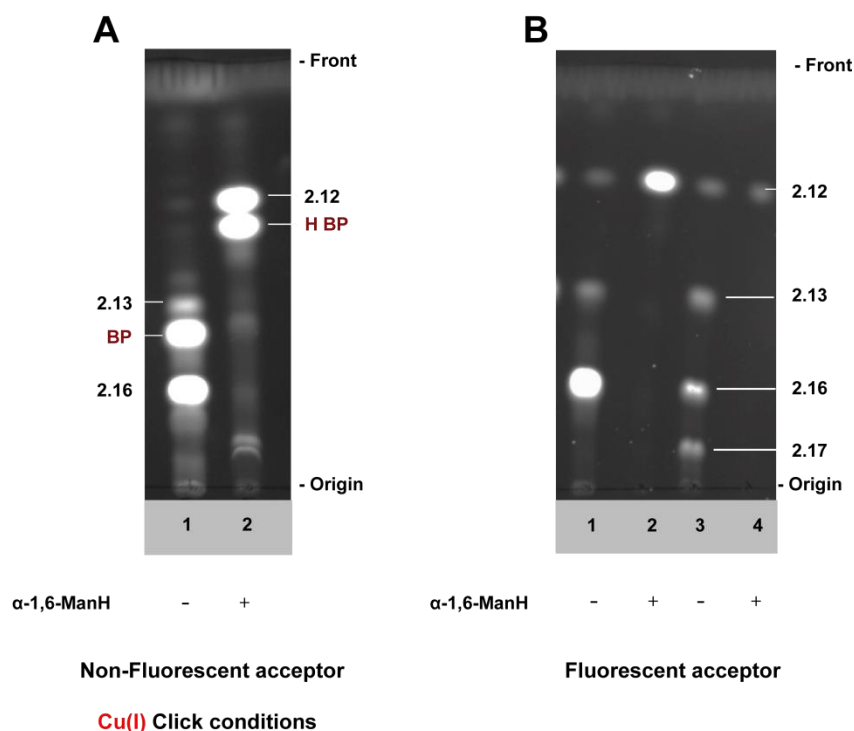


Figure 2.17 TLC analyses of *exo*-mannosidase digestions of fluorescent mannoside products with *exo*-mannosidase. *Exo*-mannosidase hydrolysis of mixed products obtained (A) from H- α -Man- α -1,6-Man (2.10); (B) from α -Man-1,6- α -Man-HTC (2.13). Enzyme used in this assay is *Xanthomonas manihotis* α -1,6-mannosidase (α -1,6-ManH). TLC plates were eluted with CHCl₃:MeOH:H₂O (10:8:1) and visualised using mid-wave length range UV light. Starting acceptors and products are shown to the left and right of each TLC image; BP by-product originated from click reaction and H-BP hydrolysed by-product.

2.7.8 Summary of fluorescence-based methodologies in *Mycobacterium smegmatis*

The immediate answer that we were able to obtain from the first round of validation was that non-fluorescent α -Man-EtC (2.04) and fluorescent α -Man-EtTC (2.05) compounds used in fluorescence-based methodology I were not able to act as substrates for α -1,6-ManTs present in *M. smegmatis* membranes. This could be attributed to the poor association of both aglycones with mycobacterial membranes and as a result it affects acceptor presentation and recognition by mannosyltransferase enzymes. Another possible consideration is that both compounds carry only one mannose residue which makes them unsuitable acceptors for the active site of these enzymes. The radiolabelled assays⁸⁷ only examined the synthetic disaccharides and no monosaccharides were mentioned in this publication.

In contrast, the non-fluorescent H- α -Man- α -1,6-Man (2.10) and fluorescent α -Man-1,6- α -Man-HTC (2.13) compounds used in methodology II were able to act as substrates for α -1,6-ManTs, resulting in fluorescent trisaccharide (2.16) from 2.10 and the same

fluorescent trisaccharide (**2.16**) and tetrasaccharide (**2.17**) from **2.13**, as depicted in Figure 2.18. Non-fluorescent **2.10** was a weaker acceptor compared to fluorescent **2.13** which gave the same number of products as acceptor substrates employed before in the radiolabelled assays.⁸⁷ Again, this difference could be due to slight variation in the aglycone length and hydrophobicity that could possibly affect acceptor association with mycobacterial membranes.

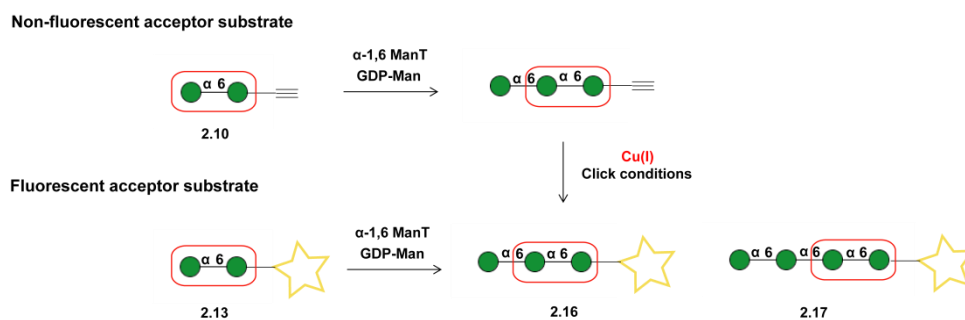


Figure 2.18 Schematic representation of α -1,6-mannosyltransferase reaction with non-fluorescent and fluorescent acceptor substrates using fluorescence-based methodology II.

2.8 Validation of fluorescence-based methodology II against established radiolabelled assay

Published results from radiolabelled assays used to investigate the biosynthesis of cell surface glycoconjugates in *Trypanosoma brucei* were used in the second round as a benchmark for our fluorescence-based methodology II. At this stage, we targeted GalTs involved in decoration of the core GPI anchor structures in *Trypanosoma brucei*.

2.8.1 Insight into studying biosynthesis of glycoconjugates in *Trypanosoma brucei*

Trypanosoma brucei is an extracellular protozoan parasite that lives in the blood, lymph and intestinal fluids of the infected mammalian host causing a devastating and often fatal African sleeping sickness in human and related disease Nagana in cattle. The parasite undergoes a complex life cycle between an insect (tsetse fly) vector and its mammalian host.¹³⁶ The blood form of the parasite is able to survive inside the human host due to the presence of variant surface glycoprotein (VSG) (10^7 molecules of 55 kDa) tightly packed on the cell surface.¹³⁷ This layer protects the parasite from the immune system of the host and the subject to antigenic variation of the VSG in order to

escape host recognition.¹³⁸ This means that the VSG layer is shed once the host develops an immune response to the predominant parasite population and replaced it with a new immunologically distinct layer that overexpressed by a new VSG gene.¹³⁹

Each VSG protein is anchored to the plasma membrane via covalent linkage of C-terminal amino acid to glycosyl-phosphatidylinositol (GPI) moiety. The survival of the parasite completely depends on the VSG coat and the coat depends on its GPI anchors; therefore, intervention in the biosynthesis of GPI anchors makes an attractive therapeutic target. Nevertheless, GPI anchors are present in mammalian cells too and the difference in the biosynthetic pathways between mammalian and *T. brucei* have been extensively studied (see chapter 1, section 1.2.1).

2.8.2 Literature radiolabelled assay to probe galactosyltransferase activities responsible for decoration of GPI anchors in *Trypanosoma brucei*

The core structure of GPI anchors consists of ethanolamine-PO₄-6Man α -1,2-Man α -1,6-Man α -1,4-GlcN α -1,6-*mio*-inositol with the ethanolamine phosphate linked to the C-terminus of the protein (Fig. 2.19).^{3, 17} The structural variations of GPI anchors between *T. brucei* and mammals are observed on the side chain and lipid moieties of the anchor. A unique feature of GPIs from *T. brucei* is the presence of a galactoside side chain attached through Gal α -1,3-Man linkage to the mannose residue adjacent to the α -GlcNH₂ residue of the core structure. Two additional single galactose residues are linked either through Gal β -1,3-Man or Gal α -1,2-Man linkages to second and third mannose residue of the core structure, respectively. Galactosylation occurs after the transfer of the VSG to the GPI precursor and its role is to fill space in order to preserve the tight packed integrity of the VSG coat.¹⁸ Finding parasite-specific inhibitors for the glycosyltransferases involved in the biosynthesis of GPI anchors has clear potential in treating African sleeping sickness.

Acceptor substrates used in the literature radiolabelled assays

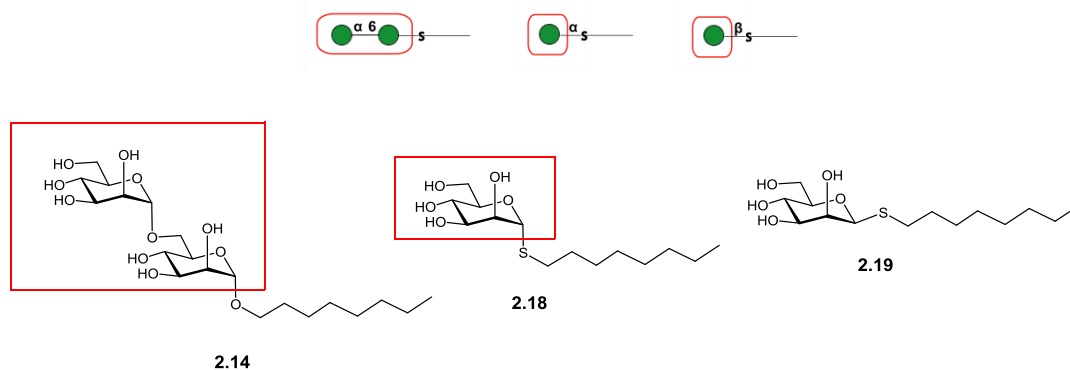
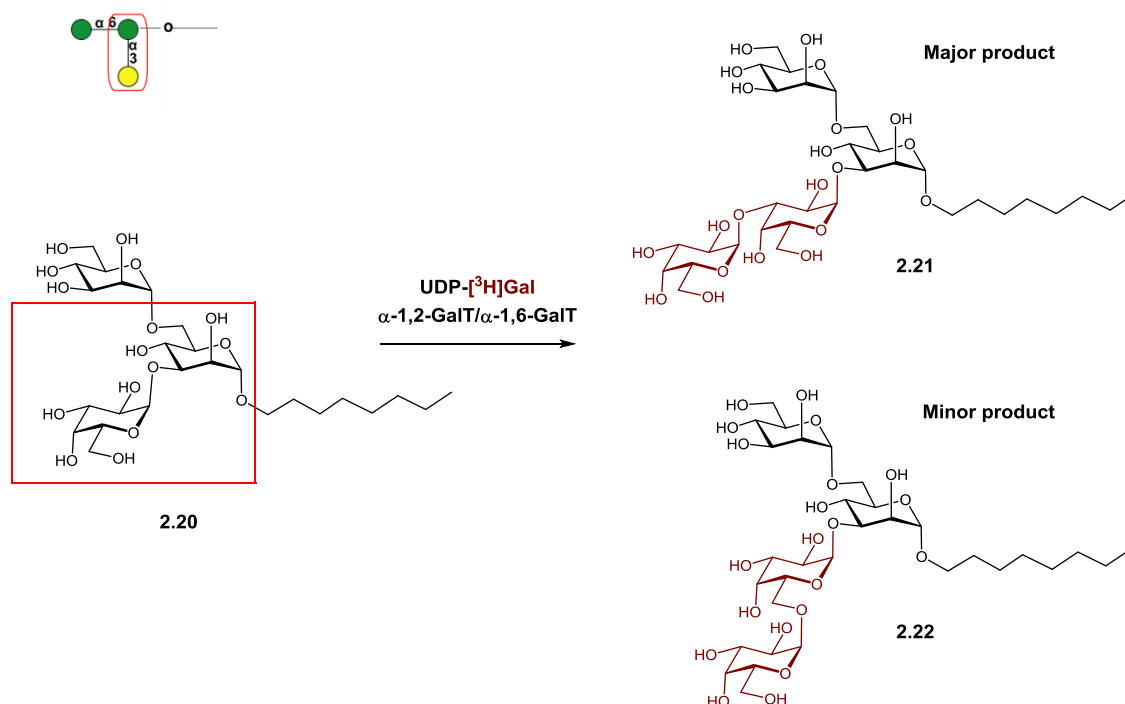


Figure 2.20 Structures of acceptor substrates used in the literature cell-free radiolabelled assays. (Top image) The diagrammatic representation of acceptor substrates. (Bottom image) Chemical structures. The red box area indicates the site of authentic intermediate mimicked by the synthetic acceptors.

The published results of these assays indicated that mannoside **2.14** and thioglycosides **2.18** and **2.19** were capable of accepting one galactose residue in either α - or β -configuration, with the α -linked products representing approximately 90, 40 and 10 %, respectively of these galactosylated products. The type of the glycosidic bond has been investigated only in **2.14** because the main aim of that study was to detect α -GalT activity in *T. brucei* membranes. The type of glycosidic linkage in this assay has been confirmed through utilisation of tandem negative-ion electrospray mass spectroscopy prior to periodate oxidation and reduction with NaBH_4 and indicated formation of major product with α -1,3-linkage and two minor products with α -1,2 and α -1,4-linkages.

Furthermore, in a separate study it has been demonstrated that chemically synthesised trisaccharide octyl α -D-galactopyranosyl-(1 \rightarrow 3)-(α -D-mannopyranosyl-(1 \rightarrow 6))- α -D-mannopyranoside (**2.20**) can act as a substrate for galactosyltransferases involved in formation of branching oligo-galactose side chains of GPI anchors.¹⁴¹ Incubation of **2.20** with radiolabelled UDP-[^3H]Gal donor in the presence of *T. brucei* microsomal membranes generated two radiolabelled tetrameric isomers (Scheme. 2.7). Using non-specific *exo*-glycosidase digestion and tandem negative-ion electrospray mass spectrometry prior to periodate oxidation and reduction with NaBH_4 the major product (**2.21**) has been assigned to bear an α -1,2- and the minor product (**2.22**) α -1,6-glycosidic linkages in approximately 9:1 ratio. Activities of both enzymes were believed to reside in the Golgi apparatus.

Acceptor substrate used in the literature radiolabelled assays



Scheme 2.7 Enzymatic transformations of synthetic acceptor substrate by galactosyltransferases responsible for branching of GPI anchors as detected by literature radiolabelled assay. (Top left image) The diagrammatic representation of acceptor substrates. The red box area indicates the site of authentic intermediate mimicked by the synthetic acceptors.

As for previous validation experiments described in section 2.7, in order to benchmark our fluorescence-based methodology II we were looking to obtain similar results to the radiolabelled assay that utilised octyl 6-*O*- α -D-mannopyranosyl-1-thio- α -D-mannopyranoside (**2.14**) as an acceptor substrate.

2.8.3 Fluorescence-based methodology II to probe galactosyltransferase activities responsible for α -galactosylation of GPI anchors in *Trypanosoma brucei*

In this round of validation of fluorescence-based methodology II, the main aim was to demonstrate that non-fluorescent H- α -Man- α -1,6-Man (**2.10**) and fluorescent α -Man-1,6- α -Man-HTC (**2.13**) compounds, already used in benchmarking against *M. smegmatis* radiolabelled assays can equally act as acceptor substrates for galactosyltransferases involved in the decoration of the core structure of GPI anchors in *T. brucei* microsomal membranes (Fig. 2.21).

Acceptor substrates for fluorescence-based methodology II

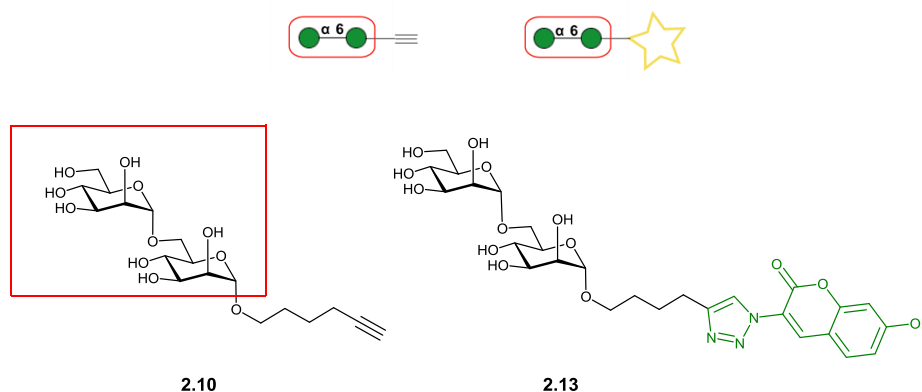


Figure 2.21 Structures of non-fluorescent and fluorescent compounds used to benchmark fluorescence-based methodology II against radiolabelled literature assay. (Top image) The diagrammatic representation of acceptor substrates. The red box area indicates the site of authentic intermediate mimicked by the synthetic acceptors.

In order to detect the GalT activity, both examined mannoside acceptor substrates (**2.10** and **2.13**) were incubated with UDP-Gal in the presence of trypanosome membranes under the same conditions as used in the literature radiolabelled assay.¹⁴⁰ Trypanosome membranes were kindly donated by Professor Ferguson's group. Bloodstream *Trypanosoma brucei* (strain 427 variant MITat 1.4) were obtained from the infected rats¹³⁷ centrifuged, washed with ice-cold buffer and lysed using hypotonic buffer.¹⁹ The time course of each enzymatic reaction during 24 h of incubation at 30 °C was monitored by TLC.

During enzymatic assays, aliquots (20 μ L) of each reaction mixture that contained H- α -Man- α -1,6-Man (**2.10**) and α -Man-1,6- α -Man-HTC (**2.13**) at 2 h, 6 h, and 24 h were obtained and stopped by addition of methanol-chloroform (1:1) solution. Aliquots of reaction mixtures from the non-fluorescent **2.10** were made fluorescent by addition of 3-azido-7-hydroxycoumarin, catalytic amount of CuSO₄ and sodium ascorbate (NaAsc). Reaction mixtures were left overnight to ensure complete fluorescent labelling of starting material and any potential products. In order to visualise the progress of enzymatic reaction 2 μ L were spotted onto the TLC plate, eluted and visualised under the UV light (Fig. 2.22 A and C).

TLC analysis showed no enzymatic activities for H- α -Man- α -1,6-Man (**2.10**) indicating that this compound cannot act as an acceptor substrate for GalTs present in *T. brucei* microsomal membranes. According to the R_f value and the same intensity at each time

point, the faint fluorescent band observed below the acceptor fluorescent band was assigned to Cu(I)-catalysed by-product (section 2.4.2.).

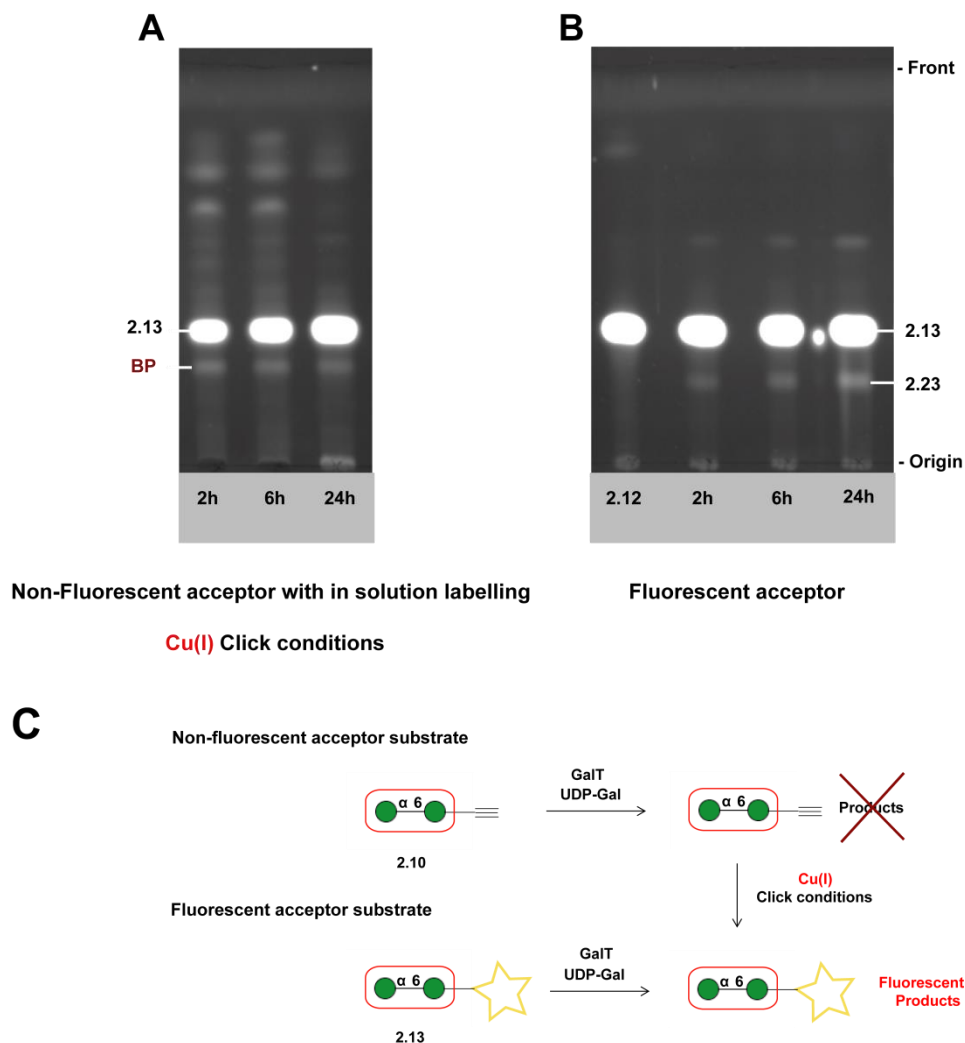


Figure 2.22 TLC analyses of enzymatic assays of non-fluorescent and fluorescent acceptors used in detection of galactosyltransferase activities in *Trypanosoma brucei* membranes utilising fluorescent methodology II. (A) The TLC plate features reaction mixture of **2.10** after fluorescent labelling with 3-azido7-hydroxycoumarin; (B) The TLC plate features reaction mixture of **2.12**. Assay conditions: acceptor substrate (1 mM), UDP-Gal (1 mM), reaction buffer HEPES/KOH (100 mM, pH 7.4), KCl (50 mM), MgCl₂/MnCl₂ (10 mM), DTT (2 mM), ATP (2 mM), *N*-tosyl-L-lysine chloromethyl ketone (0.2 mM), leupeptin (2 μg/mL), tunicamycin (2.5 μg/mL), Triton (0.05%); *T. brucei* microsomal membranes (50 μL, 10×10⁷ cells); Total reaction volume of 200 μL. TLC plates were eluted with CHCl₃:MeOH:H₂O (10:6:1) and visualised under UV light. Reaction time points are shown below the corresponding TLC image and starting acceptors and products are shown to the left of each TLC image (**BP**) by-product. (C) Reaction schemes from **2.10** leading to no fluorescent products

The enzymatic reaction that involved fluorescent α -Man-1,6- α -Man-HTC (**2.13**) acceptor substrate was visualised on the TLC plate without further modifications (Fig. 2.22 B). TLC analysis showed formation of one fluorescent band with R_f value of expected trisaccharide (**2.23**) product.

In order to increase amount of fluorescent product formed in the enzymatic reaction of α -Man-1,6- α -Man-HTC (**2.13**) with UDP-Gal in the presence of *T. brucei* microsomal membranes variation in two parameters were examined. Firstly, the reaction was carried out with a double amount of *T. brucei* microsomal membranes, and secondly with sequential addition of donor to the reaction mixture over time. The increase in the amount of *T. brucei* microsomal membranes resulted in little change in formation of trisaccharide (**2.23**) product as followed from a similar fluorescent intensity when compared to previous TLC analyses (Fig. 2.23 A vs Fig. 2.22 B). On the other hand, the increase in the amount of enzyme led to increase in hydrolysis of the starting acceptor resulting in increased fluorescent intensity of α -Man-HTC (**2.12**). The sequential addition of UDP-Gal donor resulted in an overall increase in acceptor substrate conversion as judged by the increase in intensity of fluorescent band of **2.23** (Fig. 2.23 B).

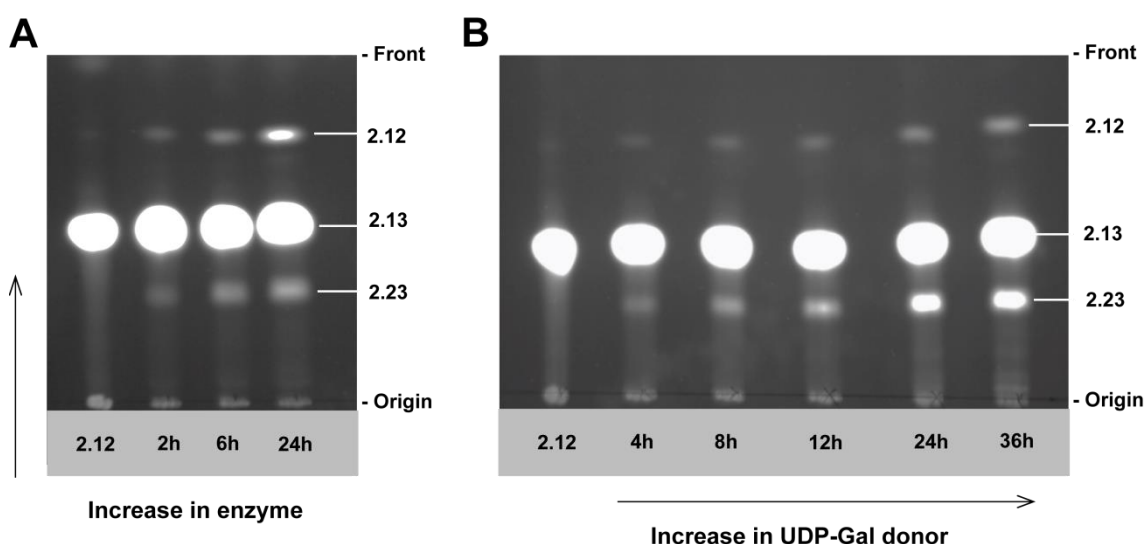


Figure 2.23 TLC analyses of enzymatic assays of fluorescent mannoside acceptor to improve galactosyltransferase activities in *Trypanosoma brucei* microsomal membranes utilising fluorescent methodology II. (A) The TLC plate features reaction mixture with addition of enzyme (25 μ L 10×10^8 cells); (B) The TLC plate features reaction mixture with addition of UDP-Gal donor (5 μ L of 4mM at each time point). Initial assay conditions: acceptor substrate (1 mM), UDP-Gal (1 mM), reaction buffer HEPES/KOH (100 mM, pH 7.4), KCl (50 mM), $MgCl_2/MnCl_2$ (10 mM), DTT (2 mM), ATP (2 mM), *N*-tosyl-L-lysine chloromethyl ketone (0.2 mM), Leupeptin (2 μ g/mL), Tunicamycin (2.5 μ g/mL), Triton (0.05%); *T. brucei* microsomal membrane (25 μ L, 10×10^7 cells); Total reaction volume of 100 μ L. TLC plates were eluted with $CHCl_3:MeOH:H_2O$ (10:6:1) visualised under UV light. Reaction time points are shown below the corresponding TLC image and starting acceptor and products are shown to the left of the TLC image.

2.8.4 Identification of fluorescent product by LC-MS

In order to confirm formation of trisaccharide (**2.23**) compound the reaction mixture from α -Man-1,6- α -Man-HTC (**2.13**) was subjected to LC-MS analysis. The ion extracted chromatogram of m/z 788.29 indicated presence of two peaks that were designated as **2.23a** (retention time 6.14 min) and **2.23b** (6.23 min) (Fig. 2.24 A). The MS spectrum of two peaks from the ion extracted chromatogram indicated a signal with m/z of 788.29 corresponded to a molecular ion $[M+H]^+$ thereby confirming the addition of a single galactose residue to **2.13** and formation of trisaccharide fluorescent products (**2.23a/b**). Masses with m/z of 626.23, 462.16 and 302.12 were assigned to the fragmentation of molecular ion $[M+H]^+$ and corresponded to the sequential loss of hexose unit (m/z 162) and release of α -Man-1,6- α -Man-HTC (**2.13**), α -Man-HTC (**2.12**) and HTC (**2.11**), respectively (Fig. 2.24 B).

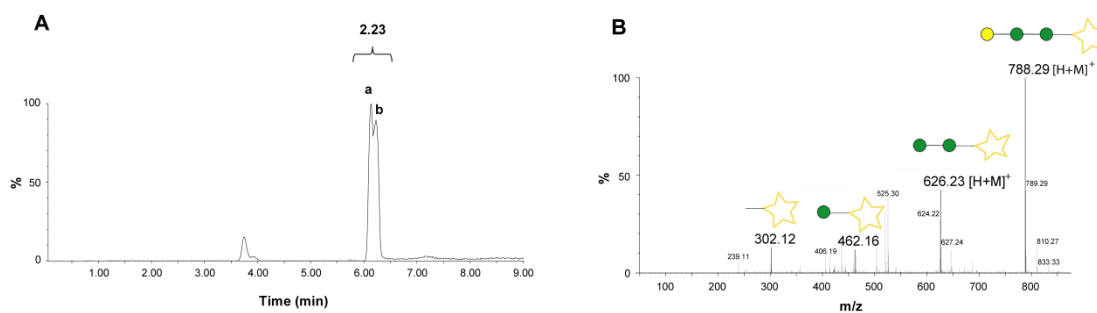


Figure 2.24 UPLC analyses of reaction mixture obtained from incubation of fluorescent acceptor with UDP-Gal in the presence of *Trypanosoma brucei* microsomal membranes. (A) Extracted ion chromatogram of **2.23**. UPLC conditions: Acquity UPLC BEH C18 (100 mm/1.0 mm/1.7 μ m), mobile phase: water- CH₃CN (0.1% formic acid) (10 to 90 %, 12 min, flow rate: 0.08 mL/min) MS detector. (B) MS spectrum of **2.23a/b**.

2.8.5 Linkage analysis through *exo*-galactosidase digestions

Assessment of the anomeric configuration of newly formed glycosidic linkages in trisaccharide (**2.23**) was achieved through utilisation of enzymatic digestions with α -galactosidase from green coffee beans and β -galactosidase from *Escherichia coli*. The purification of **2.23** from starting **2.13** was attempted by a reverse phase HPLC method. The obtained fraction contained some starting material due to the human error. The semi-purified fraction was subjected to *exo*-galactosidase digestion with α -galactosidase from green coffee beans and β -galactosidase from *E. coli* and the progress of both reactions were monitored by TLC.

TLC analysis of mixed fraction treated with α -galactosidase resulted in hydrolysis of significant amount of α -linked trisaccharide (**2.23a**) compound releasing fluorescent α -Man-1,6- α -Man-HTC (**2.13**) and leading to increase in fluorescent intensity of this compound compared to the intensity of control sample without the enzyme (Fig. 2.25 lane 1 and 2). In contrast, TLC analysis of mixed fraction with β -galactosidase indicate some hydrolysis of **2.23b** compared to the control sample without enzyme (Fig. 2.25 lane 1 and 3). Moreover, there is a slight difference in R_f value of **2.23a** and **2.23b** where the R_f value of **2.23a** is slightly higher compared to the R_f value of **2.23b** (Fig. 2.25 lane 2 and 3).

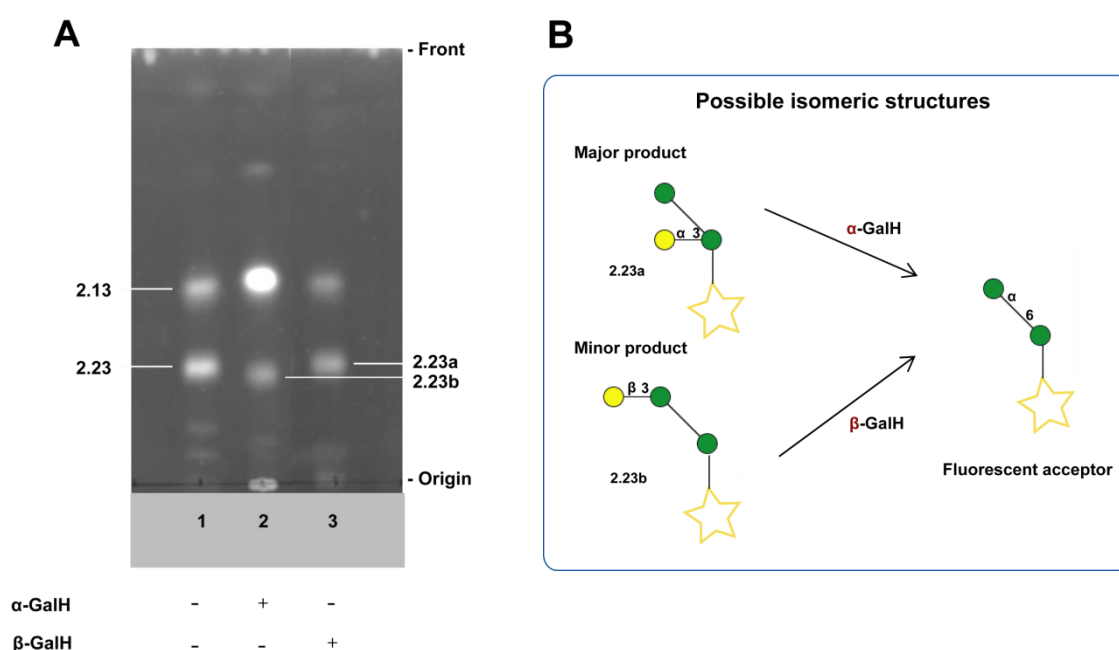


Figure 2.25 Analyses of *exo*-glycosidase digestion of fluorescent products with α -galactosidase from green coffee beans and β -galactosidase from *Escherichia coli*. (A) The TLC plate after *exo*-galactosidase digestion. Control experiment L1 (without enzyme) were conducted in parallel with hydrolysis reactions. The TLC plate were eluted with CHCl_3 :MeOH:H₂O (10:6:1) and visualised using mid-wave length range UV light. The starting acceptor and products are shown to the left of the TLC image. (B) Schematic representation of degradation of two possible products by *exo*-galactosidases and release of fluorescent acceptor.

According to *exo*-galactosidase digestion data obtained from radiolabelled assays and the structural information of GPI anchor side chains in *T. brucei*, the major trisaccharide (**2.23a**) product hydrolysed by α -galactosidase was tentatively assigned to have an α -1,3-linkage to the reducing mannose of **2.13**. The minor (**2.23b**) product was assigned to have a β -1,3-linkage to the non-reducing mannose of **2.13** (Fig. 2.25 B).

2.8.6 Investigation of number of isomeric structures by IM-MS

Ion mobility coupled to mass spectrometry (IM-MS) was used as a platform in order to confirmed presence of two isomeric structures in trisaccharide (**2.23a/b**). The IM-MS technique is very fast (in the millisecond time scale) and requires a nanoscale amount of investigated compound. This technique provides separation and differentiation of carbohydrate isomers from biological mixtures¹⁴²⁻¹⁴⁴ on the basis of both ion collisional cross section and m/z by IM and MS respectively.¹⁴⁵⁻¹⁴⁷ During the IM-MS experiment ionised compounds are generated by electrospray ionisation (ESI) which then directed into the IM drift tube under electric field that filled with a neutral drift gas. Separation is achieved through interaction of ions with a neutral drift gas. Ions with a smaller collisional cross section experience fewer collisions with the neutral drift gas. Hence, they are transmitted through the drift tube faster than an ion with a larger collisional cross section. This gives each ionised compound a unique drift time (t_D) value. When coupled to the MS it produces 2D spectrum (m/z over t_D) which reveals how many isomers are present in the given sample.

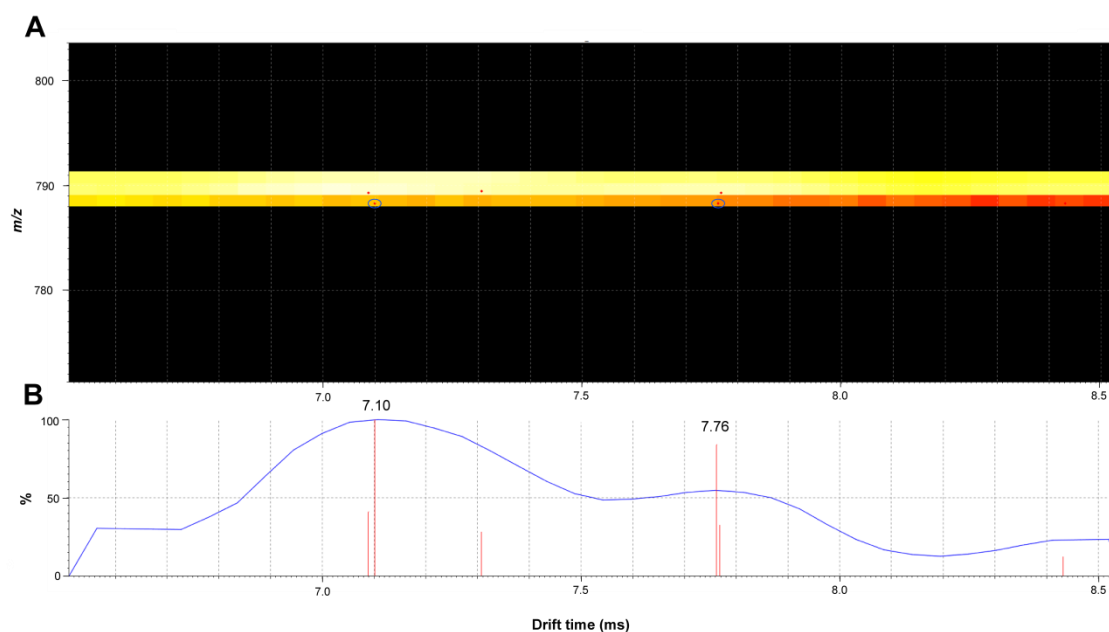


Figure 2.26 Ion mobility spectrum to represent isomeric structures present in trisaccharide fluorescent products obtained from incubation of UDP-Gal with *Trypanosoma brucei* membranes. (A) m/z /drift time spectrum of **2.23a/2.23b** (m/z 788.29). (B) % intensity/drift time spectrum of **2.23a/b** (m/z 788.29).

To access this information mixed fraction obtained from reverse phase HPLC purification was subjected to IM-MS and drift time of m/z 788.29 was investigated. The mobility spectrum of trisaccharide **2.23** revealed two distinct peaks with m/z of 788.29 at 7.10 ms corresponding to **2.23a** and at 7.76 ms corresponding to **2.23b** (Fig. 2.26 A

and B). The peak assignment was based on fluorescent intensities of the released product as observed on the TLC plate after *exo*-galactosidase digestion of **2.23** (Fig. 2.25 A). The IM-MS data confirmed formation of two isomers major **2.23a** and minor **2.23b**.

2.8.7 Summary of fluorescence-based methodology II in *Trypanosoma brucei*

In this round of validation of our fluorescence-based methodology II we obtained encouraging results with fluorescent α -Man-1,6- α -Man-HTC (**2.13**) compound, which once more proved to be a good acceptor substrate for a new set of glycosyltransferases, this time present in *T. brucei* microsomal membranes. The obtained data and structural information on GPI anchors led us to believe that **2.13** targeted α -1,3- and β -1,3-GalT enzymes involved in the decoration of core structure of GPI anchors and resulted in formation of two isomeric fluorescent trisaccharide products (**2.23a** and **2.23b**) in an approximate 7:3 ratio (Fig. 2.27).

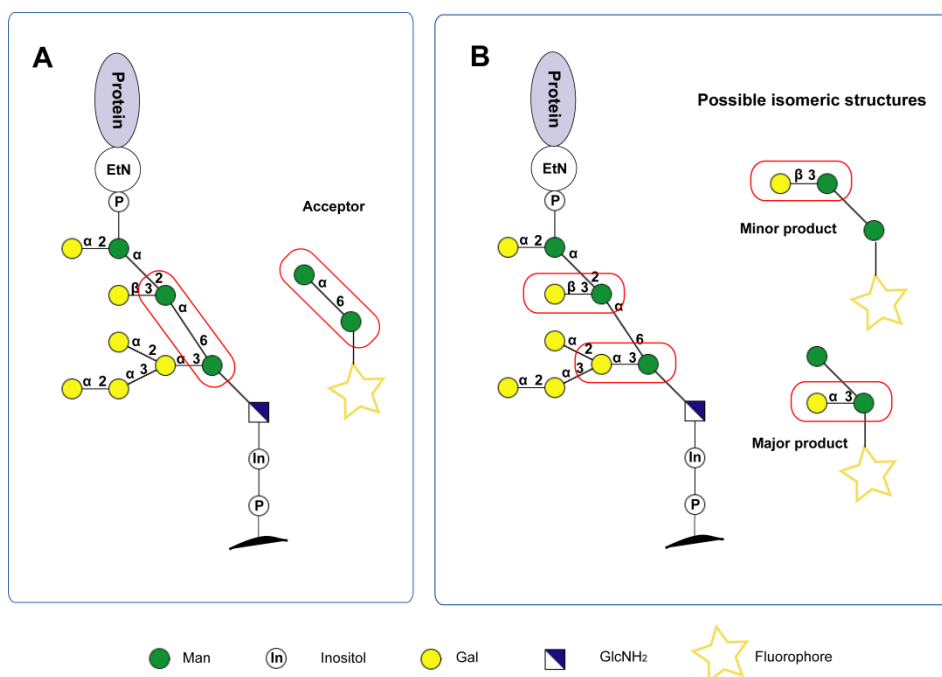


Figure 2.27 Diagrammatic representation of fluorescent acceptor mimicked sites on the GPI anchor and resulted fluorescent products. (A) Acceptor mimicked site. (B) Structure of possible isomeric products.

According to TLC analyses the major **2.23a** compound was sensitive to α -galactosidase digestion suggesting that a galactose residue was attached to α -Man-1,6- α -Man-HTC (**2.13**) in the α -anomeric configuration. On the other hand, β -galactosidase digestion of

minor **2.23b** compound was not that evident on the TLC plate due to the presence of some starting fluorescent material in the sample. Nevertheless, the incomplete α -galactosidase digestion of **2.23a** as well as the presence of two peaks in the IM-MS spectrum pointed towards formation of second compound with β -anomeric configuration. Incontrovertibly, additional analysis of digestion reaction mixture using the LC-MS method in order to confirm presence of **2.23b** compound by observing m/z of 626 as well as additional *exo*-digestion with α -mannosidase to confirm presence of branch isomer are required to strengthen above conclusions. In contrast, non-fluorescent H- α -Man-1,6-Man (**2.10**) acceptor substrate in this round of validation showed no enzymatic activity towards galactosyltransferases present in *T. brucei* microsomal membranes.

2.9 Conclusion and future work

To this point we have designed three fluorescence-based methodologies and benchmarked methodology I and II against established radiolabelled assays that were used to investigate substrate specificities of chemically synthesised acceptors towards GT present in *M. smegmatis* and *T. brucei* with insight to find suitable inhibitors.^{87, 140, 141} Both of these methodologies have shown positive and negative aspects that surfaced during validation. In methodology I non-fluorescent α -Man-EtC (**2.04**) and fluorescent α -Man-EtTC (**2.05**) compounds showed no activity towards α -1,6-ManT enzymes present in *M. smegmatis* microsomal membranes. However, it provided a clean and rapid method to visualise progress of enzymatic reactions on the TLC plates with compound visualisation within minutes on heating the plate. The cyclooctyne used in the TLC visualisation could also be replaced with 4-dibenzocyclooctynol because cyclooctyne is a volatile and pungent oil which is difficult to handle and 4-dibenzocyclooctynol is synthetically quite accessible, nontoxic solid material with excellent stability.¹⁴⁸ In future investigations acceptors used in methodology I should undergo some modifications to suite the particular biosynthetic pathways. For instance the hydrophobic linker on α -Man-EtC (**2.04**) could be extended from ethyl to pentyl to improve the membrane association.

In methodology II the fluorescent labelling prior the biotransformation provided a cleaner way to assess the enzymatic activities on the TLC plate compared to the

fluorescent labelling after the biotransformation. Primarily, it is due to formation of Cu(I)-catalysed by-product in the latter one. This creates complication in TLC analyses of formed fluorescent products and especially in case of multiple products formation. In general for both methodologies, the fluorescent labelling prior the biotransformation proven to be a more straight forward way to assess the enzymatic activities on the TLC plate compared to the fluorescent labelling after the biotransformation. Methodology III was not taken beyond the design due to non-existing or poor substrate activities of non-fluorescent acceptors.

In terms of enzymatic activities we have demonstrated that fluorescence-based methodology II is a feasible method that can be used to study glycosyltransferases responsible for the biosynthesis of various glycoconjugates in two different organisms. To this point we have shown that fluorescent compound α -Man-1,6- α -Man-HTC (**2.13**) used in this methodology targeted both α -1,6-ManT involved in the biosynthesis of LM in *M. smegmatis* as well as α - and β -GalT responsible for decoration of GPI anchor side chains in *T. brucei*.

Results from mycobacterial fluorescent study with **2.13** resulted in formation of fluorescent α -1,6-linked mannoside trimer and tetramer which was consistent with the result obtained from the radiolabelled study. In our fluorescent study formation of high molecular weight products, such as pentamer and higher were not observed. However, literature publication shown that cyclohexylmethyl α -D-mannopyranosyl-(1 \rightarrow 6) α -D-mannopyranoside (**2.24**) and cyclohexylethyl α -D-mannopyranosyl-(1 \rightarrow 6) α -D-mannopyranoside (**2.25**) were capable of accepting up to ten additional mannose residues when incubated with radiolabelled GDP-[14 C]Man and mycobacterial membranes (Fig. 2.28).¹⁴⁹ Furthermore, the publication is stating that the transfer of mannose residue was not affected by the aglycone. In our study the obtained results lead to slightly different conclusion. We have shown that incubation of H- α -Man-1,6-Man (**2.10**), which has a shorter slightly less hydrophobic aglycone, with mycobacterial membrane resulted in formation of α -1,6-linked trisaccharide whereas incubation of **2.13** resulted in α -1,6-linked trisaccharide and tetrasaccharide fluorescent products. The difference in aglycone between **2.10** and **2.13** is more pronounced compared to the difference in **2.24** and **2.25** therefore we can observe a more profound effect of aglycone association with the mycobacterial membrane. In another publication α -D-mannopyranosyl-(1 \rightarrow 6) α -D-mannopyranoside and α -D-mannopyranosyl-(1 \rightarrow 6)- α -D-

mannopyranosyl-(1→6) α -D-mannopyranoside that contained no aglycone shown an excellent substrate activities toward the α -1,6-ManT in *M. smegmatis* leading to formation of radiolabelled products up to a dodecamer, which is the longest oligomer found by addition of [^3H]mannose to endogenous acceptor.¹⁵⁰

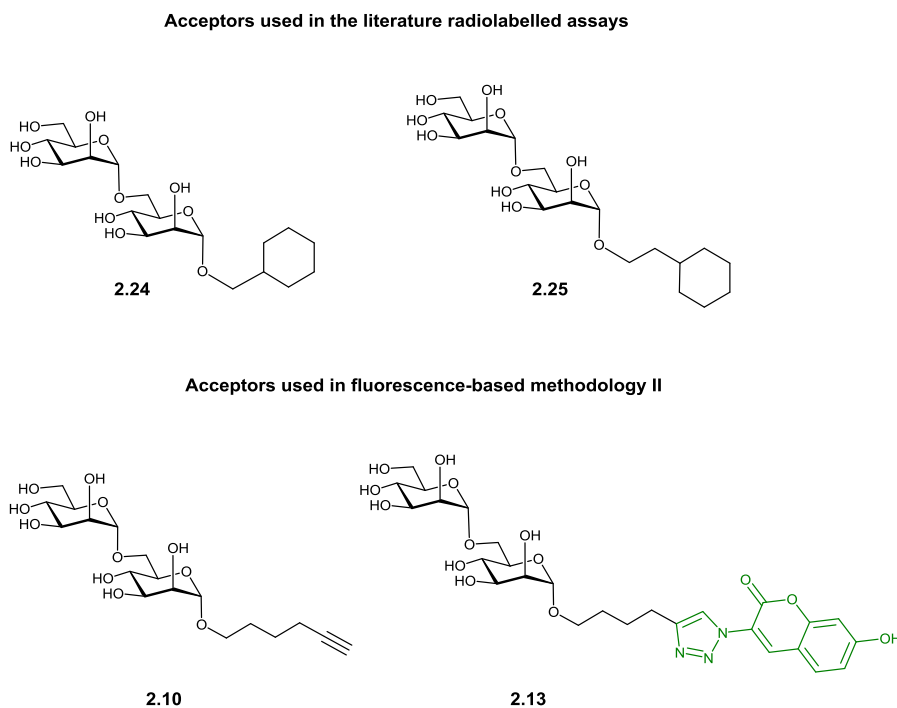


Figure 2.28 Structural comparison between acceptors used in the literature radiolabelled assays and in the fluorescence-based methodology.

Recently, activities of two α -1,6-ManTs were identified in *Corynebacterium glutamicum* species that share similar orthologue enzymes involved in cell wall assembly with *M. tuberculosis* and *M. smegmatis*. The first α -1,6-ManT (MptB) enzyme has been shown to be involved in initial stage of AcPIM₄ elongation where the second α -1,6-ManT involved in further elongation of LM to produce mature LM. Therefore, all together these results indicate that with our fluorescent acceptors probably target MptB α -1,6-ManT that perhaps requires acceptor association with *M. smegmatis* resulting in activity decrease as the aglycone size is reduced. While mannoside acceptors without aglycone and cyclohexylmethyl/cyclohexylethyl mannoside acceptors target MptA α -1,6-ManT. Nevertheless, in ongoing research where our fluorescence-based methodology II perhaps can be of assistance and find its place in the research by simplifying enzymatic assays and eliminating the need for utilisation of radiolabelled donors.

Results from trypanosome fluorescent studies utilising α -Man-1,6- α -Man-HTC (**2.13**) had demonstrated addition of one galactose residue to the acceptor leading to formation of α - and β -linked fluorescent products. These results were consistent with the results obtained from the radiolabelled study. Overall using our fluorescent acceptor the proportion of galactose product in the β -linkage was approximately 20% as judged by peaks intensity in the IM-MS chromatogram compared to 10% for octyl 6-*O*- α -D-mannopyranosyl-1-thio- α -D-mannopyranoside acceptor from the radiolabelled assays. In addition we did not detect either α -1,2 or α -1,4-linked products.

Results presented above shown that fluorescence-based methodology II, with fluorescent labelling prior to the biotransformation, can be successfully applied to probe membrane bound glycosyltransferases involved in the biosynthesis of variety of glycoconjugates. This methodology can be strongly considered as a replacement for traditional radiolabelled techniques. Further, in our study we utilise fluorescence-based methodology II to probe the biosynthesis of glycoconjugates in *Euglena gracilis*.

3 The quest for glycosyltransferase activities in *Euglena gracilis*

3.1 Insight into *Euglena*

Euglena is a unicellular flagellated and free living microorganism which mainly inhabits fresh water, although it has a high degree of adaptability and can survive in harsher environmental conditions, such as low pH (as low as 0.9), high salinity and highly energetic ionising radiation.^{151, 152} *Euglena* is a unique organism which exhibits both plant- and animal-like characteristics: it can live in the light by producing food autotrophically employing photosynthesising chloroplast, or it can exist in the dark and utilise nourishments heterotrophically from the environment and store it as a paramylon (starch-like β -1,3-glycan). Structurally, it is composed of all organelles present in the eukaryotic cell (Fig. 3.1). It does not have a cell wall like plant; on the contrary, the outer part is composed of repetitive membrane domains know as ridges and groves, that have a topographic relationship with fibrils and subpellicular ER.^{153, 154}

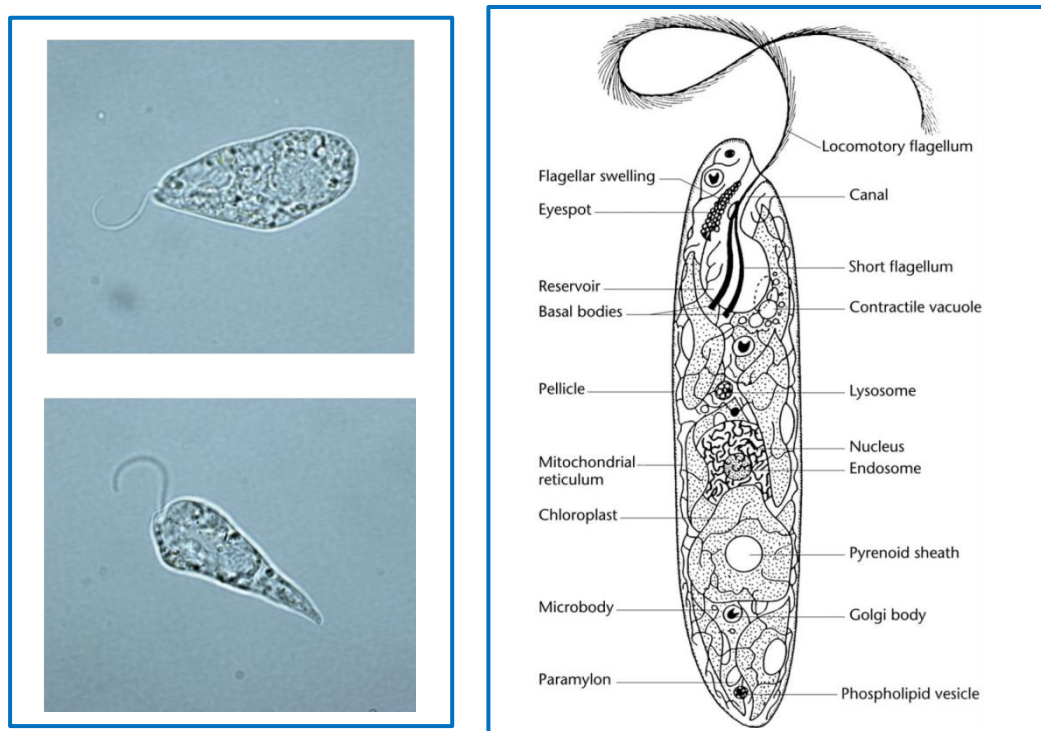


Figure 3.1 The *Euglena gracilis* cell. (Left) Electron microscope images to represent different shapes *E. gracilis* can adopt; (Right) Diagrammatic representation of *Euglena* cell to show main organelles.¹⁵¹

Euglena has been placed in the common phylum of Euglenozoa,^{155, 156} that also includes parasitic trypanosomatids, one of which is *Trypanosoma brucei*. Glycoconjugates, such as GPI anchors and *N*-linked glycoproteins, on the cell surface of parasites, play an important role in their survival and infectivity inside the vector and host organisms (refer to Chapter 2 section 2.7.9).¹⁷ Recently in our group, Dr. Ellis O'Neill resolved

the transcriptome of *E. gracilis* and, based on the homology with known enzymes, he was able to demonstrate that it contains sequences for all enzymes involved in the biosynthesis of *N*-linked glycoproteins and GPI anchors.¹⁵⁷ To the best of our knowledge no structural information of GPI anchors or characterisation of glycosyltransferase activities involved in their biosynthesis has been investigated in *E. gracilis* (Fig. 3.2). Previous study described the extraction of glycoproteins rich in xylose, mannose, glucose and galactose residues from the outer membrane of the *E. gracilis* flagellum.¹⁵⁸ The extraction of these glycoproteins was accomplished with detergents and under conditions which perturbed hydrophobic interactions, therefore, authors suggested that these glycoproteins could contain a hydrophobic, presumably membrane-associated region. Furthermore, no further research has been performed to obtain information on whether glycoproteins were GPI anchored or how oligosaccharide regions are bound to the protein for these particular glycoproteins.

Limited research has been performed to elucidate the structural composition of *N*-linked glycoproteins in *E. gracilis*.¹⁵⁹ In this study, intact *E. gracilis* cells were incubated with the UDP-[¹⁴C]Glc and radiolabelled lipid-linked *N*-glycans and *N*-linked glycoproteins were extracted at different time points of incubation. Then, lipid-linked *N*-glycans were treated with mild acid hydrolysis to release monosaccharides, while *N*-linked glycoproteins were treated with site-specific endo- β -*N*-acetylglucosaminidase H enzyme, which cleaves the bond between two *N*-acetylglucosamine subunits to release *N*-linked oligosaccharide. The released monosaccharides and *N*-linked oligosaccharides were then compared to standards utilising paper chromatography. Results showed that dolichol-P-P-bound oligosaccharide migrated as Glc₃Man₉GlcNAc₂ standard and contained glucose, mannose and *N*-acetylglucosamine residues as shown by acid hydrolysis. Based on these data, the author suggested that the mechanism of protein *N*-glycosylation in *E. gracilis* is similar to that occurring in higher eukaryotic cells (Fig. 3.2) and the lipid-linked oligosaccharide intermediate is different compared to the oligosaccharide structure found in *Trypanosoma* (Man₉GlcNAc₂-P-P-Dol).

The importance of GPI anchors and *N*-linked glycoproteins on the cell surface of parasites and position of *Euglena* in the same phylum as trypanosomatids as well as lack of knowledge in this area of research prompted us to investigate biosynthesis of these glycoconjugates in *E. gracilis*, with the scope that, if relevant activities could be detected, *Euglena* can be used as an alternative model system.

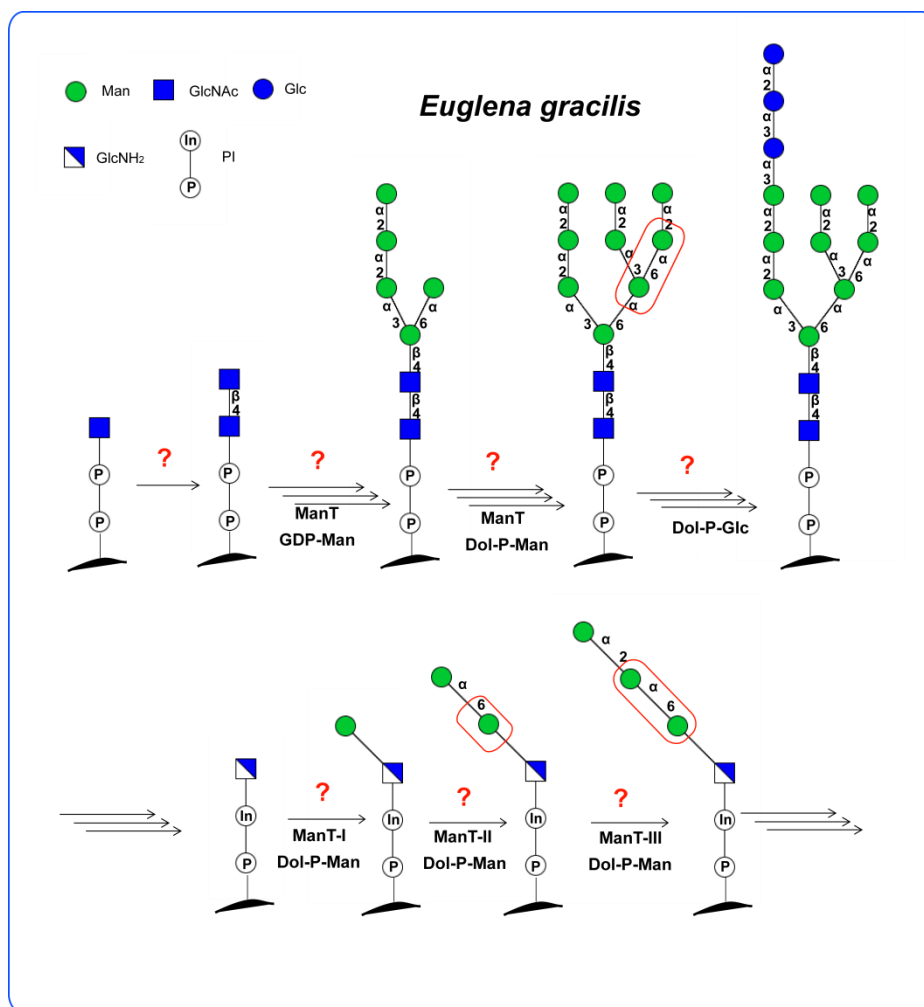


Figure 3.2 Diagrammatic representation of conserved *N*-glycan and GPI anchor biosynthesis to illustrate limited information available on glycosyltransferases present in *Euglena gracilis*. The red box area indicates the site of authentic intermediate mimicked by the synthetic acceptors in the fluorescence-based assays.

3.2 Fluorescence-based methodology II to probe mannosyltransferase activities in *Euglena gracilis*

To uncover potential mannosyltransferase (ManT) activities in *E. gracilis* responsible for the biosynthesis of either GPI anchor or lipid linked *N*-glycans we investigated the possibility of mannosylation of synthetic acceptors with GDP-mannose by microsomal membranes isolated from this organism. The detection of enzymatic activity was accomplished by fluorescence-based methodology II, which requires fluorescent labelling of monosaccharide and disaccharide acceptors prior to biotransformation (refer to Chapter 2). The fluorescent acceptors of our choice were α -Man-HTC (**2.12**) and α -Man-1,6- α -Man-HTC (**2.13**), which could potentially mimic the structure of authentic

intermediates involved in the biosynthesis GPI-anchor and lipid-linked *N*-glycan (Fig. 3.3).

Acceptor substrates for fluorescence-based methodologies II

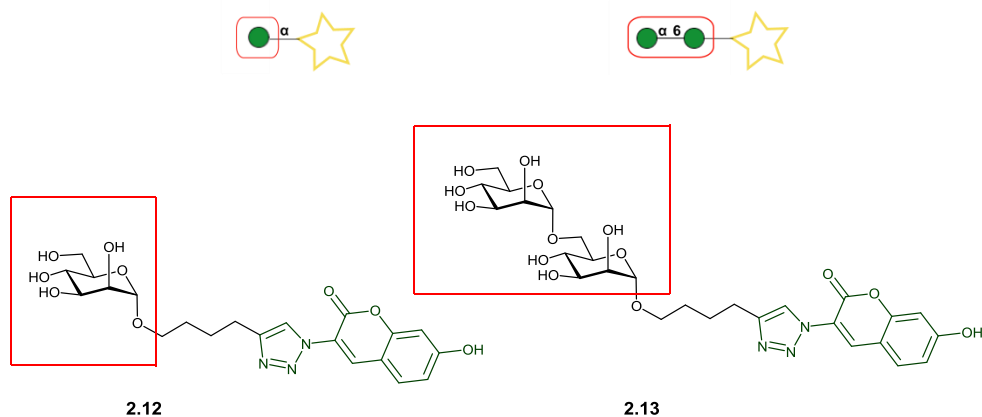


Figure 3.3 Schematic and chemical structures of fluorescent acceptors used in fluorescence-based methodology II to probe mannosyltransferases activities in *Euglena gracilis* microsomal membranes. The red box indicates the site of authentic intermediate mimicked by synthetic acceptors.

3.2.1 Microsomal membranes as a source of glycosyltransferases

Glycosyltransferases that participate in the biosynthesis of vast variety of glycoconjugates are located in the ER and Golgi apparatus.¹⁶⁰ These types of enzymes are often directly associated with microsomal membranes. This association presents a major challenge for their isolation from the microsomal membranes with retained enzymatic activities. Indeed, their isolation often leads to enzyme denaturation with subsequent loss of activity. Therefore, in this study *E. gracilis* microsomal membranes containing membrane-bound glycosyltransferases were extracted following the literature procedure,¹⁶¹ which preserves activities of membrane-bound glycosyltransferases; the latter could then be successfully utilised in fluorescence-based methodology II. Microsomal membranes were obtained by growing axenic cultures of *Euglena gracilis* var *saccharophila* Klebs (stain 1224/7a) in the dark in media supplemented with glucose. After seven days, cells were harvested and lysed by ultrasonication. The larger cell debris was then removed by centrifugation and the microsomal membranes were obtained by ultracentrifugation over a sucrose gradient. Microsomal membranes were stored at -80 °C and the same batch of microsomal membranes was used throughout a year without losing their enzymatic activities.

3.2.2 Fluorescence assays to probe mannosyltransferase activities

In these assays, fluorescent acceptors α -Man-HTC (**2.12**) and α -Man-1,6- α -Man-HTC (**2.13**) were incubated with GDP-Man in the presence of *E. gracilis* microsomal membranes. To ensure the absence of endogenous GDP-Man in the membrane preparation as well as to rule out the decomposition of starting acceptors, two control assays that contained either no enzyme or no donor substrate were run in parallel with fluorescent assays (Fig. 3.4 A and B, lane 3 and 4). The formation of fluorescent products, after 24 h of incubation at 30 °C, was monitored by TLC (Fig. 3.4).

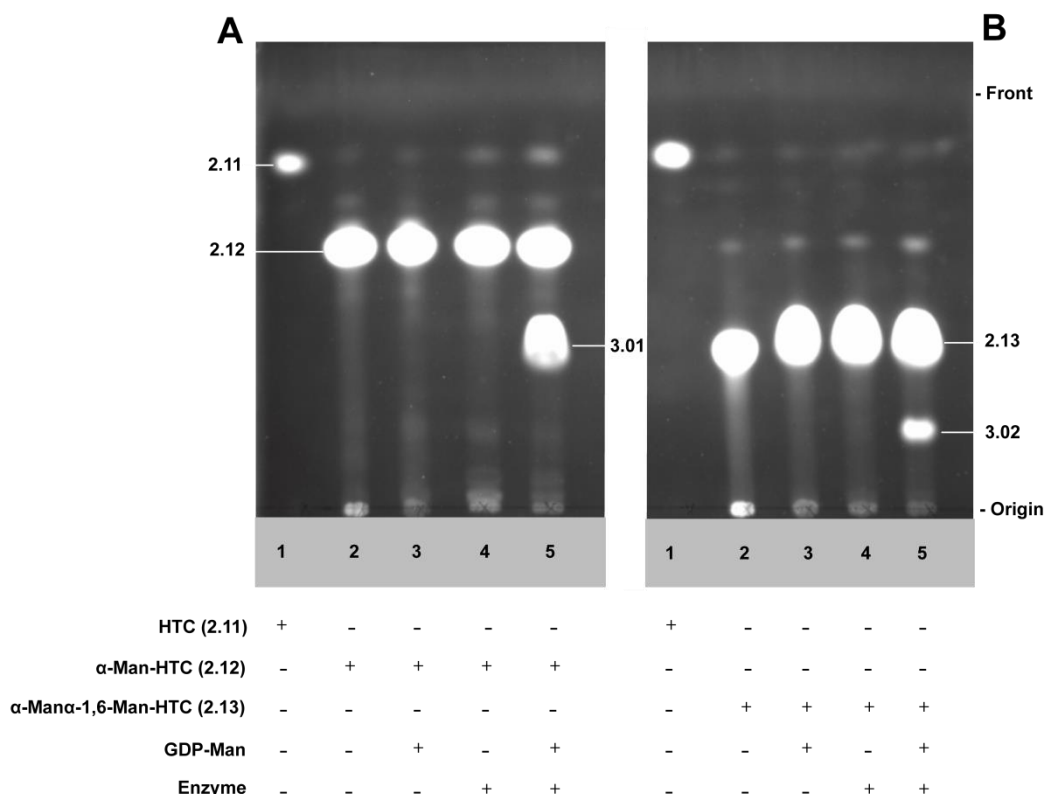


Figure 3.4 TLC analyses of fluorescence-based assays to assess mannosyltransferase activities in *Euglena gracilis* microsomal membranes. TLC images of fluorescent assays (A) α -Man-HTC acceptor (**2.12**); (B) α -Man-1,6- α -Man-HTC acceptor (**2.13**). Assay conditions: acceptor (2 mM); donor GDP-Man (4 mM); reaction buffer HEPES/KOH (10 mM, pH 7.0), MgCl₂/MnCl₂ (10 mM), KCl (25 mM), glycerol (10%), *E. gracilis* microsomal membranes (150 μ L, 195 μ g of total proteins) in total reaction volume of 200 μ L. Control experiments, lane 3 (without enzyme) and lane 4 (without donor), were conducted in parallel with enzymatic reactions. TLC plates were eluted with CHCl₃:MeOH:H₂O (10:6:1) and visualised using mid-wave length range UV light. The components of each reaction mixture are shown below the corresponding TLC image and acceptors and products are shown to the side of each TLC image.

TLC analysis of enzymatic reaction that involved α -Man-HTC (**2.12**) acceptor showed two distinct fluorescent bands (Fig. 3.4 A, lane 5). The upper band corresponded to starting acceptor substrate (**2.12**) and the lower band to the disaccharide product (**3.01**). The disaccharide product (**3.01**) had a similar R_f value as the α -Man-1,6- α -Man-HTC

(**2.13**) standard, suggesting a probable transfer of one mannose residue to the corresponding acceptor. TLC analysis of enzymatic reaction that involved α -Man-1,6- α -Man-HTC (**2.13**) acceptor also showed two distinct fluorescent bands (Fig. 3.4 B, lane 5). The upper band corresponded to starting acceptor substrate (**2.13**) and the lower band to the trisaccharide product (**3.02**) again indicative of probable transfer of one mannose residue on the corresponding acceptor. Products fluorescent band intensities visually indicated a higher enzymatic activity in case of α -Man-HTC (**2.12**) acceptor; however, a more precise measurement on the conversion should be done using HPLC method.

3.2.3 Purification of fluorescent products by HPLC

Evidently, above TLC analyses indicated the presence of mannosyltransferase activities in *E. gracilis* microsomal membranes as observed from the formation of disaccharide (**3.01**) and trisaccharide (**3.02**) products. In order to establish the structure of above fluorescent products, they were first separated from starting acceptor substrates α -Man-HTC (**2.12**) and α -Man-1,6- α -Man-HTC (**2.13**) by reverse phase and normal phase HPLC methods.

Application of reverse phase HPLC allowed separation of disaccharide (**3.01**) and trisaccharide (**3.02**) products revealing one peak at 8.1 min for **3.01** (Fig. 3.5 A, red trace) and one peak at 7.4 min for **3.02** (Fig. 3.5 A, blue trace) under this chromatographic condition. In contrast, application of normal phase HPLC enabled the separation of disaccharide (**3.01**) product into two peaks, designated as **3.01a** (retention time 5.3 min) and **3.01b** (retention time 5.6 min) (Fig. 3.5 B, red trace). Similarly, under the same chromatographic condition, trisaccharide (**3.02**) product resolved into two peaks **3.02a** (6.6 min) and **3.02b** (7.2 min) (Fig. 3.5 B, blue trace).

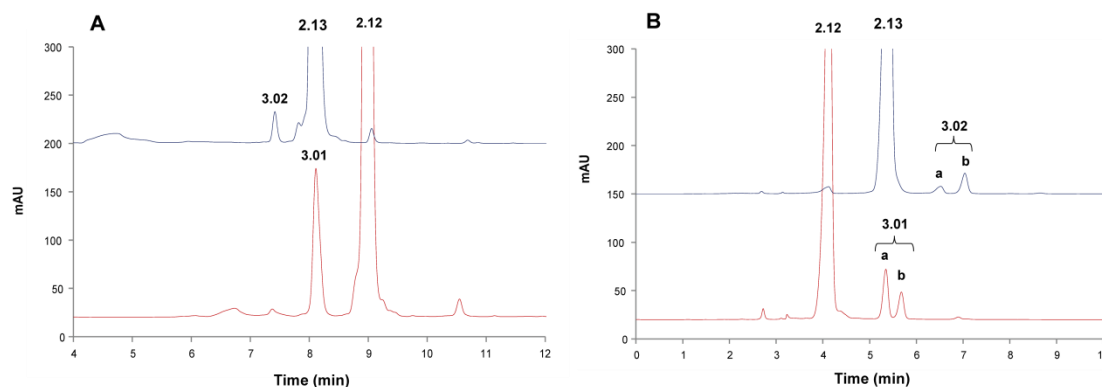


Figure 3.5 HPLC analyses of reaction mixtures obtained from incubation of fluorescent acceptors with GDP-Man in the presence of *Euglena gracilis* microsomal membranes. UV chromatograms of mannosylated products from α -Man-HTC (**2.12**) assay (red trace) and α -Man-1,6- α -Man-HTC (**2.13**) assay (blue trace). (A) Reverse phase purification of disaccharide **3.01** and trisaccharide **3.02** products. HPLC conditions: Phenomenex C18(2) (250 mm x 10 mm); mobile phase: 0.1% aq. water (0.1% TFA)-CH₃CN (10 to 90 % 36 min, flow rate: 5 mL/min); UV detector at 347 nm. (B) Normal phase HPLC purification of disaccharide **3.01** and trisaccharide **3.02** products. HPLC conditions: Phenomenex LUNA NH₂ (250 mm x 10 mm); mobile phase: CH₃CN-water (0.1% TFA) (10 to 80% 32 min, flow rate: 5 mL/min); UV detector at 347 nm.

The integration of the peak area of disaccharide (**3.01**) and trisaccharide (**3.02**) products in comparison to the peak area of starting acceptor substrates α -Man-HTC (**2.12**) and α -Man-1,6- α -Man-HTC (**2.13**) provided information about product percentage conversion. The percentage conversion obtained from the reverse phase HPLC method was consistent with the overall calculated percentage conversion obtained from the normal phase method (Table 3.1).

Reaction products	Normal Phase (NH ₂)		Reverse phase (C18)
	Peak a Conversion (%)	Peak b Conversion (%)	Peak a/b Conversion (%)
3.01	6.9	3.9	9.3
3.02	1.2	2.6	3.1

Table 3.1 Percentage conversion of fluorescent products obtained from enzymatic reactions with *Euglena gracilis* microsomal membranes.

TLC analyses of purified fractions obtained from both HPLC methods above revealed trailing of dominant starting material components (data not shown). The trailing resulted in contamination of fractions containing disaccharide (**3.01**) and trisaccharide (**3.02**) products with starting material when using normal phase HPLC. Therefore, reverse phase HPLC was used to purify fluorescent products because they eluted before the dominant acceptor substrates, resulting in a cleaner purification. Purified fractions containing fluorescent products were combined and analysed by LC-MS.

3.2.4 Identification of fluorescent products by LC-MS

Normal phase chromatographic conditions were used for the LC separation of purified disaccharide (**3.01**) and trisaccharide (**3.02**) compounds applying a steeper gradient because it allowed a quick access to the required information on the number of mannose residues added to α -Man-HTC (**2.12**) and α -Man-1,6- α -Man-HTC (**2.13**) during biotransformation (Fig. 3.6 A1, red trace and 3.6 A2, blue trace).

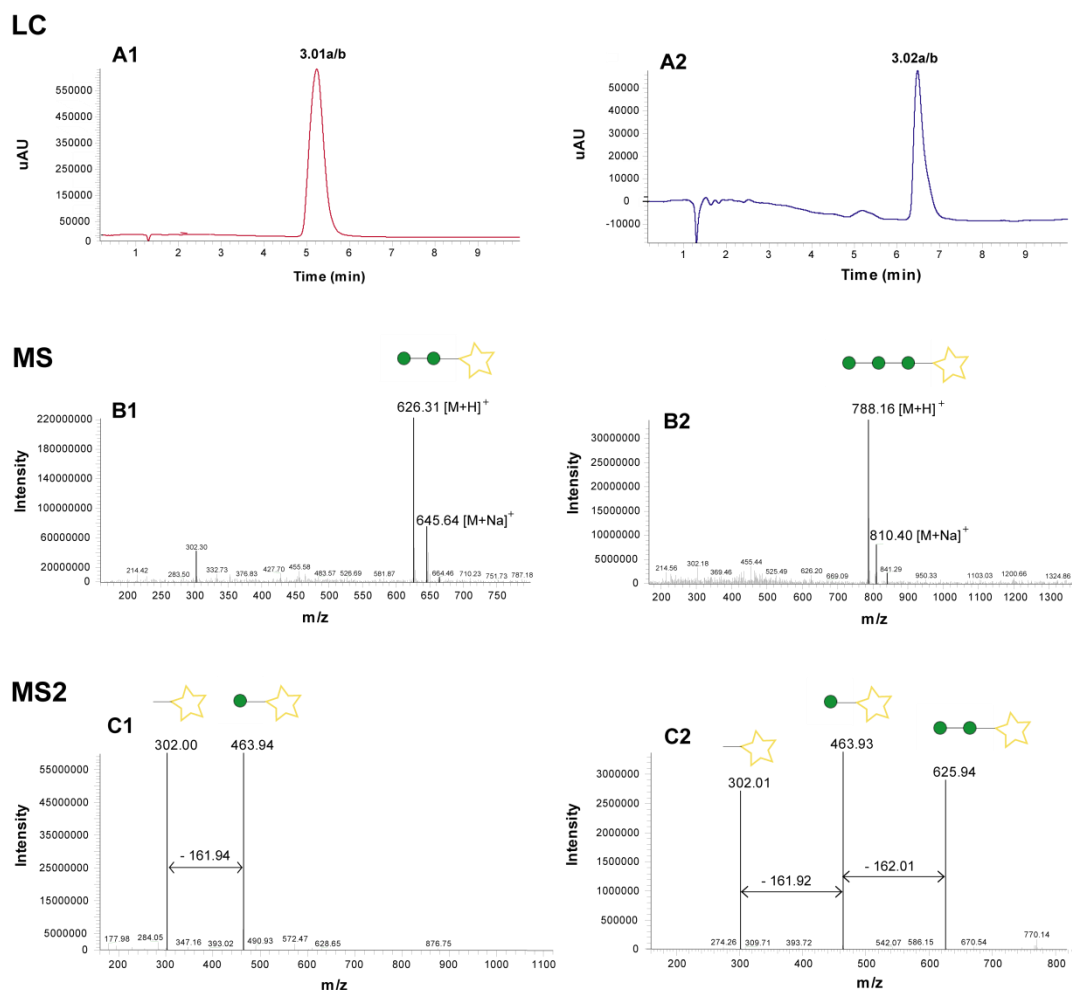


Figure 3.6 Structural identification of fluorescent products obtained from enzymatic reactions with GDP-Man and *Euglena gracilis* microsomal membranes by LC-MS. (A) UV chromatogram (**A1**) disaccharide **3.01** from α -Man-HTC (**2.12**) assay (red trace); (**A2**) trisaccharide **3.02** from α -Man-1,6- α -Man-HTC (**2.13**) assay (blue trace). LC conditions: Kinetex LUNA NH₂ (50 mm/2.1 mm/2.6 μ m); mobile phase: CH₃CN- water (0.1% TFA) (10 to 90 %, 12 min, flow rate: 0.3 mL/min); UV detector at 347 nm. (**B**) MS spectra for **3.01** (**B1**) and **3.02** (**B2**). (**C**) MS2spectra of **3.01** (**C1**) and **3.02** (**C2**).

MS data of disaccharide **3.01a/b** (retention time 5.3 min) and trisaccharide **3.02a/b** (6.7 min) confirmed addition of single mannose residues to the α -Man-HTC (**2.12**) and α -Man-1,6- α -Man-HTC (**2.13**). Thus, major peaks observed in the MS spectrum of **3.01** (m/z 626.31) and **3.02** (m/z 788.16) correspond to $[M+H]^+$ of disaccharide and

trisaccharide molecular ions (Fig. 3.6, B1 and B2), respectively. The MS2 fragmentation pattern of $[M+H]^+$ showed the sequential loss of hexose units (m/z 162) and ultimate release of fluorescent HTC (**2.11**) aglycone (m/z 302.00) in both MS2 spectra of **3.01** and **3.02** (Fig. 3.6, C1 and C2), respectively.

3.2.5 Linkage analysis through *exo*-mannosidase digestions

Information about the anomeric configuration of glycosidic linkages in disaccharide **3.01** and trisaccharide **3.02** were assessed through *exo*-glycosidase digestion with jack bean α -mannosidase.¹¹⁴ Sequential digestion of **3.01** and **3.02** with three different linkage-specific *Aspergillus saitoi* α -1,2-,⁸⁸ *Xanthomonas manihotis* α -1,6- and *Xanthomonas manihotis* α -1,2/3-mannosidases,¹⁶² capable of cleaving α -1,2-, α -1,6- and α -1,2/3-linked mannosides selectively, gave access to structural information on the regioselectivity of linkages formed between transferred mannose residues and α -Man-HTC (**2.12**) and α -Man-1,6- α -Man-HTC (**2.13**) acceptor substrates. Disaccharide **3.01** and trisaccharide **3.02** compounds were incubated with *exo*-glycosidase and the outcome of these reactions was analysed by TLC (Fig. 3.7 and 3.8).

TLC analyses of jack bean α -mannosidase digestion from disaccharide **3.01a/b** compound revealed formation of fluorescent band with the same R_f value as fluorescent HTC (**2.11**) aglycone, corresponding to removal of two mannose residues from **3.01** (Fig. 3.7 A, lane 2 and Fig. 3.7 B(i)). Incubation of disaccharide (**3.01a/b**) compound with *Xanthomonas manihotis* α -1,6-mannosidase had no effect on fluorescent compounds and therefore, formation of the α -1,6-linkage was excluded (Fig. 3.7 A, Lane 4). TLC analysis of disaccharide (**3.01a/b**) digestion with *Aspergillus saitoi* α -1,2-mannosidase released a significant amount of fluorescent product with the same R_f value as α -Man-HTC (**2.12**). However, a small amount of fluorescent disaccharide (**3.01b**) product remained unhydrolysed, which is indicative of the presence of another isomeric compound with a different linkage (Fig. 3.7 A, lane 6 and Fig. 3.7 B (ii)). In order to assess what type of glycosidic linkage the underlying mannoside possessed, it was subjected to further digestion with *Xanthomonas manihotis* α -1,2/3-mannosidase. In this case, both fluorescent products were digested. The disaccharide (**3.01 a**) was mainly converted into a fluorescent product with the same R_f value as HTC (**2.11**) aglycone, along with a minor fluorescent product with the same R_f as α -ManT-HTC

(**2.12**) (Fig. 3.7 A, lane 8 and Fig. 3.7 B (iii)). Considering the 1,3-mannosidase activity of *Xanthomonas manihotis* α -1,2/3-mannosidase, it is reasonable to suggest that the mannose residue was attached to the fluorescent acceptor substrate α -ManT-HTC (**2.12**) mainly through α -1,2-linkage and in minor amount through α -1,3-linkage.

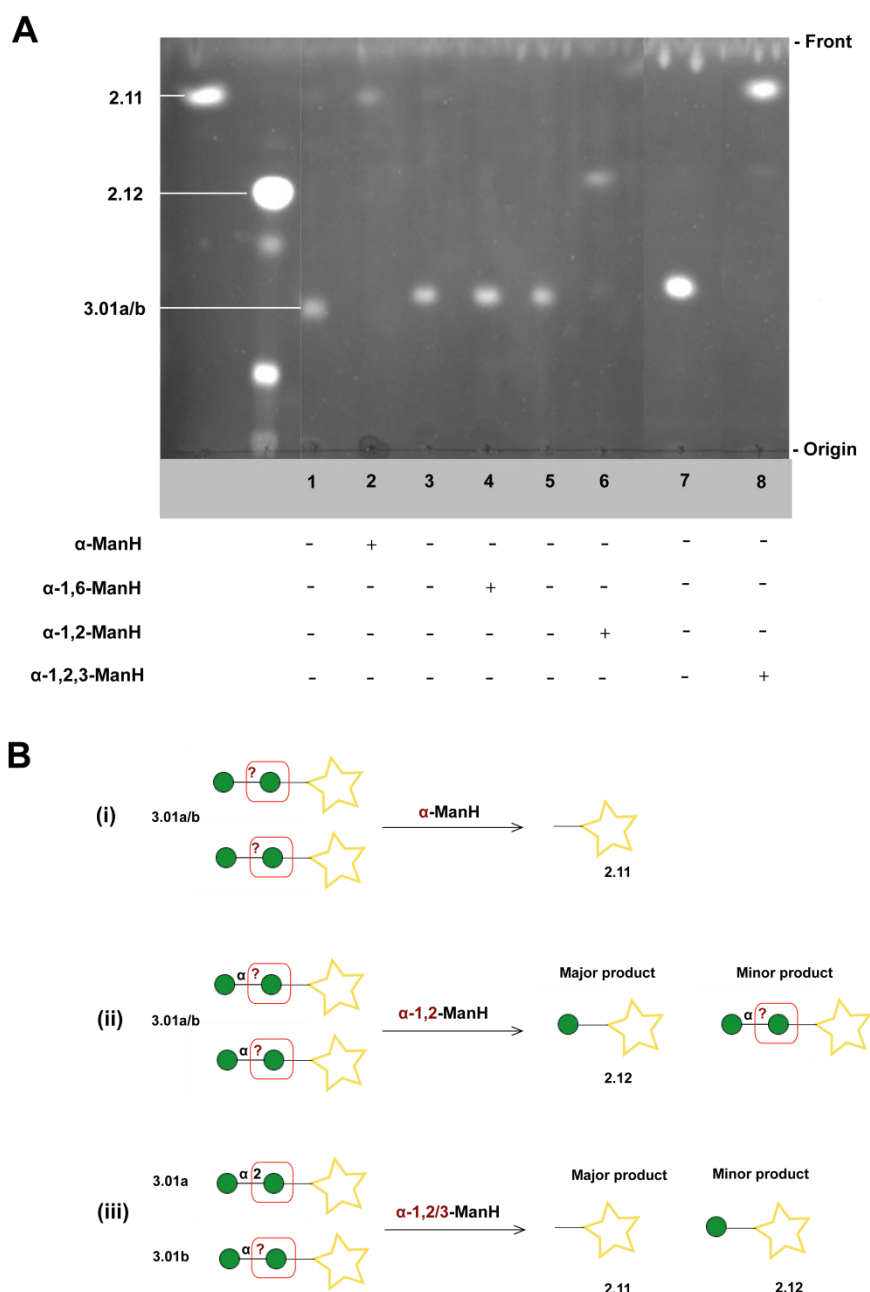


Figure 3.7 TLC analyses to assess stereoselectivity and regioselectivity of disaccharide fluorescent products by *exo*-glycosidase digestions. (A) TLC image of *exo*-glycosidase digestion of disaccharide **3.01a/b** with jack bean α -mannosidase (α -ManH), *Xanthomonas manihotis* α -1,6-mannosidase (α -1,6-ManH), *Aspergillus saitoi* α -1,2-mannosidase (α -1,2-ManH) and *Xanthomonas manihotis* α -1,2/3-mannosidase (α -1,2/3-ManH). Enzymes used in the assays are shown below the TLC traces and acceptors and products are shown to the side of each TLC image. Control experiments, lane 1, 3, 5 and 7 (without enzyme), were conducted in parallel with hydrolysis reactions. TLC plates were eluted with $\text{CHCl}_3\text{:MeOH:H}_2\text{O}$ (10:6:1) and visualised using mid-wave length range UV light. (B) Diagrammatic reaction schemes of *exo*-glycosidase digestion of **3.01a/b**

Similarly, TLC analysis from jack bean α -mannosidase digestion of trisaccharide (**3.02**) compound revealed removal of three mannose residues releasing a fluorescent product with the same R_f value as fluorescent HTC (**2.11**) aglycone (Fig. 3.8 A, lane 2 and Fig. 3.8 B(i)). Incubation of trisaccharide (**3.02**) compound with *Xanthomonas manihotis* α -1,6-mannosidase also had no effect on fluorescent compound therefore, excluding formation of the α -1,6-linkage (Fig. 3.8 A, lane 4). The hydrolysis of **3.02** with *Aspergillus saitoi* α -1,2-mannosidase resulted in formation of only one fluorescent product with the same R_f value as fluorescent α -Man-1,6- α -Man-HTC (**2.13**), thus indicating introduction of α -1,2-mannopyranosidic linkage in this product (Fig. 3.8 line 6, and Fig. 3.8 B (ii)).

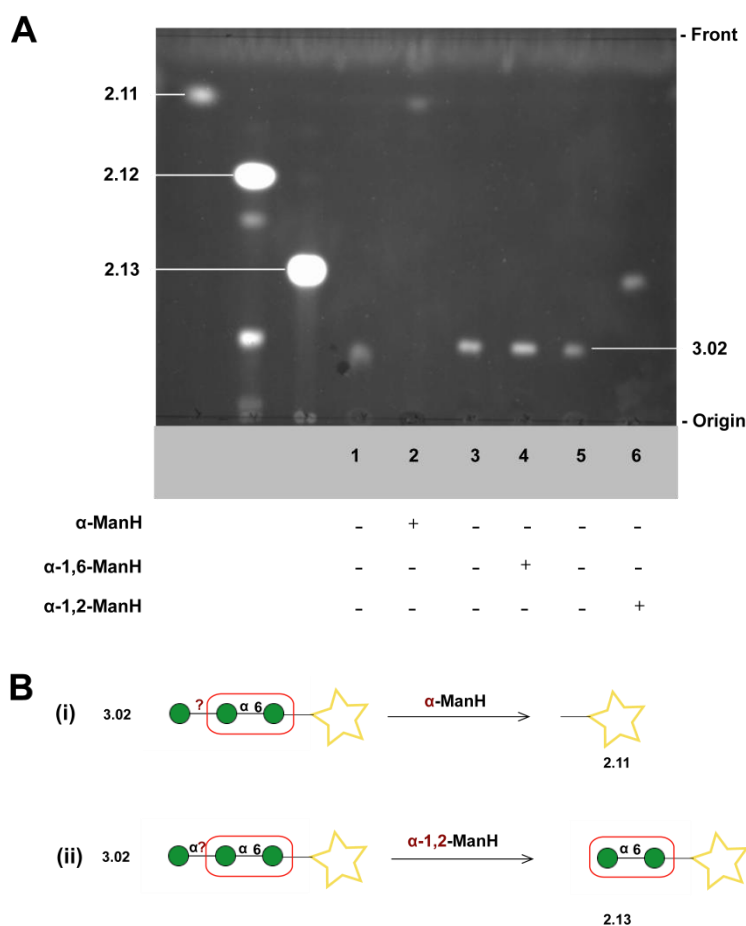


Figure 3.8 TLC analyses to assess stereoselectivity and regioselectivity of trisaccharide fluorescent products by *exo*-glycosidase digestions. (A) TLC image of *exo*-glycosidase digestion of trisaccharide **3.02** with jack bean α -mannosidase (α -ManH), *Xanthomonas manihotis* α -1,6-mannosidase (α -1,6-ManH) and *Aspergillus saitoi* α -1,2-mannosidase (α -1,2-ManH). Enzymes used in the assays are shown below the TLC traces and acceptors and products are shown to the side of each TLC image. Control experiments, lane 1, 3 and 5 (without enzyme), were conducted in parallel with hydrolysis reactions. TLC plates were eluted with CHCl_3 :MeOH:H₂O (10:6:1) and visualised using mid-wave length range UV light. (B) Diagrammatic reaction schemes of *exo*-glycosidase digestion of **3.02** with (i) α -ManH, (ii) α -1,2-ManH.

3.2.6 Confirmation of newly formed linkages in fluorescent mannoside products by LC-MS

TLC analysis of *Aspergillus saitoi* α -1,2-mannosidase digestion revealed an incomplete hydrolysis of disaccharide (**3.01a/b**) compound, indicating presence of mixed fluorescent compounds with major α -1,2- (**3.01a**) and minor α -1,3-linkages (**3.01b**) (Fig. 3.9 A). The minor fluorescent disaccharide (**3.01b**) had a low fluorescent intensity on the TLC plate, thereby making final conclusions challenging. In order to confirm these TLC observations, the reaction mixture from *Aspergillus saitoi* α -1,2-mannosidase digestion of disaccharide (**3.01**) was submitted to LC-MS analyses (Fig. 3.9 B).

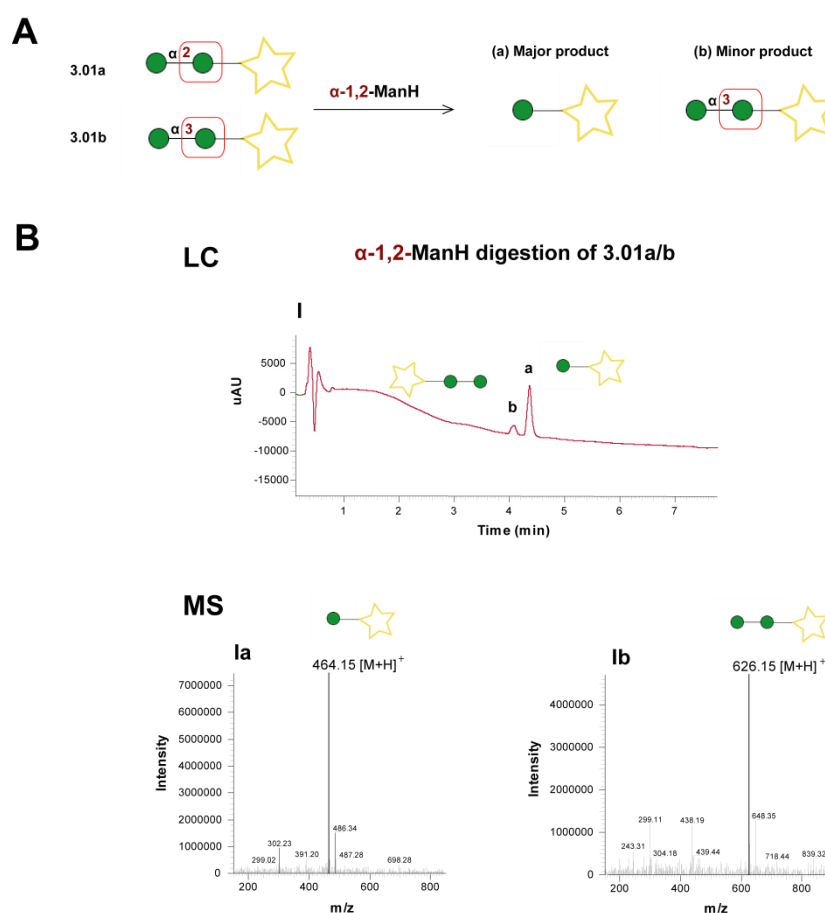


Figure 3.9 Formation of two fluorescent disaccharide isomeric compounds confirmed by LC-MS analysis. (A) Diagrammatic reaction schemes of *exo*-glycosidase digestion of **3.01a/b**. (B I) UV chromatogram of reaction mixture from *exo*-glycosidase digestion of **3.01a/b** with *Aspergillus saitoi* α -1,2-mannosidase (α -1,2-ManH). LC conditions: Kinetex C18 (50 mm/2.1 mm/2.6 micron); mobile phase: water (0.1% TFA)-CH₃CN (10 to 90 %, 18 min, flow rate: 0.3 mL/min); UV detector at 347 nm. (B Ia) MS spectrum of major monosaccharide product α -Man-HTC (**2.12**) obtained from hydrolysis of **3.01a/b**; (B Ib) MS spectrum of minor disaccharide product **3.01b** obtained from hydrolysis of **3.01a/b**.

The LC chromatogram from *Aspergillus saitoi* α -1,2-mannosidase digestion of disaccharide **3.01a/b** revealed presence of two peaks a minor peak (**b**) at retention time 4.0 min and a major (**a**) at 4.4 min (Fig. 3.9, B I). This result was in agreement with TLC observation verifying presence of two isomeric products in **3.01a/b** mixed compounds. The MS spectrum of peak (**a**) had m/z of 464.15, which corresponded to fluorescent α -Man-HTC (**2.12**) formed from **3.01a** as a result of the hydrolysis by *Aspergillus saitoi* α -1,2-mannosidase (Fig. 3.9, B Ia). The MS spectrum of peak (**b**) had m/z of 626.15, which corresponded to unhydrolysed **3.01b** (Fig. 3.9, B Ib).

The LC chromatogram of *Aspergillus saitoi* α -1,2-mannosidase digestion of trisaccharide **3.02** revealed presence of only one peak (**a**) at retention time 4.0 min (Fig. 3.10, A and BI). The MS spectrum of peak (**a**) had m/z of 626.28, which corresponds to fluorescent α -Man-1,6- α -Man-HTC (**2.13**) (Fig. 3.10, BIa) indicating the complete hydrolysis of **3.02** by α -1,2-mannosidase.

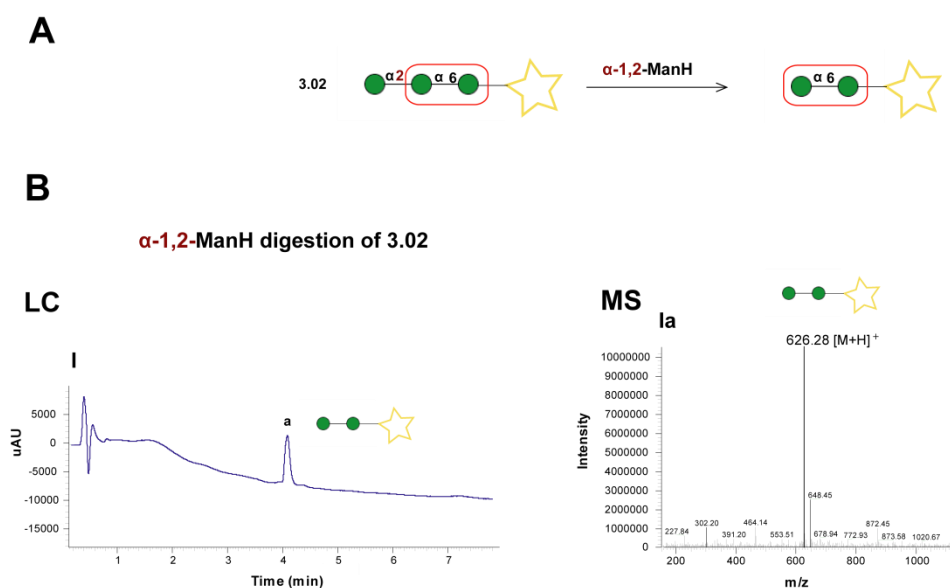


Figure 3.10 Presence of one fluorescent trisaccharide compound confirmed by LC-MS analysis. (A) Diagrammatic reaction schemes of *exo*-glycosidase digestion of **3.02**. (B I) UV chromatogram of reaction mixture from *exo*-glycosidase digestion of **3.02** with *Aspergillus saitoi* α -1,2-mannosidase (α -1,2-ManH). LC conditions: Kinetex C18 (50 mm/2.1 mm/2.6 micron), mobile phase: 0.1% aq. TFA-CH₃CN (10 to 90 %, 18 min, flow rate: 0.3 mL/min) UV detector at 347 nm. (B Ia) MS spectrum of disaccharide product α -Man α -1,6-Man-HTC (**2.12**) obtained from hydrolysis of **3.02**.

3.2.7 Investigation of number and nature of isomeric structures in fluorescent products by IM-MS

As mentioned in Chapter 2, *exo*-glycosidase digestion can be a slow method of analysing isomeric carbohydrates whereas ion mobility coupled to mass spectrometry (IM-MS) is a faster method to analyse numbers and types of isomeric compounds present in the mixture. Therefore, to access these information recorded drift times of disaccharide (**3.01a/b**) and trisaccharide (**3.02**) compounds were compared to the drift time of known α -1,6-linked standards, such as α -Man-1,6- α -Man-HTC (**2.13**) and α -Man-1,6- α -Man-1,6- α -Man-HTC (**2.16**). The latter was obtained as a product from mycobacterial validation of fluorescence-based methodology II (refer to Chapter 2, section 2.7). MS spectra of disaccharide (**3.01**) and trisaccharide (**3.02**) showed signals for both proton and sodium adducts although only proton adducts were well separated in ion mobility spectra whereas signal of sodium adducts of **3.01** and **3.02** were practically undistinguishable. These types of observations have been described in the literature; where investigated group I metal ions upon binding to several isomeric carbohydrates imposed conformational changes in collision cross section of these carbohydrate structures.^{142, 163} The authors demonstrated that out of all group I metal ions sodium ion adducts, which are the most common carbohydrate ions analysed by MS, are often not suitable charge carrier in IM separation because it resulted in identical drift time for investigated isomeric carbohydrates. For this reason in our investigation only mobility spectra of $[M+H]^+$ were analysed.

The drift time IM-MS spectrum of α -Man-1,6- α -Man α -HTC (**2.13**) standard indicated one peak at 5.92 ms (Fig. 3.11, A1). In contrast, the drift time spectrum of investigated mixed isomeric disaccharide (**3.01a/b**) (m/z 626.25) contained two distinct peaks, one at 5.60 ms corresponded to **3.01b** and another at 6.22 ms corresponded to **3.01a** (Fig. 3.11 B1). The peak assignment in this case was based on their intensities which were compared to the intensities of α -1,2-linked **3.01a** and α -1,3-linked **3.01b** observed in the UV chromatogram obtained from normal phase HPLC separation of **3.01** (refer to section 3.2.1, Fig. 3.5 B). The drift time of disaccharide (**3.01**) compound did not coincide with drift times of standard α -Man-1,6- α -Man α -HTC (**2.13**) strongly indicating the absence of non-reducing α -1,6-linkages to mannose residue in tested **3.01** (Fig. 3.11, B1).

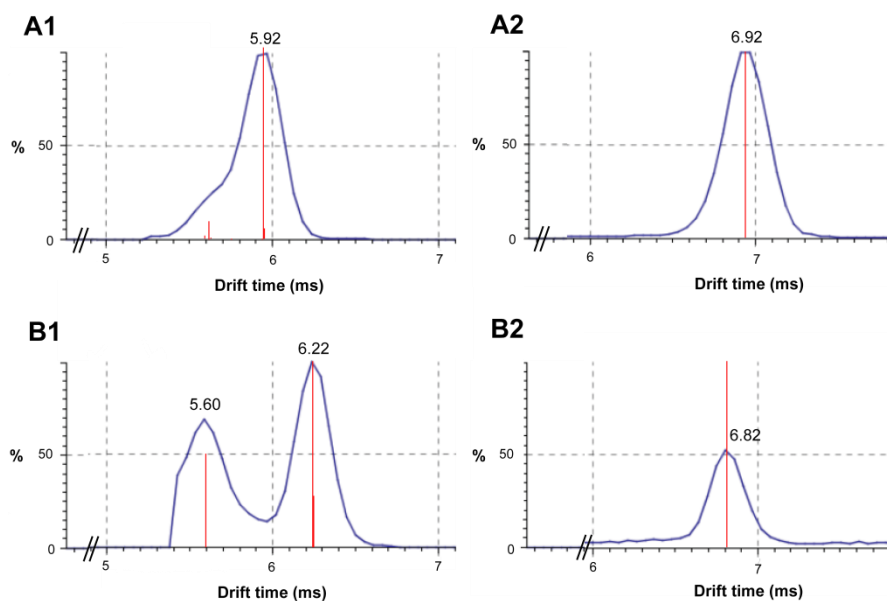


Figure 3.11 Drift time IM-MS spectra to represent number and nature of isomeric structures present in fluorescent mannoside products obtained from incubation with GDP-Man and *Euglena gracilis* microsomal membranes. (A) Drift time IM-MS spectra of standards (A1) α -Man-1,6- α -Man-HTC (**2.13**) (m/z 626.25), (A2) α -Man-1,6- α -Man-1,6- α -Man-HTC (m/z 788.16). (B) Drift time IM-MS spectra of (B1) disaccharide (**3.01a/b**) (m/z 626.25) and (B2) **3.02** (m/z 788.16).

The drift time IM-MS spectrum of α -Man-1,6- α -Man-1,6- α -Man-HTC (**2.16**) standard indicated one peak at 6.92 ms (Fig. 3.11, A2). The drift time IM-MS spectrum of trisaccharide (**3.02**) (m/z 788) revealed a single peak at 6.82 ms, which did not overlapped with α -Man-1,6- α -Man-1,6- α -Man-HTC standard at 6.92 ms (Fig. 3.11, B2). Once more, this data strongly indicated the absence of non-reducing α -1,6-linkage to mannose residue in tested **3.02**.

3.2.8 Summary of fluorescence-based methodology II used to investigate mannosyltransferase activities in *Euglena gracilis*

Fluorescent α -Man-HTC (**2.12**) and α -Man-1,6- α -Man-HTC (**2.13**) were designed to mimic α -1,6-linked intermediates and to fit into *N*-glycan and/or GPI-anchors biosynthetic pathways with a view to probing mannosyltransferases that are responsible for biosynthesis of these glycoconjugates. These compounds proved to be acceptor substrates for mannosyltransferases present in *E. gracilis* microsomal membranes. In order to establish which mannosyltransferases were detected, the structures of enzymatic fluorescent products were elucidated through a combination of HPLC, LC-MS, *exo*-glycosidase digestion and IM-MS methods. The analysed data convincingly indicated the formation of two fluorescent disaccharide (**3.01a/b**) products from α -Man-

HTC (**2.12**); the major product **3.01a**, possesses a α -1,2-mannopyranosidic linkage and the minor **3.01b**, has a α -1,3-mannopyranosidic linkage (Fig. 3.12 A).

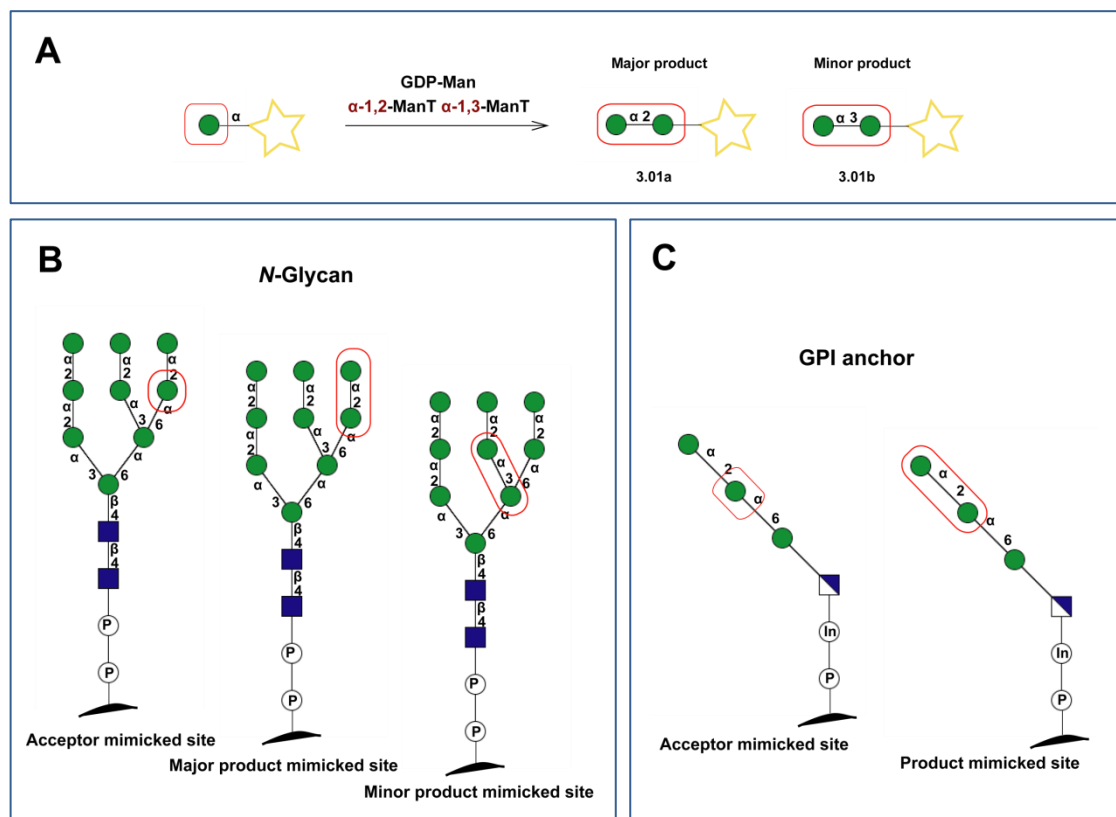


Figure 3.12 Schematic enzymatic reaction of monosaccharide acceptor and structural relationship between its disaccharide products and authentic *N*-glycan and GPI anchor intermediates. (A) Schematic representation of mannosyltransferase reactions of monosaccharide fluorescent acceptor in the presence of GDP-Man and *Euglena gracilis* microsomal membranes. (B) Structural similarity between fluorescent disaccharide products and authentic structure of *N*-glycan; (C) GPI anchor.

In contrast, normal phase HPLC data obtained from enzymatic reaction with α -Man-1,6- α -Man-HTC (**2.13**) acceptor substrate indicated formation of two fluorescent trisaccharide (**3.02a/b**) products (Fig. 3.13 A). Subsequent analysis with *exo*-glycosidase digestion as well as IM-MS analysis indicated presence of one α -1,2-linked isomer. These discrepancies could be explained by either formation of potential artefact in normal phase HPLC or by possible formation of branched product that can be hydrolysed by *Aspergillus saitoi* α -1,2-mannosidase and it can have a similar drift time in IM-MS spectrum. Nevertheless, further investigation to determine presence of the other isomer is required. The characterisation of disaccharide **3.01a/b** and trisaccharide **3.02** confirmed that α -Man-HTC (**2.12**) and α -Man-1,6- α -Man-HTC (**2.13**) acted as acceptor substrates for α -1,2- and α -1,3-ManT present in *E. gracilis*. Enzymatic product comparison to the authentic structure of *N*-glycan and GPI anchor indicates that the

detected enzymes are most likely involved in the construction of *N*-glycan in *E. gracilis*. However, the possibility of targeting α -1,2-ManT responsible for the biosynthesis of GPI anchors cannot be ruled out at this stage (Fig. 3.12 and Fig 3.13 B and C)

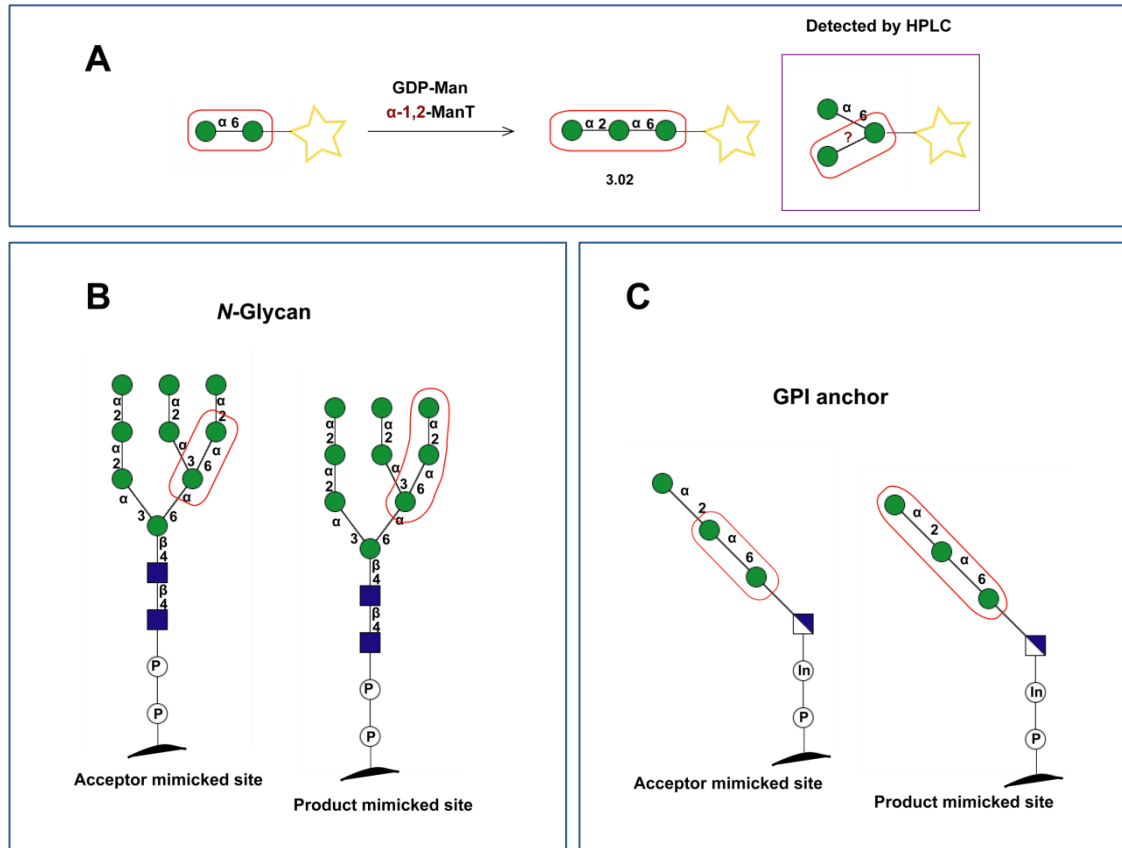


Figure 3.13 Schematic enzymatic reaction of disaccharide acceptor and structural relationship between its disaccharide products and authentic *N*-glycan and GPI anchor intermediates. (A) Schematic representation of mannosyltransferase reactions of disaccharide fluorescent acceptor in the presence of GDP-Man and *Euglena gracilis* microsomal membranes. (B) Structural similarity between fluorescent trisaccharide products and authentic structure of *N*-glycan; (C) GPI anchor.

3.3 Exploration of other glycosyltransferases in *Euglena gracilis*

Detection of α -1,2-mannosyltransferase and α -1,3-mannosyltransferase activities in *E. gracilis* microsomal membranes prompted us to probe activities of membrane-bound glycosyltransferases involved in further modification and decoration of protein-linked *N*-glycan in this organism.

The *N*-glycan biosynthesis up to $\text{Glc}_3\text{Man}_9\text{GlcNAc}_2\text{-P-P-Dol}$ oligosaccharide in all eukaryotes is conserved, however only multicellular eukaryotes can make complex protein-linked *N*-glycans (Chapter 1, section 1.2.1). In general, *N*-glycosylation of proteins in mammalian, avian, insect, fungal, and plant cells involves the transfer of glycan $\text{Glc}_3\text{Man}_9\text{GlcNAc}_2$ from dolichol-P-P derivative to asparagine residues of the emerging protein. This process occurs in the ER and is catalysed by oligosaccharyl transferase.¹⁶⁴ In the next stage, the glycoprotein is transferred to the Golgi apparatus where protein-linked oligosaccharide undergoes terminal modifications that are organism- as well as protein-specific (Fig. 3.14).

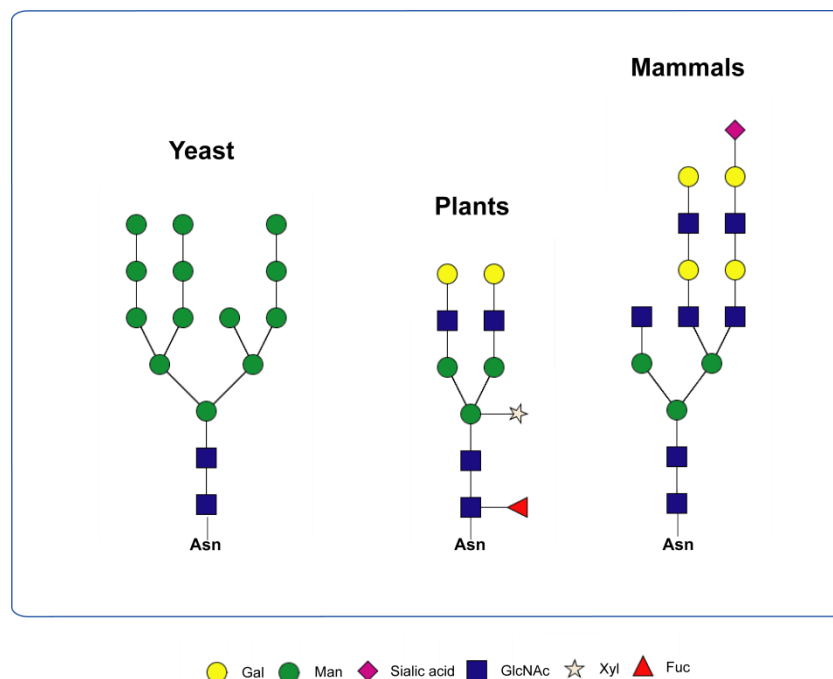


Figure 3.14 Structural variations of *N*-linked glycoproteins in plants, mammalian and yeast systems.

In mammals, the modification of the protein-linked oligosaccharide to the complex form occurs through sequential removal of glucose and mannose residues by glucosidases and mannosidases and addition of *N*-acetylglucosamine, fucose, galactose and sialic acid residues by specific transferases.¹⁶⁵ In plants, the same process takes place, but

additionally, the $\text{Man}_3\text{GlcNAc}_2$ core structure undergoes α -1,3-fucosylation and β -1,2-xylosylation, which is very specific to the plant system.¹⁶⁶ The fucosylation of the core structure is also observed in mammalian cells, however the fucose residues are α -1,6-linked in contrast to α -1,3-linked in plants. By contrast, yeast removes all glucose residues from the high mannose protein-linked oligosaccharide and extends it with extensive numbers of mannose residues without adding the peripheral *N*-acetylglucosamine, galactose and sialic acid residues that are characteristic of the mammalian cells.¹⁶⁷

The only structural information on *N*-linked glycoproteins present in *E. gracilis* is that, as in all eukaryotic cells, it produces $\text{Glc}_3\text{Man}_9\text{GlcNAc}_2\text{-P-P-Dol}$ glycan, which is then transferred onto the protein where glucose residues are removed by glucosidases to form $\text{Man}_9\text{GlcNAc}_2$ *N*-linked glycoprotein.¹⁵⁹ However, to date the *N*-glycan structure of mature glycoproteins has not been characterised yet. Given the complex nature of *Euglena* and its animal- and plants-like characteristics, we were interested to assess its glycosylation pathways.

3.3.1 Fluorescence assays to probe glycosyltransferase activities

Detecting α -1,2- and α -1,3-ManT activities in *E. gracilis* microsomal membranes prompted us to further probe glycosyltransferase activities that are involved in decoration of high mannose protein-linked *N*-glycans. In this investigation fluorescent acceptors α -Man-HTC (**2.12**) and α -Man-1,6- α -Man-HTC (**2.13**) were chosen again because the core $\text{Man}_3\text{GlcNAc}_2$ structure of *N*-glycan has Man and Man-1,6- α -Man residues that can be mimicked by these acceptors and offer potential for the detection of glycosyltransferase activities (Fig. 3.15).

Acceptor substrates for fluorescence-based methodologies II

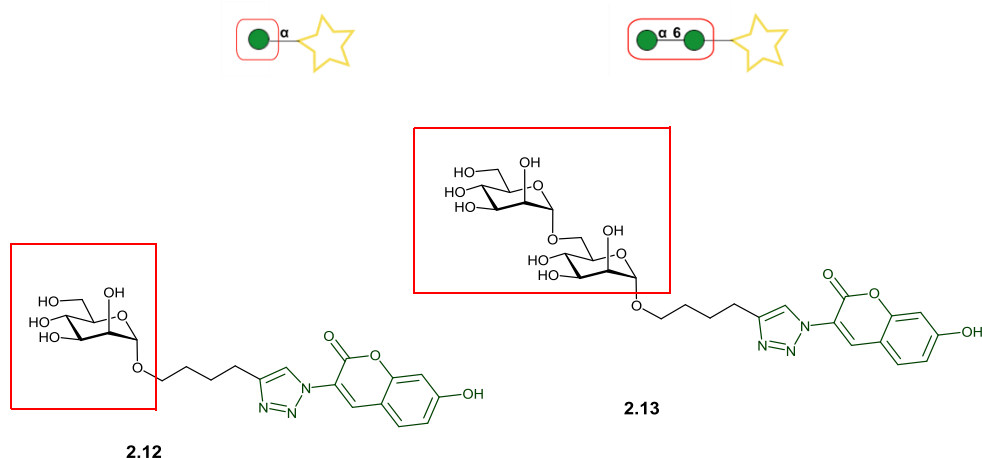


Figure 3.15 Structures of fluorescent acceptors used in fluorescence-based methodology II to probe mannosyltransferases activities present in *Euglena gracilis* microsomal membranes. (Top image) The diagrammatic representation of acceptor substrates. The red box indicates the site of authentic intermediate mimicked by synthetic acceptors.

In this assay system, acceptor substrates α -Man-HTC (**2.12**) and α -Man-1,6- α -Man-HTC (**2.13**) were incubated with various sugar nucleotides, including GDP-Fuc, UDP-Glc and UDP-GlcNAc in the presence of *E. gracilis* microsomal membranes. The absence of endogenous sugar nucleotides and the enzymatic hydrolysis of starting acceptors were monitored by running controls without donor substrate or enzyme, respectively, in parallel with fluorescence assays. The formation of fluorescent products in each enzymatic reaction, after 24 h of incubation at 30 °C, was monitored by TLC (Fig. 3.16 and Fig. 3.17 A and B).

TLC analyses of fluorescent assays with α -Man-HTC (**2.12**) and α -Man-1,6- α -Man-HTC (**2.13**) in the presence of GDP-Fuc and *E. gracilis* microsomal membranes showed that no enzymatic transformation occurred during these reactions (Fig. 3.16 A and Fig. 3.17 B, lane 3). This result is consistent with the overall structure of *N*-glycans in plants, where there is no fucose unit attached to the core mannose residue; instead, it is found on the GlcNAc residue of core *N*-glycan structure.¹⁶⁶

TLC analysis of fluorescent assay involving α -Man-HTC (**2.12**) in the presence of UDP-Glc and *E. gracilis* microsomal membranes revealed two fluorescent bands (Fig. 3.16 A, lane 4). The fluorescent band with the higher R_f value was assigned to the fluorescent disaccharide (**3.03**) product as judged by comparison with R_f value of the α -Man-1,6- α -Man-HTC (**2.13**). The fluorescent band with the lowest R_f value, initially,

was assigned as an oligosaccharide **3.04** with a possible transfer of more than one glucose residues (Fig. 3.16 B).

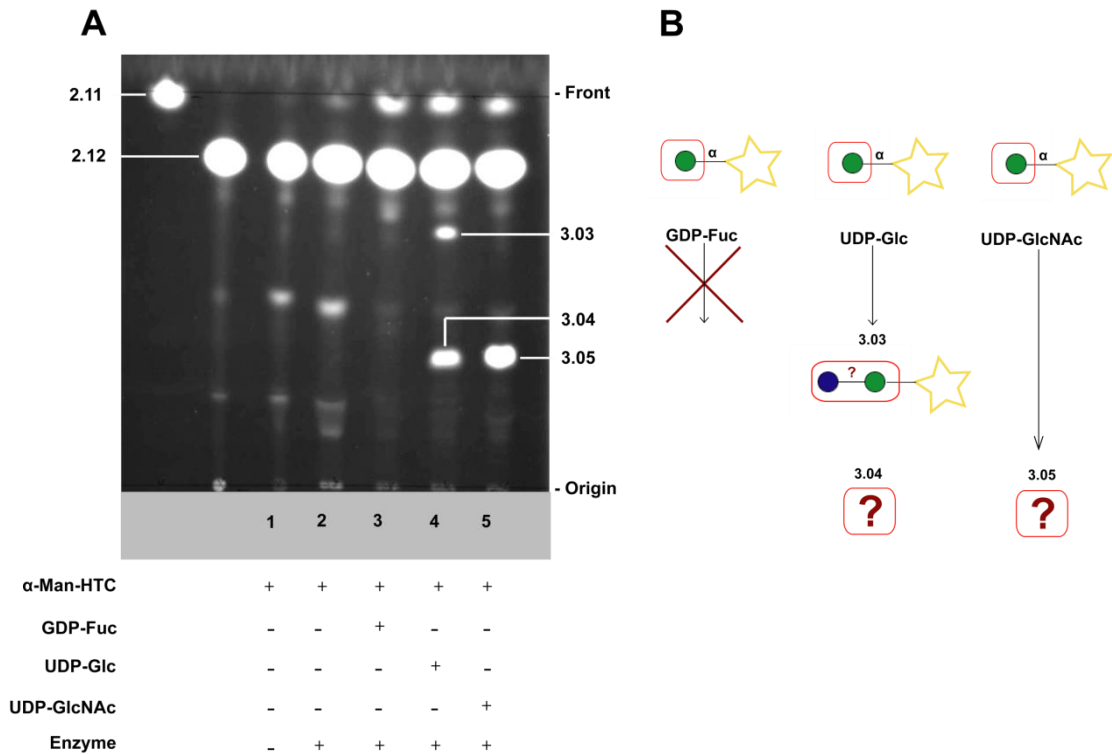


Figure 3.16 TLC analyses of enzymatic assays involving incubation of monosaccharide fluorescent acceptor substrate with number of sugar nucleotides in the presence of *Euglena gracilis* microsomal membranes. TLC images (A) α -Man-HTC acceptor (**2.12**). Fluorescent assay conditions: acceptor (2 mM); donor (4 mM); reaction buffer HEPES/KOH (10 mM, pH 7.0), $MgCl_2/MnCl_2$ (10 mM), KCl (25 mM), glycerol (10%); *E. gracilis* microsomal membrane (150 μ L, 195 μ g of total proteins). TLC plates were eluted with $CHCl_3:MeOH:H_2O$ (10:8:2) and visualised using mid-wave length range UV light. Components of each reaction mixture are shown below the corresponding TLC trace and acceptors and products to the side of the TLC image. Controls experiments, lane 1 (without enzyme) and lane 2 (without donor), were conducted in parallel with these assays. (B) Diagrammatic assignment of the TLC plate.

TLC analysis of fluorescent assays with α -Man-HTC (**2.12**) and UDP-GlcNAc in the presence of *E. gracilis* microsomal membranes revealed one fluorescent band corresponding to formation of fluorescent (**3.05**) product (Fig. 3.16 A, lane 5). Surprisingly, the R_f value of this product co-eluted with the R_f value of the fluorescent (**3.04**) product obtained in the reaction of α -Man-HTC (**2.12**) with UDP-Glc. In theory, the R_f value of product that contains more than one GlcNAc residues is expected to run slightly higher on the TLC plate compared to R_f values of **3.04** that contain more than one glucose residues due to presence of less polar acetyl group on GlcNAc sugar.¹⁶⁸ Furthermore, according to the literature^{165, 166} known structures of *N*-linked glycans from plants and mammals, one could expect a maximum of two GlcNAc residues (β -

1,2- and β -1,4-linked) to be transferred to synthetic α -Man-HTC (**2.12**) acceptor. The expected R_f value for such product should be higher compared to the observed R_f value.

Similarly, TLC analysis of fluorescent assays that contained α -Man-1,6- α -Man-HTC (**2.13**) and UDP-Glc revealed two fluorescent bands (Fig. 3.17 B, lane 4). The product with the higher R_f value was assigned to be a fluorescent trisaccharide (**3.06**) and the product with the lowest R_f was tentatively considered to be an oligosaccharide (**3.07**) with a possible addition of more than one glucose residues. TLC analysis of fluorescent assays that contained α -Man-1,6- α -Man-HTC (**2.13**) and UDP-GlcNAc has shown one fluorescent product (**3.08**) with the same R_f value as **3.07** product obtained in the reaction of α -Man-1,6- α -Man-HTC (**2.13**) with UDP-Glc (Fig. 3.17 B, lane 5). These results implied that fluorescent products **3.04/3.05** and **3.07/3.08** went through a similar modification with a possible addition of polar sugar residue to α -Man-HTC (**2.12**) α -Man-1,6- α -Man-HTC (**2.13**) acceptors.

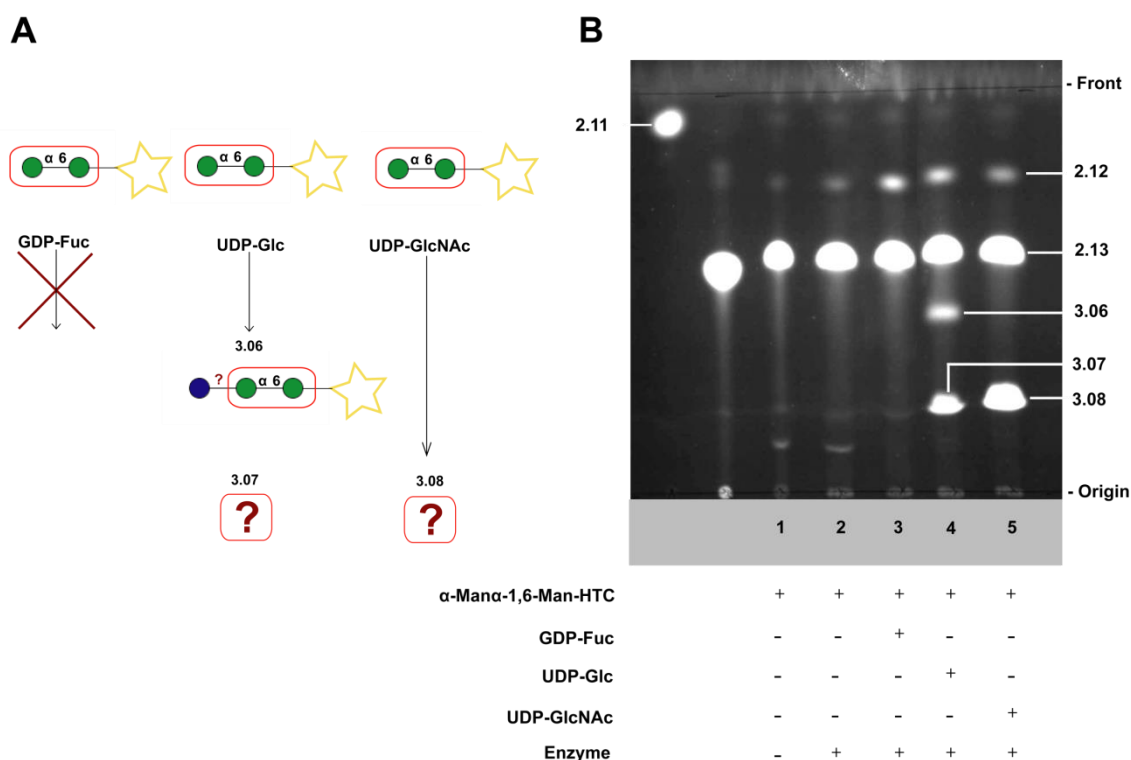


Figure 3.17 TLC analyses of enzymatic assays involving incubation of disaccharide fluorescent acceptor substrate with number of sugar nucleotides in the presence of *Euglena gracilis* microsomal membranes. (A) Diagrammatic assignment of the TLC plate. TLC images (B) α -Man-1,6 α -Man-HTC acceptor (**2.13**). Fluorescent assay conditions: acceptor (2 mM); donor (4 mM); reaction buffer HEPES/KOH (10 mM, pH 7.0), $MgCl_2/MnCl_2$ (10 mM), KCl (25 mM), glycerol (10%); *E. gracilis* microsomal membrane (150 μ L, 195 μ g of total proteins). TLC plates were eluted with $CHCl_3:MeOH:H_2O$ (10:8:2) and visualised using mid-wave length range UV light. Components of each reaction mixture are shown below the corresponding TLC trace and acceptors and products to the side of the TLC image. Controls experiments, lane 1 (without enzyme) and lane 2 (without donor), were conducted in parallel with these assays.

3.3.2 Purification of fluorescent products by HPLC

In order to establish the nature of newly formed linkages in fluorescent **3.03/3.04/3.06/3.07** products obtained from UDP-Glc incubation, and **3.05/3.08** obtained from UDP-GlcNAc incubation, all stated products were purified by reverse phase HPLC method. The purification of reaction mixture from α -Man-HTC (**2.12**) allowed separation of glucosylated products into three peaks (Fig. 3.18 A, red trace), with fluorescent (**3.03**) compound separating into two peaks, labelled as **3.03a** (retention time 8.3 min) and **3.03b** (8.4 min). These retention times corresponded to transfer of one glucose residue as judged by the comparison with the retention time of α -Man-1,6- α -Man-HTC (**2.13**). In contrast, fluorescent (**3.04**) product runs as a single peak (7.0 min). Under the same chromatographic conditions, the purification of reaction mixture obtained from α -Man-1,6- α -Man-HTC (**2.13**) allowed separation of glucosylated products into two single peaks assigned as **3.06** (retention time 7.7 min) and **3.07** (5.9 min) (Fig. 3.18 A, blue trace). The purification of reaction mixtures obtained from incubation of α -Man-HTC (**2.12**) and α -Man-1,6- α -Man-HTC (**2.13**) with UDP-GlcNAc allowed product separation into single peaks designated as (**3.05**) (retention time 7.2 min) and (**3.08**) (6.0 min) (Fig. 3.18 B, red and blue traces).

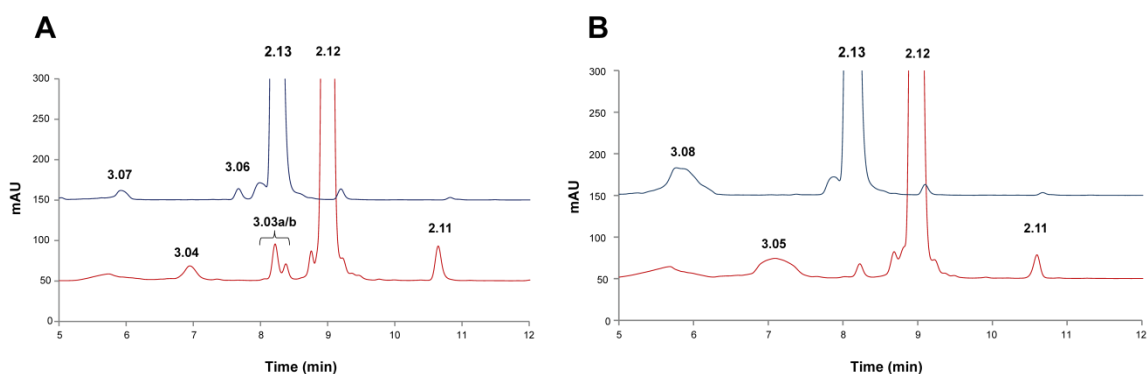


Figure 3.18 HPLC analyses of reaction mixtures obtained from incubation of fluorescent acceptors with UDP-Glc and UDP-GlcNAc in the presence of *Euglena gracilis* microsomal membranes. UV chromatogram (A) Enzymatic incubation of UDP-Glc with α -Man-HTC (**2.12**) (red trace) and α -Man-1,6- α -Man-HTC (**2.13**) (blue trace). (B) Enzymatic incubation of UDP-Glc with α -Man-HTC (**2.12**) (red trace) and α -Man-1,6- α -Man-HTC (**2.13**) (blue trace). HPLC conditions: Phenomenex C18 (250 mm x 10 mm); mobile phase: 0.1% aq. TFA-CH₃CN (10 to 90 % 36 min, flow rate: 5 mL/min); UV detector at 347 nm.

The HPLC chromatogram also allowed integration of product peak area against the peak area of starting material and gave an estimate for the percentage conversion for each enzymatic reaction (Table 3.2). Overall, the percentage conversions are low but no

further improvements were carried out at this stage. Fractions containing purified fluorescent products were combined and subjected to further analysis.

	α -ManHTC (2.12) Reaction products	Conversion (%)	α -Man-1,6 α -Man-HTC (2.13) Reaction products	Conversion (%)
UDP-Glc	3.03a/b	1.6/0.64	3.06	0.7
	3.04	1.8	3.07	1.4
UDP-GlcNAc	3.05	4.9	3.08	5.8

Table 3.2 Percentage conversion of fluorescent products obtained from enzymatic reactions with UDP-Glc and UDP-GlcNAc in the presence of *Euglena gracilis* microsomal membranes.

3.3.3 IM-MS analyses on number of isomeric structures present in trisaccharide fluorescent product obtained from UDP-Glc incubation

Reverse phase HPLC chromatogram revealed presence of two glucosylated disaccharide (**3.03a** and **3.03b**) products, which had the same retention time as α -Man-1,6- α -Man-HTC (**2.13**) indicating probable formation of mixed isomeric compound. In order to confirm this observation, purified sample of mixed isomeric disaccharide (**3.03**) compounds were subjected to ultra-performance liquid chromatography (UPLC) MS coupled to IM-MS (Fig. 3.19). The UPLC selected ion chromatogram showed no separation of mixed isomeric compounds revealing a single peak with retention time at 6.4 min (Fig. 3.19 A). In contrast, the mobility spectrum of **3.03** showed two peaks with m/z of 626 at 7.10 ms and 7.76 ms (Fig. 3.19 B). Presence of other contaminants with higher m/z value affected peaks resolution. These results together with HPLC observations confirmed the presence of two isomeric glucosylated disaccharide compounds in **3.03**. The fact that fluorescence-based assays detected glucosyltransferase activities is in agreement with the overall structure of protein linked oligosaccharide detected in *E. gracilis* (Glc₃Man₉GlcNAc₂-Protein).¹⁵⁹ IM-MS is a good technique that gives fast information on numbers of isomeric structures present in the mixed sample; however this time no standards were available to identify what linkages present in glucosylated disaccharide (**3.03a** and **3.03b**) products.

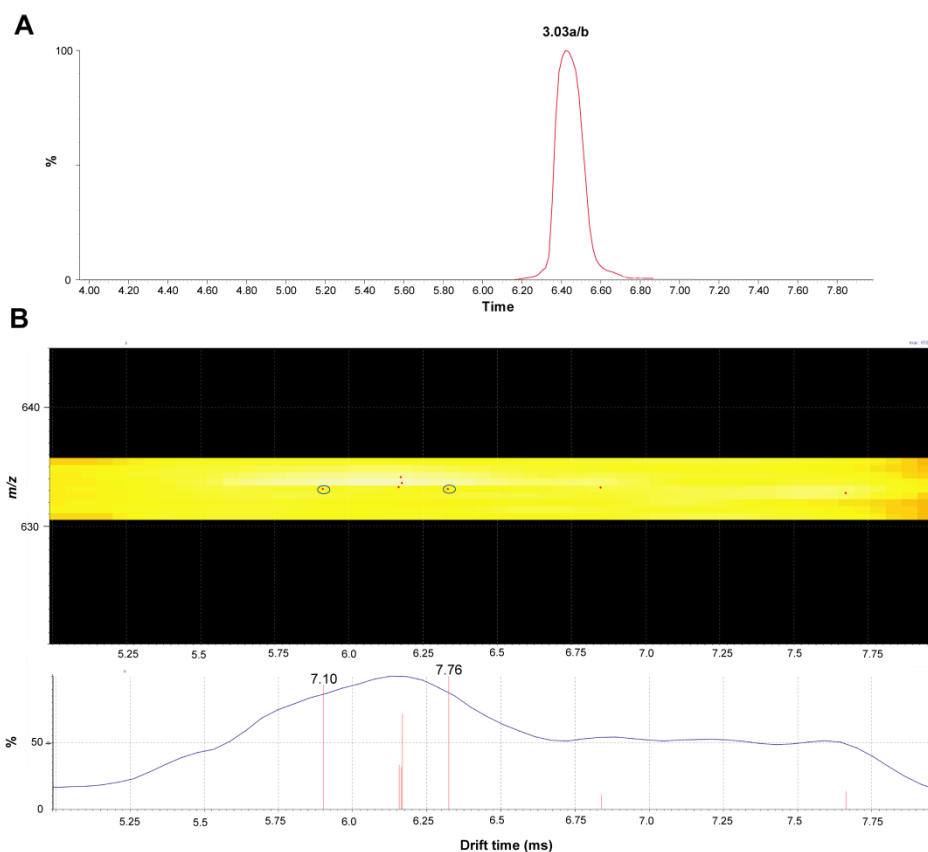


Figure 3.19 . UPLC and ion mobility analyses of isomeric structures present in glucosylated product obtained from incubation of UDP-Glc with *Euglena gracilis* microsomal membranes. (A) UPLC selected ion chromatogram for trisaccharide (**3.03a/b**) compound. UPLC conditions: Acquity UPLC BEH C18 (100 mm/1.0 mm/1.7 μ m), mobile phase: water- CH₃CN (0.1% formic acid) (10 to 90 %, 12 min, flow rate: 0.08 mL/min) MS detector. (B) **top image:** m/z/drift time spectrum of trisaccharide **3.03 a/b**(m/z 626.23); **bottom image:** % intensity/drift time spectrum of **3.03a/b**.

3.3.4 Identification of fluorescent products obtained from incubation of UDP-Glc by LC-MS

LC separation of purified glucosylated disaccharide (**3.03**) and trisaccharide (**3.06**) compounds was performed utilising reverse phase chromatographic conditions to allow a quick access to the required information on the number of glucose residues added to α -Man-HTC (**2.12**) and α -Man-1,6- α -Man-HTC (**2.13**) during biotransformation. The LC chromatogram of disaccharide (**3.03**) showed two peaks with retention time of 4.03 min and 4.16 min (see appendices A1 and A2). The extraction of a selected ion chromatogram with m/z of 626 resulted in only one peak at 4.16 min with this mass. The LC chromatogram of trisaccharide (**3.06**) showed one peak at 3.88 min with a slight shoulder at 3.94 min. These observations could be due to either a carry over or a column contamination.

LC-MS analysis of MS data from selective ion chromatogram of disaccharide (**3.03**) and trisaccharide (**3.06**) confirmed addition of a single glucose residue to α -Man-HTC (**2.12**) and α -Man-1,6- α -Man-HTC (**2.13**) (Fig. 3.20 A and B). The major peaks observed in the MS spectrum of **3.03** was m/z of 626.12 and of **3.06** was m/z of 788.23 corresponded to $[M+H]^+$ of disaccharide and trisaccharide, respectively (Fig. 3.19 B1 and B2). The MS2 fragmentation pattern of $[M+H]^+$ for both compounds showed a sequential loss of one hexose unit (m/z 162) and ultimate release of fluorescent HTC (**2.11**) aglycone (m/z 302.00) (Fig. 3.20 C1 and C2).

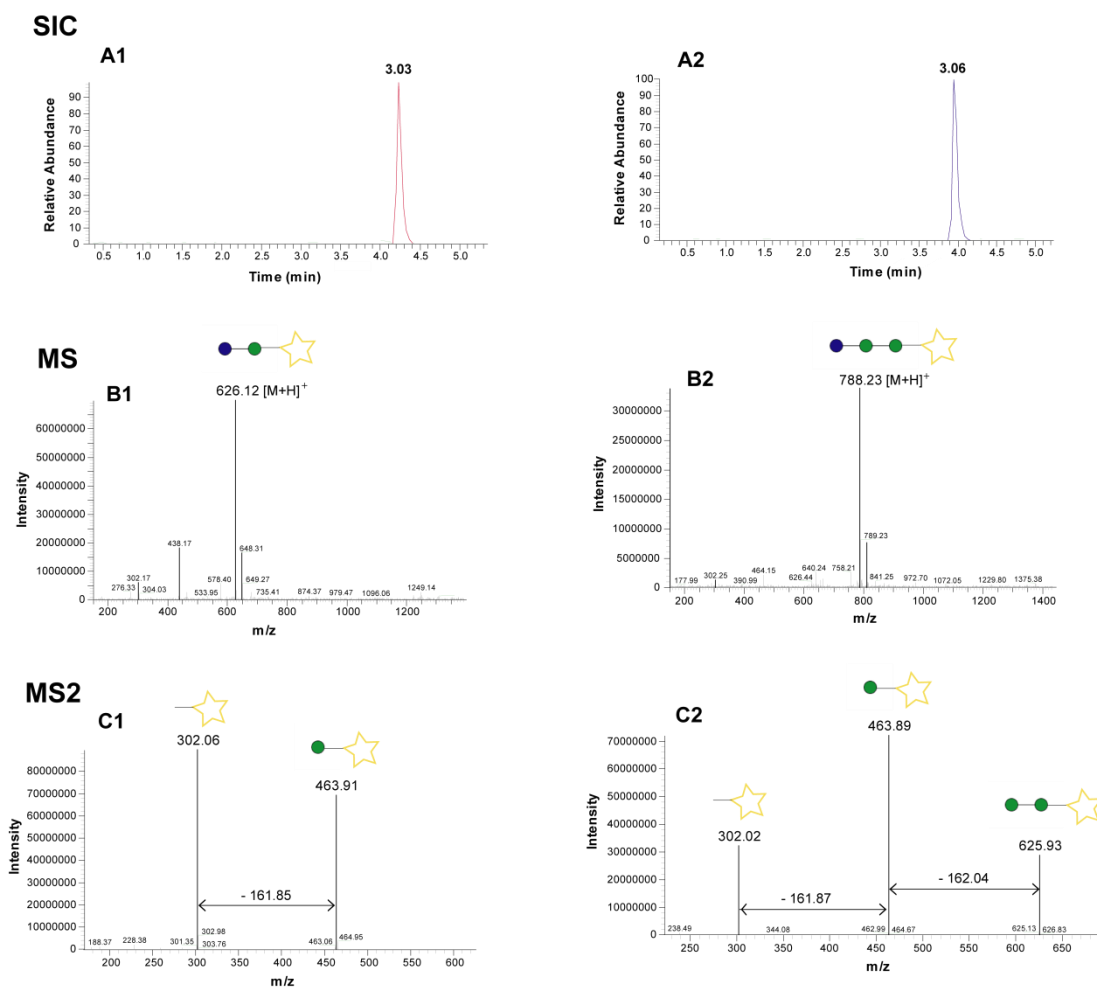


Figure 3.20 LC-MS analyses to investigate the nature of glucosylated products obtained from enzymatic biotransformation with UDP-Glc in the presence of *Euglena gracilis* microsomal membranes. (A) Selective ion chromatograms (SIC) of glucosylated products (A1) disaccharide **3.03** (red trace) and (A2) trisaccharide **3.06** (blue trace). LC conditions: Kinetex C(18) (50 mm/2.1 mm/2.6 μ m); mobile phase: 0.1% aq. TFA-CH₃CN (10 to 90 %, 18 min, flow rate: 0.3 mL/min); UV detector at 347 nm. (B) MS spectra for **3.03** (B1) and **3.06** (B2). (C) MS2 spectra of **3.03** (C1) and **3.06** (C2).

Reverse phase chromatographic conditions were also used with LC separation of purified glucosylated (**3.04**) and (**3.07**) compounds. As described above, TLC analyses of R_f values of these compounds suggested presence of more than one sugar residue

added to α -Man-HTC (**2.12**) and α -Man-1,6- α -Man-HTC (**2.13**) acceptor substrates. In contrast, LC-MS data analysis of **3.04** and **3.07** revealed addition of one sugar residue with slightly higher mass than that calculated by straight forward addition of single glucose residue occurred during these biotransformation (Fig. 3.21).

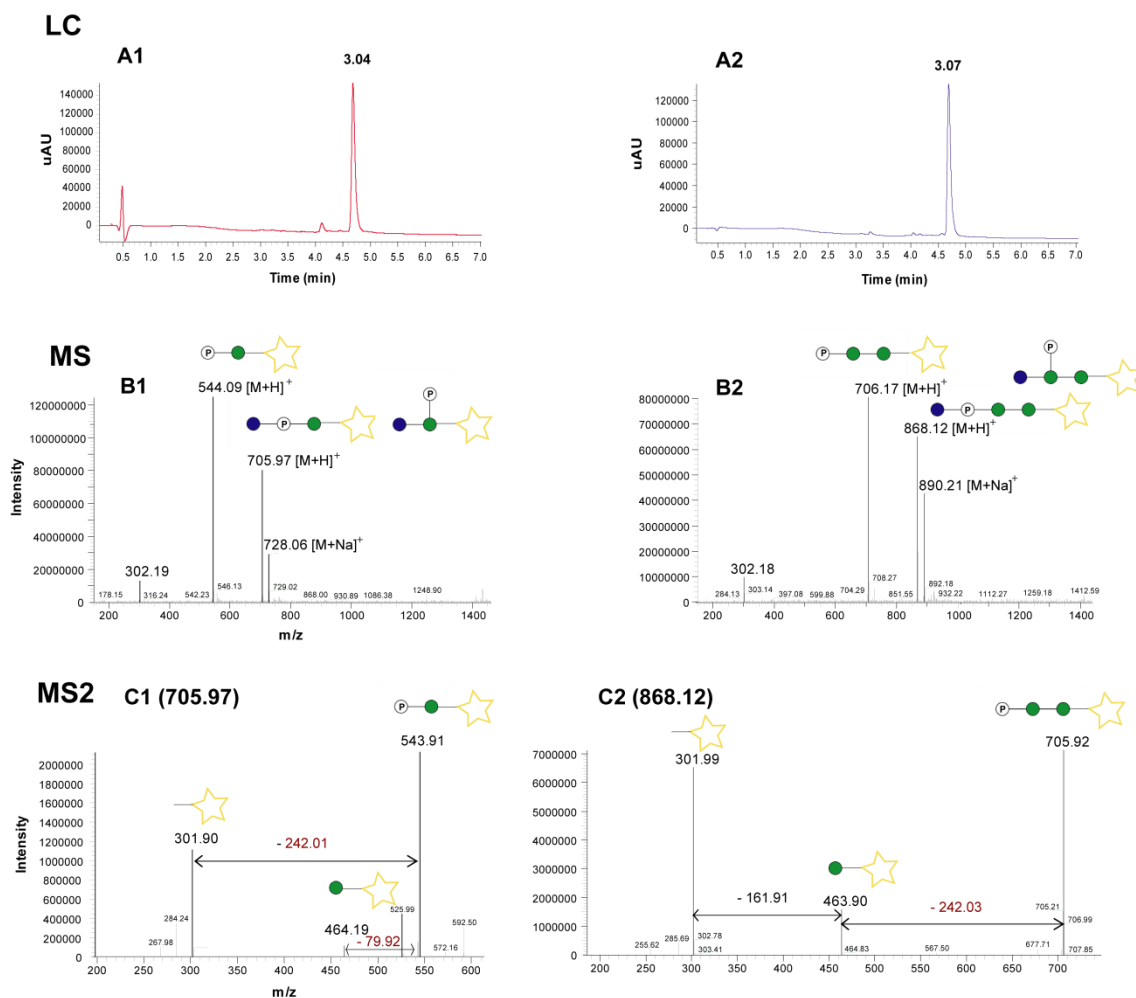


Figure 3.21 LC-MS analyses to investigate the structure of fluorescent products obtained from enzymatic biotransformation with UDP-Glc in the presence of *Euglena gracilis* microsomal membranes. (A) Selective ion chromatograms (SIC) of glucosylated products (A1) trisaccharide **3.04** (red trace) and (A2) tetrasaccharide **3.07** (blue trace). LC conditions: Kinetex C(18) (50 mm/2.1 mm/2.6 μ m); mobile phase: 0.1% aq. TFA-CH₃CN (10 to 90 %, 18 min, flow rate: 0.3 mL/min); UV detector at 347 nm. (B) MS spectra for **3.04** (B1) and **3.07** (B2). (C) MS2 spectra of **3.04** (C1) and **3.07** (C2).

The analysis of MS data of **3.04** revealed two signals. The major signal observed on the MS spectrum was m/z of 544.09 and minor m/z of 705.97 that corresponded to $[M+H]^+$ molecular ions (Fig. 3.21 B1). The MS2 fragmentation pattern of 705.97 showed loss of glucose sugar unit (m/z 162.06) and release of fluorescent fragment with m/z of 543.91 (Fig. 3.21 C1). The second fragmentation resulted in loss of m/z of 242 compared to expected loss of hexose (m/z 162) and further release of fluorescent HTC (**2.11**) aglycone (m/z 301.90). The difference between the observed and predicted

masses was calculated to be m/z of 80, which pointed towards the presence of a phosphate group and a possible formation of $\text{PO}_4\text{-}\alpha\text{-Man-HTC}$ fluorescent fragment with m/z of 543.91.

The analysis of MS data of **3.07** also revealed two signals. The major signal observed on the MS spectrum was m/z of 706.17 and minor m/z of 868.12 that corresponded to $[M+H]^+$ (Fig. 3.21 B2). The MS2 fragmentation pattern of 868.12 showed loss of glucose residue (m/z 162.20) and release of fluorescent fragment with m/z of 705.92 (Fig. 3.21 C2). The second fragmentation again resulted in loss of m/z of 242 compared to calculated loss of hexose (m/z 162) and further release of fluorescent fragment with m/z of 463.90, which corresponds to the calculated mass of $\alpha\text{-Man-HTC}$ (**2.11**). The difference between the observed and predicted masses again was calculated to be m/z of 80, which directed us towards possible formation of $\text{PO}_4\text{-}\alpha\text{-Man-1,6-}\alpha\text{-Man-HTC}$ fluorescent fragment with m/z of 705.92. Subsequently, the third fragmentation of 463.90 resulted in loss of expected hexose unit (m/z 162) and release of fluorescent HTC (**2.11**) aglycone (m/z 302.08).

3.3.5 Identification of fluorescent products obtained from incubation with UDP-GlcNAc by LC-MS

Purified fluorescent compounds (**3.05**) and (**3.08**) obtained from incubation of $\alpha\text{-Man-HTC}$ (**2.12**) and $\alpha\text{-Man-1,6-}\alpha\text{-Man-HTC}$ (**2.13**), respectively, with UDP-GlcNAc in the presence of *E. gracilis* microsomal membranes were subjected to LC-MS analysis. LC-MS analyses showed similar results to those described above for fluorescent (**3.04**) and (**3.07**) (Fig. 3.22).

Briefly, LC-MS analysis of MS data revealed signals of m/z of 746.97 for **3.05** and m/z of 909.16 for **3.08**, which corresponded to $[M+H]^+$ molecular ions of phosphorylated trisaccharide and tetrasaccharide, respectively (Fig. 3.22 B1 and B2). The MS2 fragmentation of 746.97 and 909.16 showed loss of GlcNAc sugar unit (m/z 203.23) and release of fluorescent fragment with m/z of 543.92 for **3.05** and m/z of 705.93 for **3.08** (Fig. 3.22 C1 and C2). The second fragmentation resulted in loss of m/z of 241 for both compounds compared to predicted loss of hexose (m/z 162), and further release of fluorescent HTC (**2.11**) aglycone (m/z 302.08) for **3.05** and fluorescent $\alpha\text{-Man-HTC}$ (**2.12**) (m/z 463.94) for **3.08**. The difference between the observed and predicted masses

was again calculated to be m/z of 80. The third fragmentation of m/z of 463.94 led to release of expected HTC (**2.11**) aglycone (m/z 302.08) for fluorescent (**3.08**) compound.

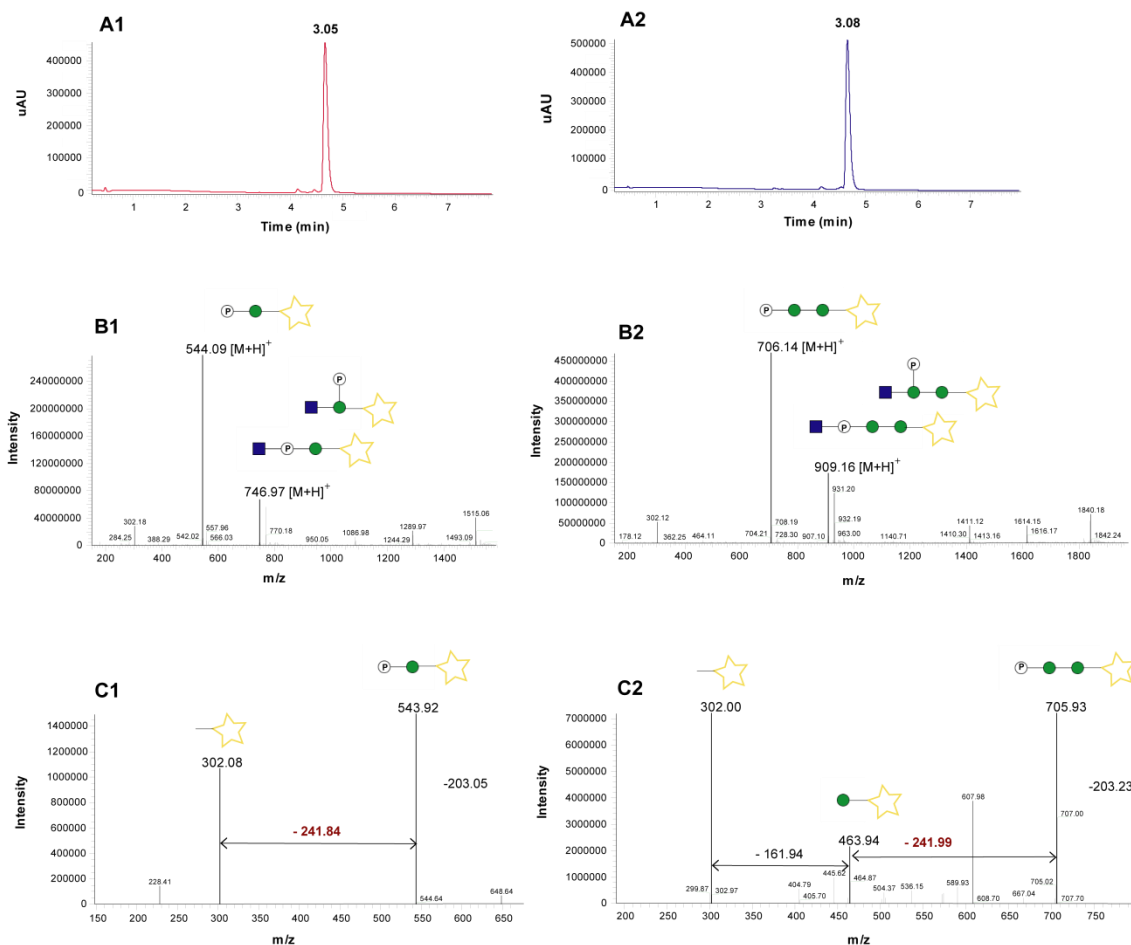


Figure 3.22 LC-MS analyses to investigate the nature of fluorescent products obtained from enzymatic biotransformation with UDP-GlcNAc in the presence of *Euglena gracilis* microsomal membranes. (A) UV chromatograms (A1) **3.05** (red trace), (A2) **3.08** (blue trace). LC conditions: Kinetex C18 (50 mm x 2.1 mm x 2.6 micron); mobile phase: CH₃CN-water (10 to 90 % 18 min, flow rate 0.3 mL/min); UV detector at 347 nm. MS. (B) MS spectra for **3.05** (B1) and **3.08** (B2). (C) MS2 spectra for **3.05** (C1) and **3.08** (C2).

LC-MS data, that described above are conclusive with formation of phosphate bonds, resulting in generation of a new phosphodiester-linkage in trisaccharide (**3.04/3.05**) and tetrasaccharide (**3.07/3.08**) products. This was also evident in the MS spectra for all analysed compounds that contain a major signal of m/z 544 and m/z 706. This signal corresponded to PO₄- α -Man-HTC and PO₄- α -Man-1,6- α -Man-HTC, respectively. At this stage the formation of isomeric phosphomonoester bond cannot be ruled out. Therefore, the nature of newly formed phosphate bonds in **3.04/3.07** (UDP-Glc) and **3.05/3.08** (UDP-GlcNAc) were investigated through a series of enzymatic hydrolysis with and without chemical degradation.

3.3.6 Investigation of newly formed linkages in fluorescent products through enzymatic and chemical degradations

In order to rule out formation of terminal phosphate, **3.04/3.07** (UDP-Glc) and **3.05/3.08** (UDP-GlcNAc) were submitted to the enzymatic degradation with alkaline phosphatase, which catalyses a hydrolytic cleavage of terminal phosphate monoesters releasing an inorganic phosphate.^{169, 170} Therefore, compounds **3.04**, **3.05**, **3.07** and **3.08** were treated with alkaline phosphatase under alkaline conditions and the progress of these reactions was monitored by TLC. A positive control experiment was performed in parallel with UDP substrate to ensure activity of alkaline phosphatase in the sample, as well as negative control without enzymes to rule out the decomposition of starting fluorescent compounds under experimental conditions. TLC analyses of all investigated compounds revealed no changes confirming that none of these compounds had terminal phosphate groups attached (Fig. 3.23 A and B).

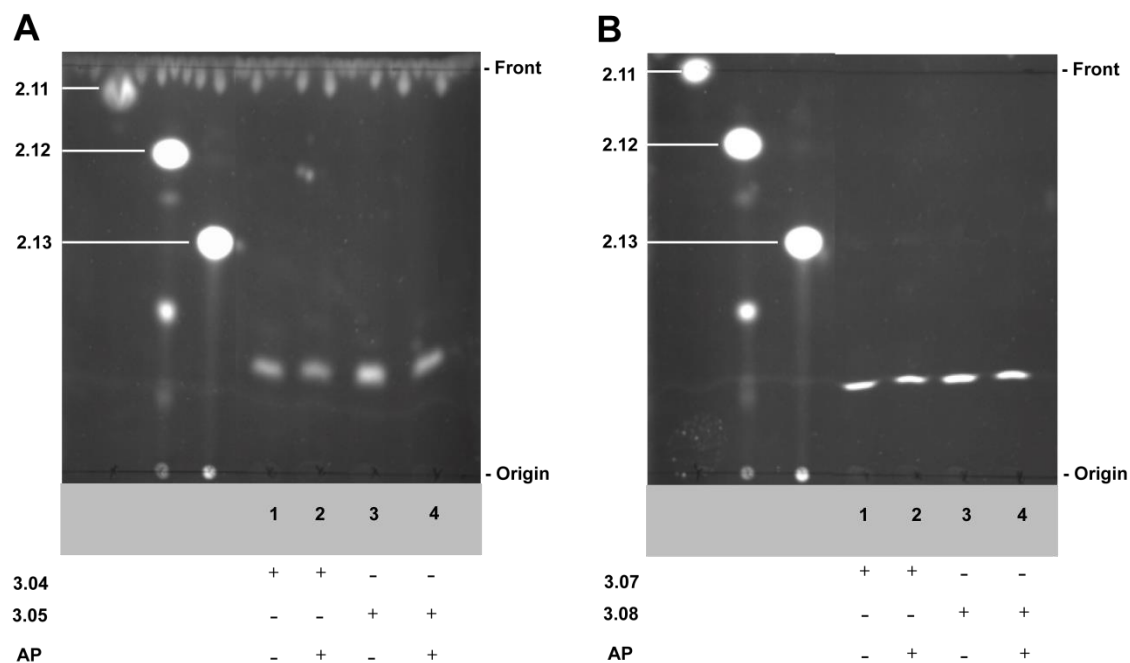


Figure 3.23 TLC analyses to investigate presence of terminal phosphate in fluorescent products through application of enzymatic hydrolysis with alkaline phosphatase. TLC images (A) Enzymatic hydrolysis of **3.04/3.05** (UDP-Glc) with alkaline phosphatase (AP); (B) Enzymatic hydrolysis of **3.07/3.08** (UDP-GlcNAc) with AP. Components and enzyme used in these assays are shown in the table below the TLC traces. Control experiments, lane 1 and 2 (without enzyme), were conducted in parallel with these assays. TLC plates were eluted with CHCl₃:MeOH:H₂O (10:8:2) and visualised using mid-wave length range UV light.

The formation of phosphodiester-linkages in **3.04**, **3.05**, **3.07** and **3.08** was examined through chemical degradation with trifluoroacetic acid (TFA) following by treatment with alkaline phosphatase. During this reaction, acidic condition promotes hydrolysis

of the glycosidic bond between Glc (**3.04/3.07**)/GlcNAc (**3.05/3.08**) residue and phosphate releasing fluorescent phosphate monoester compounds. Further treatment with alkaline phosphatase removes terminal phosphate group with possible release of either fluorescent α -Man-HTC (**2.12**) or α -Man-1,6- α -Man-HTC (**2.13**) compounds (Fig. 3.24 A and B).

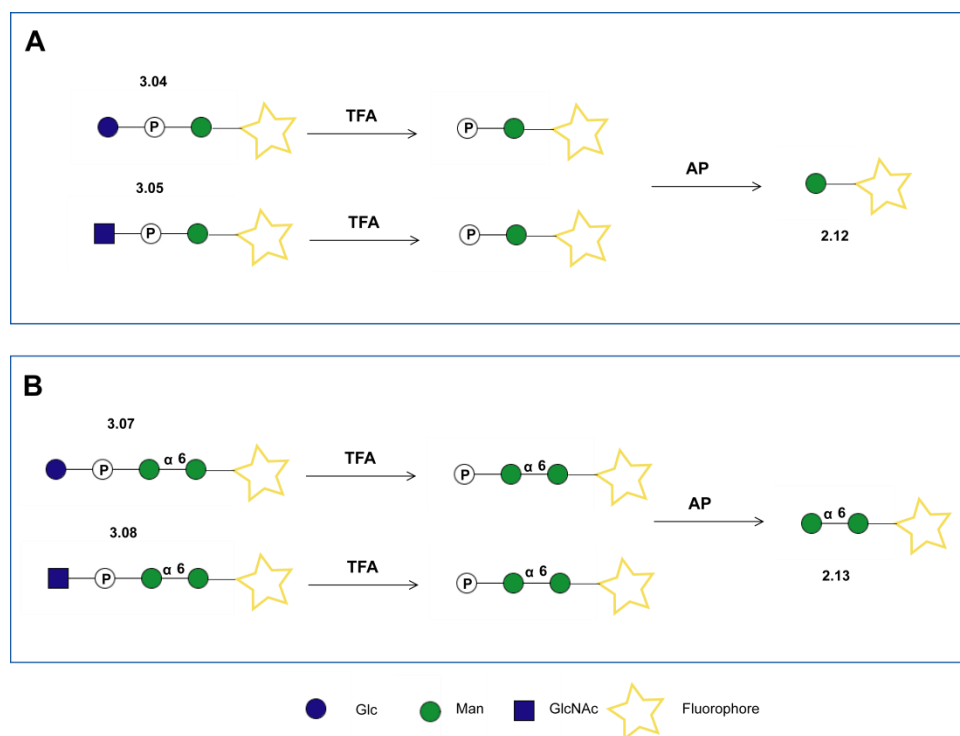


Figure 3.24 Diagrammatic representation of sequential chemical and enzymatic degradation of fluorescent trisaccharide and tetrasaccharide products containing phosphodiester bond. Trifluoroacetic acid (TFA) and alkaline phosphatase (AP).

All four compounds were subjected to acid hydrolysis and alkaline phosphatase treatment and the progress of these reactions was monitored by TLC. TLC analysis showed that after acid hydrolysis faint fluorescent bands were detected at the origin of the TLC plate for all tested compounds (Fig. 3.25 A and B, lane 1 and 3). Subsequently, on treatment with the alkaline phosphatase, the observed fluorescent bands for all tested compounds had higher R_f values compared to those detected previously. In particular, in case of **3.04** and **3.05** both fluorescent bands had the same R_f value as fluorescent α -Man-HTC (**2.12**) compound and, in case of **3.07** and **3.08**, fluorescent bands had same R_f value as fluorescent α -Man-1,6- α -Man-HTC (**2.13**) compound (Fig. 3.25 A and B, lane 2 and 4). These observations strongly indicated presence of phosphodiester bond in all tested compounds.

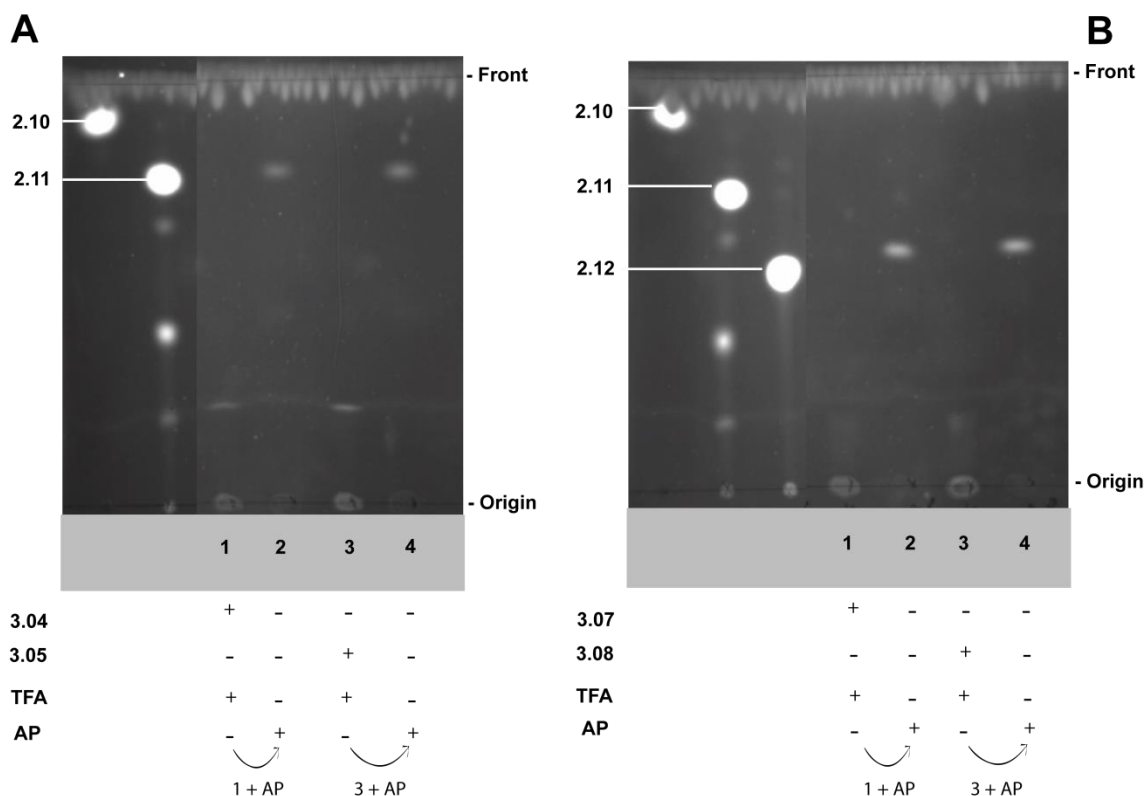


Figure 3.25 TLC analyses to investigate the presence of phosphodiester bond in fluorescent products through application of chemical degradation and enzymatic hydrolysis. Chemical degradation with TFA and enzymatic hydrolysis with AP (A) trisaccharide **3.04** and **3.05** (B) tetrasaccharide **3.07** and **3.08**. Components used in these assays are shown in the table below the TLC traces. Control experiments lane 1 and 2 (without enzyme) were conducted in parallel with these assays. The TLC plates eluted with $\text{CHCl}_3:\text{MeOH}:\text{H}_2\text{O}$ (10:8:2) and visualised using mid-wave length range UV light.

3.3.7 Characterisation and confirmation of fluorescent product by NMR spectroscopy

Results discussed above about the possible formation of phosphodiester-linkages in **3.04/3.07** (UDP-Glc) and **3.05/3.08** (UDP-GlcNAc) suggested the presence of sugar-phosphate transferase activities in *E. gracilis* microsomal membranes, which transfer sugar-phosphate moieties from UDP-sugar donor substrate to acceptor substrates forming a phosphodiester-linkage. Therefore, in order to further strengthen this proposed structural assignment, tetrasaccharide (**3.08**) compound obtained from UDP-GlcNAc incubation was subjected to NMR spectroscopy. For this purpose, the enzymatic reaction involving UDP-GlcNAc and acceptor **2.12** in the presence of *E. gracilis* microsomal membranes was scaled up to obtain approximately 0.12 mg of **3.08** with estimated 10% enzymatic conversion. In an attempt to increase the yield of product, the enzymatic reaction was run for 48 h at 30 °C with further addition of *E.*

gracilis microsomal membranes aliquot after 24 h. The obtained product was purified by reverse phase HPLC resulting in a 43% isolated product yield (0.48 mg). The purified **3.08** was submitted NMR spectroscopy in order to aid structural assignment (Fig. 3.26 and Fig. 3.27).

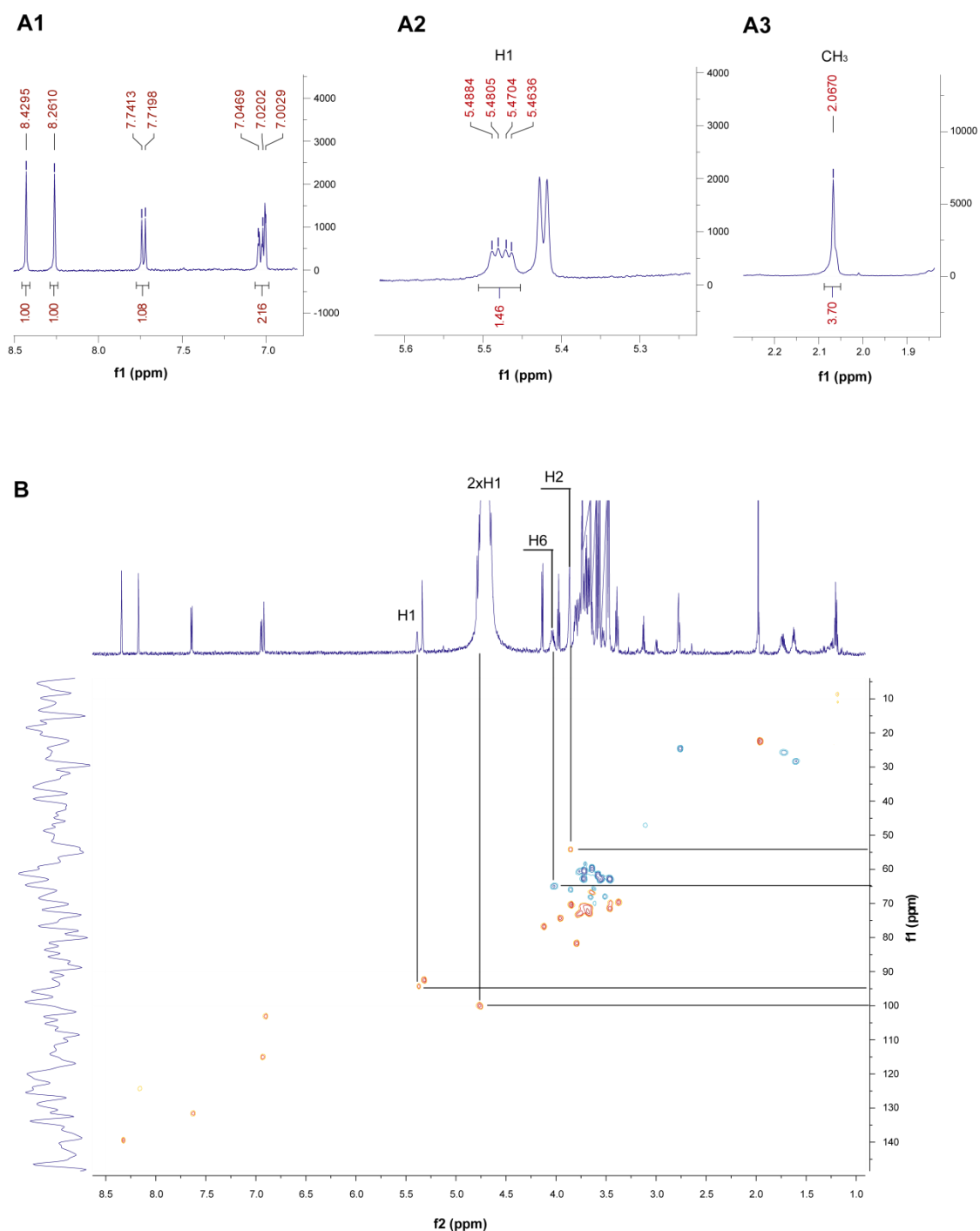


Figure 3.26 Characterisation of fluorescent phosphodiester-linked product by the NMR spectroscopy. (A) The ¹H NMR spectra of selected regions to emphasise formation of **3.08**. (B) HSQC 2D spectrum of **3.08** (in red signals for CH and CH₃ and in blue signals for CH₂). The NMR was run in D₂O.

The ^1H NMR spectrum of phosphodiester-linked (**3.08**) displayed all four coumarin signals in the aromatic region and a singlet signal at δ 8.26 ppm for the 1,4-triazole ring (Fig. 3.26 A1 and Appendices A6). The proton signal at δ 5.48 ppm was assigned to the anomeric proton of GlcNAc sugar residue by utilising 2D analysis of ^1H - ^{13}C HSQC of H1 with C1 (δ_{H} 5.48, δ_{C} 94.3 ppm) (Fig. 3.26 A2 and Fig. 3.27). The other two expected anomeric signals of two mannose sugar residues run under the solvent peak but can be again identified through the ^1H - ^{13}C HSQC correlation of H1 with C1 (δ_{C} 100 ppm). The observed doublet of doublets for the anomeric signal of the GlcNAc sugar residue, instead of expected doublet of a simple glycoside, is indicative of ^1H - ^1H spin-spin coupling between H1 and H2 ($J_{1,2}$ 3.6 Hz) and ^1H - ^{31}P spin-spin coupling between H1 and P ($J_{1,\text{P}}$ 7.2 Hz). The small value for both coupling constants suggests that anomeric centre on the GlcNAc has a α -configuration.^{171, 172} The proton signal at δ 4.14 ppm was assigned to H6a and H6b of GlcNAc sugar residue by ^1H - ^{13}C HSQC correlations of H6a and H6b with C6 (δ_{H} 5.48, δ_{C} 94.3 ppm) and the proton signal at δ 3.95 ppm was assigned to H2 of GlcNAc residue by ^1H - ^1H COSY correlations of H2 with H1. Another characteristic proton signal, such as CH_3 of acetyl group on the GlcNAc sugar residue at δ 2.06 ppm was also evident in the ^1H NMR spectrum (Fig. 3.26 A3).

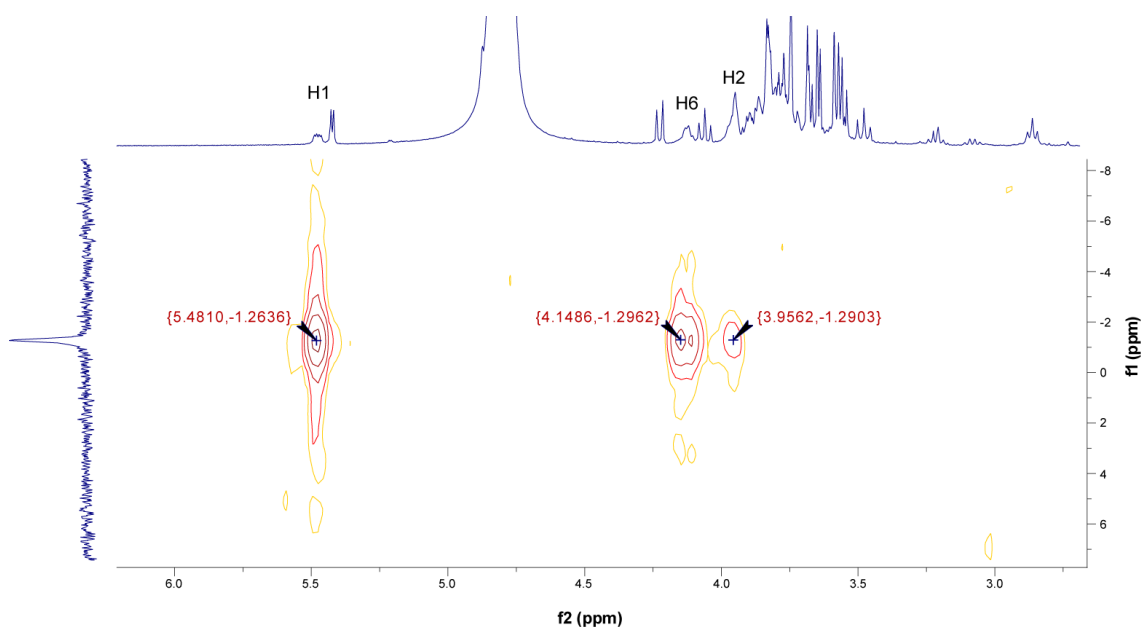


Figure 3.27 Characterisation of fluorescent phosphodiester-linked product by the NMR spectroscopy. ^1H - ^{31}P HMBC spectrum (f1 ^{31}P and f2 ^1H).

Analysis of the ^{31}P NMR spectrum showed one singlet signal at δ -1.26 ppm which is a characteristic signal of phosphodiester.¹⁷³ Subsequently, the 2D analysis of the ^{31}P

signal on the ^1H - ^{31}P HMBC spectrum had cross-peak signals at δ 5.48 ppm for H1, 4.14 ppm for H6 and 3.95 ppm for H2 (Fig. 3.27, Appendices A7). These NMR data confirmed that the sugar-phosphate transferase enzyme present in *E. gracilis* microsomal membranes catalyses transfer of a GlcNAc-P sugar residue from the UDP-GlcNAc to the 6'-hydroxyl of the mannose sugar residue of α -Man-1,6- α -Man-HTC (**2.13**) acceptor substrate with formation of **3.08** product, which possesses a phosphodiester-linkage (Fig. 3.28).

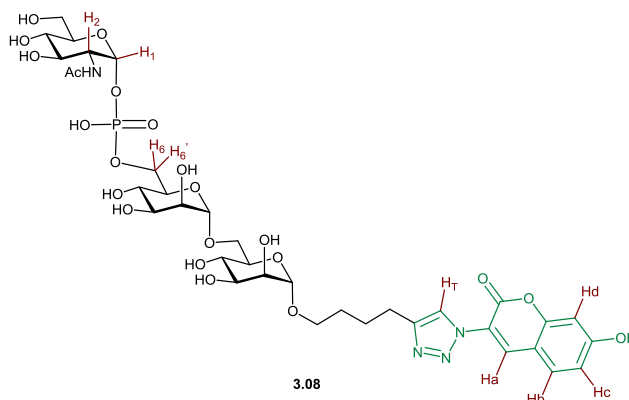


Figure 3.28 Proposed structure and assignment of fluorescent phosphodiester-linked compound for NMR analysis.

3.3.8 Summary of fluorescence-based methodology II used to investigate glycosyltransferase activities in *Euglena gracilis*

Fluorescence-based methodology II utilising α -Man-HTC (**2.12**) and α -Man-1,6- α -Man-HTC (**2.13**) acceptor substrates allowed detection of glycosyltransferase activities in *E. gracilis* microsomal membranes, which are known to be responsible for biosynthesis of lipid-linked *N*-glycan and further decoration of protein-linked *N*-glycan in eukaryotic cells. Fluorescent assays with GDP-Fuc donor substrate and fluorescent α -Man-HTC (**2.12**) as well as α -Man-1,6- α -Man-HTC (**2.13**) acceptor substrates did not give any of fluorescent product, which is consistent with overall structure of protein-linked *N*-glycan where fucose sugar residue is attached to the *N*-acetylglucosamine but not to mannose of the core structure (Fig. 3.29 AI and BI).

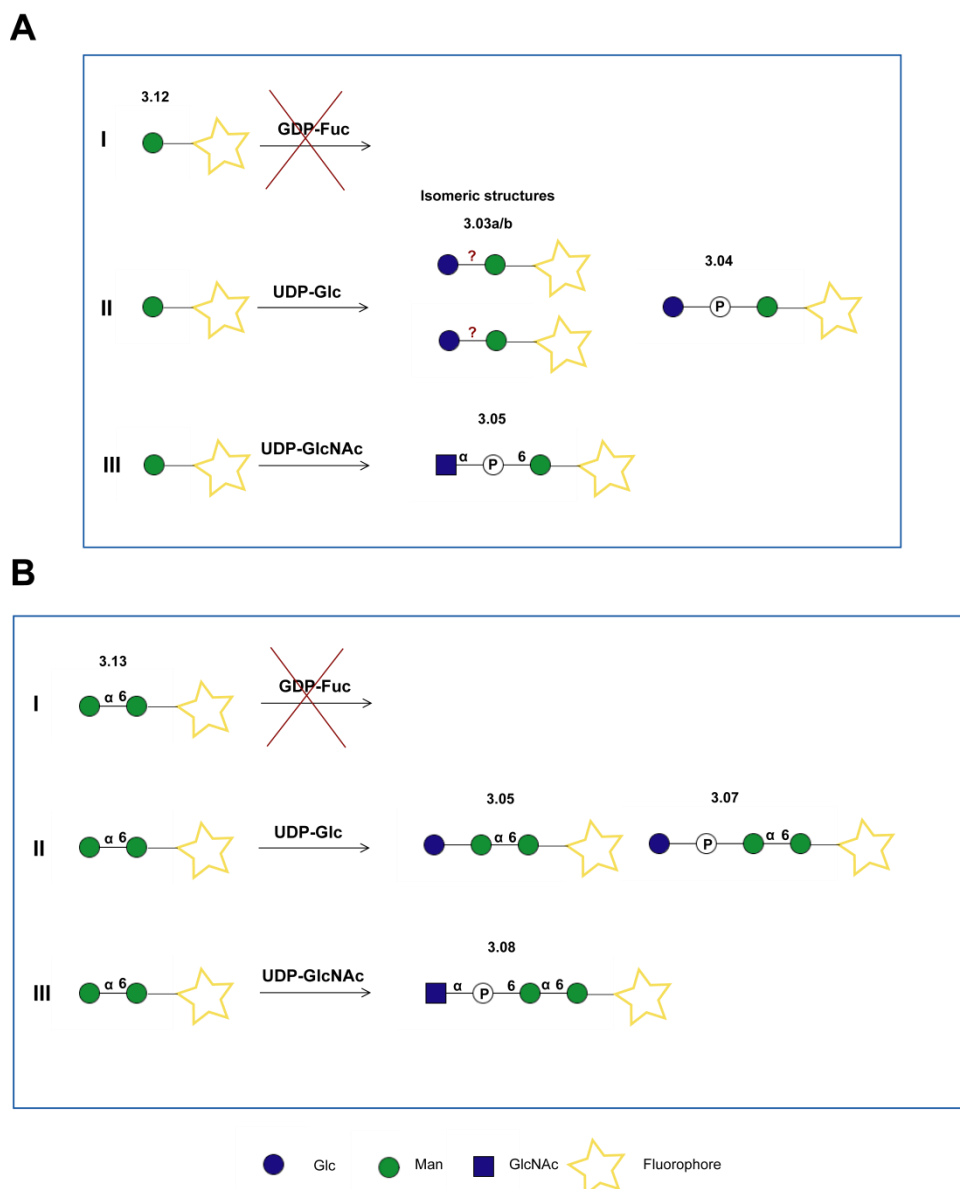


Figure 3.29 Schematic representation of enzymatic activities detected in *Euglena gracilis* microsomal membranes. (A) Enzymatic reactions and their products from incubation of α -Man-HTC (**2.12**) with sugar nucleotides (GDP-Fuc, UDP-Glc and UDP-GlcNAc). (B) Enzymatic reactions and their products from incubation of α -Man α -1,6-Man-HTC (**2.13**) with sugar nucleotides (GDP-Fuc, UDP-Glc and UDP-GlcNAc).

In contrast, fluorescent assays with UDP-Glc detected glucosyltransferase activities resulting in formation of two isomeric glucosylated disaccharides (**3.03a/b**) from incubation of fluorescent α -Man-HTC (**2.12**) and glucosylated trisaccharide (**3.05**) from incubation of α -Man-1,6- α -Man-HTC (**2.13**) (Fig. 3.29 AII and BII). These detected glucosyltransferase activities are consistent with the reported lipid-linked structure of *N*-glycan in *E. gracilis*, where three glucose residues are added to the lipid-linked oligosaccharide structure.¹⁵⁹ LC-MS and IMS MS analysis of these products gave information about structural and isomeric compositions but not about the type of linkages formed during biotransformation. According to the known conserved structure

of lipid linked *N*-glycan,⁴¹ we could predict that fluorescent isomeric mixture of disaccharide (**3.03a/b**) and trisaccharide (**3.06**) compounds to have either α -1,3- or α -1,2-linkages. Therefore, in the future, the anomeric configuration of glycosidic linkages in these compounds could be accessed through *exo*-glycosidase digestion with a non-specific α - or β -glucosidases. In contrast, regioselectivity of newly formed glycosidic linkages cannot be accessed using *exo*-glycosidase digestion with site specific enzymes due to the absence of commercially available linkage specific enzymes of these types. The regioselectivity of glycosidic linkages can be detected through application of old techniques used in radiolabelled assays, such as permethylation of sugars followed by GC-MS analysis or electrospray mass spectrometry prior to periodate oxidation and reduction with NaBH₄.^{87, 140}

The most exciting and unexpected result obtained from fluorescent assays that involved incubation of α -Man-HTC (**2.12**) and α -Man-1,6- α -Man-HTC (**2.13**) acceptor substrates with UDP-Glc and UDP-GlcNAc was the detection of *N*-acetylglucosamine-1-phosphate transferase (GlcNAc-P-Tase) activity in *E. gracilis* microsomal membranes. This enzymatic activity led to formation of glucosylated phosphodiester-linked disaccharide (**3.04**) and trisaccharide (**3.07**) products from incubation of UDP-Glc with α -Man-HTC (**2.12**) and α -Man-1,6- α -Man-HTC (**2.13**), respectively. At the same time, it was also responsible for the formation of *N*-acetylglucosaminylated phosphodiester-lined disaccharide (**3.05**) and trisaccharide (**3.08**) from incubation of UDP-GlcNAc with α -Man-HTC (**2.12**) and α -Man-1,6- α -Man-HTC (**2.13**), respectively (Fig. 3.29 AIII and BIII). Indirectly, formation of phosphodiester linkages in **3.04/3.07** and **3.05/3.08** was demonstrated through utilisation of LC-MS and chemical-enzymatic degradations. Directly, this type of linkage was confirmed in trisaccharide (**3.08**) by NMR spectroscopy, which indicated transfer of *N*-acetylglucosamine phosphate to the 6-hydroxy group of the non-reducing mannose residue in α -anomeric configuration.

Activities of *N*-acetylglucosaminyltransferases I and II were not detected in fluorescent assays with α -Man-HTC (**2.12**) and α -Man α -1,6- α -Man-HTC (**2.13**) acceptor substrates because *N*-acetylglucosaminyltransferase I requires a branched structure, such as Man α -1,3-Man(Man α -1,6)Man β -GlcNAc and *N*-acetylglucosaminyltransferase II is acceptor substrate specific enzyme (see Chapter 1, section 1.2.3).⁵⁴

Both of these enzymes belong to the asparagine-linked glycosylation gene that catalyses transfer of mannose sugar residue from Man-P-Dol to Man₈GlcNAc₂-P-P-dolichhol or Man₅GlcNAc₂-P-P-dolichhol resulting in formation of Man₉GlcNAc₂-P-P-dolichhol or Man₆GlcNAc₂-P-P-dolichhol, respectively. Amino acid sequence analysis of putative *EgAlg9* had a percent identity to *Homo sapiens*, *Saccharomyces cerevisiae*, *Arabidopsis thaliana* and not found to be present in *Trypanosoma brucei* proteins. The *EgAlg3* had identity with *Homo sapiens*, *Saccharomyces cerevisiae* and *Trypanosoma brucei* proteins (Table 3.3).

	Protein size	<i>Homo sapiens</i>	<i>Saccharomyces cerevisiae</i>	<i>Arabidopsis thaliana</i>	<i>Trypanosoma brucei</i>
		Identity (%)			
<i>EgAlg9</i>	66 kDa	31.1	25.8	27.0	N/P
<i>EgAlg3</i>	50 kDa	42.8	28.9		29.9

Table 3.3 *Euglena gracilis* percent identity of mannosyltransferase to known protein sequences from other organisms.

The *TbAlg9* is not present in *Trypanosoma brucei* because it has a Man₈GlcNAc₂-P-P-Dol glycan as a final intermediate. The depletion of *TbAlg3* gene in bloodstream *T. brucei* has shown to unable the production of oligosaccharides higher than Man₅GlcNAc₂ and had no significant effect on parasite growth, morphology or the infectivity to the host. Therefore, this enzyme is not a useful drug target against African sleeping disease.¹⁷⁴ Similarly, the mutation of *Alg3* gene in *Saccharomyces cerevisiae* and *Arabidopsis thaliana* leads to accumulation of underglycosylated intermediated resulting in no obvious growth phenotype, thereby showing that it is not essential for their viability and growth.¹⁷⁰ In contrast, the mutation of one amino acid in human *Alg3* gene leads to the deficiency of the α -1,3-mannosyltransferas resulting in no elongation of Man₅GlcNAc₂-P-P-Dol intermediates on the luminal side of the ER. The Man₅GlcNAc₂-P-P-Dol intermediate becomes a poor substrate for the oligosaccharyltransferase complex which prefers the Glc₃Man₉GlcNAc₂-P-P-Dol glycan, making difficult to move the incomplete oligosaccharide intermediate to the newly expressed protein. This leads to accumulation of this intermediate in the ER and causes under glycosylation of serum glycoproteins transferrin.¹⁷⁵ The defect of the glycosylation in humans causes type IV carbohydrate deficient glycoprotein syndrome (CDGS), which is a rare genetic disease characterised by microcephaly, severe epilepsy and minimal psychomotor development.¹⁷⁶ Similarly, single point mutation in human

Alg9 gene leads to the incipency of the α -1,3-mannosyltransferas, resulting in accumulation of $\text{Man}_8\text{GlcNAc}_2\text{-P-P-Dol}$ intermediates and also known to cause CDGS type II. Currently, there are only two people that were diagnosed with CDGS type II and six with type VI.¹⁷⁶

Overall, finding these particular enzymatic activities in *Euglena gracilis* microsomal membranes do not have real therapeutic applications, however these enzymes could be still used to aid chemo-enzymatic synthesis of complex oligosaccharides. Furthermore, to find mannosyltransferase activities that belong to the GPI anchor biosynthesis we envisaged chemical synthesis of more authentic fluorescent acceptors, which incorporate GlcNAc-*myo*-inositol sugar moiety attached to fluorescent ceramide (**3.09**) (Fig. 3.31).

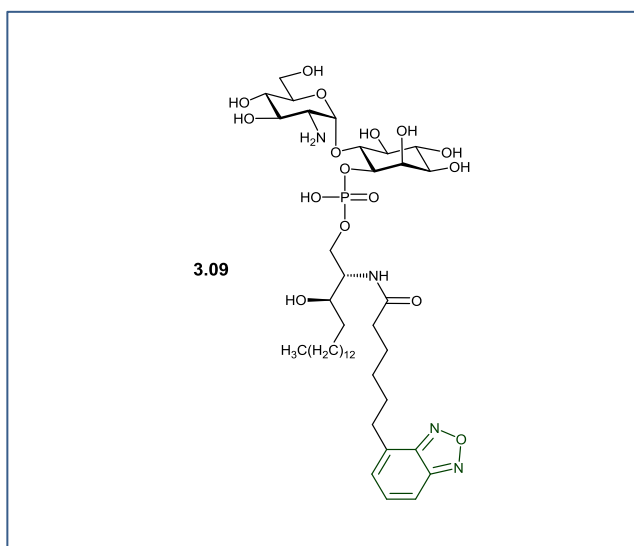


Figure 3.31 Chemical structures of authentic fluorescent acceptors to aid with detection of mannosyltransferase activities in *Euglena gracilis* microsomal membranes.

Fluorescence-based methodology II with fluorescent α -Man-HTC (**2.12**) and α -Man-1,6- α -Man-HTC (**2.13**) acceptor substrates was also able to detect *N*-acetylglucosamine-1-phosphate transferase (GlcNAc-P-Tase) activity responsible for phosphorylation of *N*-linked glycoproteins. The transcriptome search for the predicted *E. gracilis* GlcNAc-P-Tase with the identified amino acid sequence of the *Homo sapiens* (EC 2.7.8.17) gene yielded a putative *Euglena gracilis* UDP-*N*-acetylglucosamine-lysosomal-enzyme *N*-acetylglucosamine-1-phosphate transferase (GlcNAc-P-Tase). This predicted transmembrane protein consists of 1140 amino acids (124 kDa) and has 25.5% identity

with the *Homo sapiens* and 25.8% with *Dictyostelium discoideum* (slime mold) (Appendix 10).

The *Homo sapiens* GlcNAc-P-Tase is a 540 kDa hexameric transmembrane enzyme which comprise of three subunits $\alpha_2\beta_2\gamma_2$ and is coded by two genes *GNPTAB* and *GNPTG*. The $\alpha_2\beta_2$ subunits constitute the catalytic domain and carry the substrate binding sites for UDP-GlcNAc and high mannose protein-linked *N*-glycan.¹⁷⁷ The γ subunit is required for the optimum phosphorylation and especially for the addition of a second GlcNAc-P to high mannose protein-linked *N*-glycan by facilitating binding and presentation of this high mannose glycan to the catalytic domain in the favourable orientation.¹⁷⁸ In contrast, the putative *D. discoideum* GlcNAc-P-Tase¹⁷⁹ consist of 1238 amino acids and differs from human enzyme by lacking the DMAP protein binding domain in α_2 subunit. Recently, the DMAP domain has been demonstrated to participate in protein-protein interactions through recognition of conformation-dependent lysosomal protein in zebrafish model.¹⁸⁰ The gene that encode for the γ subunit was not found in the genome sequence of *D. discoideum*; therefore, the GlcNAc-P-Tase lack the γ subunit sequence in this species.¹⁸¹ Nevertheless, *D. discoideum* is still able to phosphorylate its lysosomal proteins suggesting that γ subunit is dispensable. Similar to *D. discoideum*, the *E. gracilis* GlcNAc-P-Tase lacks the DMAP domain and does not contain the γ subunit.

Deficiency in GlcNAc-P-Tase activity in *Homo sapiens* leads to lysosomal storage disorder, such as mucopolipidosis II (MLII), mucopolipidosis IIIA (MLIIIA) and mucopolipidosis IIIC (MLIIIC), where GlcNAc-P-Tase activities is absent in MLII (mutation in α/β subunit gene), reduced in MLIIIA (mutation in α/β subunit gene) and altered in MLIIIC (mutation in γ subunit gene).^{182, 183} In the course of these disorders, newly synthesised lysosomal enzymes that lack Man-6-P receptors are over secreted into the extracellular medium instead of being delivered to the lysosomes. These conditions affect sorting of multiple lysosomal enzymes and result in absent or poor degradation of carbohydrates, lipids and other material inside the lysosomes. One of the proposed methods to treat the lysosomal storage disease which affects one or more lysosomal enzymes is the generation of phosphorylated lysosomal proteins to be used in enzyme replacement therapy.¹⁸⁴ The enzyme replacement therapy is possible due to additional presence of Man-6-P receptors in the plasma membrane, which allows tagging of these lysosomal enzymes through Man-6-P recognition site back into the

lysosomes. This therapy implies overexpressing lysosomal enzymes in Chinese-hamster ovary with subsequent purification of the enzyme and treatment with *exo*-glycosidases to expose terminal Man-6-P on the *N*-glycan following by intravenous administration of these enzymes to patients. Recent studies have shown that it is possible to generate mutant of *Arabidopsis thaliana* seeds deficient in *N*-acetylglucosaminyl transferase I activity, involved in the first step of complex and hybrid *N*-glycans biosynthesis, in order to overexpress human α -L-iduronidase enzyme in high yields.¹⁸⁵ This enzyme was then modified *in vitro* with Man-6-P using soluble form of both recombinant GlcNAc-P-Tase and uncovering enzymes.^{186, 187} Despite the advances in the downstream processing of a plant-made recombinant lysosomal enzyme, the efficiency of the first step of the *in vitro* modification with GlcNAc-P residue required improvements.¹⁸⁵

The application of *D. discoideum* GlcNAc-P-Tase to decorate lysosomal enzymes with GlcNAc-P residues is proven to be unsuccessful because although this enzyme is capable of transferring GlcNAc-P to a simple chemical substrate, such as α -methylmannoside¹⁸⁸ it lacks the ability to recognise human lysosomal glycoprotein, such as cathepsin D.¹⁷⁹ The results described above, demonstrated that *E. gracilis* GlcNAc-P-Tase is capable of phosphorylating *in vitro* chemically synthesised fluorescent α -Man-HTC and α -Man- α -1,6-Man-HTC substrates. Currently, we are investigating if this enzyme can be efficient in phosphorylation of a non-lysosomal RNaseB protein using a modified sugar nucleotide (UDP-GlcNAcN₃) that was synthesised by Dr. Martin Rejzek in Professor Field's group. The modification on the sugar nucleotide allows a straightforward identification of modified protein through application of click conditions in the presence of alkyne fluorophore. The ability to demonstrate that *E. gracilis* GlcNAc-P-Tase can transfer GlcNAc-P onto the *N*-glycan of the non-lysosomal and in the future to lysosomal proteins could mean that we can then look into overexpressing this enzyme in other organisms such as yeast or plant to generate soluble form of this enzyme. Admittedly, the generation of soluble GlcNAc-P-Tase enzyme will be challenging due to its transmembrane nature and the presence of nucleotide thymine modification with β -D-glucosylhydroxymethyluracil in *E. gracilis* genome which is yet to be resolved. Nevertheless, it was possible to remove transmembrane domain from α/β subunits and produce soluble recombinant GlcNAc-P-Tase enzyme in mammalian cells¹⁸⁷ that was capable of transferring GlcNAc-P residue from UDP-GlcNAc to both synthetic small molecules, such as α -methylmannoside and

protein substrates such as lysosomal glycoprotein cathepsin D or uteroferrin and non-lysosomal glycoprotein RNaseB.¹⁷⁸ Thereby, if recombinant enzyme will be obtained, *E. gracilis* GlcNAc-P-Tase could be used in enzyme replacement therapy to modify lysosomal enzymes *in vitro* with GlcNAc-P residues. Furthermore, the nature of lysosomal enzymes in *E. gracilis* can be identified to see if they have any similarity to mammalian lysosomal enzymes. Conversely, the crude microsomal membranes can be used to aid in chemo-enzymatic synthesis of phosphodiestered bond.

4 Synthesis of triazole-linked linear and cyclic oligomers to obstruct *Trypanosoma cruzi* macrophage infection

The majority of this Chapter has been published in the primary literature:

Click chemistry oligomerisation of azido-alkyne-functionalized galactose accesses triazole-linked linear oligomers and macrocycles that inhibit *Trypanosoma cruzi* macrophage invasion

Vanesa L. Campo,* Irina M. Ivanova,* Ivone Carvalho, Carla D. Lopes, Zumira A. Carneiro, Gerhard Saalbach, Sergio Schenkman, João Santana da Silva, Sergey A. Nepogodiev, Robert A. Field

Tetrahedron, 2015, doi:10.1016/j.tet.2015.04.085

* Joint first authors

Contribution:

(10%) Vanesa L. Campo originally started the project and derived chemical synthesis of 2-(2-(2-azidoethoxy)ethoxy)ethyl 6-*O*-(prop-2-ynyl)- β -D-galactopyranoside (**4.07**).

(80%) Irina Ivanova performed improvement on the original chemical synthesis of 2-(2-(2-azidoethoxy)ethoxy)ethyl 6-*O*-(prop-2-ynyl)- β -D-galactopyranoside (**4.07**) followed by generation, purification and characterisation of cyclic and linear 1,4/1,5-triazole-linked-*pseudo*-galctooligomers and *in vitro* investigation into their substrate activities with *Trypanosoma cruzi* *trans* sialidases.

(10%) Ivone Carvalho performed *in vivo* preliminary biological evaluations in Brazil.

4.1 Introduction

Trypanosoma cruzi is a single-celled flagellated parasite that infects and replicates inside the human host in a range of tissues and cells, including macrophages, smooth and striated muscle cells and fibroblasts.¹⁸⁹ In the process, *Trypanosoma cruzi* cause a debilitating and often lethal condition known as Chagas' disease which afflicts millions of people mainly in South and Central America. According to World Health Organisation estimates 7.7 to 10 million people are chronically infected and 10,000-14,000 die each year from Chagas' disease.¹⁹⁰

T. cruzi has a very complex life cycle that involves passage of parasites through the digestive track of biting insects (Reduviidae) and gaining access to the human host through insect-generated puncture wounds.¹⁹¹ In general, inside the insect gut the parasite exists as a replicative non-infectious epimastigote form that passes to the rectum and differentiates into a non-replicative metacyclic trypomastigote form. This form of parasite is then excreted from the insect as it takes a blood meal and the parasite gains access to the human host through the mucous membrane.¹⁹² Once inside the human host the non-dividing trypomastigotes attach to macrophages or non-macrophages cells and enter the cell by stimulating signals that induce formation of lysosomes.¹⁹³ The localised fusion of lysosomes with the plasma membrane allows parasites to enter the cell through the parasitophorous vacuole. The low pH inside the lysosome triggers two events. First trypomastigotes differentiate to the amastigote form and second includes production of pore-forming enzymes that aid in the disruption of the parasitophorous vacuole.¹⁹⁴ Parasites eventually reach the cytoplasm and complete their differentiation to replicative amastigote form, which undergo several cycles of binary division and finally transform into blood trypomastigote form. Parasites then break free from the cell into the intercellular space and either begin to infect the neighbouring cells or move to the blood stream and begin to infect other tissues (Fig. 4.1).¹⁹⁵

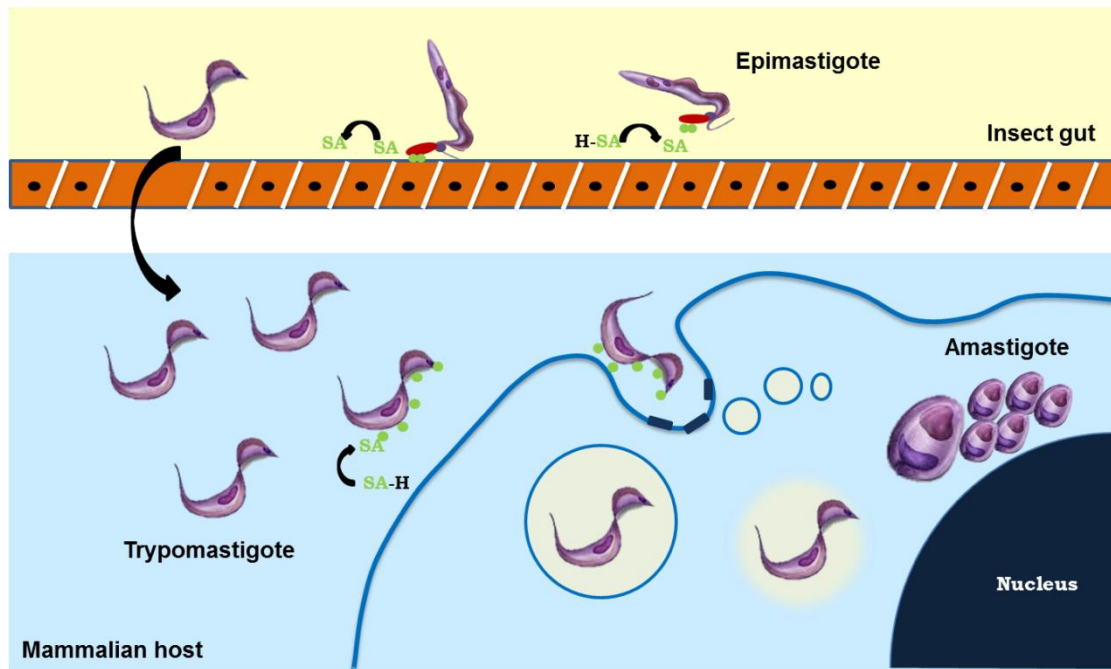


Figure 4.1 Diagrammatic representation of *Trypanosoma cruzi* invasion and differentiation inside the vector and mammalian host cells. Parasites in non-replicative epimastigote form migrate through the insect gut and differentiate to metacyclic trypomastigote form. Inside the mammalian host parasites in non-replicative trypomastigote form associate with the cell surface and invade the cell through the parasitophorous vacuole employing localised fusion of host lysosomes. Parasites are released into the cytoplasm differentiate to replicative amastigote form, which break through to infect neighbouring cells or tissues.

During the invasion process *T. cruzi* makes extensive use of cell surface molecules, such as mucins and *trans*-sialidases in its attempt to effectively adhere and invade host cells on one hand and to evade the human immune response on the other. Mucins are glycoproteins that form a dense and protective layer on the surface of the parasite. The core polypeptide is rich in serine and threonine residues, which act as acceptor sites for sequential addition of monosaccharides forming *O*-linked oligosaccharides. The first sugar residue added to the serine or threonine is GlcNAc, which is then elongated with up to five galactose residues in either furanose or pyranose configuration depending on the strain of *Trypanosoma cruzi*.¹⁹⁶ The catalytic activity of UDP-GlcNAc:polypeptide *N*-acetylglucosaminyltransferase (ppGlcNAcT) responsible for the transfer of first GlcNAc residue from UDP-GlcNAc to the peptide has been characterised⁷⁴ but there is still lack of information about the activities of the other glycosyltransferases involved in the elongation of these *O*-linked oligosaccharides.¹⁹⁷ The terminal β -galactopyranosyl residue of the *O*-linked oligosaccharide can then act as an acceptor substrate for *trans*-sialidase. The action of *Trypanosoma cruzi trans*-sialidase (TcTS) is unique because it performs sialyl transfer without utilising CMP-sialic acid due to inability of parasite to synthesis either of these compounds. Instead, TcTs prefers a host α -2,3-linked sialic

acid to β -galactosyl of glycoproteins, glycolipids and oligosaccharides as a donor substrate (Fig. 4.2).⁷⁵ In addition, not all are enzymatically active. Variants of TcTS can possess a single mutation in the active site (Tyr342His) and become catalytically inactivated but still can bind to terminal sialic acid and galactose residues, functioning as a lectin.¹⁹⁸ Both mucins and *trans*-sialidases attached to the parasite plasma membrane through the GPI.

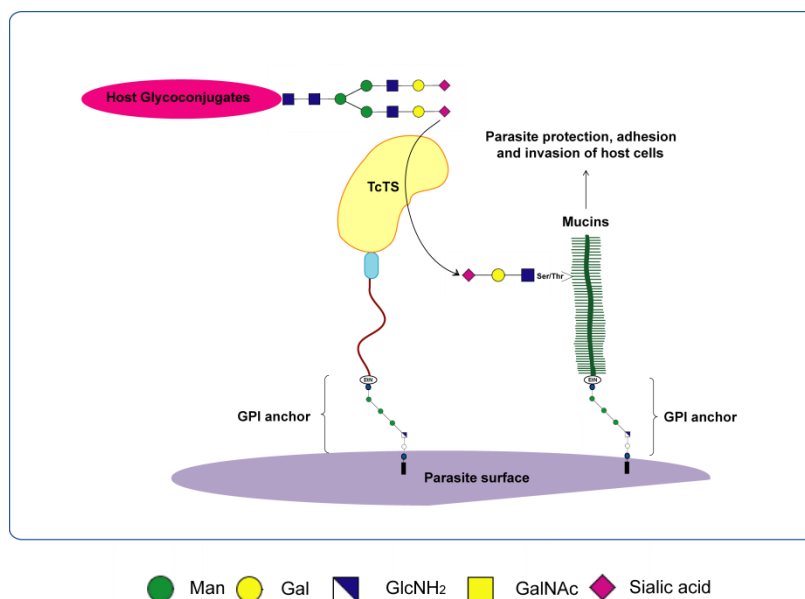


Figure 4.2 Representative transfer of sialic acid from the host glycoconjugate to the parasite cell surface mucin glycoprotein catalysed by *Trypanosoma cruzi* trans-sialidase.¹⁹⁹

There is a desperate need for new treatments for Chagas' disease, with a requirement for the identification of new drug targets and potential therapeutic agents.^{190, 200, 201} TcTS is considered to be a relevant target.²⁰² The most potent TcTs inhibitors described in the literature are compounds that are able to occupy both donor and acceptor binding sites, making the transfer of sialic acid either hindered or blocked. One of these compounds is GM3 ganglioside. When it is modified at C-4 with deoxy or methoxy group or at C-8 with deoxy demonstrated to act as the inhibitors in a concentration range of 10-100 μ M (Fig. 4.3 A).^{203, 204} With this in mind, our group have investigated glycopeptide substrates and inhibitors of TcTS,²⁰⁵ including the application of Cu(I)-catalysed alkyne-azido cycloaddition (CuAAC) click chemistry with carbohydrate building blocks to access libraries of small molecule inhibitors and multivalent TcTs ligands displayed on calixarene cores.^{204, 206-208} When generating libraries of inhibitors the azido group was placed either at C-1 or C-6 of galactose residue because the data obtained from the X-ray crystallography²⁰⁹ showed that these hydroxyl groups do not take part in the

binding process between the enzyme and substrate. In contrast, only the galactose C-3 hydroxyl group is well positioned to interact with both the enzyme and the anomeric carbon of sialic acid. Two azido galactose derivatives were coupled to a panel of structurally diverse terminal alkynes that differed in steric bulk, presence of hydrophobic groups as well as flexibility and rigidity of the side chains (Fig. 4.3 B). The *in vitro* evaluation of TcTS inhibition activities of these compounds revealed that they were only a moderate or weak inhibitors and more effective as acceptor substrates.²⁰⁷ Furthermore, in our group a series of tetravalent glycol-clusters incorporating β -lactosyl residues attached either to the upper or lower rigid rim of a central calix[4]arene core ring via 14-21 atom spacer arms were synthesised.²¹⁰ These compounds showed *in vitro* anti-trypanocidal activities with one compound showing potency comparable to the established anti-trypanosomal drug benznidazole (Fig. 4.3 C). In this compound all lactose residues were attached to the calix[4]arene core ring in *syn*-orientation. Displayed activities were not attributed to the inhibitory binding to the TcTs as the lactose residue acts as a substrate for these enzymes but it was suggested that it could be due to inability of parasite to manipulate its surface glycosylation in the presence of this compound *in vitro*.

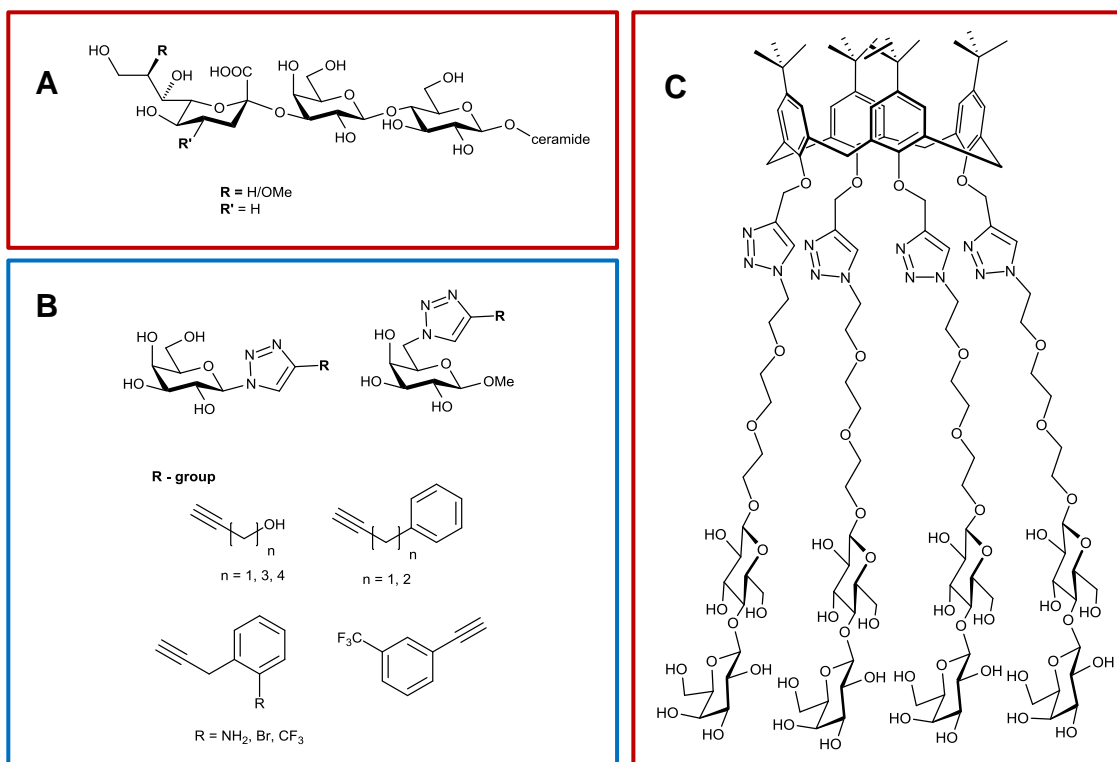


Figure 4.3 Representative examples of potent and moderate TcTs inhibitors. (A) GM3 ganglioside potent inhibitor (10-100 μM); (B) 1,2,3-Triazole-substituted derivatives moderate inhibitors (between 37-0% inhibition at 1 mM); (C) Lactose modified calix[4]arene.

The current interest lies in the application of multivalent glycoconjugates as parasite adhesion blocking agents with potential to prevent host cell invasion.^{211, 212} Click chemistry presents opportunities for the generation of oligomeric triazole-linked structures,²¹³ which have found application in the synthesis of analogues of cyclic oligosaccharides,²¹⁴ with medium size macrocycles being prepared in moderate to good yields starting both from protected and “free” sugar derivatives.²¹⁵⁻²¹⁷ There are only a few examples of the successful oligomerisation/polymerisation of such azide-alkyne-functionalised carbohydrates leading to linear oligomers, including recent proximity-driven click-polymerization of an 4-*O*-propargyl- β -D-galactopyranosyl azide in a crystal lattice.²¹⁸ Previously, in our group we showed that the cyclooligomerisation of azido-alkyne-functionalised galactose, where the azido group was incorporated either at the anomeric position or at C-6 and an alkyne group in the form of either a 6-*O*- or 1-*O*-propargyl functionality, gives rise to novel 1,6-linked cyclic *pseudo*-galactooligosaccharides that are recognised by TcTS (Fig. 4.4).²¹⁹ Computational studies of two isomeric cyclic trisaccharide structures indicated inherent differences in geometric and dynamic preferences where cyclic trimer obtained from monomer 1 is more rigid than cyclic trimer obtained from monomer 2 (Fig. 4.4).

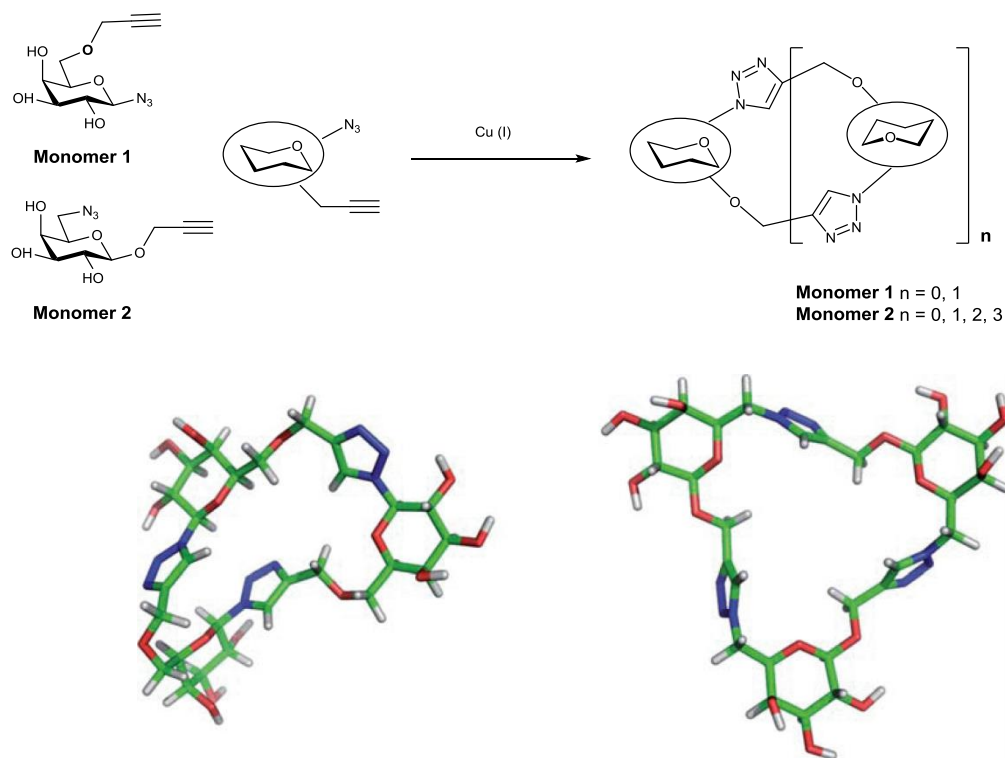


Figure 4.4 Schematic representation of cyclooligomerisation approach to the synthesis of cyclic *pseudo*-oligosaccharides. (Top) Generalised scheme. (Bottom) Lowest energy conformers for cyclic trimers. (Bottom left) Structure obtained from monomer 1; (Bottom right) Structure obtained from monomer 2.²¹⁹

In the current work, we wished to access linear oligomers and/or larger macrocycles, in order to span a greater area that might more adequately map the distribution of *trans*-sialidase on the parasite cell surface thereby blocking *trans*-sialidase-action and associated infection processes (Fig. 4.5).²²⁰ Herein we designed a galactose monomer that incorporates a propargyl group on C-6 and a linker between sugar and azide functionality, in contrast to previous Field group work where the azido group was directly attached to the C-1.²¹⁹ We selected ethylene glycol-based linker to reduce the potential for non-specific interactions with proteins and membrane components.²²¹ We anticipated that this flexible linker might promote oligomerisation at the expense of cyclisation under the CuAAC click conditions. Assessment of the interaction of triazole-linked materials with TcTS, along with initial assessment of their ability to block macrophage invasion by *Trypanosoma cruzi* parasites were investigated.

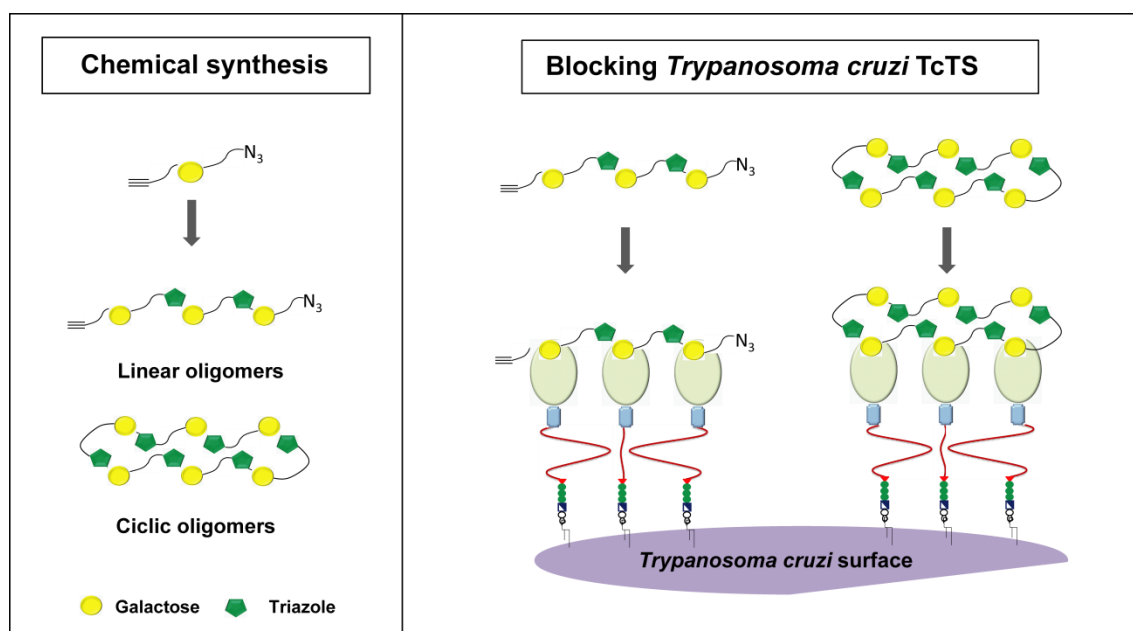
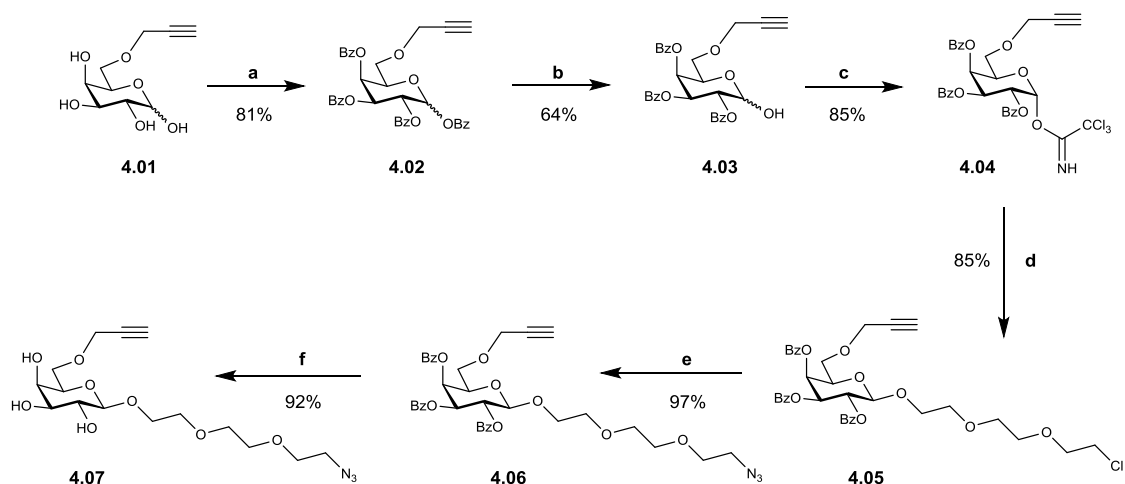


Figure 4.5 Schematic representation of cell surface-presented *Trypanosoma cruzi trans*-sialidase and potential for its blocking by 1,2,3-triazole-linked linear and cyclic *pseudo*-galactooligomers resulting in potential prevention of host cells invasion.

4.2 Synthesis of azido-alkyne galactose-containing monomer

The azido-alkyne-substituted galactose monomer **4.07** was synthesised in nine steps starting from known 6-*O*-propargyl-D-galactopyranose **4.01**,²¹⁹ as outlined in Scheme 4.1. Propargyl ether **4.01** was per-*O*-benzylated and converted into the required hemiacetal **4.03** using a solution of ammonia in methanol-THF.²²² The resulting

hemiacetal **4.03** was treated with trichloroacetonitrile and DBU to obtain the corresponding imidate donor **4.04**, which upon activation with trimethylsilyl trifluoromethanesulfonate (TMSOTf) in the presence of 2-(2-(2-chloroethoxy)ethoxy)ethanol gave chlorinated β -galactoside **4.05** in a respectable 85% yield for the glycosylation step. In the presence of NaN₃ and NaI, the chlorinated β -galactoside **4.05** was converted into the azido β -galactoside **4.06** in near quantitative yield.



Scheme 4.1 Synthetic route to azido-alkyne-containing galactose monomer. Reagents and conditions: a) BzCl, Py; b) NH₃, MeOH/THF (7:3); c) Cl₃CCN, DBU, CH₂Cl₂; d) 2-(2-(2-chloroethoxy)ethoxy)ethanol, TMSOTf, CH₂Cl₂; e) NaN₃, NaI, DMF; f) NaOMe, MeOH.

The presence of azide functionality in **4.06** was evident from a characteristic signal in the IR spectrum [2107 cm⁻¹] and the β -configuration followed from the anomeric proton signal (δ 5.75, $J_{1,2}$ =8.0 Hz) in the ¹H NMR spectrum. De-*O*-benzylation of **4.06** afforded target azido-alkyne-functionalised galactose monomer **4.07** in an overall yield of 25% from 6-*O*-propargyl galactopyranose **4.01**.

4.3 Cyclisation and oligomerisation through CuAAC reactions based on azido-alkyne-containing galactose monomer

Once synthesised, the reactivity of azido-alkyne-functionalised galactose monomer **4.07** was tested under CuAAC conditions – at 1 M concentration in DMF with CuSO₄/Cu turnings either at 110 °C (using microwave irradiation; Method A) or at ambient temperature (Method B). The progress of both reactions could conveniently be followed by TLC analysis. The reaction using Method A was complete after 30 min,

compared to 2 days for Method B. TLC analysis showed formation of multiple common products, consistent with the intended oligomerisation, while different relative spot intensities were evident from the two methods (Fig. 4.6 TLC image lanes A and B). The reaction mixtures from both methods were concentrated under reduced pressure, redissolved in water and submitted to the reverse phase HPLC purification. This allowed straightforward separation of cyclic from linear products, as well as resolution of the variously sized cyclic oligomers from each other (Fig. 4.6 A and B) resulting in samples of cyclic monomer **4.08**, cyclic dimer **4.09**, cyclic trimer **4.10**, cyclic tetramer **4.11**, cyclic pentamer **4.12** and cyclic hexamer **4.13**, along with mixed linear oligomers (Scheme 4.2). The formation of cyclic 1,4-triazole-linked structures was confirmed by virtue of singlet signals of triazole CH protons at δ 8.10 ppm²²³ and the absence of propargyl CH signals at δ 2.83 in ¹H NMR spectra.

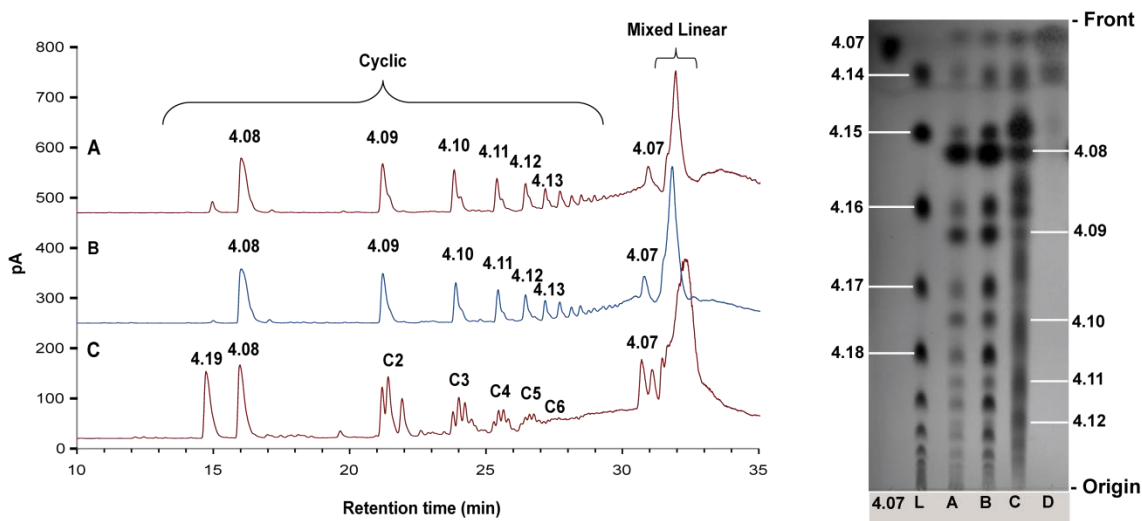
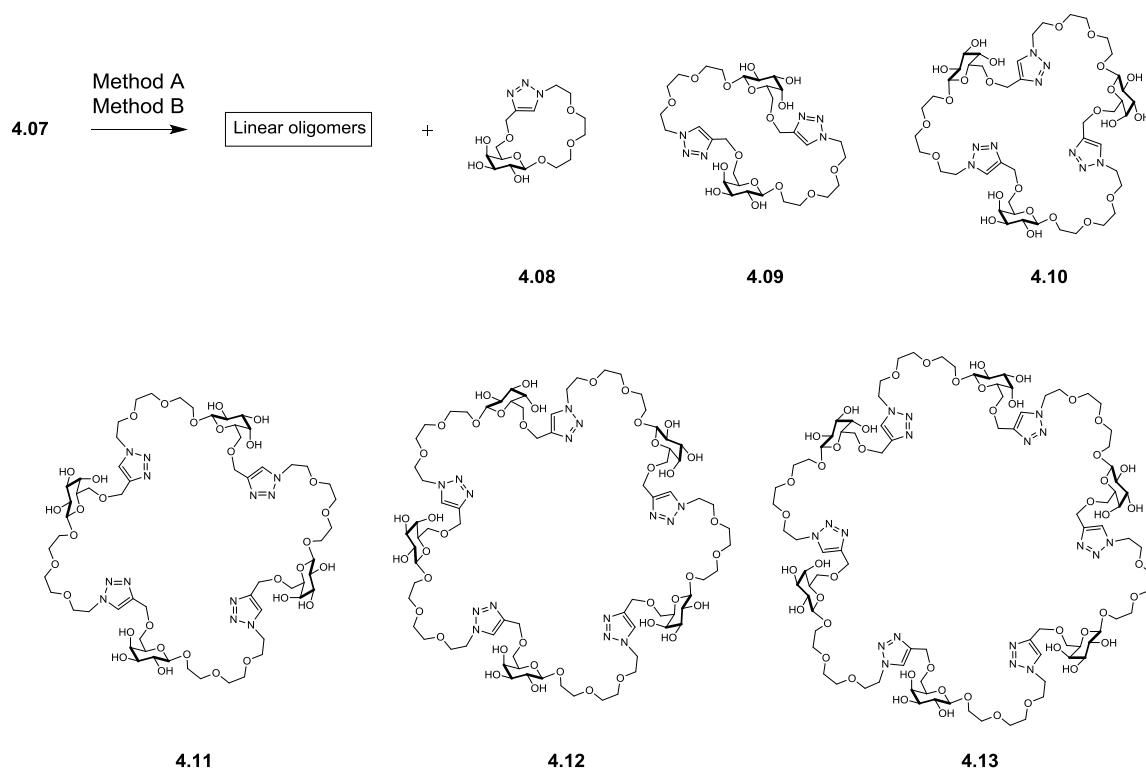


Figure 4.6 Reverse phase HPLC and normal phase TLC analyses of cyclic and linear products obtained from azido-alkyne 1,3-dipolar cycloaddition reactions of galactose monomer. (Left) Reverse phase HPLC purification of 1,4-triazol linked cyclic and linear products. HPLC conditions: Phenomenex C18(2) (250 mm x 10 mm); mobile phase: 0.1% aq. TFA-CH₃CN (0 to 35 % 50 min, flow rate: 5 mL/min); CAD detector. (Right) Normal phase TLC separation of 1,4-triazol linked cyclic and linear products. HPLC trace/TLC lane: (A) **4.07** (1M in DMF) Method A (Cu(I), 110 °C); (B), Method B (Cu(I), room temperature); (C), Method C (110 °C); (D), Method D (room temperature); TLC lane **4.07** starting galactose monomer; TLC lane L mixed linear oligomer fraction obtained from HPLC.



Scheme 4.2 Cyclisation and oligomerisation of azido-alkyne-containing galactose through CuAAC. **4.07** (1M in DMF) Method A (Cu(I), 110 °C) and Method B. (Cu(I), room temperature).

Reaction products	Method A	Method B
	Yield (%)	Yield (%)
4.08	9.0	6.7
4.09	3.0	2.2
4.10	1.6	1.0
4.11	1.1	0.8
4.12	1.3	0.6
4.13		0.5
Cyclic high mol. weight compounds	13.7	6.0
Mixture of linear compounds	25.8	35.7
Cyclic overall yield	29.7	17.8
Overall yield	55.8	53.5

Table 4.1 Yields of 1,4-triazole-linked cyclic and linear products from CuAAC reactions of galactose monomer.

Interestingly, the linear oligomeric products did not resolve under the reverse phase HPLC conditions employed to separate the corresponding cyclic materials; instead they eluted as a single broad peak at ca 32 min (Fig. 4.6 traces A and B). These linear compounds were well resolved from each other and from the corresponding cyclic oligomers on analytical TLC (Fig. 4.6, TLC image lane L) where linear oligomers **4.14-4.18** have slightly higher R_f values compared to cyclic products of the same molecular size. Galactose monomer **4.07** was shown to undergo oligomerisation up to at least a decamer. In contrast to reverse phase HPLC, gel permeation chromatography (GPC) on

TSK-HW40S enabled separation of linear oligomers up to the pentamer (Fig. 4.7). It should be noted that these linear compounds contain unreacted azido and alkyne terminal groups capable of further reactions even in the absence of Cu (I) catalyst. This gave rise to complications during handling and storage due to spontaneous cyclisation and oligomerisation of purified compounds (data not shown). These analyses alongside isolated yields (Table 4.1) illustrated that the lower reaction temperature (room temperature vs 110 °C) favours formation of linear products over the corresponding cyclic isomers.

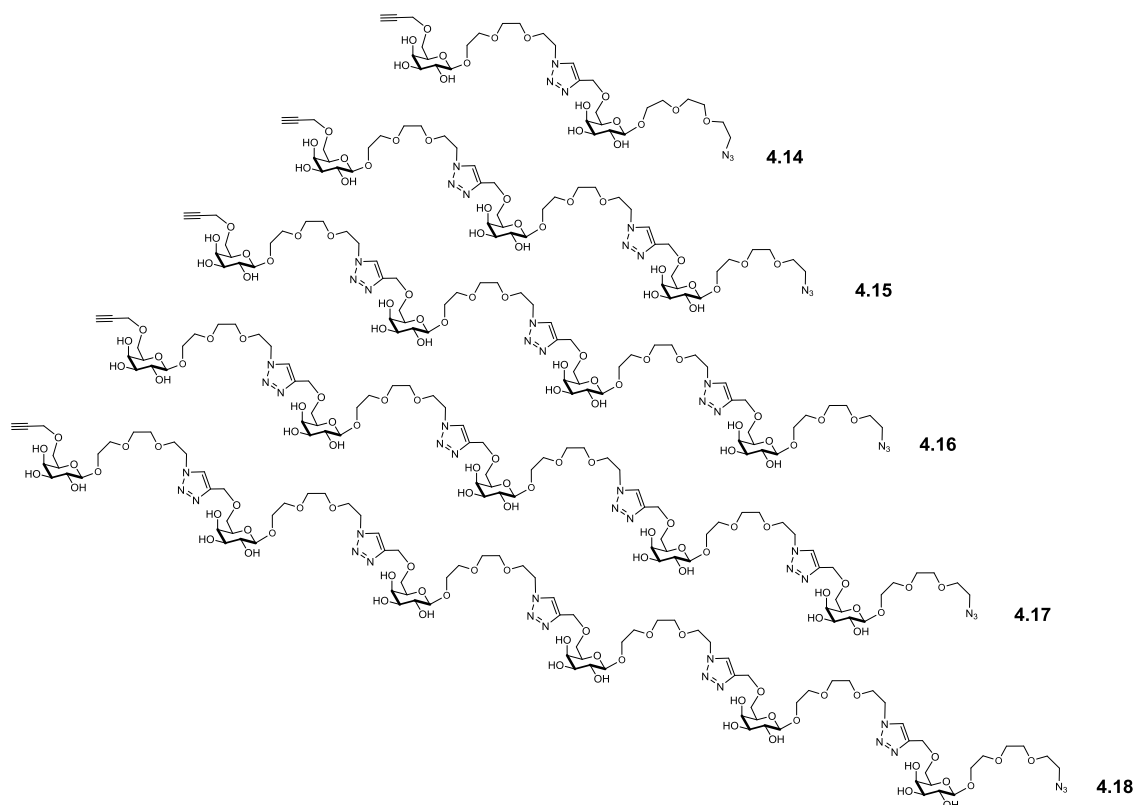


Figure 4.7 Linear oligomerisation products from the reaction of azido-alkyne-containing galactose under CuAAC conditions. Compounds **4.14-4.18** were identified by HRMS and obtained in a combined yield of 26% (Method A) and 36% (Method B).

	Calculated m/z $[M+H]^+$	Cyclic compounds	Found m/z $[M+H]^+$	Linear oligomers	Found ^a m/z $[M+H]^+$
Monomer	376.1714	4.08	376.1710	4.07	376.1708
Dimer	751.3357	4.09	751.3334	4.14	751.3351
Trimer	1126.4998	4.10	1126.4961	4.15	1126.4985
Tetramer	1501.6640	4.11	1501.6511	4.16	1501.6631
Pentamer	1876.8281	4.12	1876.8248	4.17	1876.8273
Hexamer	2251.9923	4.13	2251.9792	4.18	2251.9897

Table 4.2 HRMS data of 1,4-triazole-linked cyclic products and linear oligomers.

^aData obtained from the analysis of the mixture of linear oligomers obtained as a result of reverse-phase HPLC purification.

The 1,3-dipolar cycloaddition of azido-alkyne functionalised galactose monomer **4.07** generates isomeric cyclic and linear products that have the same molecular formula and hence the same monoisotopic mass. While linear and cyclic compounds were resolvable, we cannot rule out the formal possibility that some of the cyclic compounds may be catenated, although there is not obviously driving force for these particular monomers/intermediates to template catenate formation.²²⁴ The formation of cyclic and linear products was confirmed by high resolution MS analyses of individual isolated cyclic compounds **4.08-4.13** as well as the mixture of linear oligomers collected as a single peak from HPLC purification (Fig. 4.6 trace A and B, TLC image lane L). Cyclic and linear products from trimer upwards run in MS analyses as multiply charged species, spectra for which were de-convoluted to obtain monoisotopic masses (Table 4.2) (Appendices 11).

Cyclic oligomers are expected to have relatively simple ¹H NMR spectra of the repeat unit for macrocycles compared to more complex spectra for linear oligomers. This was demonstrated by comparing ¹H NMR spectrum of cyclic 1,4-triazole linked dimer (**4.09**) and linear 1,5-triazole linked dimer (**4.25**) (Fig. 4.8). The proton signal at around δ 4.32 ppm in both spectra was assigned to the anomeric proton of galactose residue by utilising 2D analysis of ¹H-¹³C HSQC of H1 with C1 (δ_{H} 4.32, δ_{C} 103.2 ppm for **4.09**) and (δ_{H} 4.32, δ_{C} 102.7 ppm for **4.25**). The doublet signal of **4.09** at δ 4.32 ppm had an integration value of 1H (Fig. 4.8 A blue trace), whereas the triplet signal of **4.25** at δ 4.32 ppm had integration value of 2H where two anomeric signal overlap resulting in one triplet signal (Fig. 4.8 A red trace). Furthermore, the linear dimer (**4.25**) has two CH₂ signals that belong to free propargyl group (CH₂CCH) and triazole-linked propargyl group (CH₂CC-triazole). The multiplet signal at δ 4.19 ppm was assigned to CH₂ signal of the free propargyl group (CH₂CCH) by 2D analysis of ¹H-¹³C HSQC (δ_{H} 4.19, δ_{C} 58.12 ppm). Whereas, the CH₂ signal of the triazole-linked propargyl group (CH₂CC-triazole) was present under the suppressed solvent peak and was evident from 2D analysis of ¹H-¹³C HSQC (δ_{H} 4.74, δ_{C} 60.36 ppm) (Fig. 4.8 B). The same applies to the CH₂N₃ and CH₂N signals. The 1,4-triazole ring formation was confirmed by the presence of singlet at δ 8.05 ppm in **4.09** and 1,5-triazole ring formation at δ 7.77 ppm for **4.25** (Fig. 4.8 A blue and red trace).

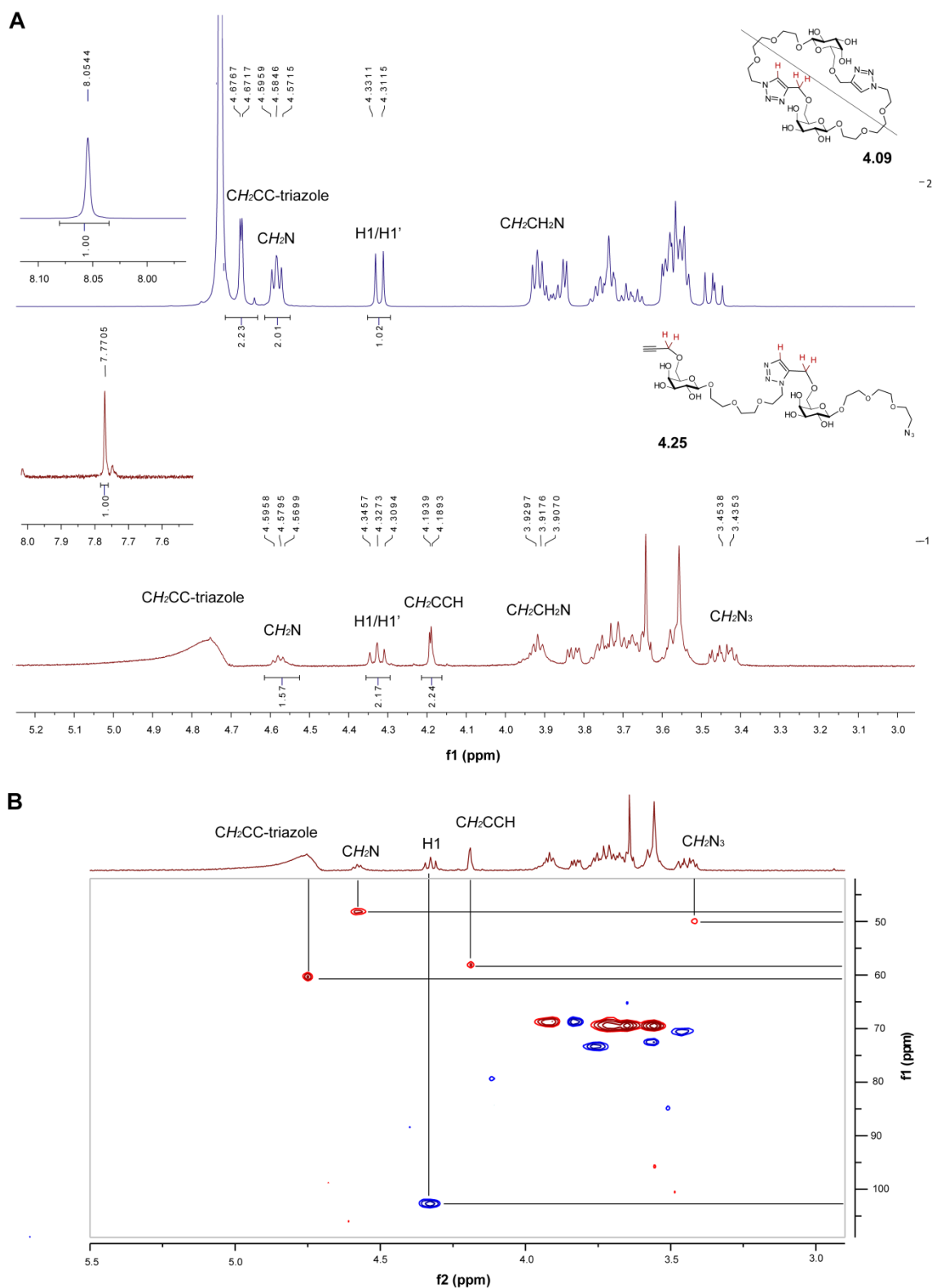


Figure 4.8 Characterisation of cyclic and linear 1,4-triazole-linked galactose dimers by NMR spectroscopy. (A) Evaluation of ^1H NMR spectra of cyclic **4.09** (blue) and linear **4.25** (red). (B) ^1H - ^{13}C HSQC spectrum of **4.25** (in blue signals for CH and CH_3 and in red signals for CH_2).

4.4 Fluorescent labelling of 1,4-triazole linked linear oligomers

Linear 1,4-triazole-linked compounds contained unreacted alkyne and azido functional groups on the same molecule. These presented difficulties in separation of these compounds on reverse phase HPLC and additional cyclisation reactions occurred when handling purified material after the GPC purification. Therefore, an analytical amount of mixed 1,4-triazole-linked linear compounds were capped with 3-azido-7-hydroxy-coumarin using Cu(I)-catalysed click conditions in order to investigate if addition of hydrophobic cap moiety can improve separation of these compounds on reverse phase reverse HPLC. The outcome of this reaction was analysed by TLC. TLC analyses clearly indicated formation of fluorescent compounds that have a slightly higher R_f value compared to the uncapped which is to be expected as the hydrophobic aromatic coumarin moiety is being attached (Fig. 4.9 TLC image lane L and F). Once more this result proves formation of linear compounds.

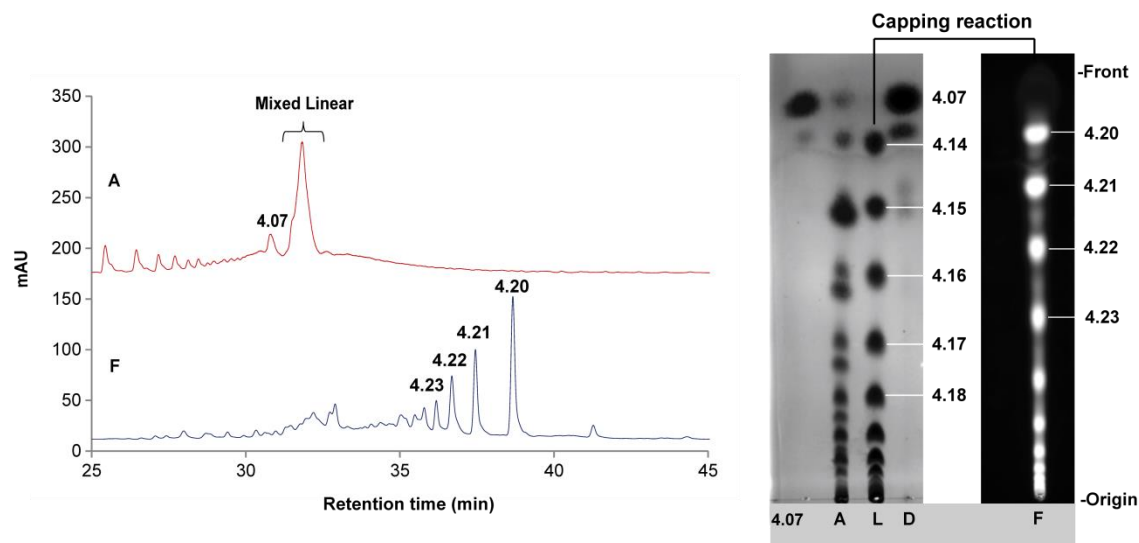


Figure 4.9 Normal phase TLC image and reverse phase HPLC chromatogram of fluorescently labelled 1,4-triazole-linked linear compounds obtained from azido-alkyne 1,3-dipolar cycloaddition reactions of mixed 1,4-triazole-linked linear compounds in the presence of 3-azido-7-hydroxy-coumarin. (Left) Image of TLC plates; TLC plates were eluted with $\text{CH}_3\text{CN}/\text{EtOAc}/i\text{PrOH}/\text{H}_2\text{O}$ (85:20:50:50). (Right) Reverse phase HPLC chromatogram, HPLC conditions: Phenomenex C18(2) (250 mm x 10 mm); mobile phase: 0.1% aq. TFA- CH_3CN (0 to 35 % 50 min, flow rate: 5 mL/min); UV detector at 347 nm. HPLC trace/TLC lane: **4.07** starting galactose monomer; (A) Method A (1M, DMF, Cu(I), 110 °C); (L) mixed linear oligomer fraction obtained from HPLC (Fig. 4.6); (D), Method D (1M, DMF, room temperature); (F) fluorescent 1,4-triazole-linked linear products.

The attachment of hydrophobic coumarin fluorophore to some extent allowed separation of capped 1,4-triazole-linked fluorescent linear compounds on reverse phase HPLC up to a pentamer compared to no separation with un-capped 1,4-triazole-linked linear

compounds (Fig. 4.9 trace A and F). During capping reaction no fluorescent monomer was formed because it was removed by HPLC purification.

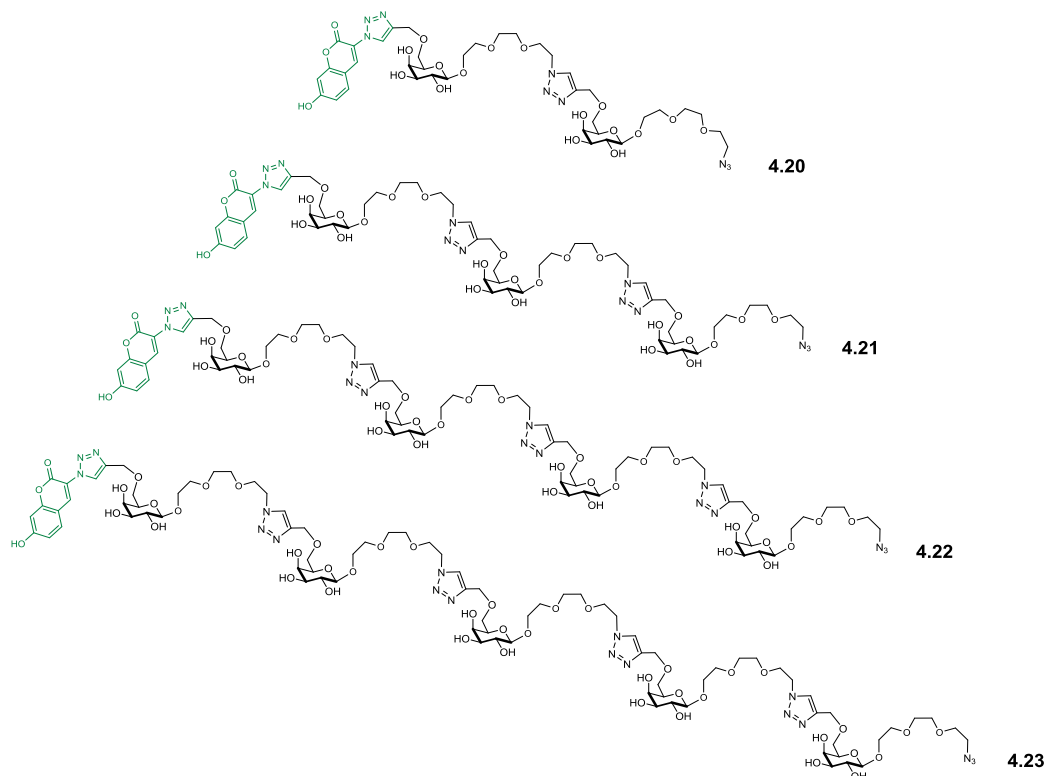


Figure 4.10 Fluorescent linear oligomerisation products from the reaction of azido-alkyne-containing galactose under CuAAC conditions. Compounds **4.20-4.23** were identified by HRMS.

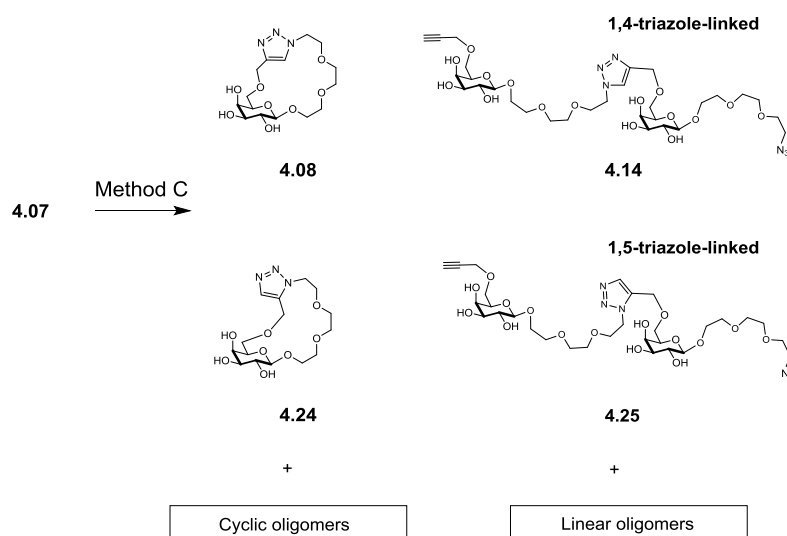
Overall capping reaction with 3-azido-7-hydroxy-coumarin resulted in formation of fluorescently labelled 1,4-triazole-linked linear products up to a decamer as judged by TLC and we were able to isolate analytical amount of 1,4-triazole-linked linear dimer (**4.20**), trimer (**4.21**), tetramer (**4.22**) and pentamer (**4.23**) which were confirmed by HRMS (Fig. 4.9, Table 4.3).

	Fluorescent linear compounds	Calculated m/z $[M+H]^+$	Found m/z $[M+H]^+$
Dimer	4.20	954.3687	954.3667
Trimer	4.21	1329.5328	1329.5308
Tetramer	4.22	1704.6970	1704.6965
Pentamer	4.23	2079.8611	2079.8662

Table 4.3 HRMS data of fluorescent 1,4-triazole-linked linear products.

4.5 Uncatalysed 1,3-dipolar cycloaddition of azido-alkyne-containing galactose monomer

Given the noted spontaneous but slow 1,3-dipolar cycloaddition of galactose monomer **4.07** on standing at room temperature (*vide supra*), the reactivity of **4.07** at 1 M concentration in DMF at 110 °C (under microwave irradiation; Method C) and at room temperature (Method D) were compared. Reaction using Method C was completed after 30 min, while Method D gave approximately 10% conversion of galactose monomer **4.07** after two weeks. TLC analysis showed even more complex multiple product mixtures than the Cu(I)-catalysed reaction (Fig. 2 TLC lanes C and D) due to the expected formation of mixed isomeric 1,4- and 1,5-linked triazoles (Scheme 4.3).



Scheme 4.3 Spontaneous cyclisation and oligomerisation of azido-alkyne-containing galactose leading to a mixture of compounds incorporating both 1,4-linked and 1,5-linked 1,2,3-triazole residues.

The reaction mixture from Method C was concentrated under reduced pressure, redissolved in water and submitted to the reverse phase HPLC purification. This procedure again allowed separation of cyclic from linear products, as well as resolution of 1,4- and 1,5-linked isomeric cyclic triazole monomer structures **4.08** and **4.24** from each other (Fig. 4.11 trace C). The rest of cyclic oligomers eluted on reverse phase HPLC as mixtures of poorly resolved regioisomers, with various combinations of 1,4- and 1,5-linked triazole rings incorporated into macrocycle structures. The ring sizes of

mixed 1,4/1,5-linked cyclic dimers (**C2**), mixed 1,4/1,5-linked cyclic trimers (**C3**), mixed 1,4/1,5-linked cyclic tetramers (**C4**), mixed 1,4/1,5-linked cyclic pentamers (**C5**) and mixed 1,4/1,5-linked cyclic hexamer (**C6**) were established by mass spectrometry and recorded in Table 4.4. The 1,5-linked cyclic monomer **4.24** was fully characterised by NMR spectroscopy and HRMS. The formation of the 1,5-linked triazole unit was confirmed by observing the triazole CH singlet signal at δ 7.71 ppm and the absence of a propargyl CH signal at δ 2.83 in the ^1H NMR spectra.

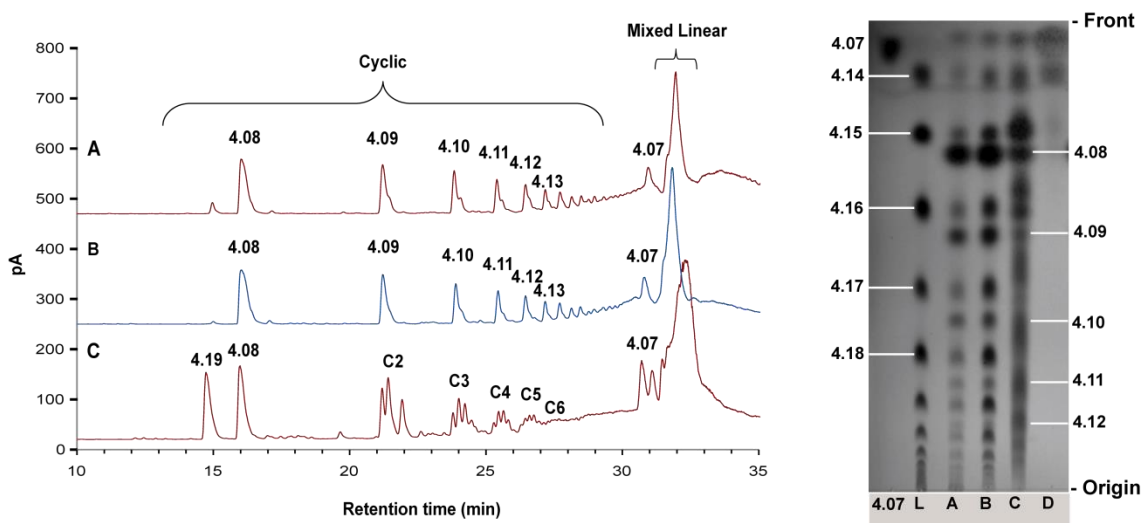


Figure 4.11 Reverse phase HPLC and normal phase TLC analyses of cyclic and linear products obtained from azido-alkyne 1,3-dipolar cycloaddition reactions of galactose monomer. (Left) Reverse phase HPLC purification of 1,4-triazol linked cyclic and linear products. HPLC conditions: Phenomenex C18(2) (250 mm x 10 mm) Mobile phase: 0.1% aq. TFA-CH₃CN (0 to 35 % 50 min, flow rate: 5 mL/min) CAD detector. (Right) Normal phase TLC separation of 1,4-triazol linked cyclic and linear products. HPLC trace/TLC lane: **4.07** (1M in DMF) (A) Method A (Cu(I), 110 °C); (B), Method B (Cu(I), room temperature); (C), Method C (110 °C); (D), Method D (room temperature); TLC lane **4.07** starting galactose monomer; TLC lane L mixed linear oligomer fraction obtained from HPLC.

		Calculated m/z [M+Na] ⁺	Found m/z [M+Na] ⁺
Dimer	C2	773.32	773.31
Trimer	C3	1148.48	1148.57
Tetramer	C4	1523.64	1524.45
Pentamer	C5	1898.81	1899.03
Hexamer	C6	2273.97	2273.33
Heptamer	C7	2649.13	2648.28

Table 4.4 MALDI-TOF data of 1,4- and 1,5-triazole-linked cyclic oligomers.

The 1,4/1,5-linked mixed linear products were submitted to GPC purification on TSK-HW40S column which enabled separation of mixed linear products up to a tetramer where linear 1,5-linked triazole dimer **4.25** and linear 1,4-linked dimer **4.14**, isolable as single compounds, were characterised by NMR spectroscopy and mass spectrometry. The linear structures of dimers **4.14** and **4.25** were confirmed by NMR spectroscopy, in particular by observation of a methylene signal of the intact propargyl group at $\delta \sim 4.18$ in the ^1H NMR spectra. The triazole linkage type in **4.14** and **4.25** was also evident from ^1H NMR spectra, which showed diagnostic proton resonances of the 1,4-linked triazoles at δ 8.04 for **4.14** and of the 1,5-linked triazole at δ 7.80 for **4.25**. In addition, DTT reduction of azido group in **4.25** produced amino-terminated compound which was detected by MS analysis showing an $[\text{M}+\text{H}]^+$ peak at m/z 725.28, compared to unreduced precursor with an $[\text{M}+\text{H}]^+$ peak at m/z 751.33.

4.6 Cyclic triazole-linked oligomers as acceptor substrates for *Trypanosoma cruzi* trans-sialidase (TcTS)

Cyclic compounds **4.08-4.10** and **4.24** were tested for their ability to act as acceptor substrates for TcTS with fetuin serving as a donor substrate for *O*-3 sialylation of the galactose residues in the triazole-linked macrocycles. Reactions were carried out over the course of 9 days, with further addition of fetuin and enzyme after 5 days, and only fetuin after 7 days. The reaction mixtures were monitored by TLC and in all cases formation of new compounds was observed (Fig. 4.12), which were identified by HRMS (Table 4.5).

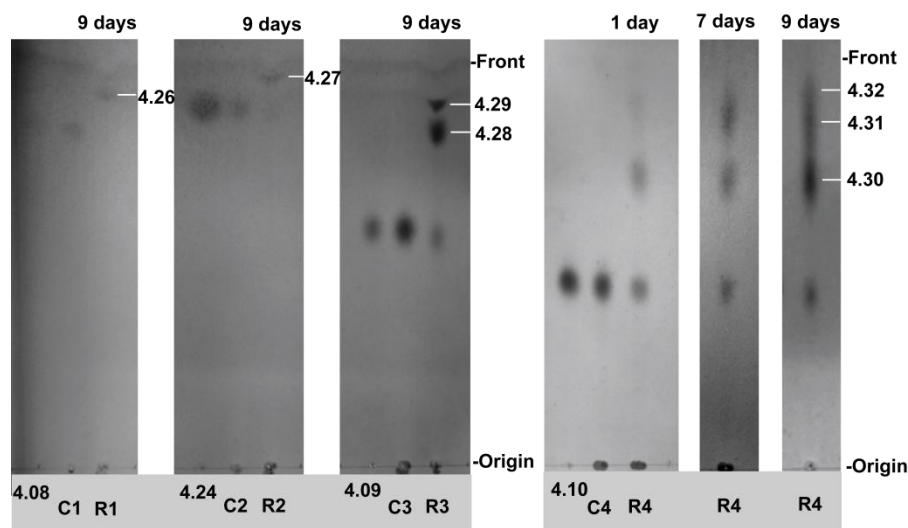
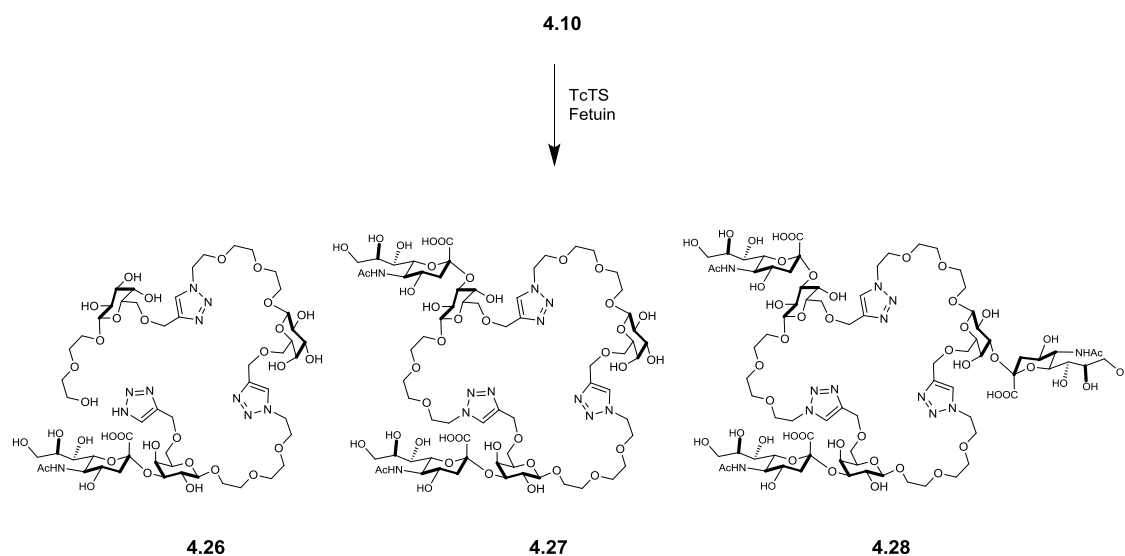


Figure 4.12 TLC analyses of enzymatic transformations of 1,4-triazole-linked cyclic monomer **4.08**, 1,5-triazole-linked cyclic monomer **4.26**, 1,4-triazole-linked cyclic dimer **4.09** and 1,4 triazole-linked cyclic trimer **4.10** into mono-, di- and tri-sialylated cyclic compounds in the presence of TcTS and a fetuin donor. Negative controls (lanes C1, C2, C3 and C4) were carried out in parallel with a donor and an acceptor without the enzyme. The progress of reactions was monitored by taking TLC samples on after 1 day, 7^h days and 9 days. TLC was eluted with CH₃CN/EtOAc/iPrOH/H₂O (85/25/50/50).

Starting material	Mono-sialylated		Di-sialylated		Tri-sialylated	
	Calcd <i>m/z</i> ([M-H] ⁻)	Found <i>m/z</i> ([M-H] ⁻)	Calcd <i>m/z</i> ([M-H] ⁻)	Found <i>m/z</i> ([M-H] ⁻)	Calcd <i>m/z</i> ([M-H] ⁻)	Found <i>m/z</i> ([M-H] ⁻)
Monomer 4.08	665.2523	665.2519				
Monomer 4.24	665.2523	665.2519				
Dimer 4.09	1040.4164	1040.4237	1331.5118	1331.5272		
Trimer 4.10	1415.5806	1415.5994	1706.6760	1706.7021	1997.7714	1997.7947

Table 4.5 HRMS data for products of enzymatic sialylation of triazole-linked cyclic oligomers.

Reaction of 1,4 triazole-linked cyclic trimer **4.10** resulted in formation of mono-, di- and tri-sialylated products **4.30**, **4.31** and **4.32**, respectively (Scheme 4.4). Related reactivity was observed for 1,4-triazole-linked cyclic dimer **4.09** which gave two sialylated products, mono-sialylated (**4.28**) and di-sialylated (**4.29**) derivatives. The 1,4-triazole-linked cyclic monomer **4.08** and 1,5-triazole-linked cyclic monomer **4.24** gave mono-sialylated products **4.26** and **4.27**, respectively. It is therefore evident that cyclic triazole-linked *pseudo*-galactooligomers are recognised by, and can act as acceptor substrates for TcTS.



Scheme 4.4 Structures of proposed sialylated products obtained from enzymatic transformation of compound 4.10. Reagents and conditions: 3 mM fetuin, 1 mM compound 4.10, *T. cruzi* *trans*-sialidase in 100 mM, pH 7.5 phosphate buffer, 28 °C, 9 days.

4.7 Preliminary biological evaluation of triazole-linked oligomers

As the *trans*-sialidase is an important enzyme associated with host cell invasion by *T. cruzi*,^{220, 225} we evaluated the biological potential of our triazole-linked oligomers as blockers of parasite mammalian cell entry. The trypomastigote form of the parasite invades mammalian cells, where it differentiates into amastigote form that replicate and subsequently de-differentiates to trypomastigotes (section 1.1). The latter then exit the cell in search of the cells to infect. Our assays were therefore twofold: assessment of the number of trypomastigotes present in the medium, or assessment of the number of amastigotes inside macrophages.

Parasites were mixed with bovine macrophages and triazole-linked oligomers, with or without a pre-incubation of the parasite and oligomers; where the pre-incubation was employed free triazole-linked oligomers were removed by washing before adding the parasites to macrophages. The parasites were left to invade the macrophages and after 6 days, the trypomastigote form found in the medium was removed and counted. As shown in Fig. 4.13 A (■), the incubation of parasite with triazole-linked oligomers substantially inhibited the invasion of macrophage by parasites (>90% for trimer-hexamer). To rule out a direct impact of the triazole-linked compounds on the macrophages, pre-incubation of parasite with triazoles, plus washing to remove excess

triazole, was accessed. While the impact on parasite invasion was more modest than when the triazole was present throughout (Fig. 4.13 A ■), this is to be expected given the dramatic reduction in concentration of the inhibitor in these experiments. Gratifyingly, inhibition of macrophage invasion was still pronounced.

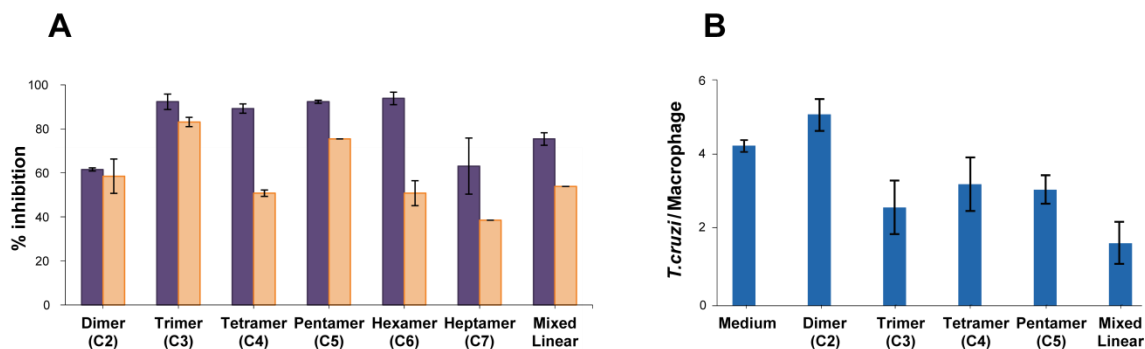


Figure 4.13 Inhibition of *T. cruzi* invasion of bovine macrophages in the presence of 1,4/1,5-triazole-linked cyclic dimers (C2), trimer (C3), tetramer (C4), pentamer (C5), hexamer (C6), heptamer (C7) and a series of mixed 1,4/1,5-triazole-linked linear oligomers. (A) Parasites were applied to macrophages without (■) or with (■) pre-incubation with triazoles and following 6 days incubation the numbers of trypomastigotes in the medium was quantified as % reduction in the numbers of parasite released from macrophages (% Inhibition). (B) Parasites and triazoles were applied to macrophages and the number of amastigotes present inside the macrophages was quantified as an average number of parasites per macrophage (*T. cruzi*/Macrophage) due to preliminary nature of these tests only two repeats were done.

To complement the above assays, we also assessed differentiated amastigote-form *T. cruzi* numbers inside infected macrophages, and the impact of triazole-linked oligomers on these numbers. In keeping with the trypomastigote results (Fig. 4 A), triazole-linked oligomers resulted in a reduction in the number of parasites found inside macrophages (Fig. 4.13 B; Fig. 4.14), with a general trend towards larger structures giving greater effect. Taken together, these data confirms the potential of triazole-linked trans-sialidase ligands to block macrophage invasion by *T. cruzi* parasites. The toxicity experiments were not carried out due to preliminary nature of these experiments.

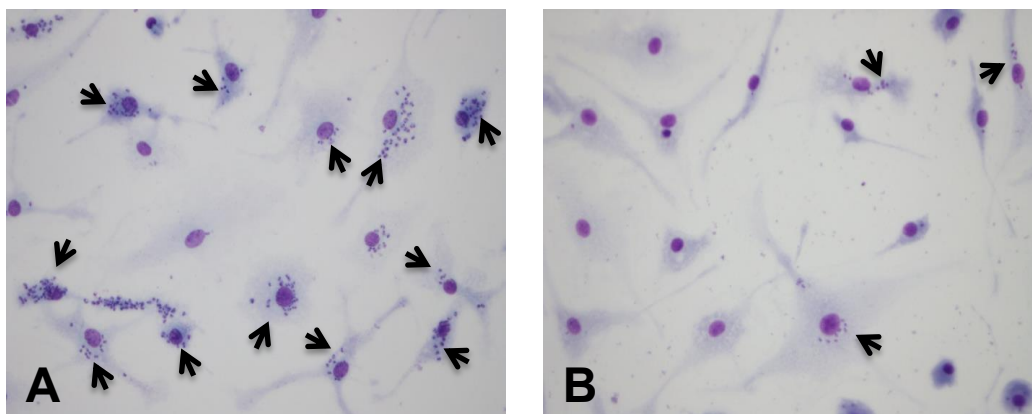


Figure 4.14 Representative images illustrating amastigote-form parasite numbers present inside macrophages infected with *T. cruzi* in (A) the absence and (B) the presence of 250 μ M mixed length 1,4/1,5 triazole-linked linear oligomers. Arrows indicate cells infected with *T. cruzi*.

4.8 Conclusion

In this study we have investigated the CuAAC-mediated oligomerisation of an azido-alkyne-functionalised galactose building block **4.07** for the development of novel oligomeric, triazole-linked compounds with potential for impact against the human parasite *T. cruzi*. Despite our initial expectation that the installation of flexible ethylene-glycol-based linker might favour polymerisation of monomer over cyclisation, mixed populations of linear and cyclic triazole-linked oligomers of d.p. 1 to >10 were evident. The cyclic compounds were separable from each other and from the corresponding linear materials by reverse phase HPLC, whilst separation of linear materials up to d.p. 5 could be achieved by gel permeation chromatography. Furthermore, capping of linear 1,4-triazole-linked compounds with 3-azido-7-hydroxy-coumarin resulted in formation of linear fluorescent compounds that were separated up to a pentamer by reverse phase HPLC compared to no separation of linear uncapped material. The overall yield of triazole-linked products obtained from polymerisation and cyclooligomerisation of galactose monomer **4.07** was around 54%, with a higher proportion of linear products (36%) compared to cyclic products (18%) formed in CuAAC reactions conducted at room temperature.

Judicious choice of the sites of galactose modification in galactose monomer **4.07** (the 1- and 6-positions) results in oligomeric triazole-linked materials that present the 2-, 3- and 4-hydroxyl groups of the sugar units that are required for binding to *T. cruzi trans-*

sialidase.²²⁶ This was borne out by *in vitro* biotransformations, which established that triazole-linked 1,6-substituted *pseudo*-galactooligomers are indeed recognised as acceptor substrates by *T. cruzi trans*-sialidase. Given the high copy number presentation of *trans*-sialidase on the surface of *T. cruzi*, multivalent ligands for the enzyme might block the surface of the parasite and inhibit TcTS-mediated host cell invasion. Encouragingly, preliminary assessment of linear and cyclic triazole-linked *pseudo*-galactooligomers clearly establishes their ability to block *T. cruzi* invasion of macrophages, with distinct advantage demonstrated by pre-incubation of triazole-linked oligomers with parasite prior to exposure to macrophages. While this phenomenon would be difficult to reproduce medicinally, it suggests that there is scope for optimisation of ligand presentation. The versatile nature of CuAAC-based oligomerisation approach offers significant scope in this regard.

5 Materials and methods

5.1 Chemical methods

5.1.1 General experimental section

Chemicals were purchased as reagent grade and used without further purification. Ammonia solution (7 N NH₃ in methanol) and methanolic sodium methoxide (0.5 M NaOMe in methanol) were purchased from Sigma Aldrich. All moisture-sensitive reactions were performed under a dry nitrogen atmosphere using oven-dried glassware. Anhydrous solvents were purchased from Sigma Aldrich and CH₂Cl₂ was freshly distilled from calcium hydride prior to use. Microwave-assisted reactions were carried out in Biotage Initiator microwave.

Thin layer chromatography (TLC)

Reactions were monitored by thin-layer chromatography (TLC) on pre-coated silica gel glass (60A) or aluminium plates (Silica Gel 60 F₂₅₄, E. Merck) with indicated eluents. Compounds were visualised under UV light (λ 254 nm), by dipping in ethanol-sulphuric acid (95:5, v/v) or in orcinol solution (20 mg/mL orcinol monohydrate in EtOH/H₂SO₄:H₂O 75:10:5, v/v) followed by heating. Fluorescent products were purified on semi-preparative TLC on pre-coated silica gel aluminium plates (Silica Gel 1000 UV254, Analtech).

Flash chromatography

Flash chromatography was performed on a Biotage Isolera MPLC system using pre-packed silica gel cartridges.

High Performance Liquide Chromatography (HPLC)

HPLC was carried out using a Dionex HPLC system with reverse phase (C18 stationary phase) column, equipped with Corona charged aerosol detector (CAD) or UV detector (at 347 nm).

Purification of cyclic and linear triazole-linked products

Cyclic and linear 1,4-triazole linked, 1,4/1,5-triazole linked and 1,4-triazole linked fluorescent products were redissolved in water and subjected to purification using semi-prep reverse phase HPLC Phenomenex Luna C18 (250 x 10 mm) column. The column was pre-conditioned with 0.1% aqueous solution of TFA. The elution program was as follows: linear gradient to 35% acetonitrile for 50 min further linear gradient to 100% acetonitrile (held at 100% for 2 min) then equilibrated back to 0.1% aqueous solution of TFA. The flow rate was 5 mL/min.

Gel Permeation Chromatography (GPC)

Non-fluorescent linear oligomers were re-dissolved in water, applied onto the TSK-HW40S gel filtration column (1.6 x 80 cm) and eluted using the Perkin Elmer Series 200 system at a flow rate of 0.5 mL/min for 400 min. Compounds were detected with IOTA 2 refractive index detector coupled to UV detector (λ 347 nm). Fractions (1 mL) were collected at rate of thirty per hour.

Optical rotation

Optical rotations were measured at 20 °C in 1 mL cell in the stated solvent using a Perkin-Elmer 341 polarimeter equipped with a sodium lamp.

Nuclear Magnetic Resonance spectroscopy (NMR)

Nuclear magnetic resonance spectra were recorded on a Bruker Avance III 400 NMR or Bruker Avance 800 spectrometer at 298 K. Chemical shifts (δ) are reported in parts per million (ppm) with respect to internal tetramethylsilane (TMS) in CDCl₃ and residual HOD signal in D₂O. NMR signal assignments were made with the aid of COSY and HSQC experiments.

Mass spectrometry (MS)

The samples were dissolved and diluted in appropriate solvent and run on the Orbitrap using manual injection from a syringe. The instrument was calibrated according to the manufacturer's instructions before use. Positive electrospray data were collected at a resolution of 60,000. Spray chamber conditions were 8 units sheath gas, no other gases, 275°C capillary temperature, 100V tube lens, and a spray voltage of 3.3kV using a steel needle kit. MS2 data were collected at various collision energies and isolation widths as appropriate to the precursor ion.

High resolution ESI MS data of linear and cyclic 1,4-triazole-linked compounds were obtained using the Waters Synapt G2 mass spectrometer. The sample was diluted into 50% methanol/water with 0.1% formic acid and infused into a Synapt G2 mass spectrometer (Waters, Manchester, UK) at 5-10 $\mu\text{l min}^{-1}$ using a Harvard Apparatus syringe pump. The mass spectrometer was controlled by Masslynx 4.1 software (Waters). It was operated in resolution and positive ion mode and calibrated using sodium formate. The sample was analysed for 2 min with 1 s MS scan time over the range of 50-1200 m/z (or as appropriate) with 3.5 kV capillary voltage, 40 V cone voltage, 100°C cone temperature. Leu-enkephalin peptide (2 ng ml^{-1} , Waters) was infused at 10 $\mu\text{l min}^{-1}$ as a lock mass (m/z 556.2766). It was measured every 10 s and was applied during the acquisition. For low mass range acquisitions it was fragmented for dual point calibration (m/z 278.1135 and 556.2766). Spectra were generated in Masslynx 4.1 by combining a number of scans, and peaks were centred using automatic peak detection. Data for multiply charged species were deconvoluted using the Mass X3 program.

Infra-Red spectrometry (IR)

Infra-red spectra were obtained on a Perkin-Elmer FTIR Spectrum BX instrument equipped with MIRacle single reflection horizontal accessory.

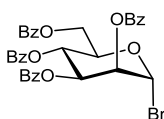
Fluorescence spectrometry

Compounds **2.05** and **2.13** were redissolved in MeOH and water, respectively, at wide concentration range and fluorescence intensities were measured on a Perkin Elmer lambda 55 instrument.

5.2 Chemical synthesis of non-fluorescent and fluorescent α -D-mannopyranoside derivatives to utilise in fluorescence-based methodology I

5.2.1 Chemical synthesis of non-fluorescent azidocoumarinyl α -D-mannopyranoside derivatives

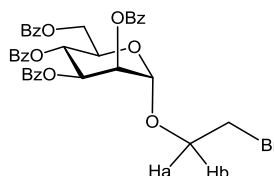
2,3,4,6-Tetra-O-benzoyl- α -D-mannopyranosyl bromide (2.01)^{116, 117}



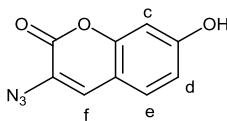
Benzoyl chloride (72 mL, 622 mmol) was added dropwise to a stirred solution of D-mannose (8.0 g, 45 mmol) in pyridine (300 mL) at 0 °C, the mixture was stirred for 1 h at room temperature and ice-cold water (300 mL) was carefully added. The product was extracted with CH₂Cl₂ (3 x 150 mL), the organic extracts were combined and washed with ice-cold 1M HCl (3 x 150 mL), saturated aqueous NaHCO₃ solution (4 x 150 mL), dried (MgSO₄), filtered, concentrated under reduced pressure, and co-evaporated with toluene. The obtained residue was purified by flash column chromatography (hexane/EtOAc, 6:4) to give perbenzoylated mannose **2.00** (31.0 g, 99%, mixture of α/β -anomers) as a colourless solid. To a solution of perbenzoylated mannose (19.4 g, 27.7 mmol) in anhydrous CH₂Cl₂ (250 mL) stirred at 0 °C, 33% HBr (glacial acetic acid, 109 mL) was added. The reaction mixture was allowed to warm to room temperature and stirred for 3.5 hours. Solvents were removed under reduced pressure followed by co-evaporation with toluene (2 x 75 mL) and the resulting residue was re-dissolved in ice-cold CH₂Cl₂ (75 mL) and neutralised with ice-cold saturated aqueous NaHCO₃ solution (75 mL). The organic phase was separated, washed with ice-cold water (3 x 75 mL), saturated aqueous NaHCO₃ solution (4 x 75 mL) and brine (3 x 75 mL). The resulting organic extract was dried (MgSO₄) and concentrated under reduced pressure to give known compound **2.01** as a colourless amorphous solid (17.8 g, 97%). ¹H NMR: (400 MHz, CDCl₃) δ 8.11-7.83 (8H, m, Ar), 7.63-7.52 (3H, m, Ar), 7.51-7.37 (7H, m, Ar), 7.30-7.26 (2H, m, Ar), 6.58 (1H, d, $J_{1,2}$ 1.4 Hz, H-1), 6.29 (1H, dd, $J_{2,3}$ =3.0 Hz, $J_{3,4}$ =10.4 Hz, H-3), 6.23 (1H, t, H-4), 5.90 (1H, dd, $J_{1,2}$ =1.4 Hz, $J_{2,3}$ =3.0 Hz, H-2), 4.74 (1H, dd, $J_{5,6a}$ =2.4 Hz, $J_{6a,6b}$ =12.4 Hz, H-6a), 4.67-4.64 (1H, m, H-5), 4.51

(1H, dd, $J_{5,6a}=3.7$ Hz, $J_{6a,6b}=12.4$ Hz, H-6b). ^1H NMR data are in accordance with the literature.^{116, 117}

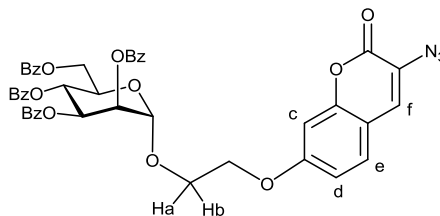
2-Bromoethyl 2,3,4,6-tetra-O-benzoyl- α -D-mannopyranoside (2.02**)²²⁷**



To a solution of mannosyl bromide **2.01** (4.0 g, 6.1 mmol) and 2-bromoethanol (0.6 mL, 9.1 mmol) in anhydrous CH_2Cl_2 (100 mL) containing 4 Å mol. sieves, at -20 °C, a solution of AgOTf (2.2 g, 8.5 mmol) in anhydrous toluene (60 mL) was added. The reaction mixture was allowed to warm to room temperature and stirred for 3 h, neutralised with Et_3N (3.0 mL), filtered through Celite and concentrated under reduced pressure. The residue was purified by flash column chromatography (hexane/EtOAc 7:3) to give protected 2-bromoethyl mannoside **2.02** as a colourless amorphous solid (3.6 g, 83%). R_f 0.73 (hexane/EtOAc, 6:4); $[\alpha]_D$ -48.9 (c 1.0, CHCl_3); ^1H NMR (400 MHz, CDCl_3) δ 8.11-8.03 (4H, m, Ar), 7.97-7.95 (2H, m, Ar), 7.85-7.82 (2H, m, Ar), 7.61-7.25 (12H, m, Ar), 6.12 (1H, t, $J=10.1$ Hz, H-4), 5.93 (1H, dd, $J_{2,3}=3.3$ Hz, $J_{3,4}=10.1$ Hz, H-3), 5.73 (1H, dd, $J_{1,2}=1.7$ Hz, $J_{2,3}=3.3$ Hz, H-2), 5.16 (1H, d, $J_{1,2}=1.7$ Hz, H-1), 4.70 (1H, dd, $J_{5a,6b}=2.4$ Hz, $J_{6a,6b}=12.1$ Hz, H-6a), 4.60-4.56 (1H, m, H-5), 4.50 (1H, dd, $J_{5a,6b}=4.6$ Hz, $J_{6a,6b}=12.1$ Hz, H-6b), 4.15-4.09 (1H, m, $\text{OCH}_a\text{CH}_2\text{Br}$), 4.03-3.98 (1H, m, $\text{OCH}_b\text{CH}_2\text{Br}$), 3.63-3.60 (2H, m, $\text{OCH}_2\text{CH}_2\text{Br}$); ^{13}C NMR (100.6 MHz, CDCl_3) δ 166.1-165.4 (C=O), 133.5-128.3 (aromatic C), 97.8 ($J_{\text{C-H}}=171$ Hz, C-1), 70.3 (C-2), 69.9 (C-3), 69.4 (C-5), 68.6 ($\text{OCH}_2\text{CH}_2\text{Br}$), 66.7 (C-4), 62.8 (C-6), 29.7 ($\text{OCH}_2\text{CH}_2\text{Br}$); HRMS (ESI): Calculated for $\text{C}_{36}\text{H}_{31}\text{BrO}_{10}$ Na, 725.0993; Found, 725.0997. This compound has been reported before but without full characterisation.²²⁷

3-Azido-7-hydroxy-2H-cromen-2-one¹¹⁸

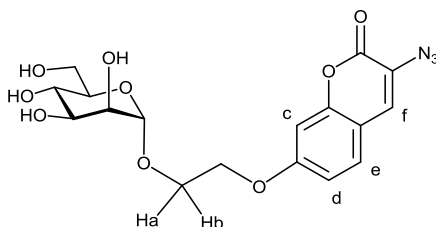
2,4-Dihydroxybenzaldehyde (20.0 g, 145 mmol), *N*-acetylglycine (16.9 g, 144 mmol) and anhydrous sodium acetate (38.0 g, 463 mmol) were suspended in acetic anhydride (500 mL) and refluxed at 140 °C under stirring for 12 h. The solvent was evaporated and resulting mixture was redissolved in water, extracted with EtOAc and organic solvent dried under reduced pressure to yield brown slurry. The resulting mixture was dispersed in a mixture of concentrated HCl and ethanol (400 mL), stirred under reflux for 2 h, then iced cold water (350 mL) was added to dilute the solution. The resulting solution was then cooled to 0 °C on ice bath, following addition of NaNO₂ (20 g, 290 mmol). The mixture was stirred for 30 min and NaN₃ (28 g, 434 mmol) was added in portions. After stirring for 12 h, the resulting precipitate was filtered off, washed with water and dried under reduced pressure to give azidocoumarin as a brown solid (3.7 g, 12%). ¹H NMR (400 MHz, DMSO) δ 7.57 (1H, s, H-f), 7.47 (1H, d, *J*_{d,e}=8.5 Hz, H-e), 6.81 (1H, dd, *J*_{c,d}=2.3 Hz, *J*_{d,e}=8.5 Hz, H-d), 6.76 (1H, d, *J*_{c,d}=2.3 Hz, H-c). ¹H NMR data are in accordance with the literature.¹¹⁸

2-(3-Azido-coumarin-7-yloxy)ethyl 2,3,4,6-tetra-*O*-benzoyl- α -*D*-mannopyranoside (2.03)

A solution containing protected 2-bromoethyl mannoside **2.02** (600 mg, 0.9 mmol), 3-azido-7-hydroxy coumarin (347 mg, 1.7 mmol), anhydrous K₂CO₃ (236 mg, 1.7 mmol) and 18-crown-6 (451 mg, 1.7 mmol) in anhydrous DMF (4 mL) was stirred at 35 °C for 14 hours. Solvent was partially evaporated and the product was extracted with ethyl acetate (3 x 30 mL), dried (Mg₂SO₄), filtered and concentrated under reduced pressure.

The obtained residue was purified by flash column chromatography (hexane/EtOAc 7:3) to give coumarinyl ether **2.03** as a yellow/orange solid (284 mg, 40%). R_f 0.58 (hexane/EtOAc, 6:4); $[\alpha]_D$ -42.6 (c 1.1, CHCl_3); IR (neat) 2122, 1720, 1618, 1602, 1584, 1450, 1256, 1067 cm^{-1} ; ^1H NMR (400 MHz, CDCl_3) δ 8.08-8.04 (4H, m, Ar), 7.94-7.91 (2H, m, Ar), 7.83-7.80 (2H, m, Ar), 7.62-7.49 (3H, m, Ar), 7.45-7.36 (7H, m, Ar), 7.30 (1H, d, $J_{d,e}$ =8.6 Hz, H-e), 7.28-7.24 (3H, m, Ar), 7.16 (1H, s, H-f), 6.95 (1H, dd, $J_{c,d}$ =2.4 Hz, $J_{d,e}$ =8.6 Hz, H-d), 6.91 (1H, d, $J_{c,d}$ =2.4 Hz, H-c), 6.10 (1H, t, J =10.0 Hz, H-4), 5.87 (1H, dd, $J_{2,3}$ =3.4 Hz, $J_{3,4}$ =10.1 Hz, H-3), 5.71 (1H, dd, $J_{1,2}$ =1.8 Hz, $J_{2,3}$ =3.3 Hz, H-2), 5.21 (1H, d, $J_{1,2}$ =1.8 Hz, H-1), 4.77-4.67 (1H, m, H-6a), 4.51-4.46 (1H, m, H-5, H-6b), 4.32-4.29 (1H, m, $\text{OCH}_a\text{CH}_2\text{O}$), 4.24-4.18 (1H, m, $\text{OCH}_b\text{CH}_2\text{O}$), 4.05-4.00 (2H, m, $\text{OCH}_2\text{CH}_2\text{O}$); ^{13}C NMR (100.6 MHz, CDCl_3) δ 166.1-165.4 (C=O), 160.7, 157.7, 152.9, 133.5-128.3 (aromatic C), 126.2, 123.6, 113.6, 113.1, 101.6, 97.1 (C-1), 70.3 (C-2), 69.8 (C-3), 69.1 (C-5), 67.4 ($\text{OCH}_2\text{CH}_2\text{O}$), 66.9 (C-4), 66.5 ($\text{OCH}_2\text{CH}_2\text{O}$), 62.9 (C-6); HRMS (ESI): Calculated for $\text{C}_{45}\text{H}_{35}\text{N}_3\text{O}_{13}$ Na, 848.2075; Found, 848.2062.

2-(3-Azido-coumarin-7-yloxy)ethyl α -D-mannopyranoside (α -Man-EtC (2.04))

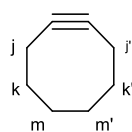


A solution of coumarinyl ether **2.03** (284 mg, 0.3 mmol) in anhydrous MeOH (2 mL) was treated with 1M NaOMe in MeOH (0.1 mL, 0.1 mmol). The solution was kept at room temperature for 24 hours, neutralised with ion-exchange resin (Amberlite IR-120 H^+) and concentrated under reduced pressure. The resulting residue was purified by flash column chromatography ($\text{CH}_2\text{Cl}_2/\text{MeOH}$ 9:1) to give unprotected mannoside **2.04** as an off-white colour solid (141 mg, 71%). R_f 0.52 ($\text{CH}_2\text{Cl}_2/\text{MeOH}$ 9:1); $[\alpha]_D$ +40.5 (c 1.0, MeOH); ^1H NMR (400 MHz, CD_3OD) δ 7.47 (1H, d, $J_{d,e}$ =9.4 Hz, H-e), 7.40 (1H, s, H-f), 6.99-6.95 (2H, m, H-c and H-d), 4.85 (1H, under D_2O signal, H-1), 4.27 (2H, t, J =4.7 Hz $\text{OCH}_2\text{CH}_2\text{O}$), 4.11-4.06 (1H, m, $\text{OCH}_a\text{CH}_2\text{O}$), 3.92-3.86 (1H, m, $\text{OCH}_b\text{CH}_2\text{O}$), 3.83-3.80 (2H, m, H-2, H-6a), 3.72-3.67 (2H, m, H-6b, H-3), 3.64-3.60

(2H, m, H-5, H-4); ^{13}C NMR (100.6 MHz, CD_3OD) δ 162.7, 159.4, 154.4, 129.8, 128.3, 124.4, 114.7, 114.3, 102.4, 101.9 (C-1), 74.8 (C-4), 72.5 (C-3), 72.1 (C-2), 69.2 ($\text{OCH}_2\text{CH}_2\text{O}$), 68.5 (C-5), 66.9 ($\text{OCH}_2\text{CH}_2\text{O}$), 62.9 (C-6); HRMS (ESI): Calculated for $\text{C}_{17}\text{H}_{19}\text{N}_3\text{O}_9\text{Na}$, 432.1014; Found, 432.1014.

5.2.2 Chemical synthesis of fluorescent coumarinyl α -D-mannopyranoside derivative under strain-promoted click condition

*Cyclooctyne*¹²⁰

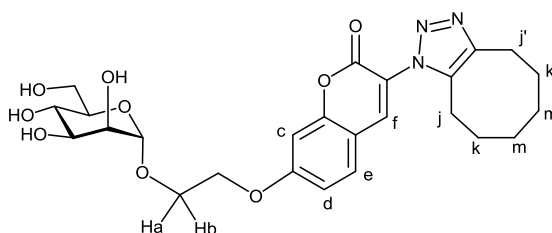


Cis-cyclooctene (500 mg, 4.54 mmol, 0.5 mL) was dissolved in CH_2Cl_2 (4 mL) and a solution of bromide (870 mg, 5.44 mmol, 0.3 mL) was added gradually at 0 °C until a yellow colour persisted. The reaction mixture was quenched with 10% Na_2SO_4 (20 mL) and the product was extracted with CH_2Cl_2 (3 x 20 mL). The resulting organic extracts were combined, dried (MgSO_4), filtered and concentrated under reduced pressure to give 1,2-dibromocyclooctane as clear oil (1.2 g, 100%). The 1,2-dibromocyclooctane (1.2 g, 4.54 mmol) was dissolved in THF (20 mL), cooled to 0 °C, and a solution of $\text{KO}t\text{Bu}$ (560 mg, 5.00 mmol) was gradually added. The reaction mixture was refluxed for 2 h, allowed to cool to room temperature and quenched with saturated aqueous NH_4Cl solution (20 mL). The product was extracted with CH_2Cl_2 (3 x 30 mL), dried (MgSO_4), filtered and concentrated under reduced pressure. The obtained residue was purified by flash column chromatography (100 % hexane) to give 1-bromocyclooctene as yellow oil (570 mg, 67 %) b.p. 90-95 °C/22torr.

To a solution of lithium diisopropylamide in anhydrous TFA (50 mL) cooled at -25 °C, 1-bromocyclooctene (570 mg, 3.01 mmol) was added. The reaction mixture was gradually brought up to 15 °C and poured onto iced cold 1 M HCL (50 mL). The product was extracted with pentane (4 x 40 mL), dried (MgSO_4) and filtered. The residue obtained was purified by flash column chromatography (100% pentane). Solvent was carefully distilled to give cyclooctyne (208 mg, 64%) b.p. 51-52°C/22torr.

^1H NMR: (400 MHz, CD_3OD) δ 2.18 (4H, m, H-j,j'), 1.88-1.84 (4H, m, H-k, k'), 1.63-1.61 (4H, m, H-m, m'); ^1H NMR data are in accordance with the literature.¹²⁰

2-(3-(4,5,6,7,8,9-Hexahydro-1H-cycloocta[d][1,2,3]triazole-1-yl)-coumarin-7-yloxy)ethyl α -D-mannopyranoside (α -Man-EtTC (2.05))

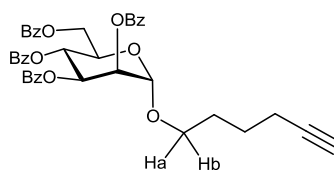


To a solution of azidocoumarin glycoside **2.04** (9.9 mg, 0.02 mmol) in MeOH (1 mL) cyclooctyne (3.1 mg, 0.03 mmol, 3.6 μL) was added. The reaction mixture was allowed to stir at room temperature for 2 h and solvent was removed under reduced pressure. The resulting residue was purified by flash column chromatography ($\text{CH}_2\text{Cl}_2/\text{MeOH}$, 9:1) to give click adduct **2.05** as an off-white amorphous solid (13 mg, 99%). R_f 0.65 ($\text{CH}_2\text{Cl}_2/\text{MeOH}$, 9:1); ^1H NMR: (400 MHz, CD_3OD) δ 8.27 (1H, s, H-f), 7.71 (1H, d, $J_{c,d}$ = 8.8 Hz, H-c), 7.09-7.07 (2H, m, H-d, H-e), 4.87 (1H, d, $J_{1,2}$ = 1.7 Hz, H-1), 4.33 (2H, t, J = 4.7 Hz, $\text{OCH}_2\text{CH}_2\text{O}$), 4.13-4.08 (1H, m, $\text{OCH}_d\text{CH}_2\text{O}$), 3.92-3.86 (1H, m, $\text{OCH}_b\text{CH}_2\text{O}$), 3.84-3.81 (2H, m, H-2, H-6a), 3.73-3.61 (2H, m, H-6b, H-3, H-5, H-4), 2.96 (2H, t, J = 6.4 Hz, H-j), 2.78 (2H, t, J = 6.2 Hz, H-j'), 1.88-1.78 (4H, m, H-k, k'), 1.61-1.52 (4H, m, H-m, m'); ^{13}C NMR (100.6 MHz, CD_3OD) δ 165.4, 159.1, 157.4, 144.1, 138.2, 131.9, 120.8, 115.3, 113.0, 102.7, 101.9 (C-1), 74.8 (C-4), 72.5 (C-3), 72.1 (C-2), 69.4 ($\text{OCH}_2\text{CH}_2\text{O}$), 68.5 (C-5), 66.9 ($\text{OCH}_2\text{CH}_2\text{O}$), 62.9 (C-6); HRMS (ESI): Calculated for $\text{C}_{25}\text{H}_{31}\text{N}_3\text{O}_9$ Na, 540.1953; Found, 540.1952.

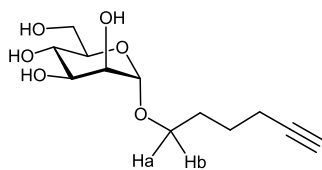
5.3 Chemical synthesis of non-fluorescent and fluorescent α -D-mannopyranoside derivatives to utilise in fluorescence-based methodology II

5.3.1 Chemical synthesis of non-fluorescent 5-hexynyl α -D-mannopyranoside derivatives

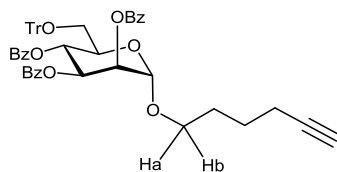
5-Hexynyl 2,3,4,6-tetra-O-benzoyl- α -D-mannopyranoside (2.06)



To a solution of mannosyl bromide **2.01** (11.7 g, 17.9 mmol) and 5-hexyn-1-ol (2.1 g, 21.5 mmol) in anhydrous CH_2Cl_2 (40 mL) containing 4 Å mol. sieves cooled at $-20\text{ }^\circ\text{C}$, a solution of AgOTf (6.4 g, 25.1 mmol) in anhydrous toluene (160 mL) was added. The reaction mixture was allowed to warm to room temperature and stirred for 3.5 hours. The reaction mixture was neutralised with Et_3N (2.0 mL), filtered through Celite and concentrated under reduced pressure. The residue was purified by flash column chromatography (hexane/ EtOAc 7:3) to give protected hexynyl mannoside **2.06** as a colourless amorphous solid (10.2 g, 85%). R_f 0.6 (hexane/ EtOAc , 6:4); $[\alpha]_D - 55.0$ (c 1.0, CHCl_3); $^1\text{H NMR}$: (400 MHz, CDCl_3) δ 8.11-8.05 (4H, m, Ar), 7.98-7.96 (2H, m, Ar), 7.85-7.83 (2H, m, Ar), 7.61-7.24 (12H, m, Ar), 6.12 (1H, t, $J=10.8$ Hz, H-4), 5.93 (1H, dd, $J_{2,3}=3.4$ Hz, $J_{3,4}=8.0$ Hz, H-3), 5.71 (1H, dd, $J_{1,2}=1.6$ Hz, $J_{2,3}=3.4$ Hz, H-2), 5.10 (1H, d, $J_{1,2}=1.6$ Hz, H-1), 4.70 (1H, dd, $J_{5,6a}=2.5$ Hz, $J_{6a,6b}=12.1$ Hz, H-6a), 4.50 (1H, dd, $J_{5,6b}=4.5$ Hz, $J_{6a,6b}=12.1$ Hz, H-6b), 4.45-4.41 (1H, m, H-5); 3.90-3.84 (1H, m, OCH_aH_b), 3.66-3.58 (1H, m, OCH_bH_a), 2.30-2.26 (2H, m, $\text{OCH}_2\text{CH}_2\text{CH}_2\text{CH}_2\text{CCH}$), 2.00 (1H, t, $J=2.6$ Hz $\text{OCH}_2\text{CH}_2\text{CH}_2\text{CH}_2\text{CCH}$), 1.86-1.81 (2H, m, $\text{OCH}_2\text{CH}_2\text{CH}_2\text{CH}_2\text{CCH}$), 1.72-1.66 (2H, m, $\text{OCH}_2\text{CH}_2\text{CH}_2\text{CH}_2\text{CCH}$); $^{13}\text{C NMR}$: (100.6 MHz, CDCl_3) δ 166.1-165.4 (C=O), 133.4-128.3 (aromatic C), 98.4 ($J_{\text{C-H}}=171.9$ Hz, C-1), 84.0, 70.6 (C-2), 70.1 (C-3), 68.9 (C-4), 68.8, 68.1, 67.0 (C-5), 62.9 (C-6), 28.4, 25.0, 18.2; HRMS (ESI) Calculated for $\text{C}_{40}\text{H}_{36}\text{O}_{10}\text{Na}$, 699.2201; Found, 699.2202.

5-Hexynyl α -D-mannopyranoside (H- α -Man (2.07))

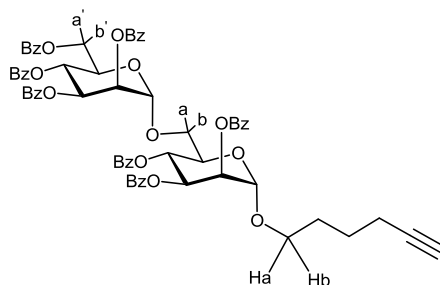
A solution of protected hexynyl mannoside **2.06** (3.10 g, 4.8 mmol) in absolute MeOH (60 mL) was treated with 1 M NaOMe in MeOH (1.9 mL, 1.9 mmol). The solution was kept at room temperature for 4 h, neutralised with ion-exchange resin (Amberlite IR-120 H⁺) and concentrated under reduced pressure. The resulting residue was re-dissolved in water (50 mL) and the aqueous phase was washed with dichloromethane (3 x 50 mL). The aqueous extract was evaporated to give unprotected hexynyl mannoside **2.07** as a colourless syrup (1.1 g, 92%). R_f 0.2 (CH₂Cl₂/MeOH, 9:1); $[\alpha]_D^{+72.0}$ (c 1.0, CHCl₃); ¹H NMR: (400 MHz, D₂O) δ 4.87 (1H, d, $J_{1,2}$ =1.7 Hz, H-1), 3.94 (1H, dd, $J_{1,2}$ =1.7 Hz, $J_{2,3}$ =3.4 Hz, H-2), 3.89 (1H, dd, $J_{5,6a}$ =1.8 Hz, $J_{6a,6b}$ =12.4 Hz, H-6a), 3.81-3.73 (3H, m, H-3, H-6b, OCH₂H_b), 3.68-3.55 (3H, m, H-4, H-5, OCH_aH_b), 2.28-2.23 (3H, m, OCH₂CH₂CH₂CH₂CCH, OCH₂CH₂CH₂CH₂CCH), 1.77-1.68 (2H, m, OCH₂CH₂CH₂CH₂CCH), 1.66-1.56 (2H, m, OCH₂CH₂CH₂CH₂CCH); ¹³C NMR; (100.6 MHz, D₂O) δ 98.4 (C-1), 84.2, 71.5 (C-5), 69.4 (C-3), 68.8 (C-2), 67.9, 66.1, 65.5 (C-4), 59.7 (C-6), 26.5, 23.3, 16.1; HRMS (ESI): Calculated for C₁₂H₂₀O₆Na, 283.1152; Found, 283.1147.

5-Hexynyl 2,3,4-tri-O-benzoyl-6-O-trityl- α -D-mannopyranoside (2.08)

To a solution of unprotected hexynyl mannoside **2.07** (1.2 g, 4.4 mmol) in anhydrous pyridine (15 mL) triphenylmethyl chloride (1.8 g, 6.6 mmol) and 4-dimethylaminopyridine (108 mg, 0.88 mmol) were added. The reaction mixture was warmed to 37 °C for 40 h, diluted with pyridine (45 mL) and cooled down to 0 °C for

benzoyl chloride (51.0 mL, 44.2 mmol) addition. The mixture was stirred for 1 h at room temperature and ice-cold water was carefully added. The product was extracted with CH_2Cl_2 (3 x 75 mL), the organic extracts were combined and washed with ice-cold 1M HCl (3 x 75 mL), saturated aqueous NaHCO_3 solution (4 x 75 mL), dried (MgSO_4), filtered and concentrated under reduced pressure. The obtained residue was purified by flash column chromatography (hexane/EtOAc 7:3) to give ester protected tritylether **2.08** as a colourless amorphous solid (3.3 g, 92%). R_f 0.77 (hexane/EtOAc, 6:4); $[\alpha]_D -95.0$ (c 1.0, CHCl_3); $^1\text{H NMR}$: (400 MHz, CDCl_3) δ 8.16-8.10 (2H, m, Ar), 7.85-7.82 (2H, m, Ar), 7.75-7.73 (2H, m, Ar), 7.50-7.40 (10H, m, Ar), 7.33-7.24 (6H, m, Ar), 7.17-7.07 (8H, m, Ar), 6.02 (1H, t, $J=10.2$, H-4), 5.78 (1H, dd, $J_{2,3}=3.4$ Hz, $J_{3,4}=10.2$ Hz, H-3), 5.67 (1H, dd, $J_{1,2}=1.6$ Hz, $J_{2,3}=3.4$ Hz, H-2), 5.12 (1H, d, $J_{1,2}=1.6$ Hz, H-1), 4.20-4.16 (1H, m, H-5), 3.93-3.87 (1H, m, OCH_aH_b), 3.65-3.59 (1H, m, OCH_aH_b), 3.38 (1H, dd, $J_{5,6a}=2.2$ Hz, $J_{6a,6b}=10.5$ Hz, H-6a), 3.28 (1H, dd, $J_{5,6b}=4.8$ Hz, $J_{6a,6b}=10.5$ Hz, H-6b), 2.30-2.26 (2H, m, $\text{OCH}_2\text{CH}_2\text{CH}_2\text{CH}_2\text{CCH}$), 1.97 (1H, t, $J=2.6$ Hz, $\text{OCH}_2\text{CH}_2\text{CH}_2\text{CH}_2\text{CCH}$), 1.86-1.81 (2H, m, $\text{OCH}_2\text{CH}_2\text{CH}_2\text{CH}_2\text{CCH}$), 1.74-1.66 (2H, m, $\text{OCH}_2\text{CH}_2\text{CH}_2\text{CH}_2\text{CCH}$); $^{13}\text{C NMR}$: (100.6 MHz, CDCl_3) δ 165.7-165.1 (C=O), 146.8-126.8 (aromatic C), 97.5 (C-1), 84.0, 70.9 (C-2), 70.6 (C-3), 70.9 (C-5), 68.7, 67.7, 67.0 (C-4), 62.3 (C-6), 28.4, 25.1, 18.2; HRMS (ESI): Calculated for $\text{C}_{52}\text{H}_{46}\text{O}_9\text{Na}$, 837.3034; Found, 837.3029.

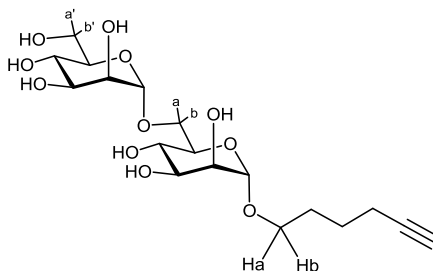
6-O-Hexyn-5-yl (2,3,4,6-tetra-O-benzoyl- α -D-mannopyranosyl)-2,3,4-tri-O-benzoyl- α -D-mannopyranoside (2.09)



To a solution of esterified tritylether **2.08** (3.7 g, 4.5 mmol) and mannosyl bromide **2.02** (4.5 g, 6.8 mmol) in anhydrous CH_2Cl_2 containing 4 Å mol. sieves, at -20 °C, a solution of AgOTf (1.6 g, 6.4 mmol) in anhydrous toluene (110 mL) was added. The

reaction mixture was allowed to warm to room temperature and stirred for 18 h, neutralised with Et₃N (3.0 mL), filtered through Celite and concentrated under reduced pressure. The resulting residue was purified by flash column chromatography (hexane/EtOAc 7:3) to give protected hexynyl disaccharide **2.09** as a colourless amorphous solid (2.3 g, 45%). R_f 0.6 (hexane/EtOAc, 1:1); [α]_D - 54.0 (c 1.0, CHCl₃); ¹H NMR: (400 MHz, CDCl₃) δ 8.17-8.15 (2H, m, Ar), 8.04-7.98 (8H, m, Ar), 7.87-7.84 (4H, m, Ar), 7.58-7.48 (6H, m, Ar), 7.44-7.34 (10H, m, Ar), 7.30-7.21 (5H, m, Ar), 6.11-6.06 (2H, m, H-4, H-4'), 6.00 (1H, dd, J_{2',3'}=3.2 Hz, J_{3',4'}=10.1 Hz, H-3'), 5.94 (1H, dd, J_{2,3}=3.3 Hz, J_{3,4}=10.1 Hz, H-3), 5.78 (1H, dd, J_{1',2'}=1.5 Hz, J_{2',3'}=3.2 Hz, H-2'), 5.75 (1H, dd, J_{1,2}=1.6 Hz, J_{2,3}=3.3 Hz, H-2), 5.15 (1H, d, J_{1',2'}=1.5 Hz, H-1'), 5.12 (1H, d, J_{1,2}=1.6 Hz, H-1), 4.51 (1H, dd, J_{5',6a'}=2.4 Hz, J_{6a',6b'}=12.2 Hz, H-6'a), 4.44-4.37 (2H, m, H-5' H-5), 4.30 (1H, dd, J_{5',6a'}=4.2 Hz, J_{6a',6b'}=12.2 Hz, H-6'b), 4.13 (1H, dd, J_{5,6a}=5.4 Hz, J_{6a,6b}=10.9 Hz, H-6b), 4.00-3.95 (1H, m, OCH_aH_b), 3.78 (1H, dd, J_{5a,6b}=2.0 Hz, J_{6a,6b}=10.8 Hz, H-6a), 3.70-3.64 (1H, m, OCH_aH_b), 2.35-2.31 (2H, m, OCH₂CH₂CH₂CH₂CCH), 1.98 (1H, t, J=2.6 Hz, OCH₂CH₂CH₂CH₂CCH), 1.95-1.87 (2H, m, OCH₂CH₂CH₂CH₂CCH), 1.80-1.72 (2H, m, OCH₂CH₂CH₂CH₂CCH); ¹³C NMR: (100.6 MHz, CDCl₃) δ 166.0-165.1 (C=O), 133.5-132.9 (aromatic C), 130.1-128.3 (aromatic C), 97.8 (C-1), 97.7 (C-1'), 84.1, 70.6 (C-2), 70.3 (C-2'), 70.2 (C-3; 3'), 69.6 (C-5), 68.9 (C-5'), 68.7, 68.1, 67.0 (C-6), 66.7 (C-4), 62.3 (C-6'), 28.5, 25.1, 18.2; HRMS (ESI): Calculated for C₆₇H₅₈O₁₈Na, 1173.3515; Found, 1173.3517.

Hexyn-5-yl α-D-mannopyranosyl-(1→6)-α-D-mannopyranoside (H-α-Man-1,6-α-Man (2.10))

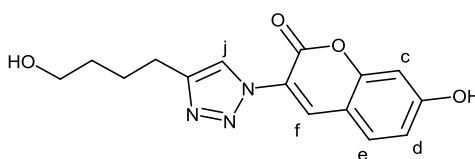


A solution of protected hexynyl disaccharide **2.09** (880 mg, 0.8 mmol) in absolute MeOH (60 mL) was treated with 1M NaOMe in MeOH (0.5 mL, 0.54 mmol). The

solution was kept at room temperature for 24 h, neutralised with ion-exchange resin (Amberlite IR-120 H⁺) and concentrated under reduced pressure. The resulting residue was purified by flash column chromatography (CH₃CN/H₂O/NH₃ 6:3:1) to give unprotected hexynyl disaccharide **2.10** as a colourless amorphous solid (323 mg, 84%). *R_f* 0.66 (CH₃CN/H₂O/NH₃ 6:3:1); [α]_D + 80.0 (*c* 1.0, MeOH); ¹H NMR: (400 MHz, D₂O) δ 4.91 (1H, d, *J*_{1',2'}=1.7 Hz, H-1'), 4.87 (1H, d, *J*_{1,2}=1.2 Hz, H-1), 4.00 (1H, dd, *J*_{1',2'}=1.7 Hz, *J*_{2',3'}=3.4 Hz, H-2'), 4.00-3.95 (2H, m, H-2; H-6b'), 3.92 (1H, dd, *J*_{5',6a'}=1.6 Hz, *J*_{6a',6b'}=11.8 Hz, H-6a'), 3.85 (1H, dd, *J*_{2,3}=3.4 Hz, *J*_{3,4}=9.0 Hz, H-3), 3.81-3.65 (8H, m, H-4', H-4, H-6a, H-6b, OCH₂H_b, H-3', H-5', H-5), 3.62-3.57 (1H, m, OCH_aH_b), 2.39 (1H, t, *J*=2.6 Hz, OCH₂CH₂CH₂CH₂CCH), 2.29-2.25 (2H, m, OCH₂CH₂CH₂CH₂CCH), 1.78-1.71 (2H, m, OCH₂CH₂CH₂CH₂CCH), 1.67-1.58 (2H, m, OCH₂CH₂CH₂CH₂CCH); ¹³C NMR: (100.6 MHz, D₂O) δ 99.8, 99.4, 85.8, 72.6 (C-5), 70.9 (C-3, 3'), 70.0 (C-2), 69.9 (C-2'), 67.3, 67.3, 66.7 (C-4), 66.6 (C-4'), 65.7 (C-6), 60.9 (C-6'), 27.6, 24.5, 17.2; HRMS (ESI): Calculated for C₁₈H₃₀O₁₁Na, 445.1680; Found, 445.1677.

5.3.2 Chemical synthesis of fluorescent coumarinyl α-D-mannopyranoside derivatives under Cu(I)-catalysed click conditions

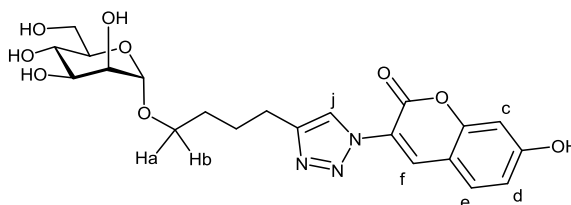
4-(1-(7-Hydroxy-coumarin-3-yl)-1H-1,2,3-triazol-4-yl)-propyl (HTC)(2.11)



A solution of 5-hexynol (25 mg, 0.1 mmol) and 3-azido-7-hydroxycoumarin (19 mg, 0.1 mmol) in MeOH (0.8 mL) was treated with 1 M aq. CuSO₄ (10 μL) and 1 M aq. sodium ascorbate (25 μL). The reaction mixture was allowed to stir at room temperature for 2 h and concentrated under reduced pressure. The resulting residue was purified by semi-prep TLC (CH₂Cl₂/MeOH/H₂O, 80:20:3) to give click adduct **2.11** as a yellow amorphous solid (29 mg, 70%). *R_f* 0.84 (CH₂Cl₂/MeOH/H₂O, 10:8:2); ¹H NMR: (400 MHz, MeOD) δ 8.37 (1H, s, H-f), 8.24 (1H, s, H-j), 7.54 (1H, d, *J*_{c,d}= 8.6

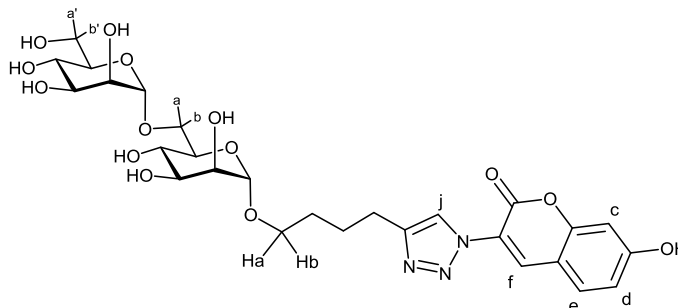
Hz, H-c), 6.80 (1H, dd, $J_{c,d}=8.6$, $J_{d,e}=2.3$ Hz, H-d), 6.72 (d, $J_{d,e}=2.3$ Hz, H-e), 3.51 (2H, t, $J=6.5$ Hz, $\underline{CH_2}$ -triazole), 2.72 (2H, t, $J=7.5$ Hz, HO- $\underline{CH_2}$), 1.74-1.66 (2H, m, $\underline{CH_2}$), 1.56-1.49 (2H, m, $\underline{CH_2}$); ^{13}C NMR (100.6 MHz, CD_3OD) δ 137.1, 131.9, 122.3, 115.6, 103.4, 33.1, 26.9, 26.0; HRMS (ESI): Calculated for $\text{C}_{15}\text{H}_{15}\text{N}_3\text{O}_4\text{Na}$, 324.0960; Found, 432.1014.

4-(1-(7-Hydroxy-coumarin-3-yl)-1H-1,2,3-triazol-4-yl)-propyl α -D-mannopyranoside (α -Man-HTC)(2.12)



A solution of hexynyl mannoside **2.07** (17 mg, 0.06 mmol) and 3-azido-7-hydroxy coumarin (16 mg, 0.05 mmol) in MeOH/ H_2O (1:1) (1 mL) was treated with 1 M aq. CuSO_4 (10 μL) and 1 M aq. NaAsc (25 μL). The reaction mixture was allowed to stir at room temperature for 2 h and concentrated under reduced pressure. The resulting residue was purified by semi-prep TLC ($\text{CH}_2\text{Cl}_2/\text{MeOH}/\text{H}_2\text{O}$, 80:20:3) to give click adduct **2.12** as a yellow amorphous solid (25 mg, 84%). R_f 0.62 ($\text{CH}_2\text{Cl}_2/\text{MeOH}/\text{H}_2\text{O}$, 10:8:2); ^1H NMR: (400 MHz, MeOD) δ 8.23 (1H, s, H-f), 8.17 (1H, s, H-j), 7.36 (1H, d, $J_{c,d}=8.8$ Hz, H-c), 6.60 (1H, dd, $J_{c,d}=8.8$, $J_{d,e}=2.2$ Hz, H-d), 6.46 (d, $J_{d,e}=2.2$ Hz, H-e), 4.64 (1H, d $J_{1,2}=1.5$ Hz, H-1), 3.76-3.67 (3H, m, H-2, H-6a, OCH_aH_b), 3.62-3.59 (2H, m, H-3, H-6b), 3.51-3.35 (3H, m, H-4, H-5, OCH_aH_b), 2.72 (2H, t, $J=7.5$ Hz, $\text{OCH}_2\text{CH}_2\text{CH}_2\text{CH}_2$), 1.78-1.71 (2H, m, $\text{OCH}_2\text{CH}_2\text{CH}_2\text{CH}_2$), 1.65-1.57 (2H, m, $\text{OCH}_2\text{CH}_2\text{CH}_2\text{CH}_2$); ^{13}C NMR; (100.6 MHz, D_2O) δ 159.3, 158.0, 138.5 131.3, 124.2, 119.5, 104.7, 101.4 (C-1), 74.7 (C-5), 72.6 (C-3), 72.3 (C-2), 68.7 (C-4), 68.2 (C-6), 30.0, 27.3, 26.0; HRMS (ESI): Calculated for $\text{C}_{21}\text{H}_{25}\text{N}_3\text{O}_9\text{Na}$, 486.1488; Found, 486.1476.

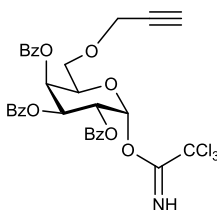
4-(1-(7-Hydroxy-coumarin-3-yl)-1H-1,2,3-triazol-4-yl)-propyl α -D-mannopyranosyl-(1 \rightarrow 6)- α -D-mannopyranoside (α -Man-1,6- α -Man-HTC)(2.13)



A solution of hexynyl disaccharide **2.10** (15 mg, 0.04 mmol) and 3-azido-7-hydroxycoumarin (7.2 mg, 0.04 mmol) in MeOH/H₂O (1:1) (1 mL) was treated with 1 M aq. CuSO₄ (10 μ L) and 1 M aq. NaAsc (25 μ L). The reaction mixture was allowed to stir at room temperature for 2 h and concentrated under reduced pressure. The resulting residue was purified by semi-prep TLC (CH₂Cl₂/MeOH/H₂O, 80:20:3) to give click adduct **2.13** as a yellow amorphous solid (20 mg, 90%). R_f 0.37 (CH₂Cl₂/MeOH/H₂O, 10:8:2); ¹H NMR: (400 MHz, CD₃OD) δ 8.37 (1H, s, H-f), 8.25 (1H, s, H-j), 7.52 (1H, d, $J_{c,d}$ = 8.7 Hz, H-c), 6.78 (1H, dd, $J_{c,d}$ = 8.7, $J_{d,e}$ = 2.3 Hz, H-d), 6.71 (1H, d, $J_{d,e}$ = 2.3 Hz, H-e), 4.72 (1H, d, $J_{1',2'}$ = 1.7 Hz, H-1'), 4.63 (1H, d, $J_{1,2}$ = 1.5 Hz, H-1), 3.81-3.50 (14H, m, H-6a, H-6b, H-2', H-2; H-3, H-3', OCH₂H_b, H-6'a, H-6'b, H-5', H-5, H-4', H-4), 3.41-3.36 (1H, m, OCH₂H_b), 2.73 (2H, t, J = 7.5 Hz, OCH₂CH₂CH₂CH₂), 1.77-1.70 (2H, m, OCH₂CH₂CH₂CH₂), 1.64-1.56 (2H, m, OCH₂CH₂CH₂CH₂); ¹³C NMR: (100.6 MHz, D₂O) δ 157.8, 156.8, 138.6, 131.8, 124.3, 115.9, 103.4, 101.6 (C-1), 101.3 (C-1'), 74.8, 74.4, 73.2, 72.8, 72.6, 72.2, 68.7 (H-4, H-4'), 68.6 (OCH₂H_b), 68.2 (C-6), 67.5, 62.9 (C-6'), 30.0, 27.4, 26.0; HRMS (ESI): Calculated for C₂₇H₃₅N₃O₁₄Na 648.2011; Found, 648.2002.

5.4 Chemical synthesis of azido-alkyne galactose-containing monomer

2,3,4-Tri-O-benzoyl-6-O-(prop-2-ynyl)-1-O-trichloroacetimidoyl- α -D-galactopyranose (4.04)

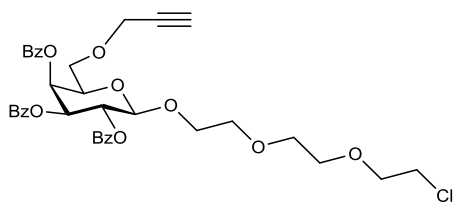


Benzoyl chloride (25 mL, 215 mmol) was added dropwise to a stirred solution of 6-*O*-propargyl galactose **4.01**³² (9.7 g, 43 mmol) in pyridine (95 mL) at 0 °C, the mixture was stirred for 1 h at room temperature and ice-cold water (100 mL) was carefully added. The product was extracted with CH₂Cl₂ (3 x 125 mL), the organic extracts were combined and washed with ice-cold 1M HCl (3 x 100 mL), saturated aqueous NaHCO₃ solution (4 x 100 mL), dried (MgSO₄), filtered and concentrated under reduced pressure. The obtained residue was purified by flash column chromatography (toluene/EtOAc, 7:3) to give compound **4.02** (21.9 g, 81%, mixture of α/β -anomers) as a colourless solid. Benzoate **4.02** (6.6 g, 104 mmol) was dissolved in anhydrous THF (70 mL), 7 N NH₃ in methanol (23 mL) was added, the solution was stirred for 26 h at room temperature and the solvent was removed under reduced pressure. The residue was purified by flash column chromatography (hexane/EtOAc, 7:3) to give compound **4.03** (3.5 g, 64%). Hemiacetal **4.03** (2.8 g, 5.2 mmol) and trichloroacetonitrile (1.9 g, 13.0 mmol) were then dissolved in anhydrous CH₂Cl₂ (10 mL), the solution was cooled to 0 °C and DBU (80 mg, 0.5 mmol) was added. The mixture was allowed to warm to room temperature, stirred for 2 h and concentrated under reduced pressure. The residue was purified by flash column chromatography (hexane/EtOAc, 7:3) to give compound **4.04** (2.9 g, 99 %) as a colourless syrup. R_f 0.55 (hexane/EtOAc, 7:3); $[\alpha]_D + 1.2$ (c 0.6, CHCl₃); δ_H (400 MHz, CDCl₃): 8.61 (1H, s, NH), 8.09-8.07 (2H, m, Ph), 7.96-7.93 (2H, m, Ph), 7.81-7.79 (2H, m, Ph), 7.63 (1H, m, Ph), 7.52-7.24 (8H, m, Ph), 6.88 (1H, d, $J_{1,2}$ =3.6 Hz, H-1), 6.08 (1H, dd, $J_{3,4}$ =3.4 Hz, $J_{4,5}$ =1.3 Hz, H-4), 6.04 (1H, dd, $J_{3,4}$ =3.4 Hz, $J_{2,3}$ =10.6 Hz, H-3), 5.92 (1H, dd, $J_{1,2}$ =3.6 Hz, $J_{2,3}$ =10.6 Hz, H-2), 4.68 (1H, m, H-5), 4.12 (2H, m, CH₂C≡CH), 3.75 (2H, d, J =6.2 Hz, H-6, H-6'), 2.24 (1H, t, J =2.3 Hz, CH₂C≡CH); δ_C (100.6 MHz, CDCl₃) 165.7-165.4, 133.6-133.2, 129.9-128.3, 93.9,

75.3, 70.3, 68.6, 68.1, 67.5, 67.1, 58.7; HRMS (ESI) m/z Calculated for $C_{32}H_{26}Cl_3NO_9Na$, 696.0571; Found: 696.0565.

2-(2-(2-Chloroethoxy)ethoxy)ethyl
galactopyranoside (4.05)

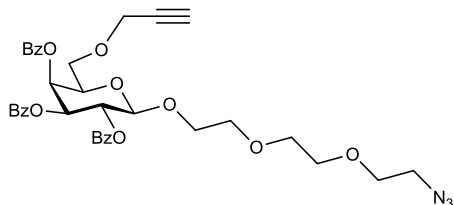
6-O-(prop-2-ynyl)-2,3,4-tri-O-benzoyl- β -D-



To a solution of imidate **4.04** (2.9 g, 5.2 mmol) and 2-(2-(2-chloroethoxy)ethoxy)ethanol (730 mg, 4.3 mmol) in anhydrous CH_2Cl_2 (50 mL) containing 4 Å mol. sieves, at $-30\text{ }^\circ\text{C}$, TMSOTf (90 μL , 0.5 mmol) was gradually added, the reaction mixture was allowed to warm to room temperature and stirred for 3 h. The reaction was quenched by addition of Et_3N (1.0 mL) and concentrated under reduced pressure. The residue was purified by flash chromatography (EtOAc/hexane, 7:3) to give compound **4.05** (2.7 g, 85%) as a colourless solid. R_f 0.17 (EtOAc/hexane, 7:3); $[\alpha]_D + 0.9$ (c 0.7, $CHCl_3$); IR (neat) 2877, 2360, 1725, 1601, 1584, 1451, 1260, 1094, 750 cm^{-1} ; δ_H (400 MHz, $CDCl_3$) 8.09-8.07 (2H, m, Ph), 7.98-7.96 (2H, m, Ph), 7.79-7.77 (2H, m, Ph), 7.61 (1H, m, Ph), 7.53-7.36 (8H, m, Ph), 5.90 (1H, dd, $J_{3,4}=3.5\text{ Hz}$, H-4), 5.75 (1H, dd, $J_{1,2}=8.0\text{ Hz}$; $J_{2,3}=10.5\text{ Hz}$, H-2), 5.56 (1H, dd, $J_{3,4}=3.5\text{ Hz}$; $J_{2,3}=10.5\text{ Hz}$, H-3), 4.90 (1H, d, $J_{1,2}=8.0\text{ Hz}$, H-1), 4.19-4.12 (3H, m, H-5, $CH_2C\equiv CH$), 4.11-4.04 (1H, m, $GalOCH_2$), 3.87-3.81 (1H, m, $GalOCH_2$), 3.76 (2H, m, H-6, H-6'), 3.69-3.60 (4H, m, CH_2), 3.59-3.53 (2H, m, CH_2Cl_2), 3.51-3.47 (2H, m, CH_2), 3.44-3.38 (2H, m, CH_2), 2.30 (1H, t, $J=2.3\text{ Hz}$, $CH_2C\equiv CH$); δ_C (100.6 MHz, $CDCl_3$) δ 165.6-165.2, 133.4-133.2, 130.0-128.3, 101.7, 79.1, 75.0, 72.7, 71.9, 71.3, 70.7, 70.5, 70.4, 69.9, 69.5, 68.5, 67.8, 58.7, 42.7; HR-MS (EI) m/z Calculated for $C_{36}H_{37}ClO_{11}Na$, 703.1922; Found: 703.1917.

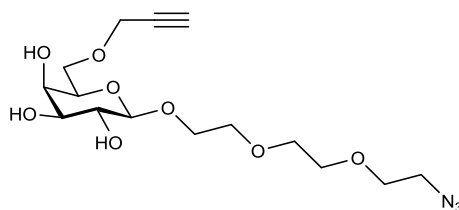
**2-(2-(2-Azidoethoxy)ethoxy)ethyl
galactopyranoside (4.06)**

6-O-(prop-2-ynyl)-2,3,4-tri-O-benzoyl- β -D-



To a solution of chloro- β -galactoside **4.05** (5.2 g, 7.6 mmol) in DMF (50 mL) NaN₃ (2.5 g, 38.0 mmol) and NaI (1.1 g, 8.0 mmol) were added and the reaction mixture was stirred at 70 °C for 28 h. The reaction mixture was diluted with water (20 mL) and extracted with CH₂Cl₂ (3 x 30 mL). The resulting organic extracts were dried (MgSO₄), and concentrated under reduced pressure to give compound **4.06** (5.0 g, 97%) as a colourless syrup. R_f 0.17 (hexane/EtOAc, 7:3); $[\alpha]_D + 0.9$ (c 0.7, CHCl₃); IR (neat) 2874, 2359, 2107, 1724, 1601, 1584, 1451, 1259, 1094, 752 cm⁻¹; δ_H (400 MHz, CDCl₃) 8.09-8.07 (2H, m, Ph), 7.98-7.96 (2H, m, Ph), 7.79-7.77 (2H, m, Ph), 7.61 (1H, m, Ph), 7.53-7.36 (8H, m, Ph), 5.90 (1H, dd, $J_{3,4}$ =3.5 Hz, H-4), 5.75 (1H, dd, $J_{1,2}$ =8.0 Hz; $J_{2,3}$ =10.5 Hz, H-2), 5.56 (1H, dd, $J_{3,4}$ =3.5 Hz; $J_{2,3}$ =10.5 Hz, H-3), 4.90 (1H, d, $J_{1,2}$ =8.0 Hz, H-1), 4.19-4.12 (3H, m, H-5, CH₂C≡CH), 4.11-4.04 (1H, m, GalOCH₂), 3.87-3.81 (1H, m, GalOCH₂), 3.76 (2H, m, H-6, H-6'), 3.69-3.59 (2H, m, CH₂), 3.57-3.52 (2H, m, CH₂), 3.52-3.46 (2H, m, CH₂), 3.44-3.37 (2H, m, CH₂), 3.51-3.29 (2H, m, CH₂N₃), 2.30 (1H, t, J =2.3 Hz, CH₂C≡CH); δ_C (100.6 MHz, CDCl₃) 165.6-165.2, 133.4-133.2, 130.0-128.3, 101.5, 79.1, 75.0, 72.7, 71.9, 71.3, 70.7, 70.5, 70.4, 69.95, 69.9, 69.5, 68.5, 67.8, 58.7, 50.6; HRMS (ESI) m/z Calculated for C₃₆H₃₇N₃O₁₁Na, 710.2326; Found: 710.2320.

2-(2-(2-Azidoethoxy)ethoxy)ethyl 6-O-(prop-2-ynyl)- β -D-galactopyranoside (4.07)



A solution of azido- β -galactoside compound **4.06** (2.4 g, 3.48 mmol) in absolute MeOH (20 mL) was treated with 0.5 M NaOMe in MeOH (2.7 mL, 1.39 mmol), the solution was kept at room temperature for 1 h, neutralized with dry ice, concentrated under reduced pressure and purified by flash chromatography (CH₂Cl₂-MeOH, 9:1) to give compound **4.07** (1.2 g, 91%) as a colourless syrup. R_f 0.89 (CH₃CN/EtOAc/*i*PrOH/H₂O, 85:20:50:50); $[\alpha]_D$ -1.6 (*c* 1.3, MeOH); δ_H (600 MHz, Methanol-*d*₄) 4.16 (1H, d, $J_{1,2}$ =7.6 Hz, H-1), 4.11 (2H, d, J =2.4 Hz, CH₂C≡CH), 3.94-3.84 (1H, m, H-6a), 3.69 (1H, dd, $J_{3,4}$ =3.4 Hz, $J_{4,5}$ =1.1 Hz, H-4), 3.67-3.54 (12H, m, H-5, H-6b, 5 x CH₂), 3.43 (1H, dd, $J_{1,2}$ =7.6 Hz, $J_{2,3}$ =9.7 Hz, H-2), 3.37 (1H, dd, $J_{2,3}$ =9.7 Hz, $J_{3,4}$ =3.4 Hz, H-3), 3.28 (2H, t, J =5.0 Hz, CH₂N₃), 2.76 (1H, t, J =2.4 Hz, CH₂C≡CH); δ_C (100.6 MHz, D₂O) 105.0, 80.6, 76.0, 75.0, 74.7, 72.5, 71.6 (2C), 71.4, 71.1, 70.4, 70.3, 69.7, 59.3, 51.8; HRMS (ESI) m/z Calculated for C₁₅H₂₅N₃O₈Na, 398.1539; Found: 398.1534.

5.5 Cu(I)-catalysed oligomerisation of azido-alkyne galactose-containing monomer

5.5.1 General procedure for catalysed cyclisation and oligomerisation

A solution of azido-alkyne monomer **4.07** (100 mg, 0.3 mmol) containing Cu turnings (260 mg, 4.1 mmol) and CuSO₄ (11 mg, 0.1 mmol) in DMF (0.27 mL) was placed into a sealed microwave tube. The tube was either submitted to microwave irradiation at 110 °C at 50 W magnetron power (*Method A*) or stirred at room temperature for 2 days (*Method B*). The reaction progress was followed by the TLC (solvent mixture F) taking samples at 15 min intervals (*Method A*) or 24 h intervals (*Method B*). After completion

the reaction mixtures were separated from Cu turnings and the solvent was removed by repeated evaporation with toluene under reduced pressure.

Cyclic monomer 4.08

HPLC retention time 16.3 min; yield 9.0 mg (9.0%) (*Method A*), 6.7 mg (6.7%) (*Method B*); δ_{H} (400 MHz, D₂O) 8.15 (1H, s, CH triazole), 4.93 (1H, d, $J=13.4$ Hz, CH_{2a}-triazole), 4.71-4.61 (3H, m, CH_{2b}-triazole, CH₂N), 4.38 (1H, d, $J_{1,2}=7.9$ Hz, H-1), 4.02-3.94 (3H, m, OCH₂CH₂N, H-6a), 3.91 (1H, d, $J_{3,4}=3.5$ Hz, H-4), 3.90-3.66 (10H, m, CH₂, H-5, H-6b), 3.64 (1H, dd, $J_{2,3}=9.7$ Hz; $J_{3,4}=3.5$ Hz, H-3), 3.50 (1H, dd, $J_{1,2}=7.9$ Hz; $J_{2,3}=9.7$ Hz, H-2); δ_{C} (100.6 MHz, D₂O) 143.6, 126.2, 102.2, 74.2, 72.7, 70.6, 69.6, 69.4, 69.4, 69.1, 68.9, 68.5, 62.4, 49.7; HR-MS (EI) m/z Calculated for C₁₅H₂₆N₃O₈, 376.1714; Found 376.1710.

Cyclic dimer 4.09

HPLC retention time 21.3 min; yield 3.0 mg (3.0%) (*Method A*), 2.2 mg (2.2%) (*Method B*); δ_{H} (400 MHz, D₂O) 8.12 (2H, s, CH triazole), 4.74 (4H, m, CH₂-triazole), 4.65 (4H, m, CH₂N), 4.38 (2H, d, $J_{1,2}=7.9$ Hz, H-1), 4.02-3.92 (6H, m, OCH₂CH₂N, H-6a), 3.91 (2H, d, $J_{3,4}=3.6$ Hz, H-4), 3.86-3.70 (8H, m, CH₂, H-5, H-6b), 3.69-3.57 (14H, m, CH₂, H-3), 3.53 (2H, dd, $J_{1,2}=7.9$ Hz, $J_{2,3}=9.9$ Hz, H-2); δ_{C} (100.6 MHz, D₂O) 143.7, 125.6, 102.8, 73.5, 72.6, 70.6, 69.6, 69.4, 68.9, 68.7, 68.6, 63.4, 50.1; HRMS (ESI) m/z Calculated for C₃₀H₅₁N₆O₁₆, 751.3357; Found: 751.3334.

Cyclic trimer 4.10

HPLC retention time 23.9 min; yield 1.6 mg (1.6%) (*Method A*), 1.0 mg (1.0%) (*Method B*); δ_{H} (400 MHz, D₂O) 8.10 (3H, s, CH triazole), 4.72 (6H, m, CH₂-triazole), 4.63 (6H, m, CH₂N), 4.39 (3H, d, $J_{1,2}=7.8$ Hz, H-1), 4.00-3.93 (9H, m, OCH₂CH₂N, H-6a), 3.90 (3H, d, $J_{3,4}=3.4$ Hz, H-4), 3.85-3.73 (12H, m, CH₂, H-5, H-6b), 3.70-3.58 (21H, m, CH₂, H-3), 3.53 (3H, dd, $J_{1,2}=7.9$ Hz, $J_{2,3}=9.9$ Hz, H-2); δ_{C} (100.6 MHz, D₂O) 143.8, 125.5, 102.8, 73.5, 72.6, 70.6, 69.7, 69.6 (2C), 69.4, 68.9, 68.7, 63.4, 50.0; HRMS (ESI) m/z Calculated for C₄₅H₇₆N₉O₂₄, 1126.4998; Found: 1126.4961.

Cyclic tetramer 4.11

HPLC retention time 25.5 min; yield 1.1 mg (1.1%) (*Method A*), 0.8 mg (0.8%) (*Method B*); δ_{H} (400 MHz, D₂O) 8.10 (4H, s, CH triazole), 4.72 (8H, m, CH₂-triazole),

4.63 (8H, m, CH₂N), 4.39 (4H, d, $J_{1,2}=7.8$ Hz, H-1), 4.00-3.93 (12H, m, OCH₂CH₂N, H-6a), 3.90 (4H, d, $J_{3,4}=3.4$ Hz, H-4), 3.85-3.73 (16H, m, CH₂, H-5, H-6b), 3.70-3.58 (28H, m, CH₂, H-3), 3.53 (4H, dd, $J_{1,2}=7.9$ Hz, $J_{2,3}=9.9$ Hz, H-2); δ_C (100.6 MHz, D₂O) 143.8, 125.5, 102.8, 73.5, 72.6, 70.6, 69.7, 69.6, 69.5, 69.4, 68.9, 68.7, 63.4, 50.0; HRMS (ESI) m/z Calculated for C₆₀H₁₀₁N₁₂O₃₂, 1501.664; Found: 1501.6511.

Cyclic pentamer 4.12

HPLC retention time 26.5 min; yield 1.3 mg (1.3%) (*Method A*), 0.6 mg (0.6%) (*Method B*); δ_H (400 MHz, D₂O) 8.10 (5H, s, CH triazole), 4.71 (10H, m, CH₂-triazole), 4.63 (10H, m, CH₂N), 4.39 (5H, d, $J_{1,2}=7.9$ Hz, H-1), 4.01-3.94 (15H, m, OCH₂CH₂N, H-6a), 3.90 (5H, d, $J_{3,4}=3.4$ Hz, H-4), 3.85-3.73 (20H, m, CH₂, H-5, H-6b), 3.70-3.58 (35H, m, CH₂, H-3), 3.53 (5H, dd, $J_{1,2}=7.9$ Hz, $J_{2,3}=9.9$ Hz, H-2); δ_C (100.6 MHz, D₂O) 143.8, 125.5, 102.8, 73.5, 72.6, 70.6, 69.6, 69.6, 69.5, 69.4, 68.9, 68.7(2 C), 63.4, 50.0; HRMS (ESI) m/z Calculated for C₇₅H₁₂₆N₁₅O₄₀, 1876.8281; Found: 1876.8248.

Cyclic hexamer 4.13

HPLC retention time 27.2 min; 0.5 mg (0.5%) (*Method B*); δ_H (400 MHz, D₂O) 8.11 (6H, s, CH triazole), 4.72 (12H, m, CH₂-triazole), 4.67-4.62 (12H, m, CH₂N), 4.39 (6H, d, $J_{1,2}=7.8$ Hz, H-1), 4.01-3.96 (18H, m, OCH₂CH₂N, H-6a), 3.90 (6H, d, $J_{3,4}=2.8$ Hz, H-4), 3.87-3.71 (24H, m, CH₂, H-5, H-6b), 3.70-3.59 (42H, m, CH₂, H-3), 3.53 (6H, dd, $J_{1,2}=7.9$ Hz, $J_{2,3}=9.8$ Hz, H-2); δ_C (100.6 MHz, D₂O) 102.8, 73.4, 72.5, 70.6, 69.5, 69.3, 68.8, 68.7, 63.4, 50.0; HRMS (ESI) m/z Calculated for C₉₀H₁₅₁N₁₈O₄₈, 2251.9923; Found: 2251.9792.

Cyclic oligomers (DP>6)

HPLC retention time min 28 to 30 min; yield 13.7 mg (13.7%) (*Method A*), 6.0 mg (6.0%) (*Method B*).

Linear oligomers

HPLC retention time 32.0 min; yield 25.8 mg (25.8%) (*Method A*), 35.7 mg (35.7%) (*Method B*); HRMS (ESI) m/z Calculated for ([M+H]⁺): 376.1751, 751.3357, 1126.4998, 1501.6640, 1876.8281, 2251.9923; Found: 376.1708; 751.3351; 1126.4985; 1501.6631; 1876.8273; 2251.9897.

5.6 Uncatalysed oligomerisation of azido-alkyne galactose-containing monomer

5.6.1 General procedure for uncatalysed cyclisation and oligomerisation

A solution of compound **4.07** (100 mg, 0.3 mmol) was placed into a sealed microwave tube. The tube was either submitted to microwave irradiation at 110 °C at 50 W magnetron power (*Method C*) or stirred at room temperature (*Method D*). The reaction progress was followed by TLC (solvent mixture F) taking samples at 15 min intervals (*Method C*). After 30 min the solvent was removed by repeated evaporation with toluene under reduced pressure.

Linear dimer (4.14)

HPLC retention time 32.0 min; yield 1.2 mg (1.2%); δ_{H} (400 MHz, D₂O) 8.02 (s, 1H), 4.60 - 4.52 (2H, m, CH₂-triazole), 4.36 - 4.27 (2 H, m, H-1, H-1'), 4.23-4.14 (2 H, m, CH₂C≡CH), 3.98-3.87 (4H, m, OCH₂CH₂N), 3.84-3.81 (2H, m, H-4), 3.78-3.52 (26H, m, CH₂, H-6, H', H5, H-3), 3.47-3.41 (4 H, m, H-2, CH₂N₃); δ_{C} (100.6 MHz, D₂O) 102.7, 76.9, 73.4, 72.5, 70.5, 68.7, 68.5, 63.3, 58.1, 50.0, 49.9.

Cyclic monomer (4.24)

HPLC retention time 14.9 min; yield 8.7 mg (8.7%); δ_{H} (400 MHz, D₂O) 7.88 (1H, s, CH triazole), 4.92-4.83 (2H, m, CH₂-triazole), 4.72-4.56 (2H, m, CH₂N), 4.42 (1H, d, $J_{1,2}=7.9$ Hz, H-1), 4.06-4.02 (2H, m, OCH₂CH₂N), 3.97-3.82 (6H, m, CH₂, H-4, H-5, H-6), 3.74-3.57 (7H, m, CH₂, H-3), 3.53 (1H, dd, $J_{1,2}=7.9$ Hz; $J_{2,3}=9.9$ Hz, H-2); δ_{C} (100.6 MHz, D₂O) 140.5, 102.2, 74.4, 72.7, 71.1, 70.6, 70.3, 69.7, 69.5, 69.3, 68.8, 61.2, 48.5; HRMS (ESI) m/z . Calculated for C₁₅H₂₆N₃O₈, 376.1751; Found: 376.1701.

Linear dimer (4.25)

HPLC retention time 32.0 min; yield 1.5 mg (1.5%); δ_{H} (400 MHz, D₂O) 7.77 (1H, s, CH triazole), 4.60 - 4.54 (2H, m, CH₂N), 4.35 - 4.29 (2 H, m, H-1, H-1'), 4.23-4.14 (2 H, m, CH₂C≡CH), 3.97-3.88 (4H, m, OCH₂CH₂N), 3.84-3.81 (2H, m, H-4), 3.78-3.52 (26H, m, CH₂, H-6, H', H5, H-3), 3.47-3.41 (4 H, m, H-2, CH₂N₃); δ_{C} (100.6 MHz, D₂O) 102.7, 73.1, 72.4, 70.6, 68.7, 68.6, 60.3, 58.1, 50.0, 48.1.

5.7 Biological methods

5.7.1 General experimental section

Mycobacterium smegmatis and *Trypanosoma bruce* membranes were kindly donated by Professor Besra's group (Birmingham) and Professor Ferguson's group (Dundee), respectively. *Euglena gracilis* var *saccharophila* Klebs (strain 1224/7a) culture was obtained from the Culture Collection of Alga and Protozoa (CCAP). All reagents used were of analytical grade and all solvents were HPLC grade. In fluorescence-based assays concentrations for buffer, acceptors and donors are stated as a total concentration used in enzymatic reactions. Stated concentration in each fluorescence-based assays is final concentration in solution.

Thin layer chromatography (TLC)

TLC separations were performed at room temperature on aluminium-backed silica gel 60 F₂₅₄ or glass plated silica gel 60Å TLC plates. Samples of reaction mixtures were applied onto the TLC plate in 2 µL aliquots and dried with a hairdryer between applications. The TLC plates were eluted with the stated eluent system (Table 1), air dried and directly visualised with the gel imager (Synoptics 2.0 MP) and processed with the GENE SYS ver 1.2.5.0 program or sprayed with cyclooctyne/EtOH (v/v 1:1), heated and then visualised with the gel imager.

A	CH ₂ Cl ₂ /MeOH	9:1
B	CH ₂ Cl ₂ /MeOH/H ₂ O	80:20:3
C	CH ₂ Cl ₂ /MeOH/H ₂ O	6:4:1
D	CHCl ₃ /MeOH/H ₂ O	10:6:1
E	CHCl ₃ /MeOH/H ₂ O	10:8:1
F	CH ₃ CN/EtOAc/iPrOH/H ₂ O	85:20:50:50

Table 5.1 Solvents mixtures used for TLC elution.

High performance liquid chromatography (HPLC)

HPLC was carried out using a Dionex HPLC system with reverse phase (C18 stationary phase) column, equipped with Corona charged aerosol detector (CAD) or UV detector (347 nm) at the flow rate of 5 mL/min.. Obtained fractions were collected using

Teledyne ISCO fraction collector. Fractions containing pure product were collected and concentrated using freeze drying.

Purification of fluorescent products under HILIC conditions

Fluorescent products (**2.16** and **2.17**) were redissolved in water and subjected to purification using semi-prep normal phase HPLC Phenomenex Luna NH₂ (250 x 10 mm). The column was pre-conditioned with 0.1% aqueous solution of TFA 90% acetonitrile. The elution program was as follows: linear gradient to 10% acetonitrile for 32 min (held at 10% for 12 min) then equilibrated back to 0.1% aqueous solution of TFA, 90% acetonitrile.

Purification of fluorescent products under reverse phase conditions

Products obtained from fluorescent assays were purified from starting fluorescent acceptor by reverse phase HPLC on the C18 reverse phase column (Phenomenex Luna C18(2) 100 A, 250 x 10 mm). The column was pre-conditioned with 0.1% aqueous solution of TFA, 10% acetonitrile. The elution program was as follows: linear gradient to 90% acetonitrile for 36 min (held at 90% for 12 min) then equilibrated back to 0.1% aqueous solution of TFA, 10% acetonitrile.

Liquid Chromatography Mass Spectrometry (LC-MS)

LC-MS was carried out using Thermo Finnigan Surveyour HPLC system with either reverse phase (C18) or normal phase (NH₂) columns equipped with UV detector and LCQ Deca XP plus (ion trap) MS detector as well as Acquity UPLC equipped with Waters Synapt G2-S MS detector and T-wave ion mobility for IM-MS.

Mass spectrometry (MS)

High resolution ESI MS and IM-MS data were obtained using the Waters Synapt G2 and Water Synapt G2-S MS detector coupled to T-wave ion mobility.

Nuclear magnetic resonance spectroscopy (NMR)

Nuclear magnetic resonance spectra were recorded on a Bruker Avance 800 spectrometer at 298 K. Chemical shifts (δ) are reported in parts per million (ppm) with respect to internal tetramethylsilane (TMS) in CDCl_3 and residual HOD signal in D_2O . NMR signal assignments were made with the aid of COSY, HSQC and HMBC experiments.

Exo-glycosidase digestions

Jack bean α -mannosidase and green coffee beans α -galactosidase were obtained from Sigma Aldrich, β -galactosidase from Calbiochem, *Xanthomonas manihotis* α -1,6-mannosidase from New England Biolabs and *Aspergillus saitoi* α -1,2-mannosidase from Prozyme.

Green coffee bean α -galactosidase

Fluorescent products (**2.20a** and **2.20b**) (30 μM) were redissolved in 50 mM phosphate buffer (pH 7.3) containing 10 mM of MgCl_2 and the reaction mixture was incubated at 37 °C for 24 h with and without 0.7 U of green coffee bean α -galactosidases (10 μL final volume). After incubation, reactions were terminated by addition of 10 μL of MeOH.

Escherichia coli β -galactosidase

Fluorescent products (**2.20a** and **2.20b**) (30 μM) were redissolved in 50 mM phosphate buffer (pH 6.5) and the reaction mixture was incubated at 21 °C for 24 h with and without 0.9 U of *E.coli* β -galactosidase (10 μL final volume). After incubation, reactions were terminated by addition of 10 μL of MeOH.

Jack bean α -mannosidase

Purified fluorescent mannosylated products (**3.01** and **3.02**) (30 μM) were redissolved in 0.1 M sodium acetate buffer (pH 5.0) and incubated at 37 °C for 24 h with and without 0.75 U of jack bean α -mannosidase (30 μL final volume). After incubation, reactions were terminated by boiling for 5 min.

***Xanthomonas manihotis* α -1,6-mannosidase**

Purified fluorescent mannosylated products Fluorescent (**2.16/2.17**) and (**3.01/3.02**) (30 μ M) were redissolved in GlycoBuffer 1 (5 mM CaCl₂, 50 mM sodium acetate, pH 5.5), supplemented with 100 μ g/mL of BSA and incubated at 37 °C for 24 h with and without 80 mU of *Xanthomonas manihotis* α -1,6-mannosidase (30 μ L final volume). After incubation, reactions were terminated by boiling for 5 min.

***Aspergillus saitoi* α -1,2-mannosidase**

Purified fluorescent mannosylated products (**3.01** and **3.02**) (30 μ M) were redissolved in reaction buffer (pH 5.0) and incubated at 37°C for 24 h with and without 80 mU of *Aspergillus saitoi* α -1,2-mannosidase from Prozyme (10 μ L final volume). After incubation, reactions were terminated by boiling for 5 min.

***Xanthomonas manihotis* α -1,2/3-mannosidase**

Purified fluorescent mannosylated products (**3.01** and **3.02**) (30 μ M) were redissolved in GlycoBuffer 1 (5 mM CaCl₂, 50 mM sodium acetate, pH 5.5), supplemented with 100 μ g/mL of BSA and incubated at 37 °C for 24 h with and without 64 mU of *Xanthomonas manihotis* α -1,2/3-mannosidase (30 μ L final volume). After incubation, reactions were terminated by boiling for 5 min.

Alkaline phosphatase digestion

To purified fluorescent product (**3.04/3.05** and **3.07/3.08**) (80 μ M, 10 μ L) were digested with 1 U of alkaline phosphatase in reaction buffer (50 mM, pH 8.0 Tris/HCl). The enzymatic reaction was mixed and incubated at 25 °C for 20 h in 20 μ L of final volume. After incubation, reactions were terminated by boiling for 5 min.

Trifluoroacetic acid and alkaline phosphatase degradation

Purified fluorescent product (**3.04/3.05** and **3.07/3.08**) (60 μ M, 10 μ L) was treated with 40 mM of trifluoroacetic for 15 min at 100 °C. After drying, the sample was dissolved in 10 μ L of water and digested with 1 U of alkaline phosphatase in reaction buffer (50 mM, pH 8.0 Tris/HCl). The enzymatic reaction was incubated at 25 °C for 20 h in 20 μ L of final volume. After incubation reactions were terminated by boiling for 5 min.

Determination of total microsomal membrane proteins concentration

Total protein concentration was determined using a commercially available Bradford test.²²⁸ In this test a standard solution of BSA (2mg/mL) was diluted to produce a series of known concentrations (from 0.1 to 1.5 mg/mL). To each known concentration of BSA standard solution a BradfordUltra reagent was added (1:15 v/v). The absorption of standard BSA solutions was measured at 595 nm to produce a standard curve. The unknown protein solution was diluted in order to fall within the linear range of known concentration of standard BSA solutions, the absorption was measured and the concentration of protein extrapolated from the standard curve.

5.8 *Mycobacterium smegmatis*

5.8.1 Fluorescence-based assays to probe mannosyltransferase activities in *Mycobacterium smegmatis*

Buffers and incubation conditions from previously established cell-free radiolabelled assay were used to probe α -1,6-mannosyltransferase activities in both fluorescence-based methodologies.⁸⁷

Fluorescence-based methodology I

In the fluorescence-based assay 50 μ L acceptor (**2.04** and **2.05**) (0.5 mM) was incubated with 50 μ L of GDP-Man (1 mM) in 50 μ L of reaction buffer (50 mM, pH 7.9 MOPS/KOH, 10 mM MgCl₂, 5 mM DTT). The reaction was initiated by the addition of 50 μ L of mycobacterial membranes (500 μ g of proteins) in a total volume of 200 μ L. Aliquots of 20 μ L at 20 min, 40 min, 60 min, 2 h, 4 h and 18 h were taken and each aliquot was stopped by addition of 20 μ L of CHCl₃/MeOH (1:1, v/v). After incubation for 18 h at 37 °C the main reaction was stopped with CHCl₃/MeOH (1:1, v/v) (80 μ L). The resulting denatured mycobacterial membranes were removed by several centrifugations (16000 g for 5 min) and washed with CHCl₃/MeOH:H₂O (10:6:1) (3 x 100 μ L). The washings were combined and solvents dried under gentle stream of air. The residue was re-dissolved in deionised water and passed through a 0.45 μ m PPTE filter, the filtrate was collected and the sample was freeze dried.

Fluorescence-based methodology II

In the fluorescence-based assay 250 μL acceptor (**2.10** and **2.13**) (1 mM) was incubated with 250 μL of GDP-Man (2 mM) in 250 μL of reaction buffer (50 mM, pH 7.9 MOPS/KOH, 10 mM MgCl_2 , 5 mM DTT). The reaction was initiated by the addition of 250 μL of mycobacterial membranes (4000 μg of protein) in a total volume of 200 μL . Aliquots of 20 μL at 2 h, 4 h, 6 h, and 29 h were taken and each aliquotes was stopped by addition of 20 μL of $\text{CHCl}_3/\text{MeOH}$ (1:1, v/v). After incubation for 29 h at 37 °C the main reaction was stopped with $\text{CHCl}_3/\text{MeOH}$ (1:1, v/v) (80 μL). The denatured mycobacterial membranes were removed by several centrifugations (16000 g for 5 min) and washed with $\text{CHCl}_3/\text{MeOH}:\text{H}_2\text{O}$ (10:6:1) (3 x 100 μL). The washings were combined and solvents dried under gentle stream of air. The residue was re-dissolved in deionised water and passed through a 0.45 μm PPTE filter, the filtrate was collected and the sample was freeze dried.

5.9 *Trypanosoma brucei*

5.9.1 Fluorescence-based assays to probe galactosyltransferase activities in *Trypanosoma brucei*

Buffers and incubation conditions from previously established cell-free radiolabelled assay were used to probe galactosyltransferase activities in fluorescence-based methodology II.¹⁴⁰

In the fluorescence-based assay *T. brucei* microsomal membranes were centrifuged (12000 rpm for 2 min) and resuspended in reaction buffer (100 mM, pH 7.4 HEPES/KOH, 50 mM KCl, 10 mM $\text{MgCl}_2/\text{MnCl}_2$, 2 mM ATP, 2 mM dithiothreitol, 2 mg/mL leupeptin, 2.5 $\mu\text{g}/\text{mL}$ tunicamycin, 0.2 mM *N*-tosyl-L-lysine chloromethyl ketone, 0.05% Triton X-100). Subsequently, 25 μL of UDP-Gal donor (1 mM) and 25 μL of acceptor (**2.10** and **2.13**) (1 mM) were dried and resuspended in 50 μL of reaction buffer. The reactions were initiated by the addition of 50 μL of *T. brucei* microsomal membranes (10×10^7 cells) in a total volume of 100 μL . Aliquots of 20 μL at 2 h, 6 h, and 24 h were taken and each reaction was stopped by addition of 20 μL of $\text{CHCl}_3/\text{MeOH}$ (1:1, v/v). After incubation for 24 h at 30 °C the main reaction was stopped with $\text{CHCl}_3/\text{MeOH}$ (1:1, v/v) (40 μL). The resulting denatured *T. brucei*

microsomal membranes were removed by several centrifugations (16000 g for 5 min) and washed with $\text{CHCl}_3/\text{MeOH}:\text{H}_2\text{O}$ (10:6:1) (3 x 50 μL). The washings were combined and solvents dried under gentle stream of air. The residue was re-dissolved in deionised water and passed through a 0.45 μm PPTE filter, the filtrate was collected and the sample was freeze dried.

Increasing enzyme concentration

The fluorescence assay was performed as described above where enzymatic reactions were initiated by the addition of 50 μL of *T. brucei* microsomal membranes (5×10^8 cells) in total volume of 100 μL .

Increasing donor concentration

The fluorescence assay was performed as described above where after incubation, at 30 °C, 10 μL aliquots were taken at 4h, 8h, 12h, 24h and 36h and supplemented with 5 μL of UDP-Gal donor (4 mM).

5.10 *Euglena gracilis*

5.10.1 Preparation of *Euglena gracilis* cells

A culture of axenic *Euglena gracilis* was grown in the dark at 30 °C, with shaking (200 rpm), in modified *Euglena gracilis* plus Jaworski's medium (1xEG + 1xJM medium) supplemented with glucose (15 g/L) for 7 days. Dark grown culture after seven days was harvested by centrifugation (800 g for 5 min), washed twice with deionised water and once in HEPES buffer (10 mM, pH 7.0 HEPES/KOH, 25 mM KCl). The harvested cells were re-suspended in HEPES buffer and de-flagellated by the method of cold-shock²²⁹ that required incubation of cells on ice for 2 h. The de-flagellated cells were removed by centrifugation (800 g for 5 min) for further isolation of microsomal membranes.

5.10.2 Isolation of microsomal membranes from *Euglena gracilis*¹⁶¹

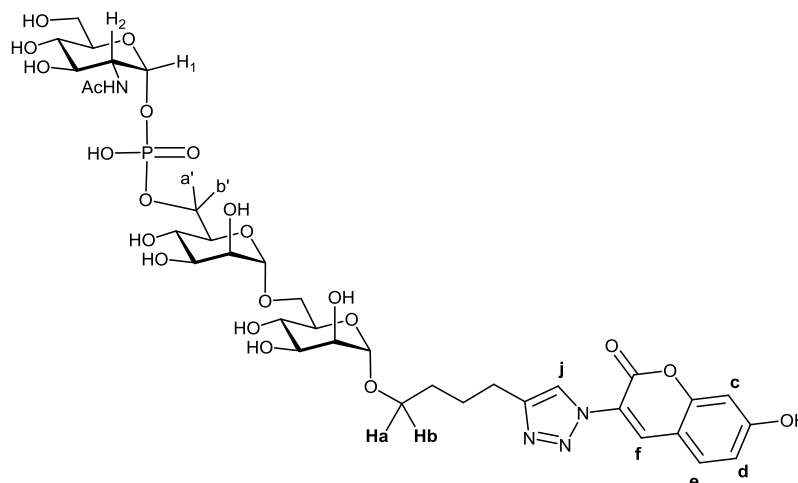
All isolation steps described were carried out at 0 to 4 °C. Dark-grown de-flagellated cells were re-suspended in Euglena lysis buffer [20 mM, pH 7.0 HEPES/KOH, 50 mM NaCl, protease inhibitor (1 tablet per 100 mL) and ribonuclease A (1 mg)] and disrupted by three 15 s bursts of ultrasonic waves (1 s ON, 3 s OFF) over three consecutive cycles. Residual cell debris (un-lysed cells, large pellicle fragments and paramylon) were removed by centrifugation (300 g for 3 min) and supernatant was centrifuged at 4200 g for 30 min to remove mitochondria. The supernatant was layered onto a 1.5 M sucrose cushion in 20 mM HEPES buffer (pH 7.0) and centrifuged at 15000 g for 45 min. The supernatant was removed and layered over a step gradient consisted of 1.3 M, 1.0 M, 0.8 M and 0.5 M sucrose in 20 mM HEPES buffer (pH 7.0). The separation of microsomal fraction was achieved by centrifugation at 150000 g for 3 h. Microsomal-enriched fractions were collected, re-suspended in 20 mM HEPES buffer (pH 7.0) and centrifuged at 150000 g for 2 h. The pellets were re-homogenised in 20 mM HEPES buffer (pH 7.0) and stored at -80 °C. *Euglena* membranes remained active for up to a year.

5.10.3 Fluorescence-based assays to probe glycosyltransferase activities in *Euglena gracilis*

In each fluorescence-based assay 4 mM donor (GDP-Man/GDP-Fuc/UDP-Glc/UDP-Gal/UDP-GlcNAc) and 2 mM acceptor (**2.10** and **2.13**) were freeze dried and re-dissolved in 50 µL reaction buffer (40 mM, pH 7.0 HEPES/KOH, 100 mM KCl, 40 mM MgCl₂/MnCl₂, 40% glycerol). The reactions were initiated by the addition of 150 µL of freshly thawed *E. gracilis* microsomal membranes (195 µg of membrane protein). Control assays without donor were also performed in parallel to correct for the presence of endogenous acceptors. After incubation for 24 h at 30 °C reactions were stopped by addition of CHCl₃/MeOH (1:1, v/v). The resulting denatured *E. gracilis* microsomal membranes were removed by several centrifugations (16000 g for 5 min) and washed with CHCl₃/MeOH:H₂O (10:6:1). The washings were combined and solvents dried under gentle stream of air. The residue was re-dissolved in deionised water and passed through a 0.45 µm PPTE filter, the filtrate was collected and the sample was freeze dried.

5.10.4 Generation of product carrying *N*-acetylglucosamine-6-Phosphate motif for structural characterisation

4-(1-(7-Hydroxy-coumarin-3-yl)-1H-1,2,3-triazol-4-yl)-propyl 6-(2-acetamido-2-deoxy- α -D-glucopyranosyl)-phosphonato-1- α -D-mannopyranosyl-(1 \rightarrow 6)- α -D-mannopyranoside (**3.08**)



A large scale reaction was performed to generate sufficient material for structural characterisation by NMR spectroscopy. In this reaction acceptor (**2.13**) (0.8 mg, 1.28 μ mol) and donor (UDP-GlcNAc) (3.2 mg, 4.9 μ mol) were dissolved in 150 μ L of reaction buffer (40 mM, pH 7.0 HEPES/KOH, 100 mM KCl, 40 mM MgCl₂/MnCl₂, 40% glycerol). The reactions were initiated by the addition of 450 μ L of *E. gracilis* microsomal membranes (585 μ g membrane proteins) in a total volume of 600 μ L. After incubation for 24 h at 30 °C the reaction was supplemented with another portion of *E. gracilis* microsomal membranes (150 μ L, 195 μ g of membrane proteins) and incubated for a further 24 h at 30 °C. The reaction was stopped by addition of CHCl₃/MeOH (1 mL). The denatured *E. gracilis* microsomal membranes were removed by several centrifugations (14000 rpm for 5 min) and washed with CHCl₃/MeOH:H₂O (10:6:1) (3 x 1 mL). The washings were combined and solvents dried under gentle stream of air. The residue was re-dissolved in deionised water and passed through 0.45 μ m PPTe filter, the filtrate was collected and the sample was freeze dried. The residue was purified by reverse phase HPLC to give compound **3.08** (0.48 mg, 43%). ¹H NMR (800 MHz, D₂O) δ 8.43 (1H, s, H-f), 8.26 (1H, s, H-j), 7.73 (1H, d, $J_{c,d}$ = 8.6 Hz, H-c), 7.06 (1H, dd, $J_{c,d}$ = 8.6, $J_{d,e}$ = 2.2 Hz, H-d), 7.01 (bd, H-e), 5.48 (1H, dd $J_{1,2}$ = 3.6 Hz, $J_{1,p}$ = 7.2

Hz, H-1), 4.13 (2H, m, H-6a' and H-6b'), 3.95 (4H, m, H-2'', H-6a, H-6b, H-2'), 3.83-3.54 (m, sugar signals, OCH_aH_b , OCH_aH_b), 2.86 (2H, t, $J_{\text{H-H}}=7.2$ Hz, $\text{OCH}_2\text{CH}_2\text{CH}_2\text{CH}_2$), 2.07 (3H, s, CH_3), 1.87-1.78 (2H, m, $\text{OCH}_2\text{CH}_2\text{CH}_2\text{CH}_2$), 1.72-1.70 (2H, m, $\text{OCH}_2\text{CH}_2\text{CH}_2\text{CH}_2$); ^{32}P NMR; (100.6 MHz, D_2O) δ 1.23; HRMS (ESI): Calculated for $\text{C}_{35}\text{H}_{50}\text{N}_4\text{O}_{22}$, 909.2649; Found, 909.2653.

5.11 *Trypanosoma cruzi*

5.11.1 *Trans*-sialidase-mediated sialylation of triazole-linked pseudo-galactooligomers

To a solution of fetuin⁴² as a donor substrate (25 μL , 3 mM in 0.1 mM phosphate buffer pH 7.0) and oligo-triazole acceptor substrates **8-10** and **19** (25 μL , 1 mM in 0.1 mM phosphate buffer pH 7.0) was added TcTS enzyme (25 μL). The mixture was incubated at 28 °C for 5 days when additional 25 μL aliquots of TcTS enzyme and fetuin were added; after a further 2 days additional 25 μL aliquot of fetuin was added. Reaction progress was followed by TLC ($\text{CH}_3\text{CN}/\text{EtOAc}/i\text{PrOH}/\text{H}_2\text{O}$, 85:20:50:50, v/v). The protein was precipitated by heating the mixture at 100 °C for 1 min and the denatured enzymes were removed by centrifugation (14000 rpm, 5 min). The supernatant was transferred to a new Eppendorf tube, concentrated by freeze drying and submitted to HR-MS analysis.

5.11.2 Macrophage invasion assays

Compounds used in macrophage invasion assays included a series of mixed 1,4/1,5-triazole-linked cyclic compounds C2, C3, C4, C5, C6, and C7 and a mixture of linear 1,4/1,5-triazole-linked oligomers generated by Method C (Section 4.6). *Trypanosoma cruzi* Y strain was cultivated in the LLC-MK2 host cells, as described elsewhere.⁴³

Preparation of macrophages

The macrophages derived from bone marrow (BMMOs) were obtained as described previously.⁴⁴ Briefly, total bone marrow cells were cultured in RPMI 1640 medium

(Sigma-Aldrich), supplemented with 10% Fetal Bovine Serum (Cutilab) and 30% L-929 cell-conditioned media at 37°C under 5% CO₂ atmosphere. On the seventh day of culture BMMOs were harvested and plated in 96 or 24 well microplates (at 5 x 10⁵ cells/mL).

Preparation of trypomastigotes

In two parallel series of tests trypomastigotes of *Trypanosoma cruzi* Y strain (1.5 x 10⁶ cells/mL) and triazole-linked compound were added into wells containing BMMOs in two different ways: (Treatment 1) trypomastigotes and tested compounds at a final concentration of 250 µM were plated at the same time and (Treatment 2) trypomastigotes and tested compounds at a final concentration of 250 µM were first pre-incubated for 1 hour, then the parasite was washed from the tested compound and plated to the wells containing BMMOs. In both methods the trypomastigotes were maintained for 2 h in contact with BMMOs. The parasites that had not invaded macrophages were removed by serial washing after 2 h incubation.

Analysis of released trypomastigotes

The free trypomastigotes were counted after six days of incubation in a Neubauer chamber and results are expressed as a percentage inhibition with respect to trypomastigotes counted released from infected cells without triazole treatment.

Analysis of amastigotes inside BMMOs

Macrophages infected with trypomastigotes as described above (Treatment 1) were maintained in culture for four days. The infected macrophages were fixed with methanol, stained with Giemsa and analysed using Leica DMI 4000B microscope. The results are expressed as an average number of amastigotes per macrophage.

6 Appendices

A1

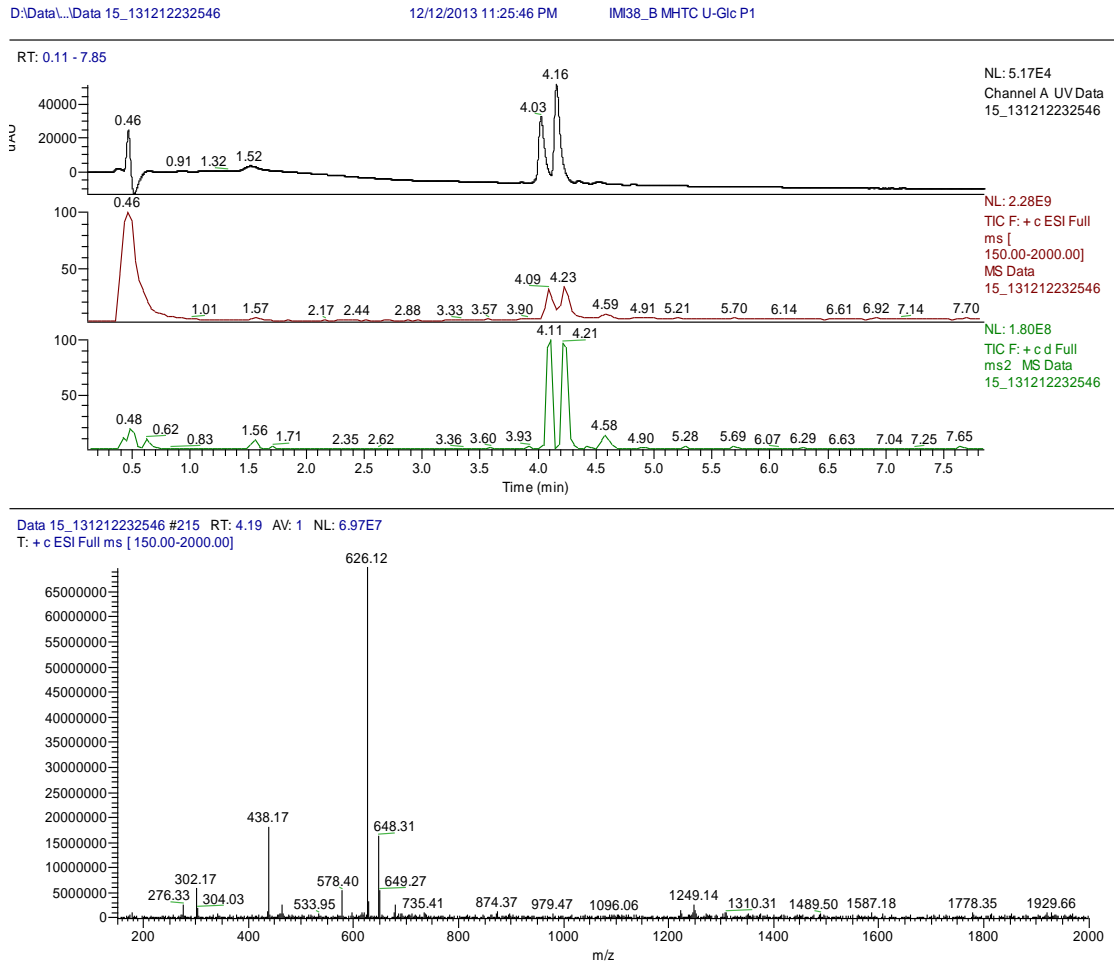
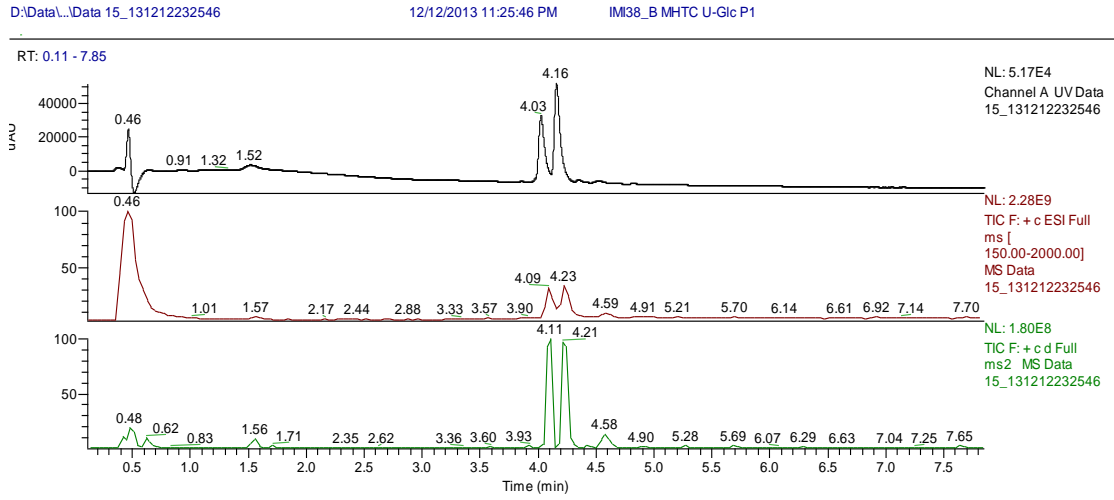


Figure 6.1 LC-MS data of peak 1 of fluorescent disaccharide (3.03) product obtained from incubation of monosaccharide acceptor substrate with UDP-Glc in the presence of *Euglena gracilis* microsomal membranes.

A2



Data 15_131212232546 #216 RT: 4.21 AV: 1 NL: 9.08E7
T: + c d Full ms 2 626.12@35.00 [160.00-1265.00]

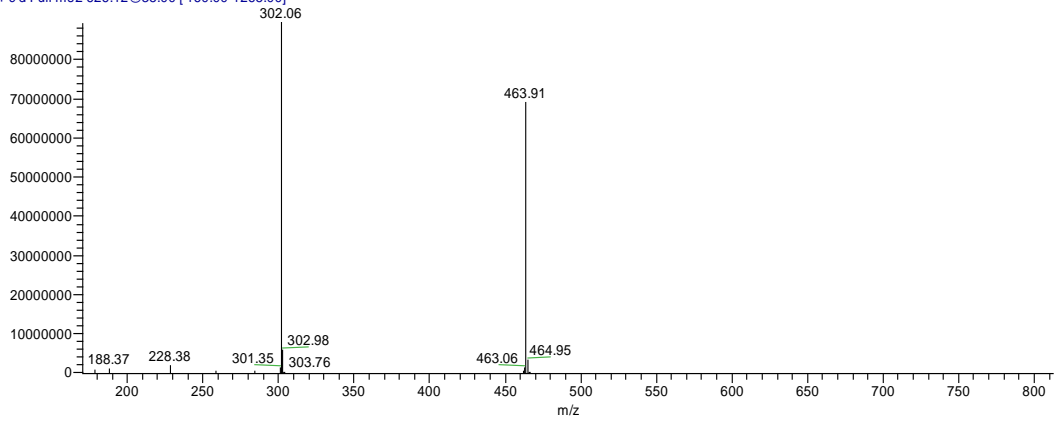


Figure 6.2 3LC-MS data of peak 2 of fluorescent disaccharide (3.03) product obtained from incubation of monosaccharide acceptor substrate with UDP-Glc in the presence of *Euglena gracilis* microsomal membranes.

A3

	Calculated m/z [M+H] ⁺	Found m/z [M+H] ⁺	MS2 fragmentation pattern		
			F1 (2.11)	F2 (2.12)	F3 (2.13)
2.11	302.11				
2.12	464.17				
2.13	626.22				
3.03	626.22	626.31	302.00	463.94	
3.06	788.27	788.16	302.01	463.93	625.94

Table 6.1 MS and MS2 data from LC-MS analysis of glucosylated fluorescent products obtained from **2.12** and **2.13**.

A4

Entry	Calculated m/z [M+H] ⁺	Found m/z [M+H] ⁺	MS2 fragmentation pattern		
			F1 (2.11)	F2 (2.12)	Difference F2-2.11
1 2.11	302.11				
2 2.12	464.17				
3 2.13	626.22				
5 3.04	706.19	705.97	301.90	543.91	79.74
6 3.07	747.21	746.97	302.08	543.92	79.75

Table 6.2 MS and MS2 data from LS-MS analysis of products obtained from **2.12** with UDP-Glc.

A5

Entry	Calculated m/z [M+H] ⁺	Found m/z [M+H] ⁺	MS2 fragmentation pattern			Difference F3-2.12
			F1 (2.11)	F2 (2.12)	F3 (2.13)	
1 2.11	302.11					
2 2.12	464.17					
3 2.13	626.22					
5 3.05	868.24	868.12	301.99	463.90	705.92	79.70
6 3.08	909.27	909.16	302.00	463.94	705.93	79.71

Table 6.3 MS and MS2 data from LS-MS analysis of products obtained from **2.13** with UDP-GlcNAc.

A6

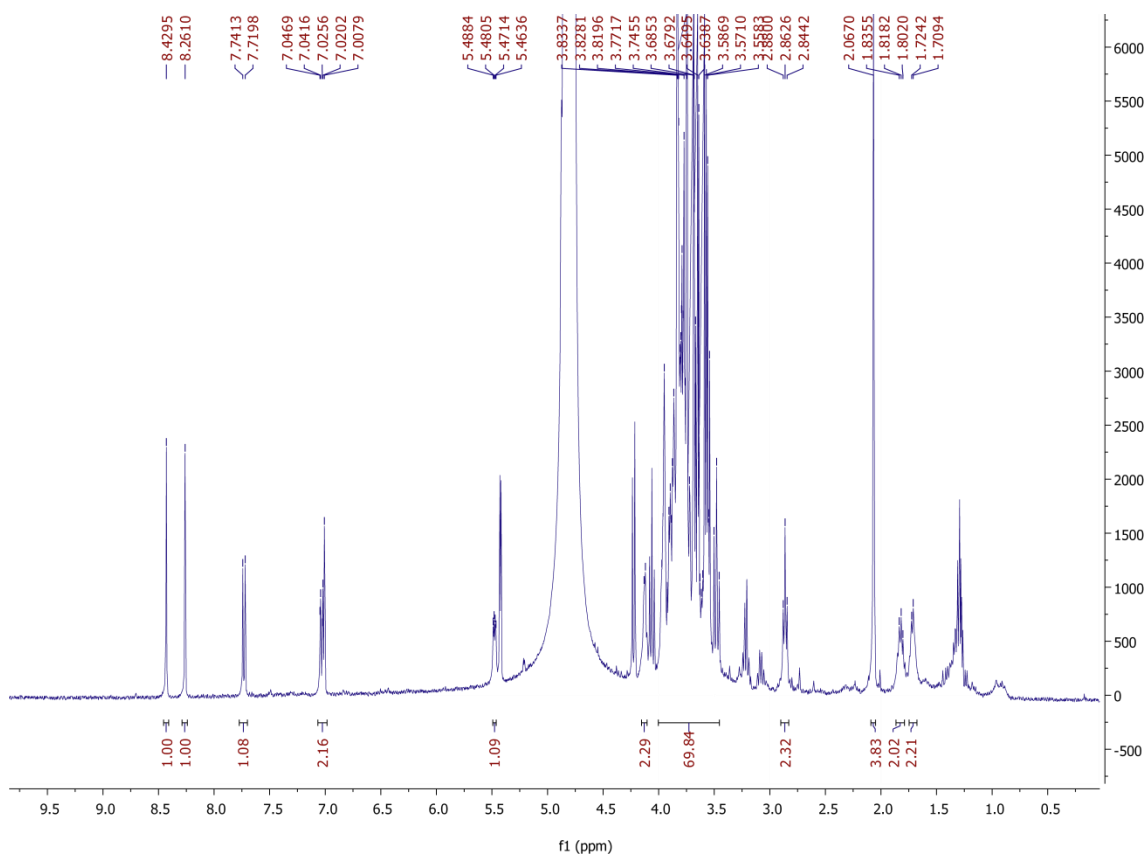


Figure 6.4 The ^1H NMR spectra of fluorescent phosphodiester-linked product.

A7

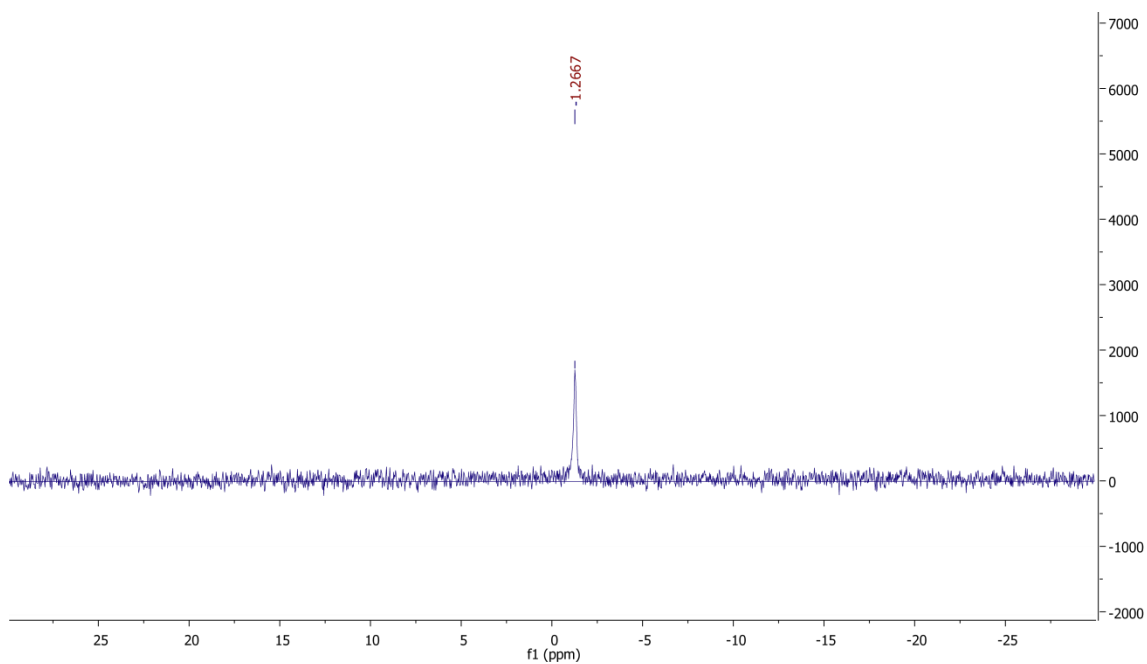


Figure 6.5 The ^{31}P NMR spectra of fluorescent phosphodiester-linked product.

A8

☑	10001	1	MKVDGRV-----AAFGAAAA-----LECLLVPLIILKVPYTEIDWRAYMQEVE	43
☑	10002	1	MKTGYS---DRRLA-----WWDARHGKRNL-----SVEDTEIDWKAYMAEVE	39
☑	10003	1	-----MEYRWLNRVLTVELCMSIIAFHLVHFTGIDWNAVMQEVK	39
☑	10004	1	MEGEQSPqgEKSLQrkqfvrrppldlWQDLKDGVRVYVifdcraNLIIVMPLLIILFESMLCKIIIKVAYTEIDYKAYMEQIE	80
☑	10001	44	AILG-GEMNYKNVRGDTGPIVYPAGFVYVYSALYYLTGSGNNIALAQQLFGVLYLVFIATVLYIYSKVKGVPSSWALLLLC	122
☑	10002	40	GVIN-GTYDYTLQGDGTGPLVYPAGFVYIFMGLYYATSRGTDIRMAQNIFAVLYLATLLLVFLIYHQTCVPPFVFFMFC	118
☑	10003	40	GFLD-GELDYMKLKGDTGPLVYPGGFVWSHSALYFMTKGGVDVEMAQWLYLGIYVMVLVVAHLY-YNSGLRGRLFIRLL	117
☑	10004	81	MIQLdGMLDYSQVSGGTGPLVYPAGHVLIIYKMMYWLTEGMDHVERGQVFFRYLYLLTLALQMACY-YLLHLPWCVWLAC	159
☑	10001	123	LS-RRIHSLFVLRNFNDCVAMFLYLAVA-----CLLR-NR-----WALGCVVYSLAVSVKMNVLFFAPGLFFLL--L	186
☑	10002	119	CAsYRVHSIFVLRNFNDPVAMVLLFLSIN-----LLLA-QR-----WGWGCCFFSLAVSVKMNVLFFAPGLFLLL--L	183
☑	10003	118	LS-KRIRSLFMFRLFNDCWAMFLVYLSVI-----CFArgRR-----WTVGCLLYSMAVSVKMNIFLFAPGLLLIL--C	182
☑	10004	160	LS-KRLHSIYVLRNFNDCFITLMMVTVLgaivaSRCH-QRpkIkslALVISATYSMAVSIKMNALLYFPAMMISLfil	237
☑	10001	187	QRFGVAGTVWKLGICAAQVVLGLPFLCTYPVEYLSRAFELSRVFFHWWSVNLKFLPEEVFQSKALALVLLALHLASIFL	266
☑	10002	184	TQFGFRGALPKLGIcAGLQVVLGLPFLLENPSGYLSRSFDLGRQFLFHWTWNWRFLPEALFLHRAFLALLTAHLTLLLL	263
☑	10003	183	KSLPFTGVVRCCLAVCALWQVWAGLPFLLNPRSYIVRSFDLGRVFTYRWTVNFKRISSEIFFSSKFSRLLVMLAVSWLL	262
☑	10004	238	NDANVILTLDDLVAIAWQVAVAVPFLRSFPQQYLHCAFNFGRKFMYQWSINWQMMDEEAfNDKRFHLALLISHLIALT	317
☑	10001	267	FAHFRWCRHSGGLVGVFRSRG-----GQQPSP--NHIVATLLEANFLGIVFARTLHYQFYVWYHSLVFLLVgcrvrdR	339
☑	10002	264	FALCRWHRTGESILSLLRDPSKRKVPQPPLT--NQIVSTLFTSNFIGICFSRSLHYQFYVWFHTLPYLLW-----A	334
☑	10003	263	VCFRRWSKRAYRRGRCEKREGTVVLVGASDEEvfHNVTLTMESNMIGVIFARSLHYQFFLWFFYFVPFVLS-----A	335
☑	10004	318	LFVTRYPRILPDLWSSSLCHPLRKNVAVLNANPA--KTIPFVLIASNFIGVLFSRSLHYQFLSWYHWTLPILIF-----W	388
☑	10001	340	AGLRLaewlgngasaqavgavAPHALRLLALGLIEVVMNVYSPRATALLLTALHLGLLHELArspapagdgppTLAQ	419
☑	10002	335	MPARW-----LTHLLRLLVLGLIELSWNTYPSTSCSSAALHICHAVILLQLW-----L--	382
☑	10003	336	TR-----LPLVKVVAFLAIQYGFVYVYPTASSVLLSGFLCVWLGML-----L---	380
☑	10004	389	SG-----MPFVGPiWVVLHEWCWNSYPPNSQASTLLALNTVLLLLLA-----LTQ	435
☑	10001	420	APDRRPAPVSHDSRDRdrwaaghQRGPTAPTLRKARps*	459
☑	10002	383	--GPQFPFKS-----TQ-----HS-----KKAH---	398
☑	10003	381	-----FPSEYSETTGK-----ETTITLTAVKRGK---	404
☑	10004	436	LSGSVALAKSHLRTTSS-----ME-----KKLN---	458

Entry	Organism	Identity %	Similarity %	Gaps %
1001	<i>Euglena gracilis</i>			
1002	<i>Homo sapiens</i>	42.8	55.4	17.7
1003	<i>Trypanosoma brucei</i>	29.9	43.9	33.7
1004	<i>Saccharomyces cerevisiae</i>	28.9	42.3	26.7

Table 6.4 *Euglena gracilis* percent identity, similarity and gaps of *EgAl3* to known protein sequences.

A9

☑	10001	1	M-----	----LAILLPLLVARLQAAMHAPVADCDEVFNFW	31
☑	10002	1	MNCK-----	AVTISL L L L L L F L T R V Y I Q P T F S L I S D C D E T F N Y W	38
☑	10003	1	MDLTTTRQRRPLISDSSSSSTKSYSKTDKPGRSNGGDAEDG	GLRWFLPFIALCYLRYMSATSNIHDCDEVFNFW	76
☑	10004	1	MASRGARQLKKGSGASSGDTAPAADKLRLLGSRAGGAEHR[12]	APEGSTAFKCLLSARLCAALLSNISDCDEFNFW	88
☑	10001	32	EPLHFLMYGSGLQPWEYSQHALRSWLYIWLHRLLFAPLATL---	PKPAVFYGRMCVAALSVAEALWNRHVARRFGPS	108
☑	10002	39	EPLNLLVRGFGKQTWEYSPEYSIRSWAFLLPFYCILYPVKNF	TDLESHWNFFITRACLGFFSFIMEFKLHREIAGSLALQ	118
☑	10003	77	EPLHYILYKSGFQTWEYSNFAIRSYLYILFHELGRPASW	FGDDKVRVYAVRFLGLVSAVSDTVLVVALSRKYGKR	156
☑	10004	89	EPTHYLIYGEFQTWEYSPAYAIRSYAYLLHAWPAFHARIL	QTNKILVFYFLRCLLAFVSCICELYFYKAVCKKFGHLH	168
☑	10001	109	VGRWGLFFSALSPAMFSAVPSILPTSFALTCFLVAHAAWIA	EERRAVGVIAAAAAavVLGWPF AALVMAPAALDCI	185
☑	10002	119	IANIWIIFQLFNPQGFHASVELLPSAVAMLLVYGATRHSR	[6]TSNFTKSLAYNFLAS--ILGWPFVILSLPLCLHYL	199
☑	10003	157	IATYAVAMLCLTSGCFFASTSFLPSSFSMYAISLSSGLLFF	-EKYAMAVAVSVVGV--ILGWPFSLAFLPVVIYSL	230
☑	10004	169	VSRMMLAFVLSTGMFCSSAFLPSSFCMYTTLIAMTGWYM	-DKTSIAVLGVAAGA--ILGWPFSAALGLPIAFDLL	242
☑	10001	186	A----RHSFLFCLWRCLPAVALLVAVSLVDSAMYGRWCST	WNLVWYNFLGADKDASSELYGVEPWHF LKNLALNFNVV	261
☑	10002	200	FNHRIISTIRTAFCCLIFSLTAFAVIVTDSIFYGKLAPV	SNILFYNVINASEESGNIFGVEPWYYPNLLNLFPLP	279
☑	10003	231	V-KRFKQAFIAGAVTTIFLLGVS---LLVDYVYKRWTS	SVLNLIIYNVLG---GGESHLYGTEGALFYIRNGFNMFNC	303
☑	10004	243	VMKHRWKSFFHWSLMALILFLVP--VVVIDSYVYKLV	IAPLNIVLYNVFT---PHGPDLYGTEPWYFYLINGFLNFVA	317
☑	10001	262	FLLALVA[7]WLLRQRL[42]RRDPRS GAAPLPWRWLLY	ISPPFWLLFWLVP AHKEERFLVPAYHCLLSAAVATDCL	383
☑	10002	280	VLVLAIL GIFHLRL-----	WPLWASLFTWIAVFTQQPHKEERFLYPIYGLITLSASIAFYKV	336
☑	10003	304	FILAMLF VAIYPVI RRKYDR-----	ALLVVISPMYIWLAFMSLQPHKEERFLYPIYPLICVSASAVIENI	368
☑	10004	318	FALALLV LPLTSLM EYLLQRFHVQNLGHPYWL	TLAPMYIWFIIFFIQPHKEERFLFPVYPLICLCGAVALSAL	390
☑	10001	384	LAVAG---QRSPSLRAGLAC----GLAAVTL	LSAGRILVQTQYYAAPLHVYGAVAHHAAGRQRTGPPAAAVPVCVGK	455
☑	10002	337	LN---LFNRKPIILKGGI-----KLSVLLIVAGQ	MSRIVALVNNYTAPIAVYEQFSSLNQGQV-----KAPVNVCTGR	402
☑	10003	369	PELFRKEYSSRESLLVTITK-YMRPVILGCILCASH	SRTFALINGYSAPLEVYKLEHDDAGPGS-----VLCVGS	439
☑	10004	391	QKCYHFVFQRYRLEHYVTsnWLALGTVFLFGLLS	FSRSVALFRGYHGPLDLYPEFYRIADPTIHTVPEGRPVNVCVGK	470
☑	10001	456	EWYRFP SHFL LHPD-QRFLFHSNFGGLLPTYFDE-	GPGGSRVVQAKLNRQNRVAVDLPVA-NATSCQYVVDLDP---	529
☑	10002	403	EWYHFPSFLPDN-HRLKFVKSGFDGLLPGDFPe	SGSIFKKIRLTPKGMNKNIYDTGKEW-PITRCDYFIDIVAPINL	480
☑	10003	440	EWHRYPSSFFVPHYiSEVRWIDDGFRGLLPFPFNN--	TLGGTSASPPYFNKNQASEEQYLKNIETCTFLIEL----QL	512
☑	10004	471	EWYRFPSSFLPDN-WQLQFIPSEFRGQLPKPFAE-	GPLATRI--VPTMNDQNLEEPSRYI-DISKCHYLDLDTMRET	545
☑	10001	530	DQAEHFTADRETWSLIAAHPFLDADHSPAWTRWLY	WYPYLSAA-----RNVFRP----YVALHRKAPPATLQDSP*	596
☑	10002	481	TKDVFNPLHLMNWNKLACAAFDIGENSKILGRAFY	VEPINR[4]VLPKQWQVYGVrYIDYCLFEKPTETTN-----	555
☑	10003	513	SRPYQYRGSDLSTWEIAVLPYLDRELSPAKYRSFF	IHPHMW-----QEKNVFG----KYVALRRVPK-----	570
☑	10004	546	PREPKYSSN-KEEWISLAYRPF LDASRSSKLLRAFY	VYP-----FLSDQYTV----YVNYTIL-KPRKAKQIRKKS	610
☑	10001	-	-	-	-
☑	10002	-	-	-	-
☑	10003	-	-	-	-
☑	10004	611	g	611	

Entry	Organism	Identity %	Similarity %	Gaps %
1001	<i>Euglena gracilis</i>			
1002	<i>Saccharomyces cerevisiae</i>	25.8	41.0	23.5
1003	<i>Arabidopsis thaliana</i>	27.0	41.2	23.3
1004	<i>Homo sapiens</i>	31.1	41.4	22.8

Table 6.5 *Euglena gracilis* percent identity, similarity and gaps of EgAlg9 to known protein sequences.

A10

☑	10001	1	MARDVLAAGKLLQRQCYTFLGSRVGLALLFIASVVTLSVQLVQIDGWFS5GIVCPHRCDD-----WRDNLQRRS	72
☑	10002	1	M-----LFKLLQRQTYTCLSHRYGLVVCFLGVVVTIVSAFQFGEVLE---WSRDQYH----VLFDSY-RDNIAGKS	64
☑	10003	1	MARLQERGSVVKLIQFKLFSFLSSRFGLFCIIGVFI5PNTILQLVRLYTDNSFIS5SDIYNQKptFFSQSYWEDNVGGS	80
☑	10001	73	FEAFLG-HEPIDVVYTVVNGSDPRL-----KATLEEWKHA --- GLP HDAH	114
☑	10002	65	FQNRLC1PMPIDVVYTVVNGDLELLKELQQVREQMEEeqkAMREILGKNTTEPTKKS[10]CIK[8]ALP[15]HSASD	166
☑	10003	81	YQNILC-SQPIDIVYTVVNGSDPKLIKEVTELRKSRDP--LIPECQKQTPEKDK-- CYR --- ----	136
☑	10001	115	APN-ATPAAPNAS RAANASAAADRADASRYQDQELRYSLSVEHFAGVVRHVIYVTVNGQVPAHLNDLNPRVTV	188
☑	10002	167	IFNvAKPKNPSTN[126]LSAISQSKQEDISASRFEDNEELRYSLSIERHAPWVRNIFVTVNGQIPSWLNDLNPRVTI	367
☑	10003	137	-----DONTASRYVDNQLKYSLSIEKFAPIRHHVYVTVNGQVPAHLNLSNPKLSI	188
☑	10001	189	VPHAALFPNHSHLPTFSSPAIEAHLHRIPGLSRRFLYLNDTFFGNVIRPEDFYTPHGHRIYLSWAVPDCSPGCTGTNI	268
☑	10002	368	VTHQDVFRNLSHLPTFSSPAIESHHRIEGLSQFIYLNDDVMFGKDVWPDFFYSHSKQKVYLTPWPNCAGECPGSHI	447
☑	10003	189	VTHQEIFANKSHLPTFSSPSIETHLHRIPGLSKFIYLNDDVMLGREIYPPDFVTQNGGQVFLSWPVPNCNDGCPNNMI	268
☑	10001	269	GDGYCDKACNVSACNFDGGDCLGKAAS5G5NMNDNYDGS-----YNYHWPYAQTSCHSGCHDNIWGDK	333
☑	10002	448	KDGYCDKACNVSACNFDGGDCLGKAAS5G5NMNDNYDGS-----YNYHWPYAQTSCHSGCHDNIWGDK	517
☑	10003	269	GDGFCDNACNVFNCFDGGDCDNSTGTVKTRMNRNGNGGTTTSTTTSTNTGNLGLTSDNRLKSYCSRGCPD5WVGDK	348
☑	10001	334	FCDTACNVEACGFATDCGVDEVRKRLHSFHLSPNLTNYSVDGRLNFAVINLTGLPAGMEVRAARhrGGGDAIRATALS	413
☑	10002	518	FCOQACNVLSGCFDAGDCGQDHFEHYKVLIPNQTHYI-IPKGECLPYF5FAEVAKRGV--EGAY--SDNPIIRHASIA	592
☑	10003	349	HCORMCKNEDCGYDAGDCGVELMFTSMKGYEINKNTSII5LPDGRSVYFNLSLIGEGTITDGS--DNAILVRTATIS	426
☑	10001	414	KPHLLVIVLKLDRRQVFALEGE-AHGAVLENFTVVVGRDRP--NTT[5]LTSMTNDNVGPTSSPQLGAPLHAL	492
☑	10002	593	NKWKTIHLIMHSGHNTTIFHNLTFQNTNDEEFKMQITVEVDTRGPKINST AQKGYENLVSPITLLPEAEILFEDI	669
☑	10003	427	QKYKIMTLTFHRDKEFQNIIVSITVEITSKKQKSIITTTTTNSTT-----NST ITT-IDSLDKGNTNSEQEELITESI	497
☑	10001	493	TPSPAPPATSH--Q5AAALDPSAAPLGH5PPAATPAATLLVAKPPTSPDPAQ-----TPAHAPSPPTPAGSSKPH	564
☑	10002	670	PKEKRFKPKFRHdvNSTRAAQEEVKIPLVNI5LLPKDAQLSLNTLDLQLEHGDITLKGYNLSK5SALRSFLHNSQHAKIK	749
☑	10003	498	--EKNF-----NITLSTKEE-----SSSSSSSI5SSEKVKDLESKTNQQTLIGTEELSPSPVESNKGKSN	559
☑	10001	565	PAPPGLDS-KDTASDPPASPPTQPSPPDVATARRLLQLRR-----RI	607
☑	10002	750	NQAIITDETDNSLVAPQEKQVHKSILPNSLGV5ERLQLTF-PAVSVKVNHDQGGQNPPLDLETTARFRVETHQKTI6G	828
☑	10003	560	FSTKAIDQLGDEIISPPIGSIEDVEGLPPASIRDREEIITGhEQVKDPNNEKQQQQQQQQQQQQQQQQQQQQQQ	639
☑	10001	608	RPAERSEVLPVMPLEPAPPYRLRLSPPTA -----APAPQGVND-----PFAD5SRPGEAP	659
☑	10002	829	NVTKEKPPSLIVPLESQMTKEKITGK---- EKENSMEENAEENHIGVTEVLLGRKLQHYTDSYLGFLPWEKXKYFQ	901
☑	10003	640	QQQQQQNQNQLTSSENKQKDYKINKKLSKM[7]QEEQKEQEEQKENKEMFDLADTLKKELEKKWQEFYD5VKK5QEN	723
☑	10001	660	RGIDPRDLQA4AVGA ERLSRLDALAQH5SPR PAVRTTPAGPG -RAGQRRLLDTFGD5LKFVNHLFTVKW6	727
☑	10002	902	DLLEEEESLKTQ--- --LAY----- --FTD---- SKNTGRQLKDTFADSLRYVNKILNSKFG	947
☑	10003	724	SNLNENNTNTNTR[8]NSLDYNDHLQLHEEK[113]PWEEFTPIDDG[7]SKPHNRKPLDMFGD5LKFVNRLYSKEFG	920
☑	10001	728	HHPRKVPAMPHMIDRDVMAALWRENPAQWEATSAAHFR5AADMQFAF5HFYIVHAKAPVDPIQFFQEhLDINGNGYLE	807
☑	10002	948	FTSRKVPAMPHMIDRIVHQLQDMFPEEFDKTSFHKVRH5EDMQFAF5FYVYVHSAVQPLNISQVFDE-VDTQ5GVLS	1026
☑	10003	921	SSPRKVPAMPHMIDVDVHVEIQAKWPAQWATSSHS5LH5PDMQYAF5FFYVYVHSAVQPLNISQVFDE-VDTQ5GVLS	999
☑	10001	808	PQEFRRLLAVLLFDKVKTESLDQITVVDG5VAPRNATVAKARN[36]NIAAT5TEEKTETGHS[42]ASHQEHEGPTMPK	957
☑	10002	1027	DREIRTLATRIHELPLSLQDLTGLEH-----MLINCSK MLPADIT--QLN-NIP PTQESYYPNLPP	1085
☑	10003	1000	DNELRTFSVNVVYVPLKV5GQFDQIKNYFYHICIQHKLNTNVEQ GIDIEATLERLNRH5 ADAPDPKREYCP	1071
☑	10001	958	EYLD[14]LLDATR5V5GLSKLVigdKQAATYKHQLVDLDEV5FFHIRDNAS5VQH5HDLAKQPKFICINDNHNHSH	1047
☑	10002	1086	VTKS LVTNCKPVTDKIHKAY---KDKNKYRFEINGEEIAFKMIRTNV5V5GQLDDIRKNRPFVCLNDNIDHNI	1158
☑	10003	1072	ITLD VIK5DNKTHEDIKKY---SKKQFYKTLT5GTD5VAF5LMDINDYV5V5KLDGIR5R5R5K5F5CLNDNIDH5AS	1144
☑	10001	1048	PENS5VAVIHDFEIVFW55FELPAGKTN5YQYLD5MAAARKARRKAA5GK5SAAV5V5L5GLAV5Y5V5GLNAV5LHNR	1127
☑	10002	1159	KDAQTVKAVLRDFYESMFP5P5QFELPREYRNRFLH5HELQ5HAYR5DKL5FW5H5CV5LATL5MFTI5F5FAEQ5LIA5LKRK	1238
☑	10003	1145	PNN5KV5V5LHNF5D5L5FAL5P5S5FEL5PP5Q5FNN5FQ5YIED5FKA----DVVEIRTKN5Y5Y5F5M5V5S5L5ALL5FIL5WK5CK5S	1219
☑	10001	1128	PGHRRQIH-----DRHDV* 1141	
☑	10002	1239	IFPRRRIHKEASPNRIRV- 1256	
☑	10003	1220	TSLH5K5FK5KGL5PTR5MSVH 1238	

Entry	Organism	Identity %	Similarity %	Gaps %
1001	<i>Euglena gracilis</i>			
1002	<i>Dictyostelium discoideum</i>	25.8	39.8	26.6
1003	<i>Homo sapiens</i>	25.5	36.4	35.5

Table 6.6 *Euglena gracilis* percent identity, similarity and gaps of GlcNAc-P-Tase to known protein sequences.

A11

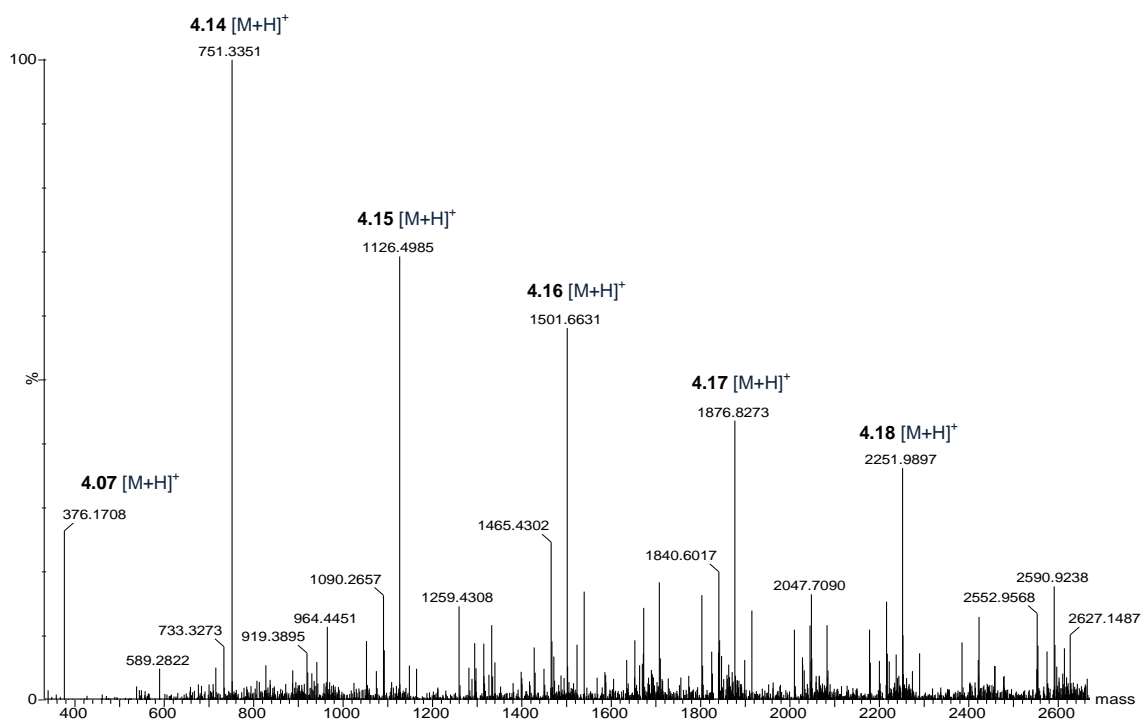


Figure 6.6 The HRMS spectrum of the series of 1,4-triazole-linked linear products obtained from CuAAC oligomerisation of galactose monomer.

7 References

1. Reuter, G.; Gabius, H. J., Eukaryotic glycosylation: whim of nature or multipurpose tool? *Cell. Mol. Life Sci.* **1999**, *55*, 368-422.
2. Bertozzi, C. R.; Rabuka, D., Structural basis of glycan diversity. *In Essentials of Glycobiology*, 2nd ed.; Varki, A.; Cummings, R. D.; Esko, J. D.; Freeze, H. H.; Stanley, P.; Bertozzi, C. R.; Hart, G. W.; Etzler, M. E., Eds.: Cold Spring Harbor (NY), **2009**.
3. Ferguson, M. A., The structure, biosynthesis and functions of glycosylphosphatidylinositol anchors, and the contributions of trypanosome research. *J. Cell Sci.* **1999**, *112*, 2799-2809.
4. Mishra, A. K.; Driessen, N. N.; Appelmelk, B. J.; Besra, G. S., Lipoarabinomannan and related glycoconjugates: structure, biogenesis and role in *Mycobacterium tuberculosis* physiology and host-pathogen interaction. *FEMS Microbiol. Rev.* **2011**, *35*, 1126-1157.
5. Sacchettini, J. C.; Baum, L. G.; Brewer, C. F., Multivalent protein-carbohydrate interactions. A new paradigm for supermolecular assembly and signal transduction. *Biochemistry* **2001**, *40*, 3009-3015.
6. Tan, F. Y.; Tang, C. M.; Exley, R. M., Sugar coating: bacterial protein glycosylation and host-microbe interactions. *Trends. Biochem. Sci.* **2015**, *40*, 342-350.
7. Karlsson, K. A., Bacterium-host protein-carbohydrate interactions and pathogenicity. *Biochem. Soc. T.* **1999**, *27*, 471-474.
8. Wiederschain, G. Y., Glycobiology: Progress, problems, and perspectives. *Biochemistry (Moscow)* **2013**, *78*, 679-696.
9. Benoff, S., Carbohydrates and fertilization: an overview. *Mol. Hum. Reprod.* **1997**, *3*, 599-637.

10. Tifft, C. J.; Proia, R. L.; Cameriniotero, R. D., The folding and cell-surface expression of CD4 requires glycosylation. *J. Biol. Chem.* **1992**, *267*, 3268-3273.
11. Varki, A., Biological roles of oligosaccharides - all of the theories are correct. *Glycobiology* **1993**, *3*, 97-130.
12. Shifrin, S.; Consiglio, E.; Kohn, L. D., Effect of the complex carbohydrate moiety on the structure of thyroglobulin. *J. Biol. Chem.* **1983**, *258*, 3780-3786.
13. Ikezawa, H., Glycosylphosphatidylinositol (GPI)-anchored proteins. *Biol. Pharm. Bull.* **2002**, *25*, 409-417.
14. Ferguson, M. A. J.; Kinoshita, T.; Hart, G. W., Glycosylphosphatidylinositol anchors. *In Essentials of Glycobiology*, 2nd ed.; Varki, A.; Cummings, R. D.; Esko, J. D.; Freeze, H. H.; Stanley, P.; Bertozzi, C. R.; Hart, G. W.; Etzler, M. E., Eds.: Cold Spring Harbor (NY), **2009**.
15. Nosjean, O.; Briolay, A.; Roux, B., Mammalian GPI proteins: sorting, membrane residence and functions. *Biochim. Biophys. Acta* **1997**, *1331*, 153-186.
16. Nozaki, M.; Ohishi, K.; Yamada, N.; Kinoshita, T.; Nagy, A.; Takeda, J., Developmental abnormalities of glycosylphosphatidylinositol-anchor-deficient embryos revealed by Cre/loxP system. *Lab. Invest.* **1999**, *79*, 293-299.
17. McConville, M. J.; Ferguson, M. A., The structure, biosynthesis and function of glycosylated phosphatidylinositols in the parasitic protozoa and higher eukaryotes. *Biochem. J.* **1993**, *294*, 305-324.
18. Homans, S. W.; Edge, C. J.; Ferguson, M. A. J.; Dwek, R. A.; Rademacher, T. W., Solution structure of the glycosylphosphatidylinositol membrane anchor glycan of *Trypanosoma brucei* variant surface glycoprotein. *Biochemistry* **1989**, *28*, 2881-2887.
19. Masterson, W. J.; Doering, T. L.; Hart, G. W.; Englund, P. T., A novel pathway for glycan assembly - biosynthesis of the glycosylphosphatidylinositol anchor of the *Trypanosome* variant surface glycoprotein. *Cell* **1989**, *56*, 793-800.

20. Orlean, P.; Menon, A. K., Thematic review series: lipid posttranslational modifications. GPI anchoring of protein in yeast and mammalian cells, or: how we learned to stop worrying and love glycopospholipids. *J. Lipid Res.* **2007**, *48*, 993-1011.
21. Kinoshita, T.; Fujita, M.; Maeda, Y., Biosynthesis, remodelling and functions of mammalian GPI-anchored proteins: recent progress. *J. Biochem.* **2008**, *144*, 287-294.
22. Urbaniak, M. D.; Yashunsky, D. V.; Crossman, A.; Nikolaev, A. V.; Ferguson, M. A., Probing enzymes late in the trypanosomal glycosylphosphatidylinositol biosynthetic pathway with synthetic glycosylphosphatidylinositol analogues. *ACS Chem. Biol.* **2008**, *3*, 625-634.
23. Smith, T. K.; Sharma, D. K.; Crossman, A.; Brimacombe, J. S.; Ferguson, M. A., Selective inhibitors of the glycosylphosphatidylinositol biosynthetic pathway of *Trypanosoma brucei*. *EMBO J.* **1999**, *18*, 5922-5930.
24. Gamage, D. G.; Hendrickson, T. L., GPI transamidase and GPI anchored proteins: oncogenes and biomarkers for cancer. *Crit. Rev. Biochem. Mol. Biol.* **2013**, *48*, 446-464.
25. Ellis, M.; Egelund, J.; Schultz, C. J.; Bacic, A., Arabinogalactan-proteins: key regulators at the cell surface? *Plant Physiol.* **2010**, *153*, 403-419.
26. Oxley, D.; Bacic, A., Structure of the glycosylphosphatidylinositol anchor of an arabinogalactan protein from *Pyrus communis* suspension-cultured cells. *Proc. Natl. Acad. Sci. U S A* **1999**, *96*, 14246-14251.
27. Nigou, J.; Gilleron, M.; Puzo, G., Lipoarabinomannans: from structure to biosynthesis. *Biochimie* **2003**, *85*, 153-166.
28. Pitarque, S.; Herrmann, J. L.; Duteyrat, J. L.; Jackson, M.; Stewart, G. R.; Lecointe, F.; Payre, B.; Schwartz, O.; Young, D. B.; Marchal, G.; Lagrange, P. H.; Puzo, G.; Gicquel, B.; Nigou, J.; Neyrolles, O., Deciphering the molecular bases of *Mycobacterium tuberculosis* binding to the lectin DC-SIGN reveals an underestimated complexity. *Biochem. J.* **2005**, *392*, 615-624.

29. Guerin, M. E.; Buschiazzo, A.; Kordulakova, J.; Jackson, M.; Alzari, P. M., Crystallization and preliminary crystallographic analysis of PimA, an essential mannosyltransferase from *Mycobacterium smegmatis*. *Acta. Crystallogr. Sect. F. Struct. Biol. Cryst. Commun.* **2005**, *61*, 518-520.
30. Guerin, M. E.; Schaeffer, F.; Chaffotte, A.; Gest, P.; Giganti, D.; Kordulakova, J.; van der Woerd, M.; Jackson, M.; Alzari, P. M., Substrate-induced conformational changes in the essential peripheral membrane-associated mannosyltransferase PimA from mycobacteria: implications for catalysis. *J. Biol. Chem.* **2009**, *284*, 21613-21625.
31. Kordulakova, J.; Gilleron, M.; Puzo, G.; Brennan, P. J.; Gicquel, B.; Mikusova, K.; Jackson, M., Identification of the required acyltransferase step in the biosynthesis of the phosphatidylinositol mannosides of mycobacterium species. *J. Biol. Chem.* **2003**, *278*, 36285-36295.
32. Morita, Y. S.; Patterson, J. H.; Billman-Jacobe, H.; McConville, M. J., Biosynthesis of mycobacterial phosphatidylinositol mannosides. *Biochem. J.* **2004**, *378*, 589-597.
33. Morita, Y. S.; Fukuda, T.; Sena, C. B.; Yamaryo-Botte, Y.; McConville, M. J.; Kinoshita, T., Inositol lipid metabolism in mycobacteria: biosynthesis and regulatory mechanisms. *Biochim. Biophys. Acta* **2011**, *1810*, 630-641.
34. Mishra, A. K.; Alderwick, L. J.; Rittmann, D.; Tatituri, R. V. V.; Nigou, J.; Gilleron, M.; Eggeling, L.; Besra, G. S., Identification of an alpha(1→6) mannosyltransferase (MptA), involved in *Corynebacterium glutamicum* lipomanann biosynthesis, and identification of its orthologue in *Mycobacterium tuberculosis*. *Mol. Microbiol.* **2007**, *65*, 1503-1517.
35. Mishra, A. K.; Alderwick, L. J.; Rittmann, D.; Wang, C.; Bhatt, A.; Jacobs, W. R.; Takayama, K.; Eggeling, L.; Besra, G. S., Identification of a novel alpha(1→6) mannosyltransferase MptB from *Corynebacterium glutamicum* by deletion of a conserved gene, NCgl1505, affords a lipomannan- and lipoarabinomannan-deficient mutant. *Mol. Microbiol.* **2008**, *68*, 1595-1613.

36. Seidel, M.; Alderwick, L. J.; Birch, H. L.; Sahm, H.; Eggeling, L.; Besra, G. S., Identification of a novel arabinofuranosyltransferase AftB involved in a terminal step of cell wall arabinan biosynthesis in *Corynebacteriaceae*, such as *Corynebacterium glutamicum* and *Mycobacterium tuberculosis*. *J. Biol. Chem.* **2007**, *282*, 14729-14740.
37. Birch, H. L.; Alderwick, L. J.; Appelmelk, B. J.; Maaskant, J.; Bhatt, A.; Singh, A.; Nigou, J.; Eggeling, L.; Geurtsen, J.; Besra, G. S., A truncated lipoglycan from mycobacteria with altered immunological properties. *Proc. Natl. Acad. Sci. U S A* **2010**, *107*, 2634-2639.
38. Alderwick, L. J.; Lloyd, G. S.; Ghadbane, H.; May, J. W.; Bhatt, A.; Eggeling, L.; Futterer, K.; Besra, G. S., The C-terminal domain of the arabinosyltransferase *Mycobacterium tuberculosis* EmbC is a lectin-like carbohydrate binding module. *PLoS Pathog.* **2011**, *7*, e1001299.
39. Larkin, A.; Imperiali, B., The expanding horizons of asparagine-linked glycosylation. *Biochemistry* **2011**, *50*, 4411-4426.
40. Lehle, L.; Strahl, S.; Tanner, W., Protein glycosylation, conserved from yeast to man: A model organism helps elucidate congenital human diseases. *Angew. Chem. Int. Edit.* **2006**, *45*, 6802-6818.
41. Lehrman, M. A., Biosynthesis of *N*-acetylglucosamine-P-P-dolichol, the committed step of asparagine-linked oligosaccharide assembly. *Glycobiology* **1991**, *1*, 553-562.
42. Takatsuk.A; Arima, K.; Tamura, G., Tunicamycin, a new antibiotic. Isolation and characterization of tunicamycin. *J. Antibiot.* **1971**, *24*, 215-223.
43. Helenius, J.; Ng, D. T. W.; Marolda, C. L.; Walter, P.; Valvano, M. A.; Aebi, M., Translocation of lipid-linked oligosaccharides across the ER membrane requires Rft1 protein. *Nature* **2002**, *415*, 447-450.
44. Burda, P.; Aebi, M., The dolichol pathway of *N*-linked glycosylation. *Biochim. Biophys. Acta-Gen. Subjects* **1999**, *1426*, 239-257.

45. Frank, C. G.; Aebi, M., ALG9 mannosyltransferase is involved in two different steps of lipid-linked oligosaccharide biosynthesis. *Glycobiology* **2005**, *15*, 1156-1163.
46. Guha-Niyogi, A.; Sullivan, D. R.; Turco, S. J., Glycoconjugate structures of parasitic protozoa. *Glycobiology* **2001**, *11*, 45R-59R.
47. Parodi, A. J., *N*-Glycosylation in trypanosomatid protozoa. *Glycobiology* **1993**, *3*, 193-199.
48. Kelleher, D. J.; Gilmore, R., An evolving view of the eukaryotic oligosaccharyltransferase. *Glycobiology* **2006**, *16*, 47R-62R.
49. Parodi, A. J., Protein glucosylation and its role in protein folding. *Annu. Rev. Biochem.* **2000**, *69*, 69-93.
50. Vembar, S. S.; Brodsky, J. L., One step at a time: endoplasmic reticulum-associated degradation. *Nat. Rev. Mol. Cell Biol.* **2008**, *9*, 944-957.
51. Munro, S., What can yeast tell us about *N*-linked glycosylation in the Golgi apparatus? *FEBS Lett.* **2001**, *498*, 223-227.
52. Schachter, H., The joys of HexNAc. The synthesis and function of *N*- and *O*-glycan branches. *Glycoconjugate J.* **2000**, *17*, 465-483.
53. Vella, G. J.; Paulsen, H.; Schachter, H., Control of glycoprotein synthesis. A terminal Man α -1-3Man β -1-sequence in the substrate is the minimum requirement for UDP-*N*-acetyl-D-glucosamine: α -D-mannoside (GlcNAc to Man α -1-3) β 2-*N*-acetylglucosaminyltransferase I. *Can. J. Biochem. Cell Biol.* **1984**, *62*, 409-417.
54. Kornfeld, R.; Kornfeld, S., Assembly of asparagine-linked oligosaccharides. *Annu. Rev. Biochem.* **1985**, *54*, 631-664.

55. Stanley, P.; Schachter, H.; Taniguchi, N., *N-Glycans. In Essentials of Glycobiology*, 2nd ed.; Varki, A.; Cummings, R. D.; Esko, J. D.; Freeze, H. H.; Stanley, P.; Bertozzi, C. R.; Hart, G. W.; Etzler, M. E., Eds.: Cold Spring Harbor (NY), **2009**.
56. Kornfeld, S.; Mellman, I., The biogenesis of lysosomes. *Annu. Rev. Cell Biol.* **1989**, *5*, 483-525.
57. Reitman, M. L.; Kornfeld, S., UDP-*N*-acetylglucosamine:glycoprotein *N*-acetylglucosamine-1-phosphotransferase. Proposed enzyme for the phosphorylation of the high mannose oligosaccharide units of lysosomal enzymes. *J. Biol. Chem.* **1981**, *256*, 4275-4281.
58. Varki, A.; Kornfeld, S., P-type Lectins. *In Essentials of Glycobiology*, 2nd ed.; Varki, A.; Cummings, R. D.; Esko, J. D.; Freeze, H. H.; Stanley, P.; Bertozzi, C. R.; Hart, G. W.; Etzler, M. E., Eds.: Cold Spring Harbor (NY), **2009**.
59. Bao, M.; Booth, J. L.; Elmendorf, B. J.; Canfield, W. M., Bovine UDP-*N*-acetylglucosamine:lysosomal-enzyme *N*-acetylglucosamine-1-phosphotransferase. Purification and subunit structure. *J. Biol. Chem.* **1996**, *271*, 31437-31445.
60. Waheed, A.; Hasilik, A.; von Figura, K., UDP-*N*-acetylglucosamine:lysosomal enzyme precursor *N*-acetylglucosamine-1-phosphotransferase. Partial purification and characterization of the rat liver Golgi enzyme. *J. Biol. Chem.* **1982**, *257*, 12322-12331.
61. Varki, A.; Kornfeld, S., Purification and characterization of rat-liver alpha-*N*-acetylglucosaminyl phosphodiesterase. *J. Biol. Chem.* **1981**, *256*, 9937-9943.
62. Ghosh, P.; Dahms, N. M.; Kornfeld, S., Mannose 6-phosphate receptors: new twists in the tale. *Nat. Rev. Mol. Cell Biol.* **2003**, *4*, 202-212.
63. Coutinho, M. F.; Prata, M. J.; Alves, S., Mannose-6-phosphate pathway: A review on its role in lysosomal function and dysfunction. *Mol. Genet. Metab.* **2012**, *105*, 542-550.

64. Tran, D. T.; Ten Hagen, K. G., Mucin-type *O*-glycosylation during development. *J. Biol. Chem.* **2013**, *288*, 6921-6929.
65. Mendonca-Previato, L.; Penha, L.; Garcez, T. C.; Jones, C.; Previato, J. O., Addition of alpha-*O*-GlcNAc to threonine residues define the post-translational modification of mucin-like molecules in *Trypanosoma cruzi*. *Glycoconj. J.* **2013**, *30*, 659-666.
66. Freeze, H. H.; Haltiwanger, R. S., Other classes of ER/Golgi-derived glycans. *In Essentials of Glycobiology*, 2nd ed.; Varki, A.; Cummings, R. D.; Esko, J. D.; Freeze, H. H.; Stanley, P.; Bertozzi, C. R.; Hart, G. W.; Etzler, M. E., Eds.: Cold Spring Harbor (NY), **2009**.
67. Bennett, E. P.; Mandel, U.; Clausen, H.; Gerken, T. A.; Fritz, T. A.; Tabak, L. A., Control of mucin-type *O*-glycosylation: a classification of the polypeptide GalNAc-transferase gene family. *Glycobiology* **2012**, *22*, 736-756.
68. Raman, J.; Guan, Y.; Perrine, C. L.; Gerken, T. A.; Tabak, L. A., UDP-*N*-acetyl-alpha-D-galactosamine:polypeptide *N*-acetylgalactosaminyltransferases: completion of the family tree. *Glycobiology* **2012**, *22*, 768-777.
69. Tetaert, D.; Ten Hagen, K. G.; Richet, C.; Boersma, A.; Gagnon, J.; Degand, P., Glycopeptide *N*-acetylgalactosaminyltransferase specificities for *O*-glycosylated sites on MUC5AC mucin motif peptides. *Biochem. J.* **2001**, *357*, 313-320.
70. Tian, E.; Ten Hagen, K. G., Recent insights into the biological roles of mucin-type *O*-glycosylation. *Glycoconj. J.* **2009**, *26*, 325-334.
71. Ju, T.; Brewer, K.; D'Souza, A.; Cummings, R. D.; Canfield, W. M., Cloning and expression of human core 1 beta-1,3-galactosyltransferase. *J. Biol. Chem.* **2002**, *277*, 178-186.
72. Hounsell, E. F.; Davies, M. J.; Renouf, D. V., *O*-linked protein glycosylation structure and function. *Glycoconj. J.* **1996**, *13*, 19-26.

73. Di Noia, J. M.; Pollevick, G. D.; Xavier, M. T.; Previato, J. O.; Mendoca-Previato, L.; Sanchez, D. O.; Frasch, A. C., High diversity in mucin genes and mucin molecules in *Trypanosoma cruzi*. *J. Biol. Chem.* **1996**, *271*, 32078-32083.
74. Previato, J. O.; Sola-Penna, M.; Agrellos, O. A.; Jones, C.; Oeltmann, T.; Travassos, L. R.; Mendonca-Previato, L., Biosynthesis of *O*-*N*-acetylglucosamine-linked glycans in *Trypanosoma cruzi*. Characterization of the novel uridine diphospho-*N*-acetylglucosamine:polypeptide *N*-acetylglucosaminyltransferase-catalyzing formation of *N*-acetylglucosamine alpha-1→*O*-threonine. *J. Biol. Chem.* **1998**, *273*, 14982-14988.
75. Schenkman, S.; Eichinger, D.; Pereira, M. E. A.; Nussenzweig, V., Structural and functional-properties of *Trypanosoma trans*-sialidase. *Annu. Rev. Microbiol.* **1994**, *48*, 499-523.
76. Lombard, V.; Golaconda Ramulu, H.; Drula, E.; Coutinho, P. M.; Henrissat, B., The carbohydrate-active enzymes database (CAZy) in 2013. *Nucleic. Acids Res.* **2014**, *42*, D490-D495.
77. Lairson, L. L.; Henrissat, B.; Davies, G. J.; Withers, S. G., Glycosyltransferases: structures, functions, and mechanisms. *Annu. Rev. Biochem.* **2008**, *77*, 521-555.
78. Lairson, L. L.; Withers, S. G., Mechanistic analogies amongst carbohydrate modifying enzymes. *Chem. Commun.* **2004**, 2243-2248.
79. Lee, S. S.; Hong, S. Y.; Errey, J. C.; Izumi, A.; Davies, G. J.; Davis, B. G., Mechanistic evidence for a front-side, *S_Ni*-type reaction in a retaining glycosyltransferase. *Nat. Chem. Biol.* **2011**, *7*, 631-638.
80. Roth, J., Subcellular organization of glycosylation in mammalian cells. *Biochim. Biophys. Acta* **1987**, *906*, 405-436.
81. El-Battari, A., Autofluorescent proteins for monitoring the intracellular distribution of glycosyltransferases. *Methods Enzymol.* **2006**, *416*, 102-120.
82. Palcic, M. M.; Sujino, K., Assays for glycosyltransferases. *Trend. Glycosci. Glycotechnol.* **2001**, *13*, 361-370.

83. Wagner, G. K.; Pesnot, T., Glycosyltransferases and their assays. *ChemBioChem* **2010**, *11*, 1939-1949.
84. Gosselin, S.; Alhussaini, M.; Streiff, M. B.; Takabayashi, K.; Palcic, M. M., A Continuous spectrophotometric assay for glycosyltransferases. *Anal. Biochem.* **1994**, *220*, 92-97.
85. Matern, H.; Heinemann, H.; Matern, S., Radioassay of UDP-glucuronosyltransferase activities toward endogenous substrates using labeled UDP-glucuronic acid and an organic solvent extraction procedure. *Anal. Biochem.* **1994**, *219*, 182-188.
86. Palcic, M. M. H., L.; Pierce, M.; Hindsgaul, O., The use of hydrophobic synthetic glycosides as acceptors in glycosyltransferase assays. *Glycoconj. J.* **1988**, *5*, 49-63.
87. Brown, J. R.; Field, R. A.; Barker, A.; Guy, M.; Grewal, R.; Khoo, K. H.; Brennan, P. J.; Besra, G. S.; Chatterjee, D., Synthetic mannosides act as accepters for mycobacterial alpha 1→6 mannosyltransferase. *Bioorgan. Med. Chem.* **2001**, *9*, 815-824.
88. Brown, J. R.; Guther, M. L. S.; Field, R. A.; Ferguson, M. A. J., Hydrophobic mannosides act as accepters for *trypanosome* alpha-mannosyltransferases. *Glycobiology* **1997**, *7*, 549-558.
89. Miyashiro, M.; Furuya, S.; Sugita, T., A high-throughput screening system for alpha1→3-fucosyltransferase-VII inhibitor utilizing scintillation proximity assay. *Anal. Biochem.* **2005**, *338*, 168-170.
90. Ahsen, O.; Voigtmann, U.; Klotz, M.; Nifantiev, N.; Schottelius, A.; Ernst, A.; Muller-Tiemann, B.; Parczyk, K., A miniaturized high-throughput screening assay for fucosyltransferase VII. *Anal. Biochem.* **2008**, *372*, 96-105.
91. Reymond, J. L.; Fluxa, V. S.; Maillard, N., Enzyme assays. *Chem. Commun.* **2009**, 34-46.

92. Qin, W.; Baruah, M.; Van der Auweraer, M.; De Schryver, F. C.; Boens, N., Photophysical properties of borondipyrromethene analogues in solution. *J. Phys. Chem. A* **2005**, *109*, 7371-7384.
93. Sarver, S. A.; Keithley, R. B.; Essaka, D. C.; Tanaka, H.; Yoshimura, Y.; Palcic, M. M.; Hindsgaul, O.; Dovichi, N. J., Preparation and electrophoretic separation of BODIPY-fluorescently-labeled glycosphingolipids. *J. Chromatogr. A* **2012**, *1229*, 268-273.
94. Schiedel, M. S.; Briehn, C. A.; Bauerle, P., Single-compound libraries of organic materials: Parallel synthesis and screening of fluorescent dyes. *Angew. Chem. Int. Edit.* **2001**, *40*, 4677-4680.
95. Owicki, J. C., Fluorescence polarization and anisotropy in high throughput screening: perspectives and primer. *J. Biomol. Screen.* **2000**, *5*, 297-306.
96. Soltero-Higgin, M.; Carlson, E. E.; Phillips, J. H.; Kiessling, L. L., Identification of inhibitors for UDP-galactopyranose mutase. *J. Am. Chem. Soc.* **2004**, *126*, 10532-10533.
97. Gross, B. J.; Kraybill, B. C.; Walker, S., Discovery of *O*-GlcNAc transferase inhibitors. *J. Am. Chem. Soc.* **2005**, *127*, 14588-14589.
98. Collier, A.; Wagner, G. K., A fast synthetic route to GDP-sugars modified at the nucleobase. *Chem. Commun.* **2008**, 178-180.
99. Batt, S. M.; Jabeen, T.; Mishra, A. K.; Veerapen, N.; Krumbach, K.; Eggeling, L.; Besra, G. S.; Futterer, K., Acceptor substrate discrimination in phosphatidyl-*myo*-inositol mannoside synthesis: structural and mutational analysis of mannosyltransferase *Corynebacterium glutamicum* PimB'. *J. Biol. Chem.* **2010**, *285*, 37741-37752.
100. Aharoni, A.; Thieme, K.; Chiu, C. P.; Buchini, S.; Lairson, L. L.; Chen, H.; Strynadka, N. C.; Wakarchuk, W. W.; Withers, S. G., High-throughput screening methodology for the directed evolution of glycosyltransferases. *Nat. Methods* **2006**, *3*, 609-614.

101. Herzenberg, L. A.; Parks, D.; Sahaf, B.; Perez, O.; Roederer, M.; Herzenberg, L. A., The history and future of the fluorescence activated cell sorter and flow cytometry: a view from Stanford. *Clin. Chem.* **2002**, *48*, 1819-1827.
102. Yoshimura, Y. T., H.; Dovichi, N.; Hindsgaul, O.; Palcic, M., Application of fluorescently-labeled glycosphingolipids to metabolic profiling in single cell using capillary electrophoresis. *Trend. Glycosci. Glycotechnol.* **2012**, *24*, 169-178.
103. Rajaganesh, R.; Ravinder, P.; Subramanian, V.; Das, T. M., FACE-selective fluorogenic cycloaddition reaction between coumarin azides and sugar terminal alkynes: an experimental and computational study. *Carbohydr. Res.* **2011**, *346*, 2327-2336.
104. Sivakumar, K.; Xie, F.; Cash, B. M.; Long, S.; Barnhill, H. N.; Wang, Q., A fluorogenic 1,3-dipolar cycloaddition reaction of 3-azidocoumarins and acetylenes. *Org. Lett.* **2004**, *6*, 4603-4606.
105. Jewett, J. C.; Bertozzi, C. R., Synthesis of a fluorogenic cyclooctyne activated by Cu-free click chemistry. *Org. Lett.* **2011**, *13*, 5937-5939.
106. Park, S.; Kim, H. J., Highly selective and sensitive fluorescence turn-on probe for a catalytic amount of Cu(I) ions in water through the click reaction. *Tetrahedron Lett.* **2012**, *53*, 4473-4475.
107. Hartman, M. C.; Dcona, M. M., A new, highly water-soluble, fluorescent turn-on chemodosimeter for direct measurement of hydrogen sulfide in biological fluids. *Analyst* **2012**, *137*, 4910-4912.
108. Paulus, A.; Klockow, A., Detection of carbohydrates in capillary electrophoresis. *J. Chromatogr. A* **1996**, *720*, 353-376.
109. Goetz, S., The molecular basis of plant cell wall oligosaccharide formation. *PhD thesis, John Innes Centre* **2012**.

110. Wang, K. L.; Jiang, D. C.; Sims, C. E.; Allbritton, N. L., Separation of fluorescently labeled phosphoinositides and sphingolipids by capillary electrophoresis. *J. Chromatogr. B* **2012**, *907*, 79-86.
111. Essaka, D. C.; Prendergast, J.; Keithley, R. B.; Palcic, M. M.; Hindsgaul, O.; Schnaar, R. L.; Dovichi, N. J., Metabolic cytometry: capillary electrophoresis with two-color fluorescence detection for the simultaneous study of two glycosphingolipid metabolic pathways in single primary neurons. *Anal. Chem.* **2012**, *84*, 2799-2804.
112. Thiele, C.; Papan, C.; Hoelper, D.; Kusserow, K.; Gaebler, A.; Schoene, M.; Piotrowitz, K.; Lohmann, D.; Spandl, J.; Stevanovic, A.; Shevchenko, A.; Kuerschner, L., Tracing fatty acid metabolism by Click chemistry. *ACS Chem. Biol.* **2012**, *7*, 2004-2011.
113. Smith, T. K.; Cottaz, S.; Brimacombe, J. S.; Ferguson, M. A. J., Substrate specificity of the dolichol phosphate mannose: Glucosaminyl phosphatidylinositol alpha 1→4-mannosyltransferase of the glycosylphosphatidylinositol biosynthetic pathway of African trypanosomes. *J. Biol. Chem.* **1996**, *271*, 6476-6482.
114. Smith, T. K.; Crossman, A.; Paterson, M. J.; Borissow, C. N.; Brimacombe, J. S.; Ferguson, M. A. J., Specificities of enzymes of glycosylphosphatidylinositol biosynthesis in *Trypanosoma brucei* and HeLa cells. *J. Biol. Chem.* **2002**, *277*, 37147-37153.
115. Urbaniak, M. D.; Crossman, A.; Ferguson, M. A. J., Probing *Trypanosoma brucei* glycosylphosphatidylinositol biosynthesis using novel precursor-analogues. *Chem. Biol. Drug Des.* **2008**, *72*, 127-132.
116. Ness, R. K.; Fletcher, H. G. JR.; Hudson, C. S., The Reaction of 2,3,4,6-tetrabenzoyl- α -D-glucopyranosyl bromide and 2,3,4,6-tetrabenzoyl- α -D-mannopyranosyl bromide with methanol. Certain benzoylated derivatives of D-glucose and D-mannose. *J. Am. Chem. Soc.* **1950**, *72*, 2000-2205.

117. Dowlut, M.; Hall, D. G.; Hindsgaul, O., Investigation of nonspecific effects of different dyes in the screening of labeled carbohydrates against immobilized proteins. *J. Org. Chem.* **2005**, *70*, 9809-9813.
118. Simmons, J. T.; Allen, J. R.; Morris, D. R.; Clark, R. J.; Levenson, C. W.; Davidson, M. W.; Zhu, L., Integrated and passive 1,2,3-triazolyl groups in fluorescent indicators for zinc(II) ions: thermodynamic and kinetic evaluations. *Inorg. Chem.* **2013**, *52*, 5838-5850.
119. Mehta, V. P.; Punji, B., Recent advances in transition-metal-free direct C-C and C-heteroatom bond forming reactions. *RSC Adv.* **2013**, *3*, 11957-11986.
120. Brandsma L.; Verkruijsse, H. D., An improved synthesis of cyclooctyne. *Synthesis* **1978**, 290.
121. Hanessian, S.; Masse, R.; Capmeau, M. L., Aminoglycoside antibiotics: synthesis of 5"-amino-5"-deoxyneomycin and 5"-amino-5"-deoxyparomomycin. *J. Antibiot.* **1977**, *30*, 893-896.
122. Key, J. A.; Koh, S.; Timerghazin, Q. K.; Brown, A.; Cairo, C. W., Photophysical characterization of triazole-substituted coumarin fluorophores. *Dyes Pigments* **2009**, *82*, 196-203.
123. Angell, Y.; Burgess, K., Base dependence in copper-catalyzed Huisgen reactions: efficient formation of bistriazoles. *Angew. Chem. Int. Edit.* **2007**, *46*, 3649-3651.
124. Key, J. A.; Cairo, C. W.; Ferguson, F. J., 7,7'-(3,3'-Dibenzyl-3*H*,3'*H*-4,4'-bi-1,2,3-triazole-5,5''-diyl)bis(4-methyl-2*H*chromen-2-one). *Acta Crystallogr. Sect. E* **2008**, *E64*, o1910.
125. Rao, V. S.; Perlin, A. S., Influence on direct, ¹³C-¹H coupling, and ¹³C-chemical shift, of replacement of oxygen-atoms in aldopyranoses by sulfur - evidence of differential, gamma-anti effects. *Carbohydr. Res.* **1981**, *92*, 141-148.

126. Hoshiyama, M.; Kubo, K.; Igarashi, T.; Sakurai, T., Complexation and proton dissociation behavior of 7-hydroxy-4-methylcoumarin and related compounds in the presence of beta-cyclodextrin. *J. Photochem. Photobiol. A* **2001**, *138*, 227-233.
127. Bruckner, J., Estimation of monosaccharides by the orcinol-sulphuric acid reaction. *Biochem. J.* **1955**, *60*, 200-205.
128. Bass, J. B.; Farer, L. S.; Hopewell, P. C.; O'Brien, R.; Jacobs, R. F.; Ruben, F.; Snider, D. E.; Thornton, G., Treatment of tuberculosis and tuberculosis infection in adults and children. *Am. J. Resp. Crit. Care* **1994**, *149*, 1359-1374.
129. Dover, L. G.; Cerdeno-Tarraga, A. M.; Pallen, M. J.; Parkhill, J.; Besra, G. S., Comparative cell wall core biosynthesis in the mycolated pathogens, *Mycobacterium tuberculosis* and *Corynebacterium diphtheriae*. *FEMS Microbiol. Rev.* **2004**, *28*, 225-250.
130. Besra, G. S.; Brennan, P. J., The mycobacterial cell wall: biosynthesis of arabinogalactan and lipoarabinomannan. *Biochem. Soc. T.* **1997**, *25*, 845-850.
131. Banerjee, D. K.; Scher, M. G.; Waechter, C. J., Amphomycin - Effect of the lipopeptide antibiotic on the glycosylation and extraction of dolichyl monophosphate in calf brain membranes. *Biochemistry* **1981**, *20*, 1561-1568.
132. Tam, P. H.; Besra, G. S.; Lowary, T. L., Exploring the substrate specificity of a mycobacterial polyprenol monophosphomannose-dependent alpha-(1→6)-mannosyltransferase. *ChemBioChem* **2008**, *9*, 267-278.
133. Subramaniam, V.; Gurucha, S. S.; Besra, G. S.; Lowary, T. L., Modified mannose disaccharides as substrates and inhibitors of a polyprenol monophosphomannose-dependent alpha-(1→6)-mannosyltransferase involved in mycobacterial lipoarabinomannan biosynthesis. *Bioorg. Med. Chem.* **2005**, *13*, 1083-1094.
134. Alpert, A. J.; Shukla, M.; Shukla, A. K.; Zieske, L. R.; Yuen, S. W.; Ferguson, M. A. J.; Mehlert, A.; Pauly, M.; Orlando, R., Hydrophilic-interaction chromatography of complex carbohydrates. *J. Chromatogr. A* **1994**, *676*, 191-202.

135. Churms, S. C., Recent progress in carbohydrate separation by high-performance liquid chromatography based on hydrophilic interaction. *J. Chromatogr. A* **1996**, 720, 75-91.
136. Langousis, G.; Hill, K. L., Motility and more: the flagellum of *Trypanosoma brucei*. *Nat. Rev. Microbiol.* **2014**, 12, 505-518.
137. Cross, G. A., Identification, purification and properties of clone-specific glycoprotein antigens constituting the surface coat of *Trypanosoma brucei*. *Parasitology* **1975**, 71, 393-417.
138. Pays, E.; Vanhamme, L.; Berberof, M., Genetic controls for the expression of surface antigens in African trypanosomes. *Annu. Rev. Microbiol.* **1994**, 48, 25-52.
139. Boothroyd, J. C., Antigenic variation in African trypanosomes. *Annu. Rev. Microbiol.* **1985**, 39, 475-502.
140. Pingel, S.; Field, R. A.; Guther, M. L. S.; Duszenko, M.; Ferguson, M. A. J., The hydrophobic mannoside Man- α -1 \rightarrow 6Man- α -1-S-(CH₂)₇-CH₃ acts as an acceptor for the UDP-Gal-glycosylphosphatidylinositol anchor α -1,3-galactosyltransferase of *Trypanosoma brucei*. *Biochem. J.* **1995**, 309, 877-882.
141. Brown, J. R.; Smith, T. K.; Ferguson, M. A. J.; Field, R. A., A synthetic acceptor substrate for *Trypanosoma brucei* UDP-Gal: GPI anchor side-chain α -galactosyltransferases. *Bioorg. Med. Chem. Lett.* **1998**, 8, 2051-2054.
142. Clowers, B. H.; Dwivedi, P.; Steiner, W. E.; Hill, H. H.; Bendiak, B., Separation of sodiated isobaric disaccharides and trisaccharides using electrospray ionization-atmospheric pressure ion mobility-time of flight mass spectrometry. *J. Am. Soc. Mass Spectr.* **2005**, 16, 660-669.
143. Dwivedi, P.; Bendiak, B.; Clowers, B. H.; Hill, H. H., Rapid resolution of carbohydrate isomers by electrospray ionization ambient pressure ion mobility spectrometry-time-of-flight mass spectrometry (ESI-APIMS-TOFMS). *J. Am. Soc. Mass Spectr.* **2007**, 18, 1163-1175.

144. Levin, D. S.; Vouros, P.; Miller, R. A.; Nazarov, E. G., Using a nanoelectrospray-differential mobility spectrometer-mass spectrometer system for the analysis of oligosaccharides with solvent selected control over ESI aggregate ion formation. *J. Am. Soc. Mass Spectr.* **2007**, *18*, 502-511.
145. Fenn, L. S.; McLean, J. A., Biomolecular structural separations by ion mobility-mass spectrometry. *Anal. Bioanal. Chem.* **2008**, *391*, 905-909.
146. Verbeck, G. F.; Ruotolo, B. T.; Sawyer, H. A.; Gillig, K. J.; Russell, D. H., A fundamental introduction to ion mobility mass spectrometry applied to the analysis of biomolecules. *J. Biomol. Tech.* **2002**, *13*, 56-61.
147. Kanu, A. B.; Dwivedi, P.; Tam, M.; Matz, L.; Hill, H. H., Ion mobility-mass spectrometry. *J. Mass Spectrom.* **2008**, *43*, 1-22.
148. Ning, X.; Guo, J.; Wolfert, M. A.; Boons, G. J., Visualizing metabolically labeled glycoconjugates of living cells by copper-free and fast huisgen cycloadditions. *Angew. Chem. Int. Edit.* **2008**, *47*, 2253-2255.
149. Lattova E., S. Z., Mikusova K. Perreault H., Polakova M., Novel synthetic (1→6)-alpha-D-mannodisaccharide substrates support processive mannosylation catalysed by the mycobacterial cell envelope enzyme fraction. *RSC Adv.* *39*, 17784-17792.
150. Yokoyama, K.; Ballou, C. E., Synthesis of alpha 1,6-mannooligosaccharides in *Mycobacterium smegmatis*. Function of beta-mannosylphosphoryldecaprenol as the mannosyl donor. *J. Biol. Chem.* **1989**, *264*, 21621-21628.
151. Buetow, D. E., Euglena. *Encyclopedia of Life Sciences* **2011**, 1-5.
152. Buetow, D. E., Differential effects of temperature on growth of *Euglena gracilis*. *Exp. Cell Res.* **1962**, *27*, 137-142.
153. Sommer, J. R., The ultrastructure of the pellicle complex of *Euglena gracilis*. *J. Cell Biol.* **1965**, *24*, 253-257.

154. Nakano, Y.; Urade, Y.; Urade, R.; Kitaoka, S., Isolation, purification, and characterization of the pellicle of *Euglena gracilis*. *J. Biochem.* **1987**, *102*, 1053-1063.
155. Ahmadinejad, N.; Dagan, T.; Martin, W., Genome history in the symbiotic hybrid *Euglena gracilis*. *Gene* **2007**, *402*, 35-39.
156. Krnacova, K.; Vesteg, M.; Hampl, V.; Vlcek, C.; Horvath, A., *Euglena gracilis* and *Trypanosomatids* possess common patterns in predicted mitochondrial targeting presequences. *J. Mol. Evol.* **2012**, *75*, 119-129.
157. O'Neill, E. C., An exploration of phosphorylases for the synthesis of carbohydrate polymers. *PhD thesis, John Innes Centre* **2013**.
158. Rogalski, A. A.; Bouck, G. B., Characterization and localization of a flagellar-specific membrane glycoprotein in *Euglena*. *J. Cell Biol.* **1980**, *86*, 424-435.
159. Delacanal, L.; Parodi, A. J., Glycosylation of proteins in the protozoan *Euglena gracilis*. *Comp. Biochem. Phys. B* **1985**, *81*, 803-805.
160. Varki, A.; Esko, J. D.; Colley, K. J., Cellular Organization of Glycosylation. *In Essentials of Glycobiology*, 2nd ed.; Varki, A.; Cummings, R. D.; Esko, J. D.; Freeze, H. H.; Stanley, P.; Bertozzi, C. R.; Hart, G. W.; Etzler, M. E., Eds.: Cold Spring Harbor (NY), **2009**.
161. Gillott, M. A.; Triemer, R. E.; Vasconcelos, A. C., Isolation of dictyosomes from *Euglena gracilis*. *Protoplasma* **1980**, *105*, 45-51.
162. Corfield, A. P., Analysis of sugar sequences in glycoproteins by glycosidase digestion and gel filtration. *Methods Mol. Biol.* **1993**, *19*, 269-286.
163. Huang, Y. T.; Dodds, E. D., Ion mobility studies of carbohydrates as Group I adducts: isomer specific collisional cross section dependence on metal ion radius. *Anal. Chem.* **2013**, *85*, 9728-9735.

164. Imperiali, B.; O'Connor, S. E.; Hendrickson, T.; Kellenberger, C., Chemistry and biology of asparagine-linked glycosylation. *Pure Appl. Chem.* **1999**, *71*, 777-787.
165. Dorner, A. J.; Kaufman, R. J., Analysis of synthesis, processing, and secretion of proteins expressed in mammalian-cells. *Method. Enzymol.* **1990**, *185*, 577-596.
166. Strasser, R., Biological significance of complex *N*-glycans in plants and their impact on plant physiology. *Front. Plant Sci.* **2014**, *5*, 363.
167. Ziegler, F. D.; Gemmill, T. R.; Trimble, R. B., Glycoprotein-synthesis in yeast - early events in *N*-linked oligosaccharide processing in *Schizosaccharomyces pombe*. *J. Biol. Chem.* **1994**, *269*, 12527-12535.
168. Zhang Z., X. Z., Linhardt R. J., Thin layer chromatography for the separation and analysis of acidic carbohydrates. *J. Liq. Chromatogr. R. T.* **2009**, *32*, 1711-1732.
169. Lee, D. H.; Choi, S. L.; Rha, E.; Kim, S. J.; Yeom, S. J.; Moon, J. H.; Lee, S. G., A novel psychrophilic alkaline phosphatase from the metagenome of tidal flat sediments. *BMC. Biotechnol.* **2015**, *15*, 1-15.
170. Kajiura, H.; Seki, T.; Fujiyama, K., *Arabidopsis thaliana* ALG3 mutant synthesizes immature oligosaccharides in the ER and accumulates unique *N*-glycans. *Glycobiology* **2010**, *20*, 736-751.
171. Sarma, R. H.; Mynott, R. J., Conformation of pyridine-nucleotides studied by phosphorus-31 and hydrogen-1 fast Fourier-transform nuclear magnetic resonance spectroscopy. Oxidized and reduced mononucleotides. *J. Am. Chem. Soc.* **1973**, *95*, 1641-1649.
172. Tsuboi, M.; Takahash.S; Kyogoku, Y.; Hayatsu, H.; Ukita, T.; Kainosho, M., Phosphorus-proton spin-spin coupling and conformation of a dinucleoside phosphate. *Science* **1969**, *166*, 1504-1505.

173. Liu, Y. P.; Chen, G., Chemical synthesis of *N*-linked glycans carrying both mannose-6-phosphate and GlcNAc-mannose-6-phosphate motifs. *J. Org. Chem.* **2011**, *76*, 8682-8689.
174. Manthri, S.; Guether, M. L. S.; Izquierdo, L.; Acosta-Serrano, A.; Ferguson, M. A. J., Deletion of the TbALG3 gene demonstrates site-specific *N*-glycosylation and *N*-glycan processing in *Trypanosoma brucei*. *Glycobiology* **2008**, *18*, 367-383.
175. Korner, C.; Knauer, R.; Stephani, U.; Marquardt, T.; Lehle, L.; von Figura, K., Carbohydrate deficient glycoprotein syndrome type IV: deficiency of dolichyl-P-Man : Man₍₅₎GlcNAc₍₂₎-PP-dolichyl mannosyltransferase. *EMBO J.* **1999**, *18*, 6816-6822.
176. Cylwik, B.; Naklicki, M.; Chrostek, L.; Gruszewska, E., Congenital disorders of glycosylation. Part I. Defects of protein *N*-glycosylation. *Acta Biochim. Pol.* **2013**, *60*, 151-161.
177. Kudo, M.; Bao, M.; D'Souza, A.; Ying, F.; Pan, H.; Roe, B. A.; Canfield, W. M., The alpha- and beta-subunits of the human UDP-*N*-acetylglucosamine:lysosomal enzyme *N*-acetylglucosamine-1-phosphotransferase are encoded by a single cDNA. *J. Biol. Chem.* **2005**, *280*, 36141-36149.
178. Qian, Y.; Lee, I.; Lee, W. S.; Qian, M.; Kudo, M.; Canfield, W. M.; Lobel, P.; Kornfeld, S., Functions of the alpha, beta, and gamma subunits of UDP-GlcNAc:lysosomal enzyme *N*-acetylglucosamine-1-phosphotransferase. *J. Biol. Chem.* **2010**, *285*, 3360-3370.
179. Lang, L.; Couso, R.; Kornfeld, S., Glycoprotein phosphorylation in simple eucaryotic organisms. Identification of UDP-GlcNAc:glycoprotein *N*-acetylglucosamine-1-phosphotransferase activity and analysis of substrate specificity. *J. Biol. Chem.* **1986**, *261*, 6320-6325.
180. Qian, Y.; Flanagan-Steet, H.; van Meel, E.; Steet, R.; Kornfeld, S. A., The DMAP interaction domain of UDP-GlcNAc:lysosomal enzyme *N*-acetylglucosamine-1-phosphotransferase is a substrate recognition module. *Proc. Natl. Acad. Sci. U S A* **2013**, *110*, 10246-10251.

181. Qian, Y.; West, C. M.; Kornfeld, S., UDP-GlcNAc:Glycoprotein *N*-acetylglucosamine-1-phosphotransferase mediates the initial step in the formation of the methylphosphomannosyl residues on the high mannose oligosaccharides of *Dictyostelium discoideum* glycoproteins. *Biochem. Biophys. Res. Commun.* **2010**, *393*, 678-681.
182. Raas-Rothschild, A.; Cormier-Daire, V.; Bao, M.; Genin, E.; Salomon, R.; Brewer, K.; Zeigler, M.; Mandel, H.; Toth, S.; Roe, B.; Munnich, A.; Canfield, W. M., Molecular basis of variant *pseudo-hurler* polydystrophy (mucopolipidosis IIIC). *J. Clin. Invest.* **2000**, *105*, 673-681.
183. Kollmann, K.; Pohl, S.; Marschner, K.; Encarnacao, M.; Sakwa, I.; Tiede, S.; Poorthuis, B. J.; Lubke, T.; Muller-Loennies, S.; Storch, S.; Braulke, T., Mannose phosphorylation in health and disease. *Eur. J. Cell Biol.* **2010**, *89*, 117-123.
184. Lachmann, R., Treatments for lysosomal storage disorders. *Biochem. Soc. Trans.* **2010**, *38*, 1465-1468.
185. He, X.; Pierce, O.; Haselhorst, T.; von Itzstein, M.; Kolarich, D.; Packer, N. H.; Gloster, T. M.; Vocadlo, D. J.; Qian, Y.; Brooks, D.; Kermode, A. R., Characterization and downstream mannose phosphorylation of human recombinant alpha-L-iduronidase produced in *Arabidopsis complex glycan-deficient (cgl)* seeds. *Plant Biotechnol. J.* **2013**, *11*, 1034-1043.
186. Do, H.; Lee, W. S.; Ghosh, P.; Hollowell, T.; Canfield, W.; Kornfeld, S., Human mannose 6-phosphate-uncovering enzyme is synthesized as a proenzyme that is activated by the endoprotease furin. *J. Biol. Chem.* **2002**, *277*, 29737-29744.
187. Kudo, M.; Canfield, W. M., Structural requirements for efficient processing and activation of recombinant human UDP-*N*-acetylglucosamine:lysosomal-enzyme-*N*-acetylglucosamine-1-phosphotransferase. *J. Biol. Chem.* **2006**, *281*, 11761-11768.
188. Freeze, H. H.; Ichikawa, M., Identification of *N*-acetylglucosamine-alpha-1-phosphate transferase activity in *Dictyostelium discoideum*: an enzyme that initiates phosphoglycosylation. *Biochem. Biophys. Res. Commun.* **1995**, *208*, 384-389.

189. Andrade, L. O.; Andrews, N. W., The *Trypanosoma cruzi* host-cell interplay: location, invasion, retention. *Nat. Rev. Microbiol.* **2005**, *3*, 819-823.
190. Zingales, B.; Miles, M. A.; Moraes, C. B.; Luquetti, A.; Guhl, F.; Schijman, A. G.; Ribeiro, I., Drug discovery for Chagas disease should consider *Trypanosoma cruzi* strain diversity. *Mem. Inst. Oswaldo Cruz.* **2014**, *109*, 828-833.
191. Coura, J. R.; Dias, J. C. P., Epidemiology, control and surveillance of Chagas disease-100 years after its discovery. *Mem. Inst. Oswaldo Cruz.* **2009**, *104*, 31-40.
192. Osorio, L.; Rios, I.; Gutierrez, B.; Gonzalez, J., Virulence factors of *Trypanosoma cruzi*: who is who? *Microb. Infect.* **2012**, *14*, 1390-1402.
193. Tardieux, I.; Webster, P.; Ravesloot, J.; Boron, W.; Lunn, J. A.; Heuser, J. E.; Andrews, N. W., Lysosome recruitment and fusion are early events required for *Trypanosome* invasion of mammalian cells. *Cell* **1992**, *71*, 1117-1130.
194. Andrews, N. W.; Abrams, C. K.; Slatin, S. L.; Griffiths, G., A *T. cruzi* secreted protein immunologically related to the complement component C9: evidence for membrane pore-forming activity at low pH. *Cell* **1990**, *61*, 1277-1287.
195. Alves, M. J. M.; Colli, W., *Trypanosoma cruzi*: adhesion to the host cell and intracellular survival. *IUBMB Life* **2007**, *59*, 274-279.
196. Previato, J. O.; Jones, C.; Goncalves, L. P.; Wait, R.; Travassos, L. R.; Mendonca-Previato, L., O-glycosidically linked N-acetylglucosamine-bound oligosaccharides from glycoproteins of *Trypanosoma cruzi*. *Biochem. J.* **1994**, *301*, 151-159.
197. Giorgi, M. E.; de Lederkremer, R. M., Trans-sialidase and mucins of *Trypanosoma cruzi*: an important interplay for the parasite. *Carbohydr. Res.* **2011**, *346*, 1389-1393.

198. Buschiazzo, A.; Amaya, M. F.; Cremona, M. L.; Frasch, A. C.; Alzari, P. M., The crystal structure and mode of action of trans-sialidase, a key enzyme in *Trypanosoma cruzi* pathogenesis. *Mol. Cell* **2002**, *10*, 757-768.
199. Buscaglia, C. A.; Campo, V. A.; Frasch, A. C.; Di Noia, J. M., *Trypanosoma cruzi* surface mucins: host-dependent coat diversity. *Nat. Rev. Microbiol.* **2006**, *4*, 229-236.
200. Andrade, D. V.; Gollob, K. J.; Dutra, W. O., Acute Chagas disease: new global challenges for an old neglected disease. *PLOS Neglect. Trop. D.* **2014**, *8*, e3010.
201. Buckner, F. S., Experimental chemotherapy and approaches to drug discovery for *Trypanosoma cruzi* infection. *Adv. Parasitol.* **2011**, *75*, 89-119.
202. Neres, J.; Bryce, R. A.; Douglas, K. T., Rational drug design in parasitology: trans-sialidase as a case study for Chagas disease. *Drug Discov. Today* **2008**, *13*, 110-117.
203. Vandekerckhove, F.; Schenkman, S.; Pontes de Carvalho, L.; Tomlinson, S.; Kiso, M.; Yoshida, M.; Hasegawa, A.; Nussenzweig, V., Substrate specificity of the *Trypanosoma cruzi* trans-sialidase. *Glycobiology* **1992**, *2*, 541-548.
204. Campo, V. L.; Sesti-Costa, R.; Carneiro, Z. A.; Silva, J. S.; Schenkman, S.; Carvalho, I., Design, synthesis and the effect of 1,2,3-triazole sialylmimetic neoglycoconjugates on *Trypanosoma cruzi* and its cell surface trans-sialidase. *Bioorg. Med. Chem.* **2012**, *20*, 145-156.
205. Campo, V. L.; Carvalho, I.; Allman, S.; Davis, B. G.; Field, R. A., Chemical and chemoenzymatic synthesis of glycosyl-amino acids and glycopeptides related to *Trypanosoma cruzi* mucins. *Org. Biomol. Chem.* **2007**, *5*, 2645-2657.
206. Meldal, M.; Tornøe, C. W., Cu-catalyzed azide-alkyne cycloaddition. *Chem. Rev.* **2008**, *108*, 2952-3015.

207. Carvalho, I.; Andrade, P.; Campo, V. L.; Guedes, P. M. M.; Sesti-Costa, R.; Silva, J. S.; Schenkman, S.; Dedola, S.; Hill, L.; Rejzek, M.; Nepogodiev, S. A.; Field, R. A., Click chemistry synthesis of a library of 1,2,3-triazole-substituted galactose derivatives and their evaluation against *Trypanosoma cruzi* and its cell surface *trans*-sialidase. *Bioorg. Med. Chem.* **2010**, *18*, 2412-2427.
208. Junqueira, G. G.; Carvalho, M. R.; de Andrade, P.; Lopes, C. D.; Carneiro, Z. A.; Sesti-Costa, R.; Silva, J. S.; Carvalho, I., Synthesis and *in vitro* evaluation of novel galactosyl-triazolo-benzenesulfonamides against *Trypanosoma cruzi*. *J. Brazil. Chem. Soc.* **2014**, *25*, 1872-1884.
209. Da Silva, C. H.; Campo, V. L.; Carvalho, I.; Taft, C. A., Molecular modeling, docking and ADMET studies applied to the design of a novel hybrid for treatment of Alzheimer's disease. *J. Mol. Graph. Model.* **2006**, *25*, 169-175.
210. Galante, E.; Geraci, C.; Sciuto, S.; Campo, V. L.; Carvalho, I.; Sesti-Costa, R.; Guedes, P. M. M.; Silva, J. S.; Hill, L.; Nepogodiev, S. A.; Field, R. A., Glycoclusters presenting lactose on calix[4]arene cores display trypanocidal activity. *Tetrahedron* **2011**, *67*, 5902-5912.
211. Bernardi, A.; Jimenez-Barbero, J.; Casnati, A.; De Castro, C.; Darbre, T.; Fieschi, F.; Finne, J.; Funken, H.; Jaeger, K. E.; Lahmann, M.; Lindhorst, T. K.; Marradi, M.; Messner, P.; Molinaro, A.; Murphy, P. V.; Nativi, C.; Oscarson, S.; Penades, S.; Peri, F.; Pieters, R. J.; Renaudet, O.; Reymond, J. L.; Richichi, B.; Rojo, J.; Sansone, F.; Schaffer, C.; Turnbull, W. B.; Velasco-Torrijos, T.; Vidal, S.; Vincent, S.; Wennekes, T.; Zuilhof, H.; Imberty, A., Multivalent glycoconjugates as anti-pathogenic agents. *Chem. Soc. Rev.* **2013**, *42*, 4709-4727.
212. Bhatia, S.; Dimde, M.; Haag, R., Multivalent glycoconjugates as vaccines and potential drug candidates. *MedChemComm* **2014**, *5*, 862-878.
213. Kempe, K.; Krieg, A.; Becer, C. R.; Schubert, U. S., "Clicking" on with polymers: a rapidly expanding field for the straightforward preparation of novel macromolecular architectures. *Chem. Soc. Rev.* **2012**, *41*, 176-191.

214. Xie, J.; Bogliotti, N., Synthesis and applications of carbohydrate-derived macrocyclic compounds. *Chem. Rev.* **2014**, *114*, 7678-7739.
215. Bodine, K. D.; Gin, D. Y.; Gin, M. S., Synthesis of readily modifiable cyclodextrin analogues via cyclodimerization of an alkynyl-azido trisaccharide. *J. Am. Chem. Soc.* **2004**, *126*, 1638-1639.
216. Muthana, S.; Yu, H.; Cao, H. Z.; Cheng, J. S.; Chen, X., Chemoenzymatic synthesis of a new class of macrocyclic oligosaccharides. *J. Org. Chem.* **2009**, *74*, 2928-2936.
217. Pathigoolla, A.; Gonnade, R. G.; Sureshan, K. M., Topochemical Click reaction: spontaneous self-stitching of a monosaccharide to linear oligomers through lattice-controlled azide-alkyne cycloaddition. *Angew. Chem. Int. Edit.* **2012**, *51*, 4362-4366.
218. Pathigoolla, A.; Sureshan, K. M., A Crystal-to-crystal synthesis of triazolyl-linked polysaccharide. *Angew. Chem. Int. Edit.* **2013**, *52*, 8671-8675.
219. Campo, V. L.; Carvalho, I.; Da Silva, C. H. T. P.; Schenkman, S.; Hill, L.; Nepogodiev, S. A.; Field, R. A., Cyclooligomerisation of azido-alkyne-functionalised sugars: synthesis of 1,6-linked cyclic pseudo-galactooligosaccharides and assessment of their sialylation by *Trypanosoma cruzi* trans-sialidase. *Chem. Sci.* **2010**, *1*, 507-514.
220. Butler, C. E.; de Carvalho, T. M. U.; Grisard, E. C.; Field, R. A.; Tyler, K. M., Trans-sialidase stimulates eat me response from epithelial cells. *Traffic* **2013**, *14*, 853-869.
221. Chen, S. F.; Li, L. Y.; Zhao, C.; Zheng, J., Surface hydration: Principles and applications toward low-fouling/nonfouling biomaterials. *Polymer* **2010**, *51*, 5283-5293.
222. Ma, Y.; Cao, X.; Yu, B., Synthesis of oligosaccharide fragments of the rhamnogalacturonan of *Nerium indicum*. *Carbohydr. Res.* **2013**, *377*, 63-74.

223. Dondoni, A.; Marra, A., C-glycoside clustering on calix[4]arene, adamantane, and benzene scaffolds through 1,2,3-triazole linkers. *J. Org. Chem.* **2006**, *71*, 7546-7557.
224. Xu, L.; Li, Y. J.; Li, Y. L., Application of Click chemistry to the construction of supramolecular functional systems. *Asian. J. Org. Chem.* **2014**, *3*, 582-602.
225. Dc-Rubin, S. S.; Schenkman, S., *Trypanosoma cruzi* trans-sialidase as a multifunctional enzyme in Chagas' disease. *Cell Microbiol.* **2012**, *14*, 1522-1530.
226. Harrison, J. A.; Kartha, K. P. R.; Fournier, E. J. L.; Lowary, T. L.; Malet, C.; Nilsson, U. J.; Hindsgaul, O.; Schenkman, S.; Naismith, J. H.; Field, R. A., Probing the acceptor substrate binding site of *Trypanosoma cruzi* trans-sialidase with systematically modified substrates and glycoside libraries. *Org. Biomol. Chem.* **2011**, *9*, 1653-1660.
227. Chen, Y. X.; Zhao, L.; Huang, Z. P.; Zhao, Y. F.; Li, Y. M., Facile synthesis of cyclopeptide-centered multivalent glycoclusters with click chemistry and molecular recognition study by surface plasmon resonance. *Bioorg. Med. Chem. Lett.* **2009**, *19*, 3775-3778.
228. Bradford, M. M., A rapid and sensitive method for the quantitation of microgram quantities of protein utilizing the principle of protein-dye binding. *Anal. Biochem.* **1976**, *72*, 248-254.
229. Bouck, G. B.; Rogalski, A.; Valaitis, A., Surface organization and composition of *Euglena*. II. Flagellar mastigonemes. *J. Cell Biol.* **1978**, *77*, 805-826.